## AD NUMBER

**AD811146**

## NEW LIMITATION CHANGE

TO

**Approved for public release, distribution unlimited**

FROM

**Distribution authorized to U.S. Gov't. agencies and their contractors; Administrative/Operational use; 11 Apr 1966. Other requests shall be referred to Naval Ordnance Systems Command, Attn: Code ORD 9132, Washington DC 20360.**

## AUTHORITY

**USNOSC notice, 27 Apr 1967.**

# CERAMIC SYSTEMS FOR MISSILE STRUCTURAL APPLICATIONS

31 October 1966

Prepared under Navy, Bureau of Naval Weapons

Contract NOw-63-0143-d

FINAL SUMMARY REPORT

(QUARTERLY REPORT NO. 16 INCLUSIVE)

1 November 1965 through 31 October 1966



Engineering Experiment Station
Georgia Institute of Technology
Atlanta, Georgia

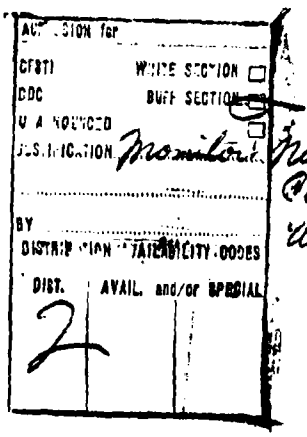


Monitor Naval ORDNANCE Systems Command
Code ORD-9132
Wash., D.C. 20360 a4
11 Apr 67

1473

(6) CERAMIC SYSTEMS FOR MISSILE STRUCTURAL APPLICATIONS.

(12) 242 p.

(11) 31 Oct 66

Prepared under Navy, Bureau of Naval Weapons

(15) Contract NOw-63-0143

(16) A-651

FINAL SUMMARY REPORT

(QUARTERLY REPORT NO. 16 INCLUSIVE)

1 November 1965 through 31 October 1966

(9) Quarterly rept. no. 16 (Final), 1 Nov 65 - 31 Oct 66,

Engineering Experiment Station, Georgia Institute of Technology, Atlanta, Georgia; N. E. Poulos, C. A. Murphy, W. J. Corbett, P. Boland, and C. W. Gorton, authors.

(10) Nick E. Poulos, Charles A. Murphy, William J. Corbett, Paul Boland Charles W. Gorton

mlk U53 850)

mk

## FOREWORD

This report was prepared by the Engineering Experiment Station of the Georgia Institute of Technology under U. S. Navy, Bureau of Naval Weapons, Contract NOw-63-0143-d. This contract is administered under the Bureau of Naval Weapons, Missile Guidance and Air Frame Division, Advanced Technology Branch (RMGA-8).

This report covers the period from 1 November 1965 through 31 October 1966. Principal personnel participating in this work include: N. E. Poulos, J. N. Harris, C. A. Murphy, W. J. Corbett, Paul Boland, C. W. Gorton, and J. D. Walton, Jr.

## ABSTRACT

Five slip-cast fused silica radomes were fabricated and evaluated in a Mach 2.2, 4000° F, 140 psia Typhon ramjet exhaust at General Dynamics/Pomona Ordnance Aerophysics Laboratory July 6-18, 1966. Test data are to be presented in a separate report prepared and published by the Johns Hopkins University, Applied Physics Laboratory, Silver Spring, Maryland. Preliminary observations are presented herein and it is estimated that 65 to 70 per cent of the test objectives were realized. Materials development and characterization studies of slip-cast alumina-fused silica composites and fused silica grinding for strength improvement are presented. Studies for applying metal films on slip-cast fused silica substrates for antenna applications were completed. Fabrication of felts from refractory fibers of fused silica, boron nitride, zirconia, magnesia, and silicon carbide coated graphite fibers and impregnation of a phenolic embedded ablator in these felts and comparison of thermal evaluation results of these embedded felts with standard ablators under a heat flux of 450 and 1500 BTU/ft$^2$-sec are described.

TABLE OF CONTENTS



(Continued)

TABLE OF CONTENTS (Continued)



This report contains 242 pages.

## LIST OF FIGURES



(Continued)

LIST OF FIGURES (Continued)



(Continued)

LIST OF FIGURES (Continued)



(Continued)

LIST OF FIGURES (Concluded)

## LIST OF TABLES



(Continued)

## LIST OF TABLES (Continued)

# I. PURPOSE

The purpose of Contract No. NOw-63-0143-d was to perform a research and development program directed toward development of techniques to exploit the full potential of readily available ceramic systems for use as structural components in hypersonic missile applications.

## II. INTRODUCTION

The objective of this program is the development of high temperature structural components for use in hypersonic missile applications. The work of the three phases or parts presented in this report is consistent with the Navy's material needs and requirements for Naval Missiles and Rockets.

### A. Slip-Cast Fused Silica (SCFS) Radome Structures for Thermal Evaluation at General Dynamics/Pomona Ordnance Aerophysics Laboratory

This work was continued from the past year's work. The thermomechanical test program of this effort was coordinated between Georgia Tech, Johns Hopkins University, and General Dynamics/Pomona. Each of these organizations have made significant contributions to the program such as fabrication and instrumentation of the test radomes, data reduction, and correlation with theoretical analysis.

It is anticipated that this program will not only provide valuable case histories on the thermal performance of SCFS radome structures, but also on the fabrication of and attachment systems for SCFS radomes. The program is directed towards the evaluation of the epoxy bond to the attachment ring and complete characterization of the material for the radome structure and the proof testing of the composite radome structure prior to instrumentation and subsequent evaluation at OAL.

### B. Materials Development and Characterization

This effort was divided into four areas of study. These are slip-cast fused silica-alumina composites, fused silica grinding, metal films, and felted ceramics. The felted ceramic studies are in part a continuation of the felted ceramic work of the past contract year, and the major effort of

this phase was devoted to the development of slip-cast fused silica-alumina composites and thick metal films for integrated radome thermosensors and antennas.

C. Composite Thermal Protection Systems

The purpose of this work was to assess the state-of-the-art of heat shields and to examine promising thermal protection concepts in a complementary experimental program. Interest was focused on materials selection, processing techniques, attachment methods, design guides, testing methods, and refurbishment for the types of systems suitable for the thermal protection of leading edges and other hot spot geometries where the special arrangement of highly refractory materials is required. The design philosophy included the environmental parameters of moderate to high heat flux and relatively short-time exposure with the following design criteria: moderate temperature rise at the back surface, mechanical stability although penetrated by foreign objects, retention of aerodynamic contour, and minimal wake contamination through the loss of heat shield material during hypersonic flight.

## III. EXPERIMENTAL WORK

### A. Slip-Cast Fused Silica (SCFS) Radome Structures Thermal Evaluation at General Dynamics/Pomona Ordnance Aerophysics Laboratory

#### 1. Test Program

The thermal testing of slip-cast fused silica radome structures in the exhaust stream of the Typhon Combustor at General Dynamics/Pomona Ordnance Aerophysics Laboratory, Lone Star, Texas was continued during this contract year. The previous tests 1/ were conducted in the exhaust stream of the Typhon Combustor which had a straight nozzle approximately 10 inches in diameter. The stream Mach number at the model tip was estimated to be from 1.6 to 1.8 in these tests. For the tests during this contract year the Typhon Combustor was modified to use a water cooled supersonic exit nozzle to give an exit flow of about Mach 2.2. The stream stagnation temperature with this nozzle was computed to be 3800° to 4000° F with a total pressure of 140 psia.

Fabrication and instrumentation of the test radomes, and analysis of the test data, has been a coordinated effort between the Georgia Institute of Technology, Engineering Experiment Station, Atlanta, Georgia, Johns Hopkins University, Applied Physics Laboratory, Silver Spring, Maryland, and General Dynamics/Pomona, Pomona, California. The contributions of each organization are presented in Table I.

A meeting was held 2 February 1966 at General Dynamics/Pomona, Ordnance Aerophysics Laboratory, Lone Star, Texas for the purpose of discussing the test program. Representatives of the Georgia Institute of Technology, Engineering Experiment Station, Atlanta, Georgia, and the Johns Hopkins

TABLE I

PARTICIPANT CONTRIBUTIONS TO THE ORDNANCE AEROPHYSICS LABORATORY THERMAL TESTS OF SLIP-CAST FUSED SILICA RADOME [illegible] CYCLES

| Organization | Contribution | | | |
|---|---|---|---|---|
| | Primary Hardware | Secondary Hardware | Instrumentation | Analysis |
| Georgia Institute of Technology | Four drain cast SCFS Radome structures; two X-band and two C-band. One X-band and one C-band to have 7 - w/o $Cr_2O_3$ modified surface of forward region. | Attachment-mounting systems for all primary hardware. | Attach all thermocouples (Cr:AL and Ir:$Ir_{60}Rh_{40}$). | Primary hardware characterization, i.e. strength and cristobalite content. Attachment-mounting system analysis in association with JHU/APL and GD/P. |
| Johns Hopkins University | None | None | Recommendations for T/C and strain gage locations. Attach all strain gauges and calibrate. | Thermal analyses for temperature distributions and stress distributions. |
| General Dynamics/Pomona | One precision cast SCFS X-band radome structure. | None | None | Bore sighting of precision cast SCFS X-band radome before and after thermal testing. |

University, Applied Physics Laboratory, Silver Spring, Maryland met with representatives of the Ordnance Aerophysics Laboratory. The discussions were primarily oriented towards delineating the facility requirements for the tests. The test program schedule was considered as was the instrumentation to obtain the thermo-mechanical material response to the supersonic hot gas stream from the Typhon combustor for correlation to the analytically predicted behavior. Preliminary data shown in Table II and in Figures 1 and 2 were generated by Suess 2/ to provide the basis for instrumentation selection.

TABLE II

PREDICTED TEMPERATURES AND THERMAL STRESSES IN SCFS RADOMES DURING 1966 OAL TESTS 2/

| Radome | Maximum Outer Surface Temperature[1] (°F) | Maximum Inner Surface Temperature[1] (°F) | Maximum Tensile Stress[1] (psi) |
|---|---|---|---|
| X-Band[2] | 3090 | 1550 | 1950 |
| C-Band[3] | 3090 | 220 | 2200 |

[1]Computations made at 4-inch axial distance from tip.

[2]Actual wall thickness considered was 0.400-inch.

[3]Actual wall thickness considered was 0.746-inch.

Thermal testing of the five SCFS radomes was accomplished during the period 6 July through 18 July 1966. Representatives from The Johns Hopkins University, Applied Physics Laboratory, and Georgia Institute of Technology, Engineering Experiment Station were present for the testing of four of the

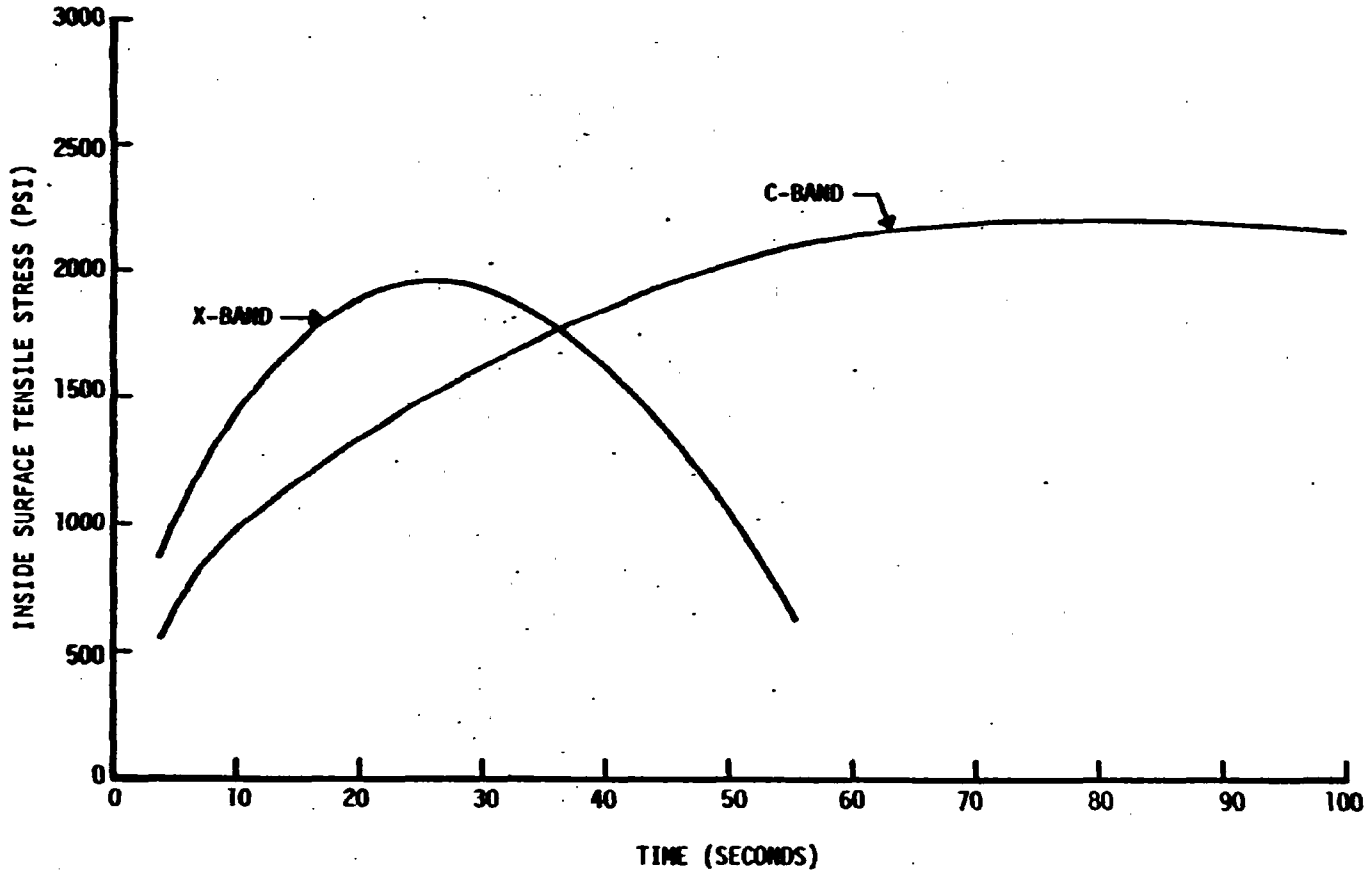


Figure 1. Predicted Inside Surface Tensile Stress vs Time for X and C-band SCFS Radomes (Reference 2).

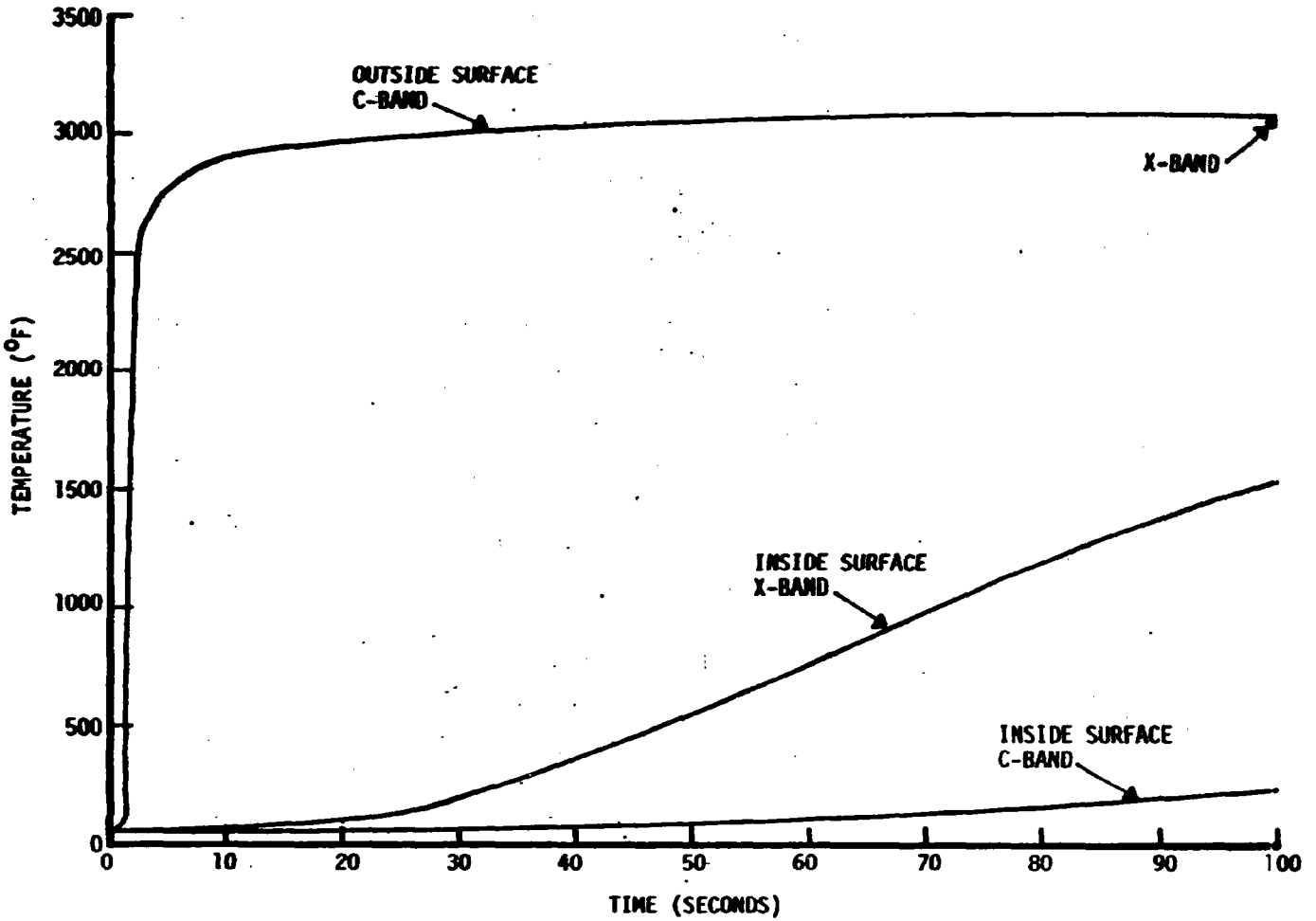


Figure 2. Predicted Surface Temperature vs Time for X and C-band SCFS Radomes (Reference 2).

radomes, and the fifth radome was tested after the representatives had returned to their laboratories.

The SCFS radomes were tested in the exhaust stream of the Typhon combustor. The planned stream conditions were: total temperature = 4000° F, velocity = Mach 2.2 and total pressure = 140 psi. The test conditions varied slightly from the planned values for each test due to the inherent fluctuations associated with the operation of the Typhon combustor. The descriptions of the radomes are presented in Table III.

TABLE III

OAL TEST NUMBER AND ORDER OF TESTING OF THE SCFS RADOMES

| OAL Test Number | Radome Number | Radome Description |
|---|---|---|
| 6167 | 1 | Drain casting, ≈ x-band thickness |
| 6168}<br>6169 | 2 | Drain casting, ≈ x-band thickness, with $Cr_2O_3$ modified forward region surface |
| 6170 | 3 | Precision casting, x-band thickness |
| 6171 | 4 | Drain casting, ≈ c-band thickness, with $Cr_2O_3$ modified forward region surface |
| 6172 | 5 | Drain casting, ≈ c-band thickness |

The reduction of the experimental data for correlation with the theoretical predictions of temperature and stress profiles has been undertaken by personnel of the Applied Physics Laboratory. This was not completed at the time of publishing this report. A preliminary report by APL is presented as Appendix III to this report. No attempt was made to incorporate any of the experimental results into this report for two reasons: (1) the ra

experimental data will be compiled in a report covering the tests which will be prepared and released in the near future by the Ordnance Aerophysics Laboratory, and (2) a report will be prepared and released in early 1967 by the Applied Physics Laboratory covering the data reduction and correlation with the theoretical analyses. The tests were not as successful as originally planned, but it is estimated that 65 to 70 per cent of the objectives were realized. A synopsis of each test is presented in Appendix IV.

## 2. OAL Test Radome Fabrication

Radomes were fabricated and sintered to determine the processing requirements of the test radomes which were supplied by Georgia Tech for the OAL thermal evaluation. The objectives of this study were to minimize the out-of-roundness of the radome structure and hold the maximum cristobalite content to 8 per cent. Previous studies 3/ showed that the out-of-roundness of slip-cast fused silica radomes occurs during the high temperature sintering cycle and not during the casting-drying cycle. These studies also showed the out-of-roundness of a 1/2-inch wall thickness, 2 feet base diameter by 4 feet tall radome was decreased during sintering by using an unsintered annular ring of slip-cast fused silica as a setter plate. The final stages of the work by General Dynamics/Pomona 4/ with slip-cast fused silica radome structures was conducted using a presintered annular ring of slip-cast fused silica in conjunction with a matter of refractory fiber wool.

As an extension of the above works, the effect of annular ring setter plates of resin bonded fused silica grain for reducing or eliminating the out-of-roundness in slip-cast fused silica radome structures was investigated. The composition of these rings is as follows:

74.40 w/o - 100 + 200 mesh fused silica grain

25.15 w/o - polyester resin

0.45 w/o - resin activator

The resin and activator are mixed together and then slowly blended with the grain. The mixture is tamped into a plywood ring mold and cured at 120° F for 16 hours and at 250° F for 7 hours.

A Von Karman configuration slip-cast fused silica radome 13.5 inches base diameter by 28.3 inches long was fabricated by pressure casting at 20 psig for 65 minutes. Based on previous experience a radome wall thickness of approximately 0.36 inches can be obtained with this pressure and time. Prior to removal from the mold, the cast radome was thoroughly dried tip-down in the mold. A layer of refractory fiber wool was then placed over the open mold and base of the included dry casting. The resin bonded fused silica annular ring was then placed with its center in approximate coincidence with the radome axis on the fiber wool. This was followed by three layers of fiber wool and a presintered foam fused silica support pedestal which was bolted subsequently to the mold frame. The entire assembly was then rotated 180° to a tip-up position. The fused silica foam pedestal was unbolted from the mold frame and the plaste mold was then lifted away. A roundness profile 3/ was then obtained at stations 1-inch above the radome base and at 13 inches above the radome base. No out-of-roundness was present at either position. The slip-cast fused silica radome (VK-5T) was then heated in a rotating bed electric furnace 3/ following the schedule presented in Table IV. Roundness profiles were again obtained at stations 1-inch and 13 inches above the radome base. The maximum observed

TABLE IV

TIME-TEMPERATURE SCHEDULE USED TO SINTER SLIP-CAST FUSED SILICA RADOME STRUCTURES

| | |
|---|---|
| Room Temperature to 1800° F | 16 hours |
| 1800° to 1900° F | 1/4 hour |
| Soak at 1900° F | 4 hours |
| 1900° to 2200° F | 1-1/4 hours |
| Soak at 2200° F | 1-1/4 hours |
| 2200° to 500° F (furnace power off) | 16-18 hours |
| 500° F to Room Temperature (open furnace) | --- |

out-of-roundness was 45 mils and occurred at the 1-inch station. No out-of-roundness was apparent at the 13-inch station. However, the radome axis did shift through an angle of 7° during sintering.

The wall thickness of the sintered radome was measured by selectively breaking the radome and measuring the wall thickness. These measurements are presented in Figure 3. The slight increase in wall thickness at the approximate 22-inch station is characteristic of two stage casting which is used to fabricate the $Cr_2O_3$ modified surface (compare with Figure 4). Cristobalite concentrations at selected stations on the radome are presented in Table V with modulus of rupture strength data in Table VI.

A second radome (VK-6T) was pressure cast for 59 minutes at 20 psig. The cast time was decreased to decrease wall thickness since the wall thickness of the VK-5T radome was greater than the desired 0.36 inches. However, as shown in Figure 4, this decrease was not obtained. The radome was cast following the same procedures as before and sintered in the same manner (Table IV) with the exceptions that this radome was supported on three layers of refractory

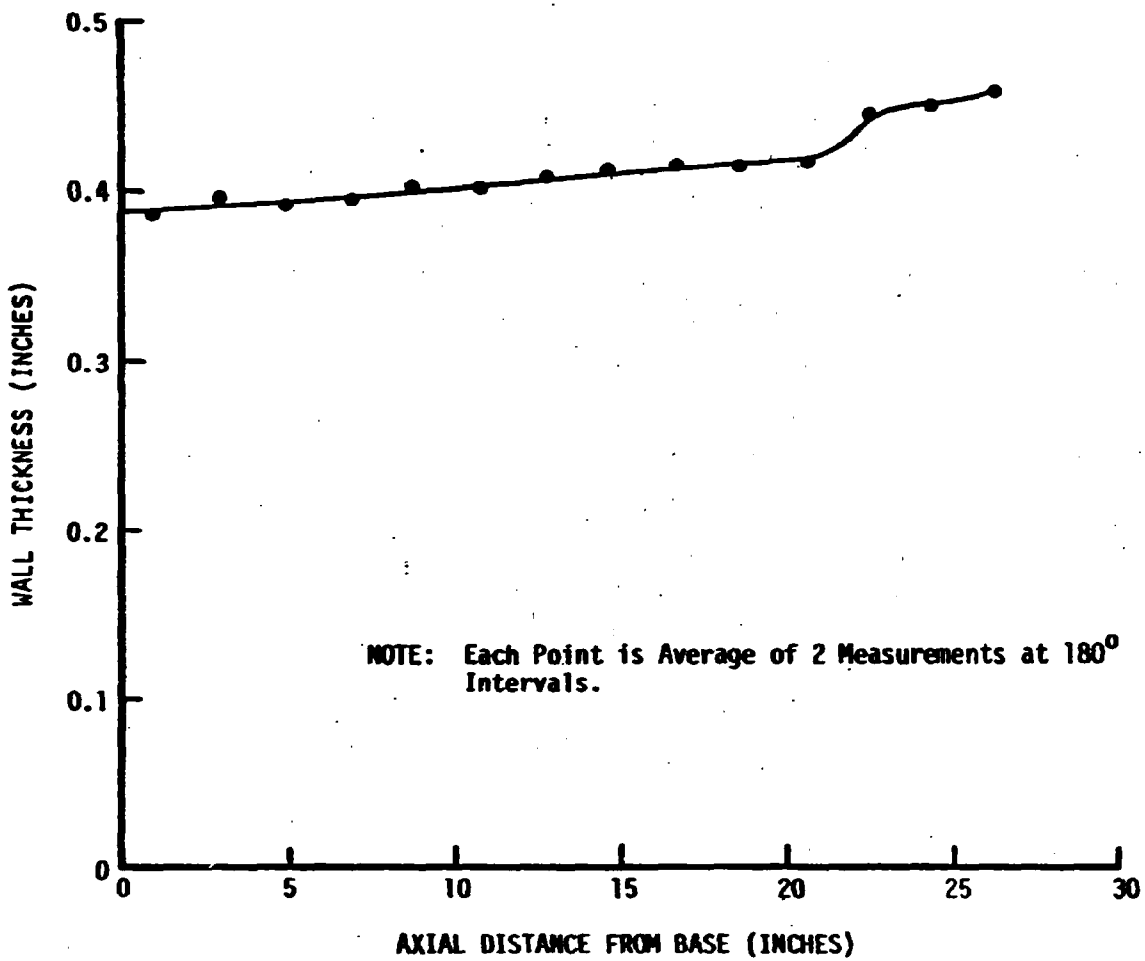


Figure 3. Measured Wall Thickness of $Cr_2O_3$ Modified Forward Surface Region Slip-Cast Fused Silica Radome Cast for 65 Minutes at 20 psig (VK-5T).

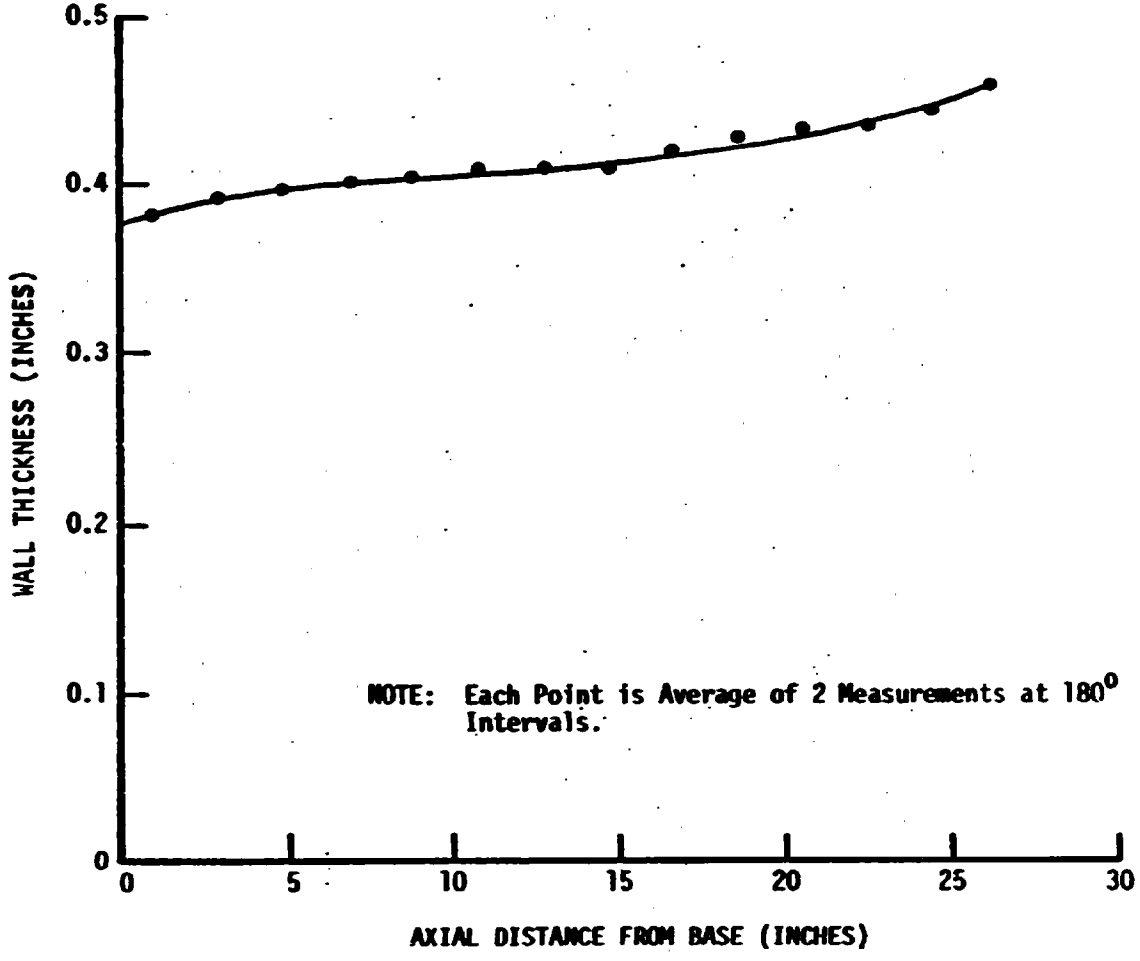


Figure 4. Measured Wall Thickness of Slip-Cast Fused Silica Radome Cast for 59 Minutes at 20 psig (VK-6T).

TABLE V

MEASURED CRISTOBALITE CONTENT OF SELECTED SEGMENTS CUT FROM VK-5T AND VK-6T RADOMES

| Radome | Cristobalite Content at Position | | | |
|---|---|---|---|---|
| | Bulk* Tip | Outer Tip | Bulk Base | Outer Base |
| VK-5T | 9.5 | 8.9 | 6.6 | 7.6 |
| VK-6T | 10.1 | 10.5 | 7.8 | 7.5 |

*Note: "Bulk" refers to specimen cut through the radome wall and with a thickness equal to the radome wall thickness. "Outer" refers to specimen cut with a thickness equal to one-half the radome wall thickness.

TABLE VI

MODULUS OF RUPTURE DATA ON SPECIMENS CUT FROM VK-5T AND VK-6T RADOMES

| Radome | Modulus of Rupture at Position | |
|---|---|---|
| | I* | II** |
| | ($lb/in^2$) | ($lb/in^2$) |
| VK-5T | $3060 \pm 209$*** | $3609 \pm 464$*** |
| VK-6T | $3329 \pm 181$ | $3012 \pm 433$ |

*Specimens cut from segment consisting of first 6 inches of radome as measured from base of radome.

**Specimens cut from segment consisting of second 6 inches of radome as measured from base of radome.

***95% Confidence Interval.

felt and was soaked at 2200° F for 70 minutes instead of 15 minutes. Roundness profiles before and after sintering showed no out-of-roundness before sintering and a maximum out-of-roundness of 35 mils after sintering. As before this out-of-roundness occurred at the 1-inch station. The radome axis shifted 9.5° during sintering. Cristobalite concentrations are presented in Table V, and modulus of rupture data in Table VI.

The out-of-roundness of the sintered SCFS radomes using a resin bonded fused silica grain ring as a setter plate did not differ significantly from radomes sintered using three layers of refractory felt between the radome and furnace pedestal, i.e. the radome-to-radome out-of-roundness was found to vary between 15 and 50 mils. Therefore, in the absence of a better solution to the problem of eliminating the out-of-roundness, subsequent test radomes were sintered using three layers of refractory felt between the radome and furnace pedestal.

As shown previously, the cristobalite content of the sintered SCFS radome shapes varied from ≈ 7-1/2 per cent at the base to ≈ 10 per cent at the tip. This spread was reduced by raising the radomes into the upper two-thirds of the furnace cavity during the sintering operation (this was an obvious approach since the furnace was shown to have a nearly uniform temperature in this region).

The fabrication studies offered a means of determining the usefulness of sintering SCFS test bars, 3/4-inch diameter by 6 inches long, along with the radome shapes for characterization of the properties of the sintered radomes. It was found, as illustrated in Table VII, that the properties of the SCFS control bars bore some relationship in some cases to the properties of specimens cut from the individual test radomes. However, it was concluded

TABLE VII

MODULUS OF RUPTURE AND CRISTOBALITE CONTENT OF SPECIMENS FROM SCFS RADOMES AND 3/4-INCH DIAMETER SCFS BARS

| Radome | Radome Specimens | | 3/4-Inch Test Bars | |
|---|---|---|---|---|
| | Modulus of Rupture ($lb/in^2$) | Cristobalite Content (v/o) | Modulus of Rupture ($lb/in^2$) | Cristobalite Content (v/o) |
| HT-18 | 3078 ± 143* | 7.6 ± 0.8* | 2857 ± 598* | 6.8 ± 0.1* |
| HT-20 | 3705 ± 143 | 8.9 ± 1.1 | 2423 ± 354 | 10.0 ± 1.6 |
| HT-21 | 3375 ± 145 | 7.5 ± 1.3 | 3326 ± 280 | 7.7 ± 1.5 |
| HT-22 | 3132 ± 163 | 6.7 ± 1.1 | 3070 ± 493 | 6.5 ± 0.9 |
| HT-28 | 3400 ± 200 | 6.5 ± 0.8 | 1979 ± 205 | 5.8 ± 1.0 |
| HT-31 | 3905 ± 125 | 4.6 ± 0.5 | 2306 ± 316 | 7.7 ± 0.5 |

*95% Confidence Interval.

that observations made on test bars sintered with SCFS radome shapes does not provide a consistently meaningful picture of the properties of the radome shapes and, thus, should not be adopted as a production measure. It was then decided that a section of the radome would have to be used for the determination of the strength and cristobalite content of the individual radome. Therefore, a 3.3-inch skirt was cut from the base of each radome and was used as a characterization sample. It was thought to be worthwhile to evaluate the uniformity of the entire radome with the idea of generating two numbers which should characterize each radome. This was done using the strength-cristobalite parameters which were assessed using conventional statistical methods (as opposed to Weibull statistics). The results are listed in Table VIII along

TABLE VIII

COMPARISON OF MODULUS OF RUPTURE AND CRISTOBALITE CONTENT OF ENTIRE RADOMES VERSUS 3.3-INCH SECTION

| Radome | Entire Radome | | 3.3-Inch Section | |
|---|---|---|---|---|
| | Modulus of Rupture ($lb/in^2$) | Cristobalite Content (v/o) | Modulus of Rupture ($lb/in^2$) | Cristobalite Content (v/o) |
| HT-21 | 2876 ± 145* | 7.5 ± 1.3* | 2826 ± 131* | 8.0 ± 0.8* |
| HT-22 | 3132 ± 163 | 6.7 ± 1.1 | 2978 ± 302 | 8.6 ± 0.3 |
| HT-28 | 3400 ± 200 | 6.5 ± 0.8 | 3266 ± 202 | 6.6 ± 0.4 |
| HT-31 | 3905 ± 125 | 4.6 ± 0.5 | 3612 ± 156 | 4.7 ± 0.3 |

*95% Confidence Interval.

with the data measured from the specimens taken from the 3.3-inch skirt cut from the base of the radome. These data clearly show the 3.3-inch length of the radome is sufficient to evaluate the properties of the total radome.

Test radome shapes were fitted* with water cooled Invar attachment rings. A drawing of the test radome-attachment system assembly is shown in Figure 5. The ring is attached to the SCFS radome with Shell 901/B-1 adhesive system. This is a room temperature cure system reported to have a tensile shear strength of 2000 psi after 24 hours at 75° F. Two cylinders, 6.7-inch O.D. with a wall thickness of ≈ 0.5-inch, were fabricated and fitted with simulated attachment rings made of aluminum, and the shear strength was measured by failing the system under axial loading as shown in Figure 6. The average shear

*The machining of the SCFS in the attachment region was accomplished with diamond tooling and is described in Appendix I.

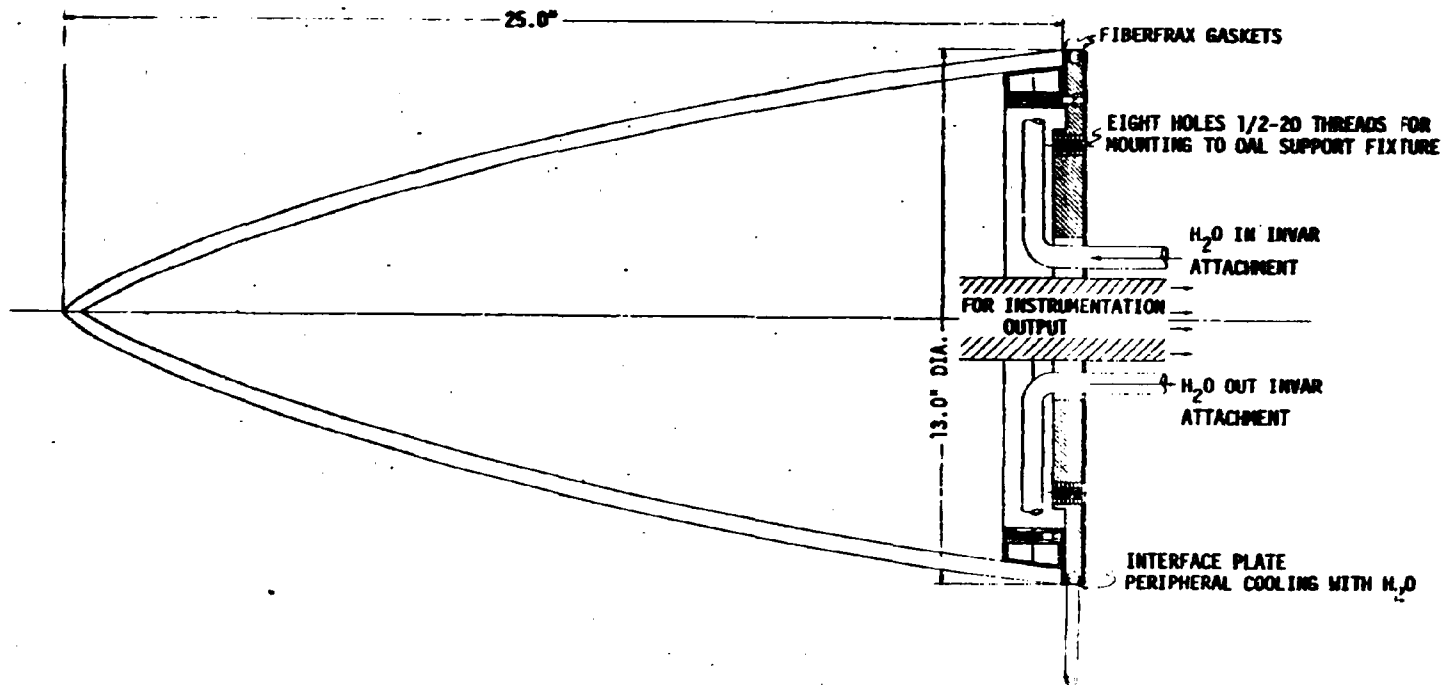


Figure 5. Drawing of SCFS OAL Test Radome - Attachment System.

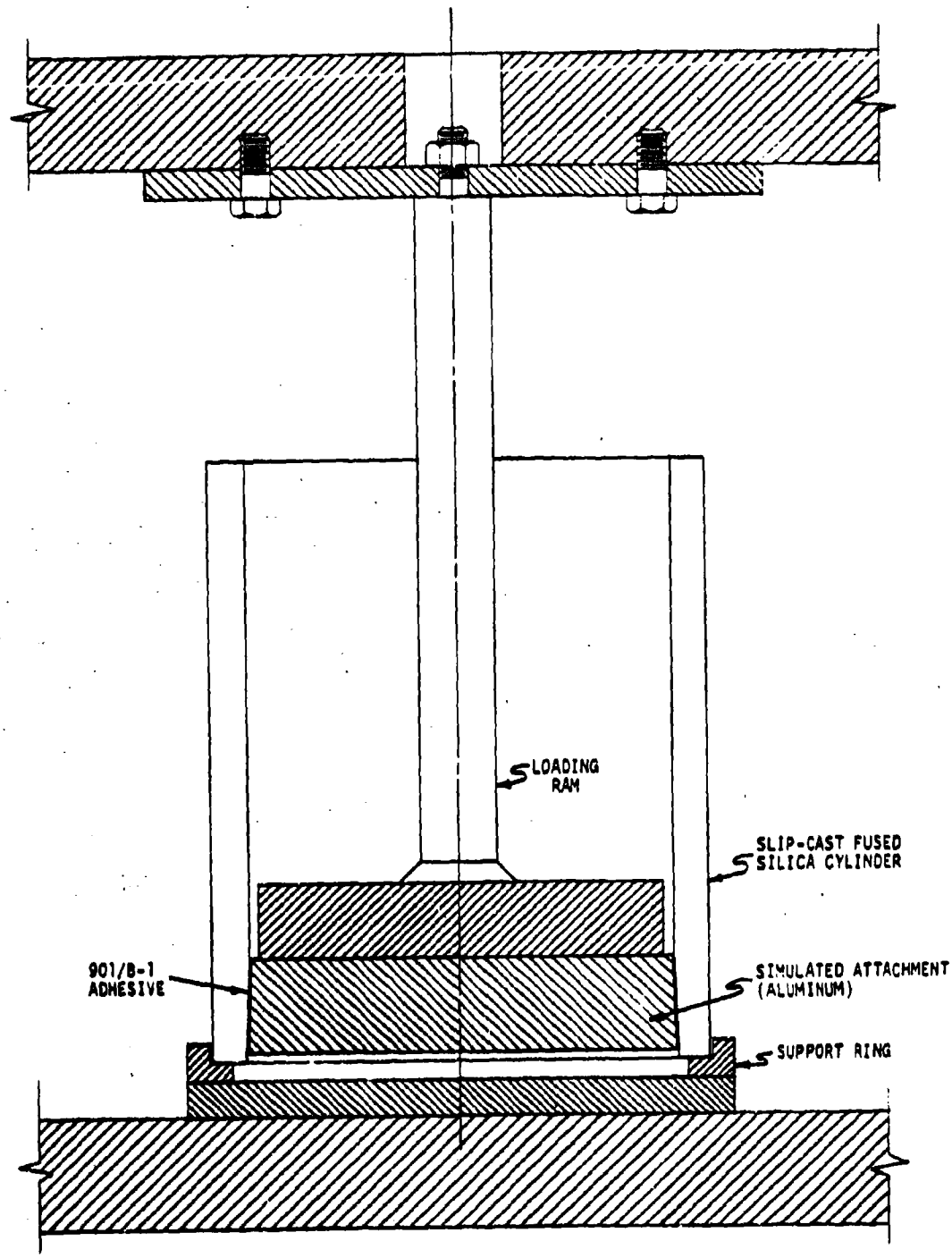


Figure 6. Drawing Illustrating Tensile Shear Strength Test of 901/B-1 Adhesive.

strength was 1794 psi. Two cylinders of SCFS were then fabricated, fitted with simulated aluminum attachment rings and failed under cantilever loading as shown in Figure 7. The failure loads, computed SCFS tensile stress failure levels, and SCFS compression stress levels at the instant of failure are presented in Table IX.

TABLE IX

FAILURE LOAD, SCFS TENSILE STRESS, AND SCFS COMPRESSIVE STRESS FOR CANTILEVER-TESTED CYLINDERS

| Cylinder No. | Failure Load[1] (lb) | Tensile Stress ($lb/in^2$) | Compressive Stress ($lb/in^2$) |
|---|---|---|---|
| 3 | 3740 | 2475 | 3320 |
| 4 | 3460 | 1550 | 2860 |

[1]Load applied 7 inches from attachment.

Note: The mechanism of failure on these specimens was not distinguishable, i.e. the origin of the failure could not be determined. It is thought that the tensile stress values are not indicative of the true strength of the material.

In an effort to assess the test environment temperature effects on the epoxy bond a simple steady state heat conduction analysis was made on the attachment system, assuming the surface was operating at 3000° F. The results indicated the epoxy would not reach a critical temperature during the CAL tests. A laboratory test was conducted with a SCFS cylinder fitted with a water cooled simulated attachment ring (Figure 8). It was planned to obtain a steady state condition in a furnace at 2700° F with the simulated water-cooled attachment system. However, the rate at which the water cooled ring removed heat by conduction through the silica and epoxy was such that the furnace could

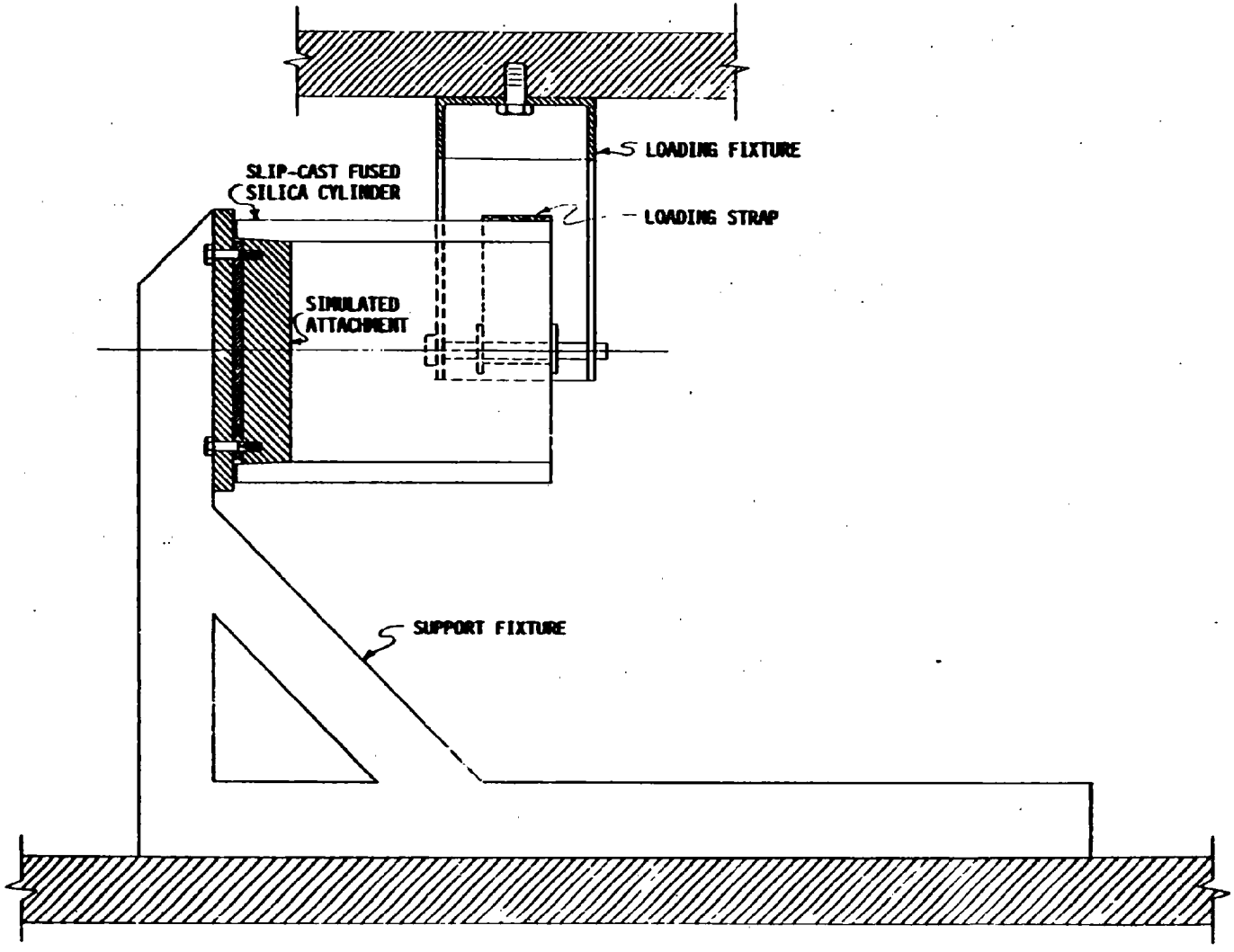


Figure 7. Drawing Illustrating Cantilever Test of SCFS Cylinders.

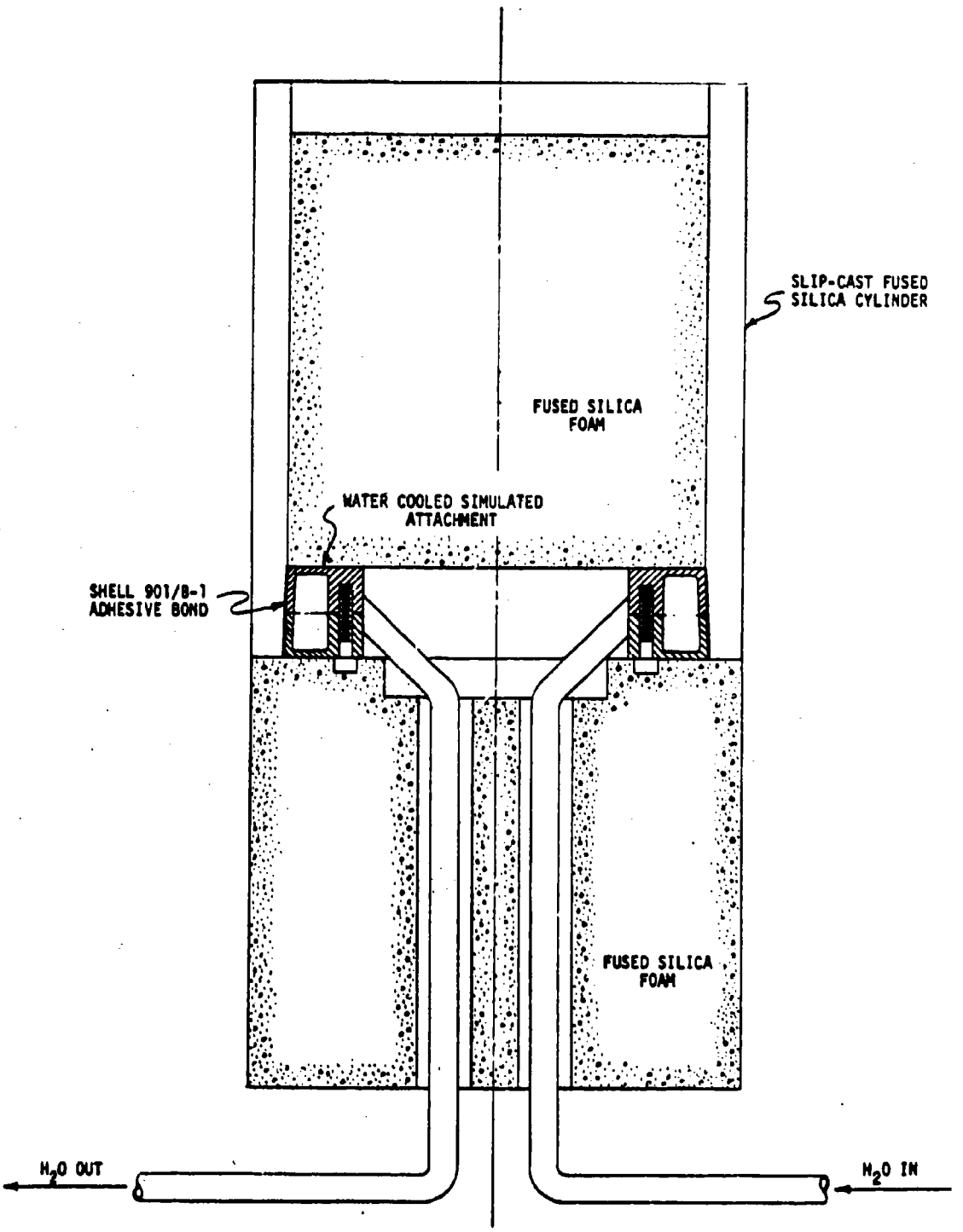


Figure 8. Drawing Illustrating Thermal Test SCFS Cylinder with Water Cooled Simulated Attachment.

not recover to 2700° F. The maximum recovery temperature obtained after 1-1/2 hours was 2330° F. The shear strength of the 901/B-1 adhesive after testing was 560 psi.

On the basis of the previous observations and the attachment system analysis in Appendix II it appeared the attachment system using the water-cooled Invar ring bonded to the SCFS radome with Shell 901/B-1 system would be satisfactory.

Initial consideration of internal pressurization as a proof test method suggested that it would suffice for the OAL test radomes. A schematic of the hydrostatic test system used for this purpose is shown in Figure 9.

An x-band test radome was fitted with an Invar ring and set up for hydrostatic testing. Computations were made to determine the required pressure level which would impart stresses predicted from the analysis of mechanical loads that the radome would experience going into the hot gas stream of the OAL Typhon combustor. The pressure level was computed to be 50 psig. The assembly was filled with water and pressurized. Catastrophic failure of the radome occurred at 35 psig. The reason for the failure at this pressure and stress level (hoop stress = 808 psi, meridional stress = 395 psi) was not obvious. However, personnel at the Applied Physics Laboratory pointed out a probable reason: a resultant bending moment at the junction of the radome and forward surface of the attachment ring 5/. It was determined that the stress (discontinuity stress) caused by this bending moment was 1534 psi, which, when superposed with the meridional stress of 395 psi gave a total stress of 1929 psi. It was still questionable that the radome would fail at this stress since the measured modulus of rupture for specimens from the 3.3-inch section was 3030 $\pm$ 170 psi. Even though the modulus of rupture determination is not

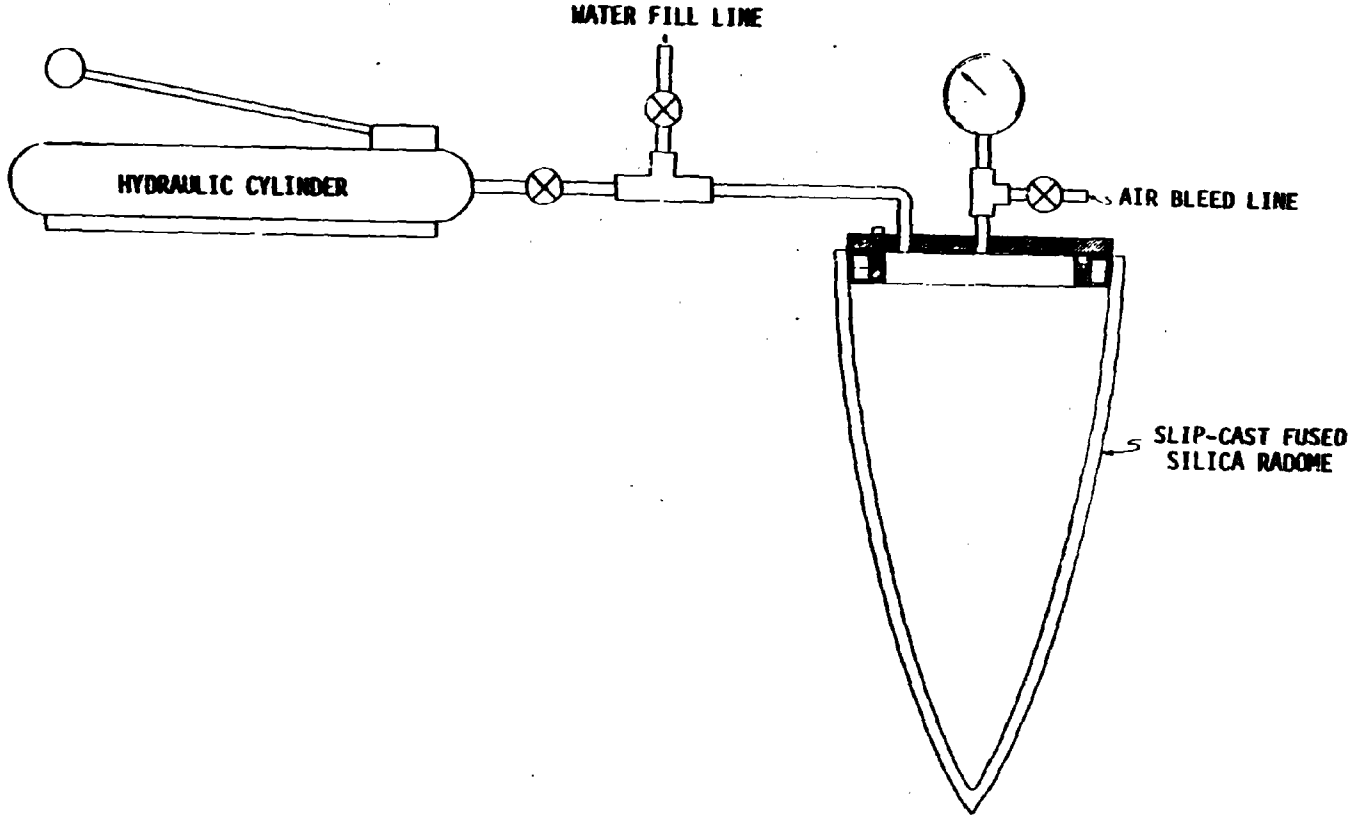


Figure 9. Schematic of Hydrostatic Test System.

considered a true representation of the tensile strength of a ceramic it was thought to be applicable to this case since the major stress developed (discontinuity stress) was a bending stress. Therefore, the effects of water saturation and notching* were determined. The observed data are presented in Table X. The effect of the 901/B-1 resin on dry specimens with and without notching was also determined. These data are also presented in Table X. It is apparent from these data, that with water saturation, coupled with the presence of a notch, failure could occur at the 1929 psi stress level. With these observations it was decided, therefore, that a cantilever proof test would be more applicable due to the significant magnitude of the discontinuity stress over the meridional stress.

TABLE X

MODULUS OF RUPTURE FOR UNNOTCHED AND NOTCHED, WATER SATURATED, DRY, AND RESIN COATED SCFS TEST SPECIMENS

| Specimen Code | Modulus of Rupture ($lb/in^2$) |
|---|---|
| Dry | 2822 ± 361* |
| Dry - Notched | 2271 ± 225 |
| Wet | 2461 ± 419 |
| Wet - Notched | 2063 ± 103 |
| Resin | 2827 ± 205 |
| Resin - Notched | 2494 ± 176 |

*95% Confidence Interval.

*Note: The notches were cut in the tensile surfaces of the MR specimens with a diamond saw, ≈ 25 mils deep by 80 mils wide.

The five test radomes fabricated for the scheduled CAL tests were fitted with water cooled Invar rings. With the exception of Radome No. 4 (c-band thickness, with $Cr_2O_3$ modified surface of forward region), each of these radomes were proof tested by loading to a bending moment of 21,100 inch-pounds. CAL test time scheduling did not permit the proof testing of Radome No. 4, and since the other four radomes survived the proof test, it was reasoned that it too would have survived. The test assembly is shown in Figure 10. These five test radomes were submitted to the Applied Physics Laboratory for installation of strain gages and thermocouples. This instrumentation is described in Appendix V.

Of major interest is the effort that was made to measure adequately the outer surface temperatures during the tests. To this end, special water cooled brightness pyrometers were fabricated at the Applied Physics Laboratory and used during the tests. These instruments operate at a wavelength of 9000 Å. Also, thermocouples were cast directly into the walls of two radomes (CAL Test numbers 6171 and 6172, Table III) with the junctions located on the outer surface. The thermocouple leads were extended circumferentially along the surface for at least 1/4-inch before passing through the radome wall to minimize conduction errors. It was hoped that these thermocouples could be used to accurately relate the true surface temperature to the apparent temperatures measured using the 9000 Å wavelength pyrometers.

The test radomes were characterized by obtaining the modulus of rupture, dynamic elastic modulus, critical strain, and cristobalite content of the excess skirt section. The measured values for these determinations are presented in Table XI. The dynamic elastic modulus values are to be used in

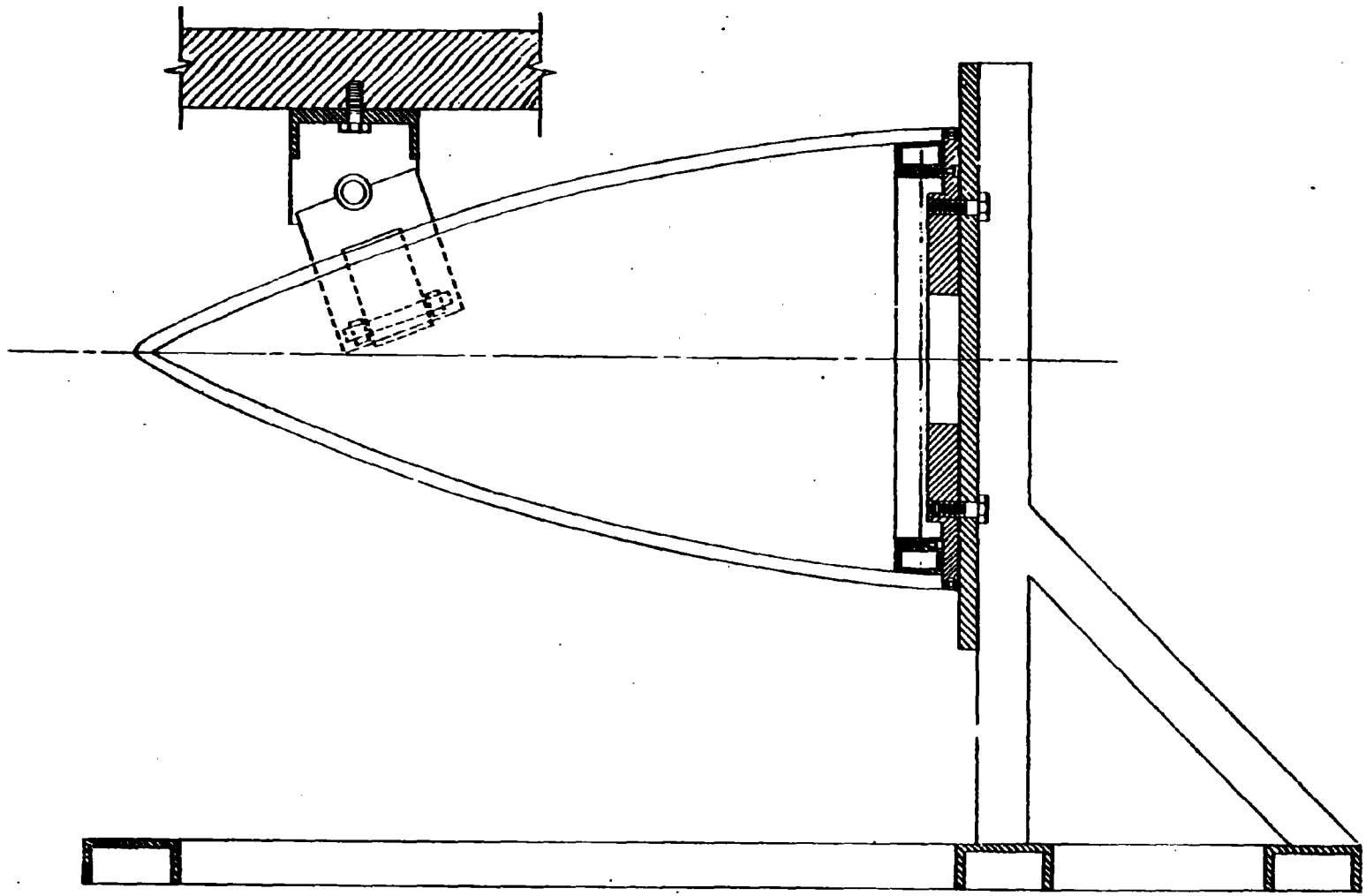

Figure 10. Drawing Illustrating Bending Test of SCFS OAL Test Radomes.

TABLE XI

MODULUS OF RUPTURE, ELASTIC MODULUS, CRITICAL STRAIN AND CRISTOBALITE CONTENT OF SPECIMENS FROM THE EXCESS SKIRT SECTIONS OF THE OAL TEST RADOMES

| Radome No. | Modulus of Rupture ($lb/in^2$) | Elastic Modulus ($10^6$ $lb/in^2$) | Critical Strain ($10^3$ in/in) | Cristobalite Content (v/o) |
|---|---|---|---|---|
| 1 | 2877 ± 169* | 3.9 ± 0.2* | 0.74 | 4.5 ± 0.5* |
| 2 | 2896 ± 350 | 3.8 ± 0.1 | 0.76 | 4.3 ± 0.6 |
| 3 | 3133 ± 201 | 3.6 ± 0.1 | 0.87 | 4.1 ± 0.5 |
| 4 | 3676 ± 349 | --- | --- | 5.6 ± 0.6 |
| 5 | 2623 ± 190 | 4.0 ± 0.1 | 0.66 | 3.5 ± 0.3 |

*95% Confidence Interval.

the APL analytical program to predict the thermal stresses that each radome experienced during testing for comparison with the measured stresses.

The particle size distributions of the three batches of fused silica slip designated OAL-1, -2, and -3 and used to fabricate OAL test radomes were measured using a Coulter Counter®. The results are presented in Figures 11, 12, and 13.

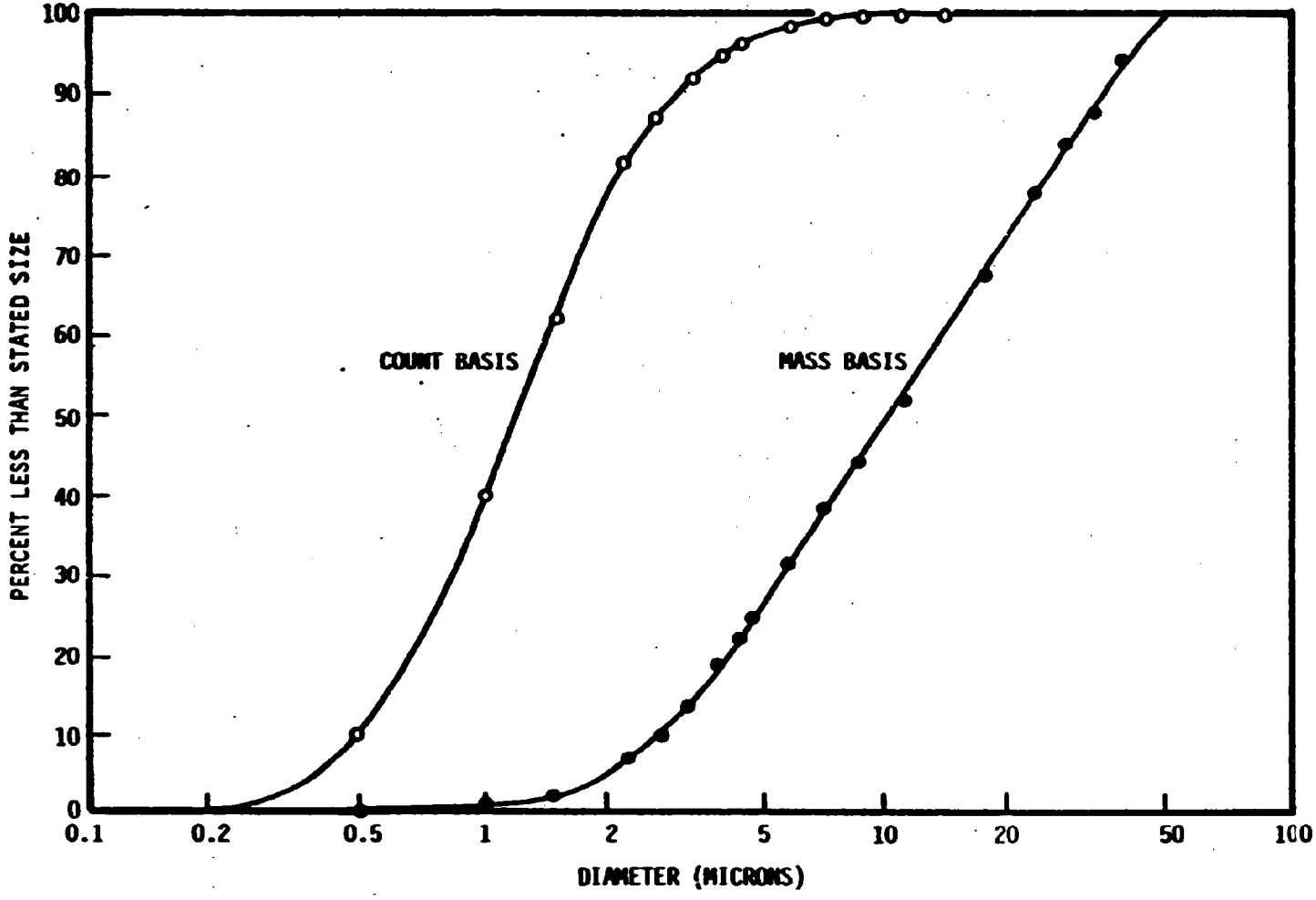


**Figure 11.** Count and Mass Basis Distributions of Particle Sizes in Fused Silica Slip Batch OAL-1.

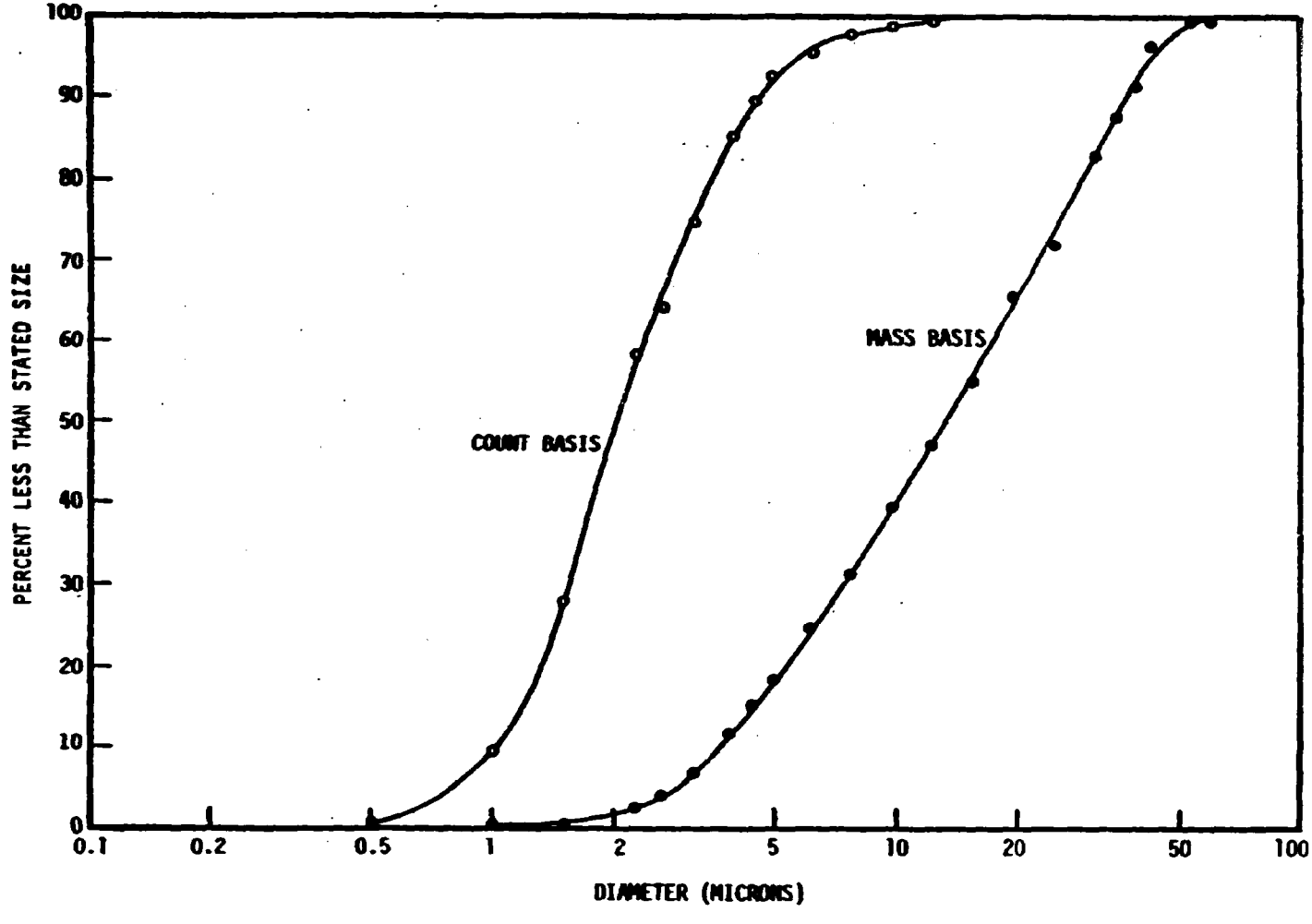


Figure 12. Count and Mass Basis Distributions of Particle Sizes in Fused Silica Slip Batch OAL-2.

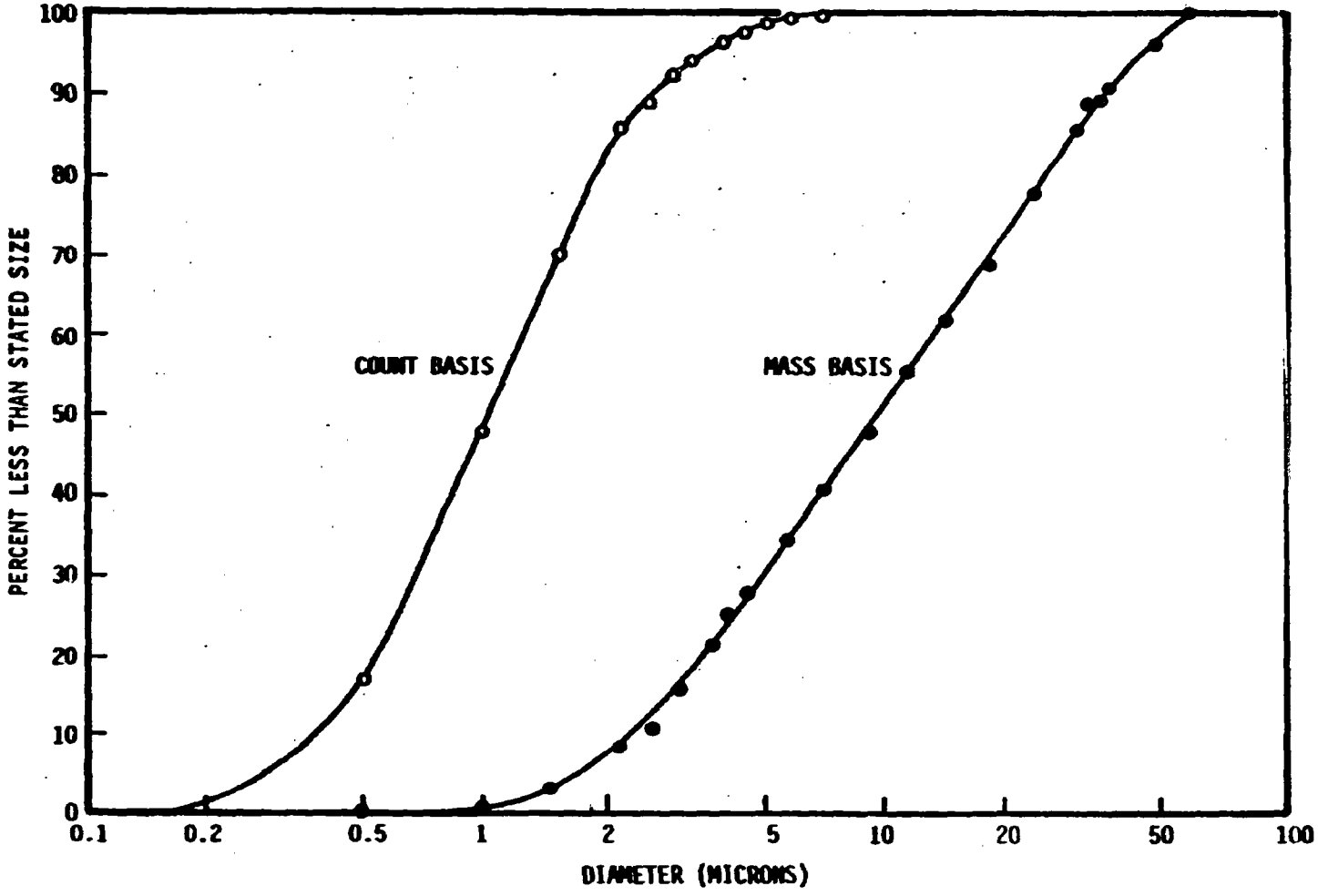


Figure 13. Count and Mass Basis Distributions of Particle Sizes in Fused Silica Slip Batch OAL-3.

B. Materials Development and Characterization

1. Slip-Cast Alumina-Fused Silica Composites

That alumina can be slip-cast, has been recognized for some time 6,7/. An examination of the conditions necessary for slip-casting alumina has shown that these are quite similar to those for slip-casting fused silica. That is, the particle size distributions are quite similar and the alumina slip can be deflocculated under acidic conditions. Also, previous work on the firing of slip-cast alumina bodies, performed at Georgia Tech 8/, indicated that sintering can be obtained at similar temperatures, and that the volumetric shrinkage obtained for the alumina bodies is quite close to that obtained with slip-cast fused silica. However, the modulus of rupture of sintered alumina bodies was substantially higher than slip-cast fused silica: the order of 15,000 psi. Therefore, consideration was given to the possibility of slip-casting composites structures consisting of discrete particles of alumina and discrete particles of fused silica. The potential of such composites is very attractive, i.e. such composites should have thermal shock resistance similar to, and strengths substantially superior to, that of slip-cast fused silica. Composite structures tailored with certain desired physical properties (e.g. dielectric constant) could be possibly obtained by grading the relative concentrations of alumina and fused silica either axially or radially through a structure. This gradation could be accomplished by progressive replacement of the slips during casting.

Because of the apparent feasibility and attractive potential of slip-cast fused silica-alumina composites, an investigation was begun to develop and examine such composites. The initial phase of this investigation has been

concerned with the development and complete characterization of a suitable alumina slip. Previous investigators prepared slips using commercial alumina which contained from 0.3 to 0.4 weight per cent of $Na_2O$. Their investigations indicated that the presence of the sodium is principally responsible for the deterioration of alumina slips on aging 9/. That is, the pH of the slip changes drastically with time and with this change the system usually becomes flocculated. Also, from the standpoint of ultimately mixing the alumina slip with a slip of fused silica, it is desirable to hold the sodium level as low as possible. Sodium has a drastic effect on the devitrification rate of fused silica and can seriously degrade the properties of sintered fused silica through the development of excessive amounts of cristobalite. For the above reasons a high-purity, commercial alumina, containing less than 0.03 weight per cent $Na_2O$, was selected for this investigation. This high-purity, tabular alumina was obtained as a sized fraction passing a 325-mesh screen. The particle size distribution of the material was subsequently determined using a Coulter Counter®. The distribution is presented in Figure 14.

The effect of solids concentration on the rheological properties of alumina slips was examined initially, by preparing slips with alumina concentrations of 70, 75, 80, 82, and 85 weight per cent (w/o). These slips were prepared by grinding 2000 grams of the alumina with HCl and the required amount of water. These slips were milled for 17 hours in 1 gallon jar mills containing 3750 grams of 3/4-inch diameter grinding cylinders. The flow properties of these slips were determined. The data are contained in Table XII. Particle size determinations were made for the 70 w/o and 82 w/o slips. These analyses were made using a Coulter Counter® and the data are presented in Figure 15.

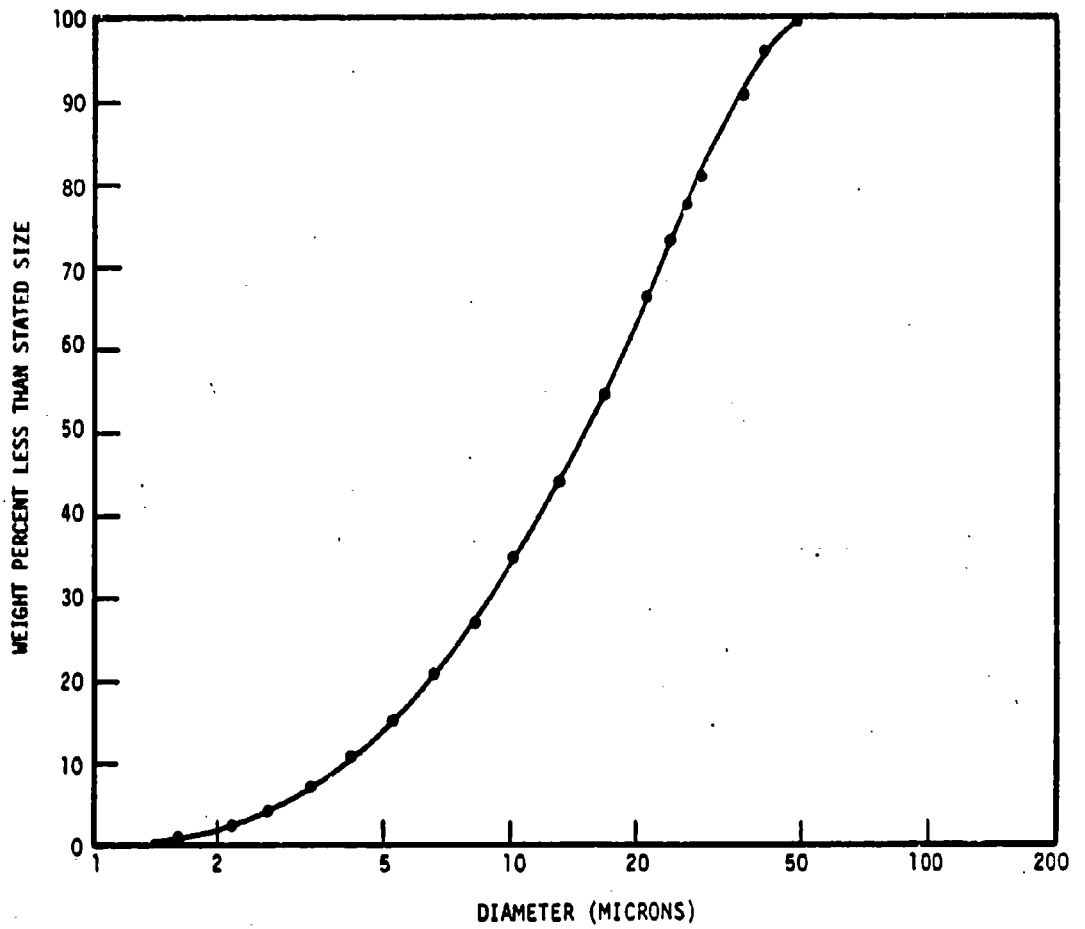


Figure 14. Distribution of Particle Sizes for -325 Mesh High-Purity, Tabular Alumina.

TABLE XII

APPARENT VISCOSITIES OF ALUMINA SLIPS WITH VARIOUS SOLIDS CONCENTRATIONS

| Alumina Content (w/o) | pH | Apparent Viscosity[1] (centipoise) |
|---|---|---|
| 70 | 4.60 | 20 |
| 75 | 4.60 | 30 |
| 80 | 4.70 | 196 |
| 82 | 3.90 | 260 |
| 85 | 4.10 | 2000 |

[1]Determined with a Brookfield Viscosimeter, Model LVF using a number 3 spindle at 30 rpm.

The effect of grinding time on the properties of an alumina slip were investigated by preparing four different slips, all at concentrations of 82 w/o alumina. These slips were prepared from 2000 grams of alumina, 428 ml of water and 11 ml of 5.0 N HCl. These slips were milled in 1 gallon jar mills with 3750 gm of 3/4-inch diameter grinding cylinders for 24, 48, 72, and 96 hours respectively. The slips were adjusted to a pH of 4.0 and examined for apparent viscosity and settling behavior. The viscosity data are presented in Table XIII. The settling behavior of the slips was examined by filling a 2.5-cm I.D. glass tube, that was closed at one end, to a depth of 50 cm with slip and measuring the sediment height, and depth of clear liquid at the top of the column, as a function of time. Similar measurements were made with a slip of fused silica that exhibited satisfactory casting behavior. The alumina slip that had been milled for only 24 hours had a settling rate greater than the

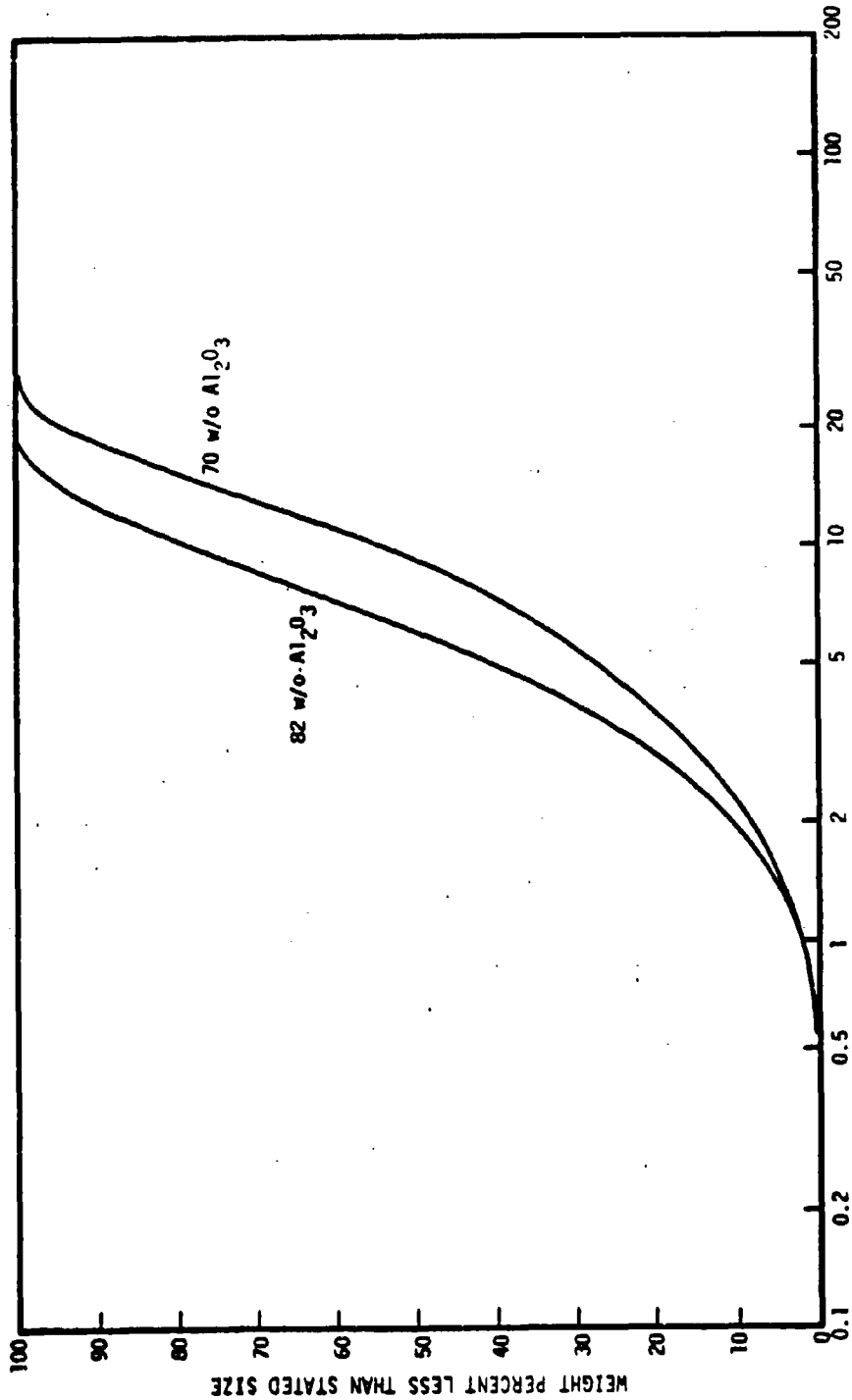


Figure 15. Distribution of Particle Sizes for Alumina Slips After 18 Hours of Milling.

TABLE XIII

APPARENT VISCOSITIES OF ALUMINA SLIPS SUBJECTED TO VARIOUS GRINDING TIMES

| Alumina Content (w/o) | Grinding Time (hr) | pH | Apparent Viscosity[1] (centipoise) |
|---|---|---|---|
| 82 | 24 | 4.0 | 340 |
| 82 | 48 | 4.0 | 540 |
| 82 | 72 | 4.0 | 1000 |
| 82 | 96 | 4.0 | 980 |

[1] Determined with a Brookfield Viscosimeter, Model LVF using a number 3 spindle at 30 rpm.

silica slip. The alumina slip that had been milled for 48 hours had a settling rate that was approximately the same as the silica slip. The settling rates for the alumina slips that had been milled for 72 and 96 hours and settling rates approximately one-half and one-third that of the silica slip, respectively.

In the course of the investigations on alumina slips it was noted that the pH of the slips did not change very significantly with a rather large change in the amount of acid added, when the pH was in the neighborhood of 4. Therefore, the relationship between the acid concentration and the pH of alumina slips was examined. Progressive amounts of HCl were added to alumina slips containing a known amount of alumina and having a solids concentration of 82 w/o. The slips were allowed to equilibrate after each addition of acid, by rolling for 24 hours in suitable containers and without grinding media. After equilibration the pH was determined with a pH meter. These data are presented in Figure 16.

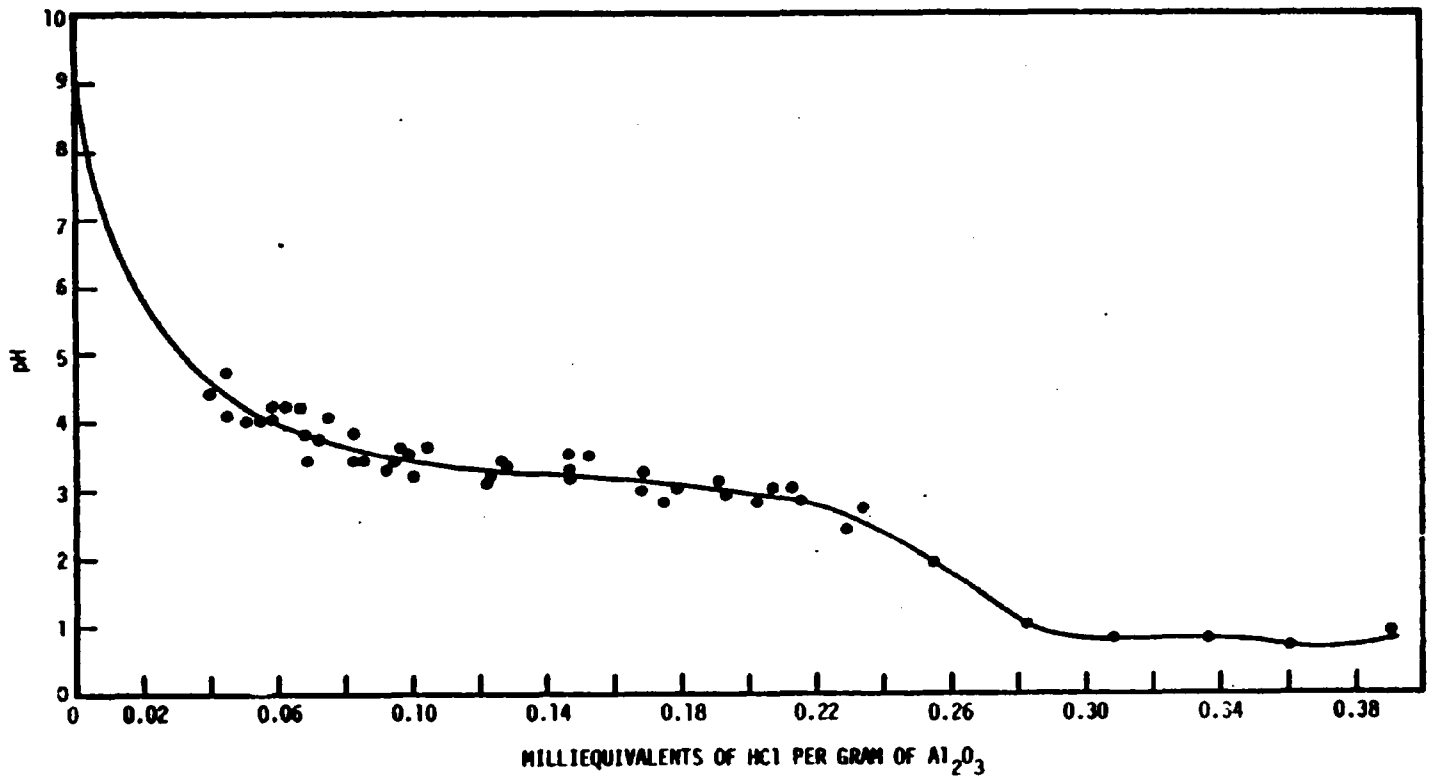


Figure 16. pH as a Function of Acid Concentration for Slips Containing 82 w/o Alumina.

Since the pH of the alumina slips was found to be rather insensitive to the amount of acid addition in the range of a pH of 4 to a pH of 3 (Figure 16), the apparent viscosity as a function of the amount of acid addition was determined for a number of alumina slips. The same slips used in the determination of pH as a function of acid addition were used in these studies, and again the viscosity determinations were made only after a 24 hour equilibration period following the acid additions. The apparent viscosities were determined using a Brookfield Model LVF viscosimeter. The data obtained with a number 3 spindle are presented in Figure 17.

On the basis of the preceding data, the properties of an alumina slip containing about 82 w/o solids, prepared by milling for 48 hours and having an acid concentration of about 0.05 milliequivalents per gram of alumina, appeared to be satisfactory for slip-casting. Therefore, approximately 4 gallons of such a slip were prepared. This slip was prepared in batches by milling 2000 gm of alumina with 419 ml of $H_2O$ and 10 ml of 5.0 N HCl in 1 gallon jar mills with 3750 gm of 3/4-inch diameter grinding media. After milling an additional 10 ml of 5.0 N HCl was added to bring the acid concentration to the desired level of 0.05 milliequivalents per gram of alumina. Approximately 16 such batches were prepared and blended to produce the desired 4 gallons of slip. A sample of the blended slips was taken for particle size analysis. The distribution of particle sizes is presented in Figure 18.

Other investigators [9,10] have reported significant changes in the properties of alumina slips on aging. Therefore, a sample of the slip prepared here was examined for changes in pH and apparent viscosity with time. It was found that these properties changed significantly with time during the first 24 hours following any addition of acid to a slip. However, after this initial

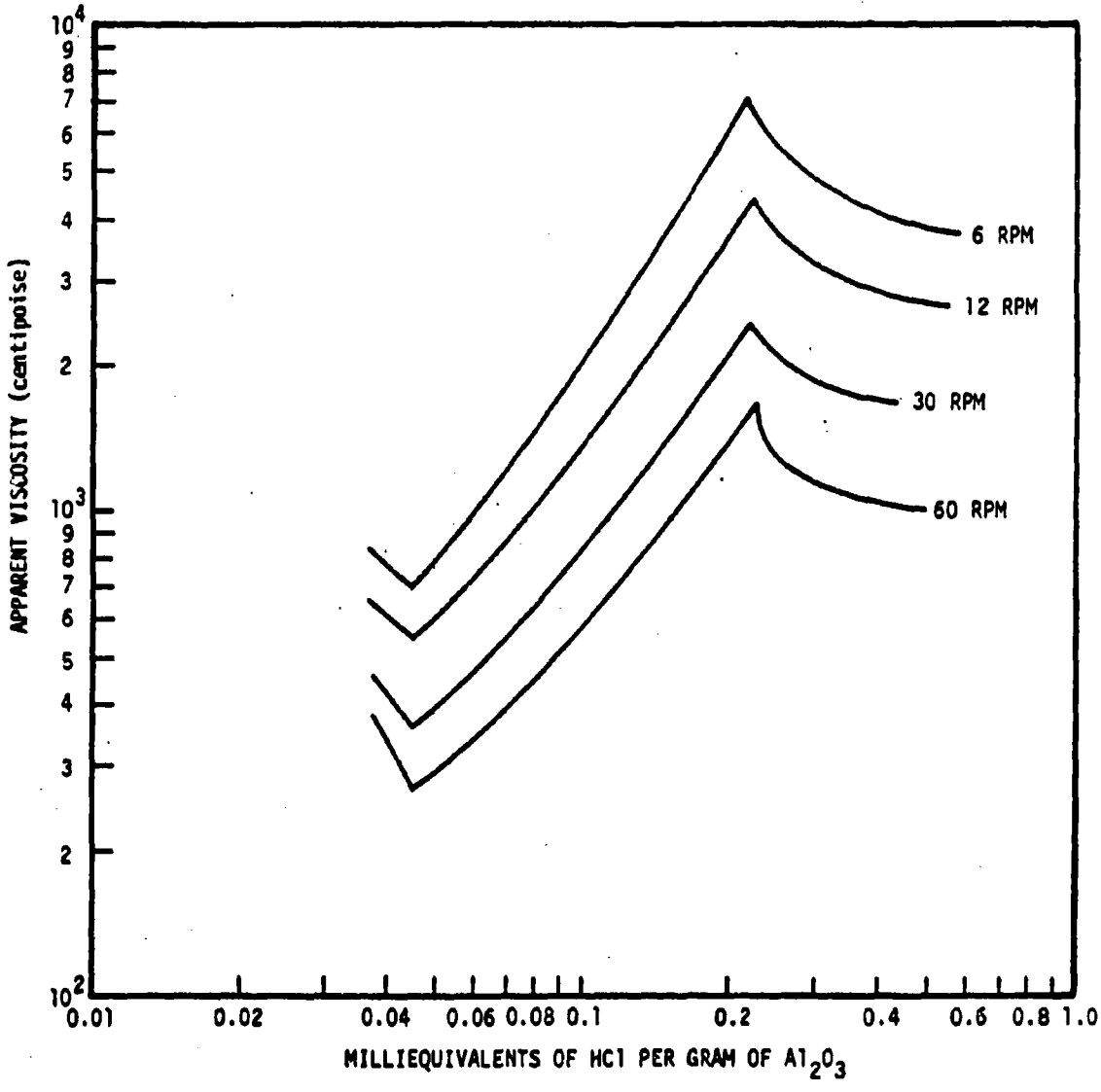


Figure 17. Apparent Viscosity as a Function of Acid Content for a Slip Containing 82 w/o Alumina.

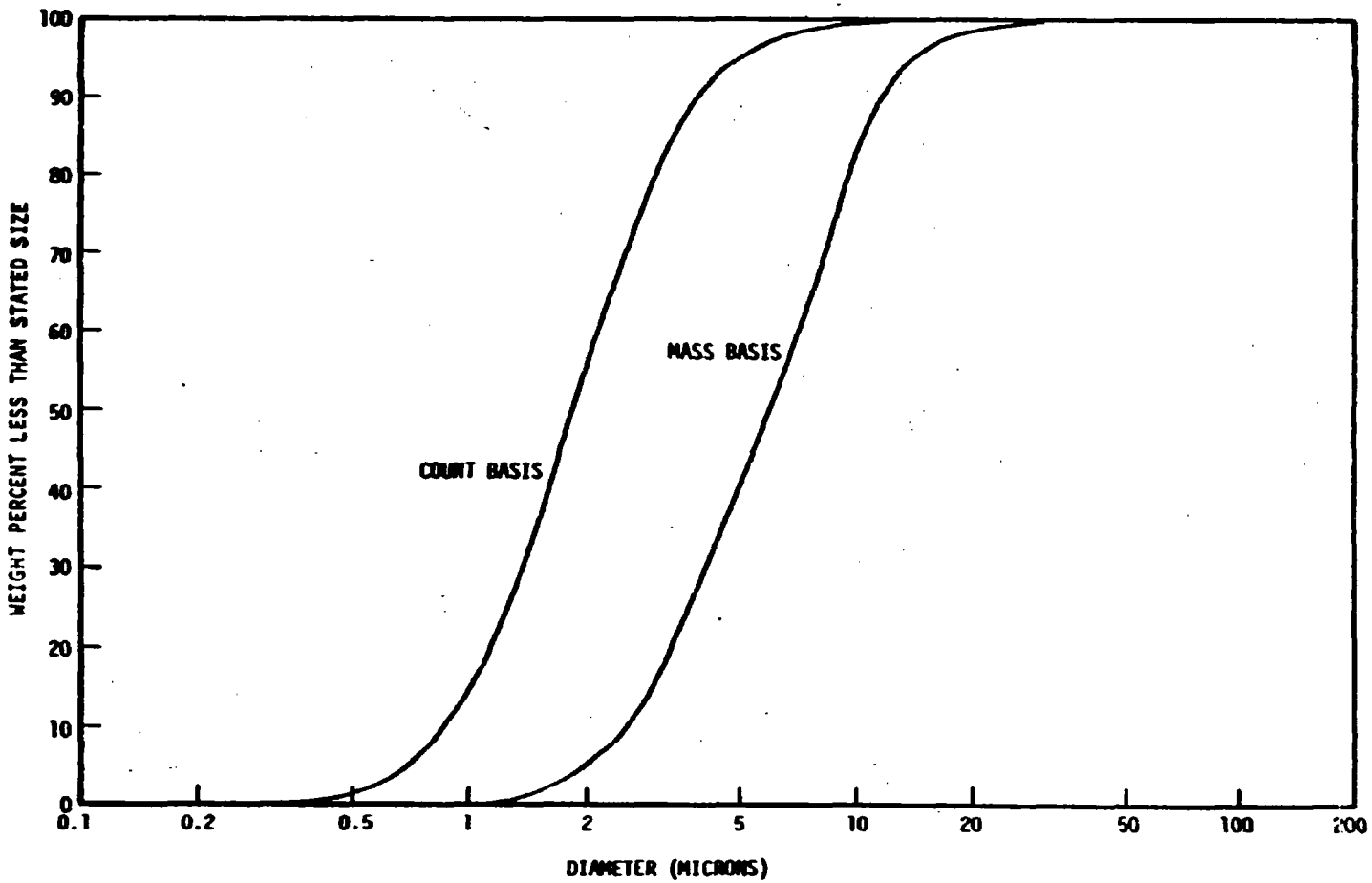


Figure 18. Distribution of Particle Sizes for the Alumina Slip.

period these properties did not change significantly with time. The slip still retained satisfactory flow properties after an aging time of at least 3 weeks. These data are presented in Figure 19.

Samples of the 82 w/o alumina slip were mixed with fused silica slips in ratios of 1:3, 1:1, and 3:1. The slips mixed satisfactorily with no visual evidence of flocculation. Data on the pH and apparent viscosities of the mixed slips, along with similar data for the fused silica and alumina slips, are presented in Table XIV. Sample bars cast from the mixed slips indicated satisfactory casting behavior for these slips.

TABLE XIV

PROPERTIES OF ALUMINA-FUSED SILICA SLIPS

| Weight Ratio of Alumina to Fused Silica | Solids Content of Slip (w/o) | pH | Apparent Viscosity[1] (centipoise) |
|---|---|---|---|
| 1:0 | 82 | 4.3 | 830 |
| 3:1 | 82 | 4.3 | 440 |
| 1:1 | 82 | 4.1 | 290 |
| 1:3 | 82 | 3.9 | 200 |
| 0:1 | 82 | 5.0 | 110 |

[1]Determined with a Brookfield Viscosimeter, Model LVF using a number 3 spindle at 30 rpm.

Cylindrical specimens, 3/4-inch in diameter and 5 inches in length, were slip-cast with slips containing alumina to fused silica weight ratios of 1:3, 1:1, and 3:1. Studies were then conducted to determine the optimum sintering

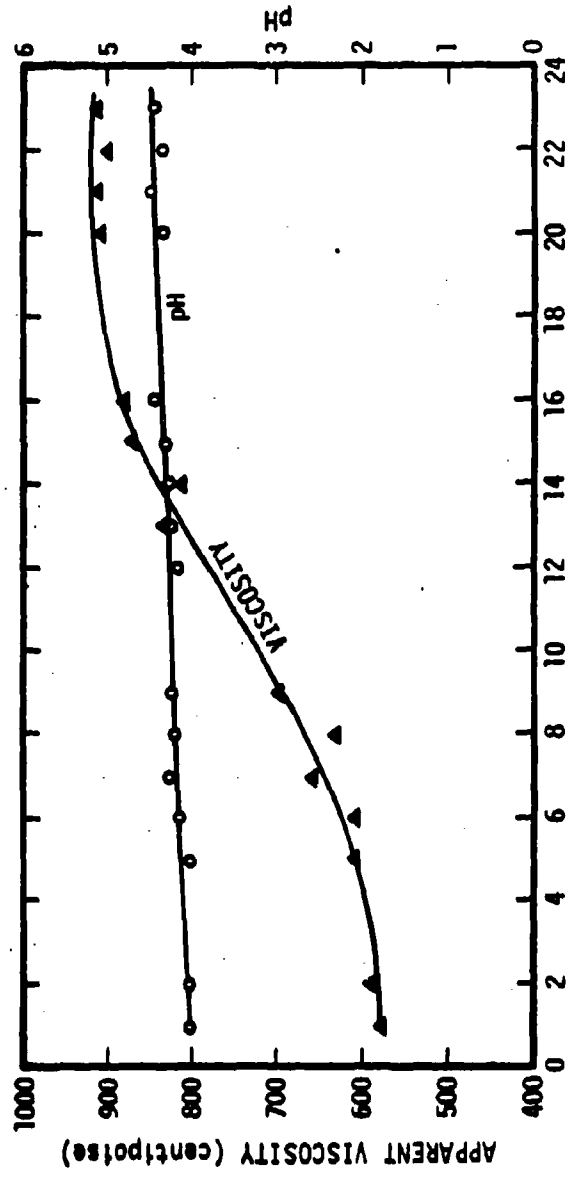


Figure 19. Change in Viscosity and pH with Time for 82 w/o Alumina Slip.

conditions for these composites. It has been previously determined [11] that during the sintering of slip-cast fused silica a point is reached where the deleterious effect of microcracking due to devitrification overcomes the effect of increased densification. When this point is reached the strength and elastic modulus decrease with increased sintering time. Recognizing that such an effect may also be found in the composites containing fused silica, studies of the rate of fused silica devitrification and the effect of this devitrification on the elastic modulus were conducted.

Identical sets of composite bars, composed of alumina to fused silica ratios of 3:1, 1:1, 1:3, and 0:1, were sintered progressively at 2200° F in an electric kiln. The bars were sintered for a specific time interval, removed from the furnace hot, and allowed to air cool. A portion of each bar from one set was taken for cristobalite determinations, and measurements of porosity and dynamic elastic modulus were made on the other set. All the bars were then replaced in the kiln, sintered further for a specific time interval, removed and air cooled, and additional measurements made of cristobalite content, elastic modulus and porosity. This procedure was repeated until a total sintering time of 510 minutes had been reached. The results of the total amount of devitrification as a function of time are presented in Figure 20 and the variation in elastic modulus with porosity and amount of devitrification are presented in Figures 21 through 24.

Approximately 25 specimens, 3/4-inch diameter, 5 inches long, of each of the three alumina-fused silica combinations, the 100 per cent alumina, and the 100 per cent fused silica were slip-cast. These specimens were all sintered simultaneously at 2200° F for a time sufficient to develop the maximum elastic

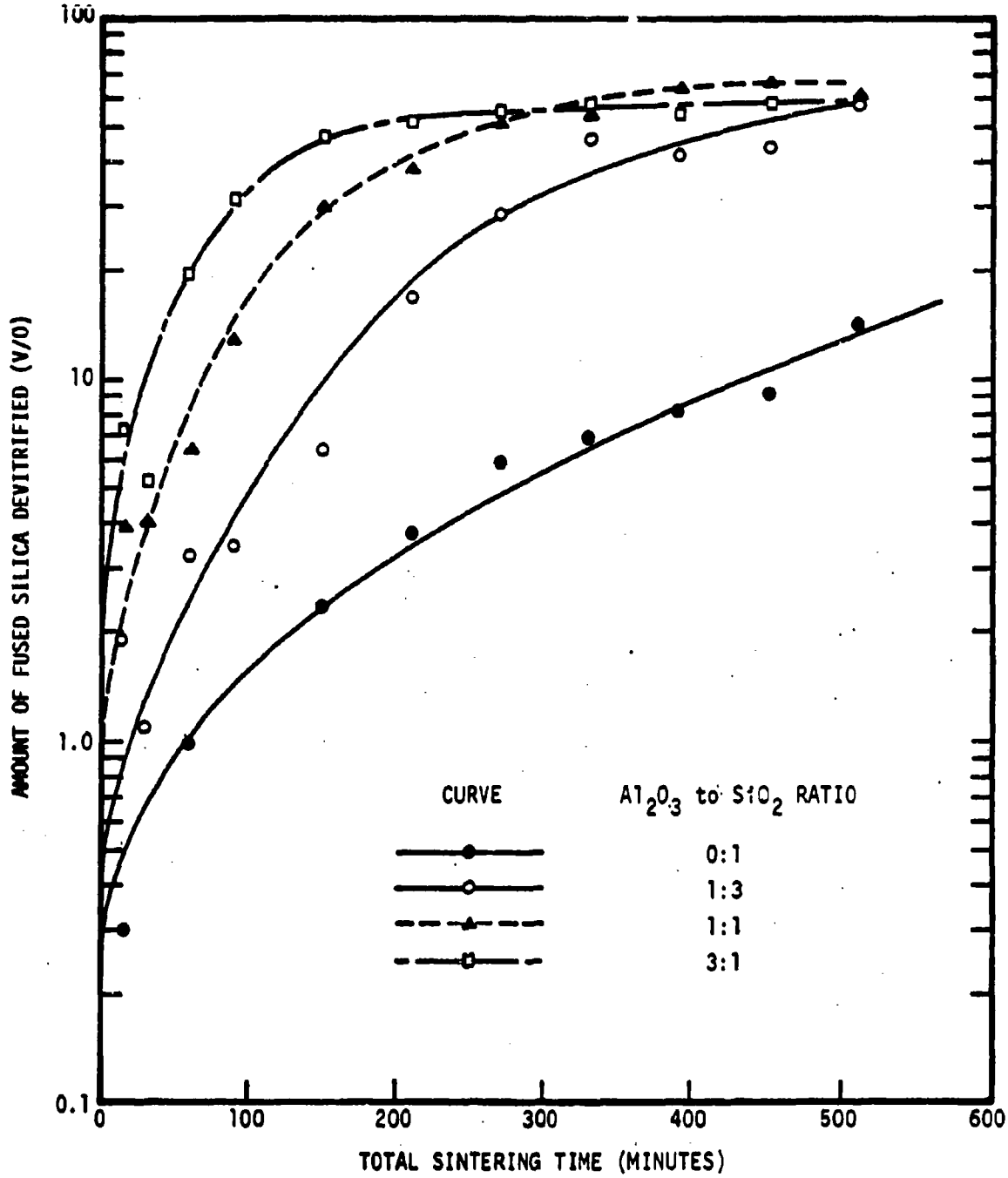


Figure 20. Per Cent of Total Fused Silica Devitrified as a Function of Total Time at 2200° F.

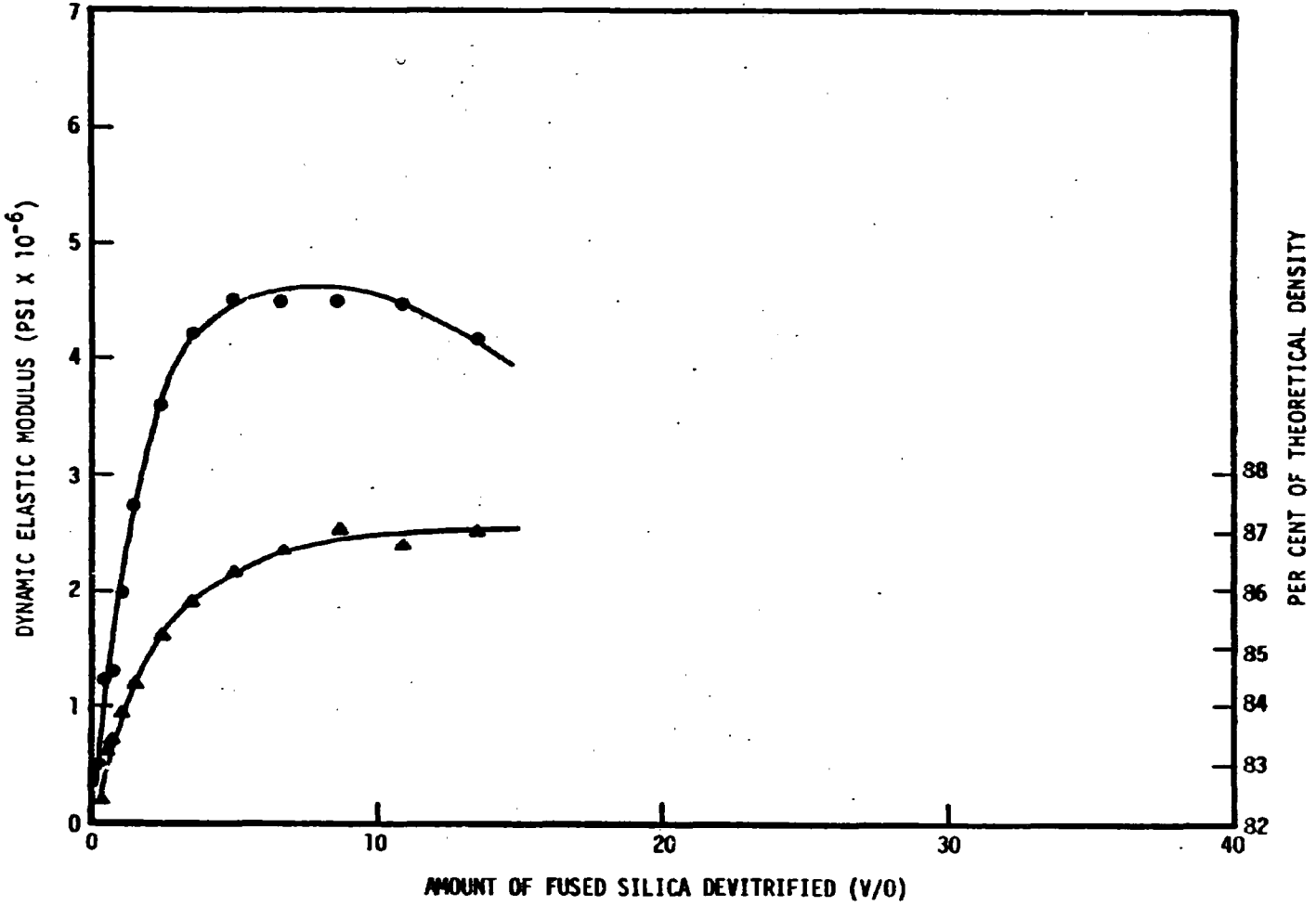


Figure 21. Dynamic Elastic Modulus of Slip-Cast Fused Silica as a Function of Density and Amount of Devitrification.

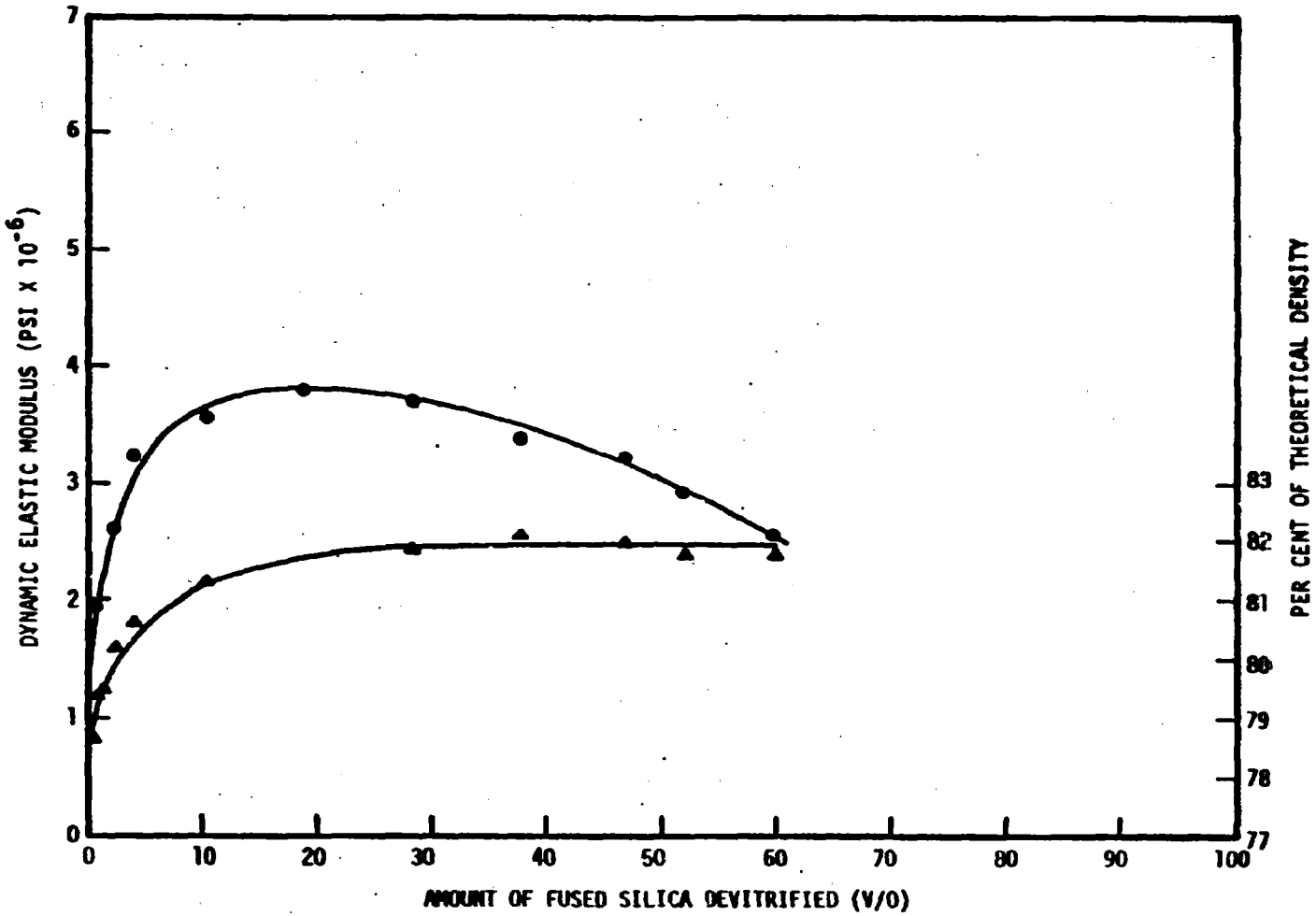


Figure 22. Dynamic Elastic Modulus of 1:3 Alumina-Fused Silica Composite as a Function of Density and Amount of Fused Silica Devitrified.

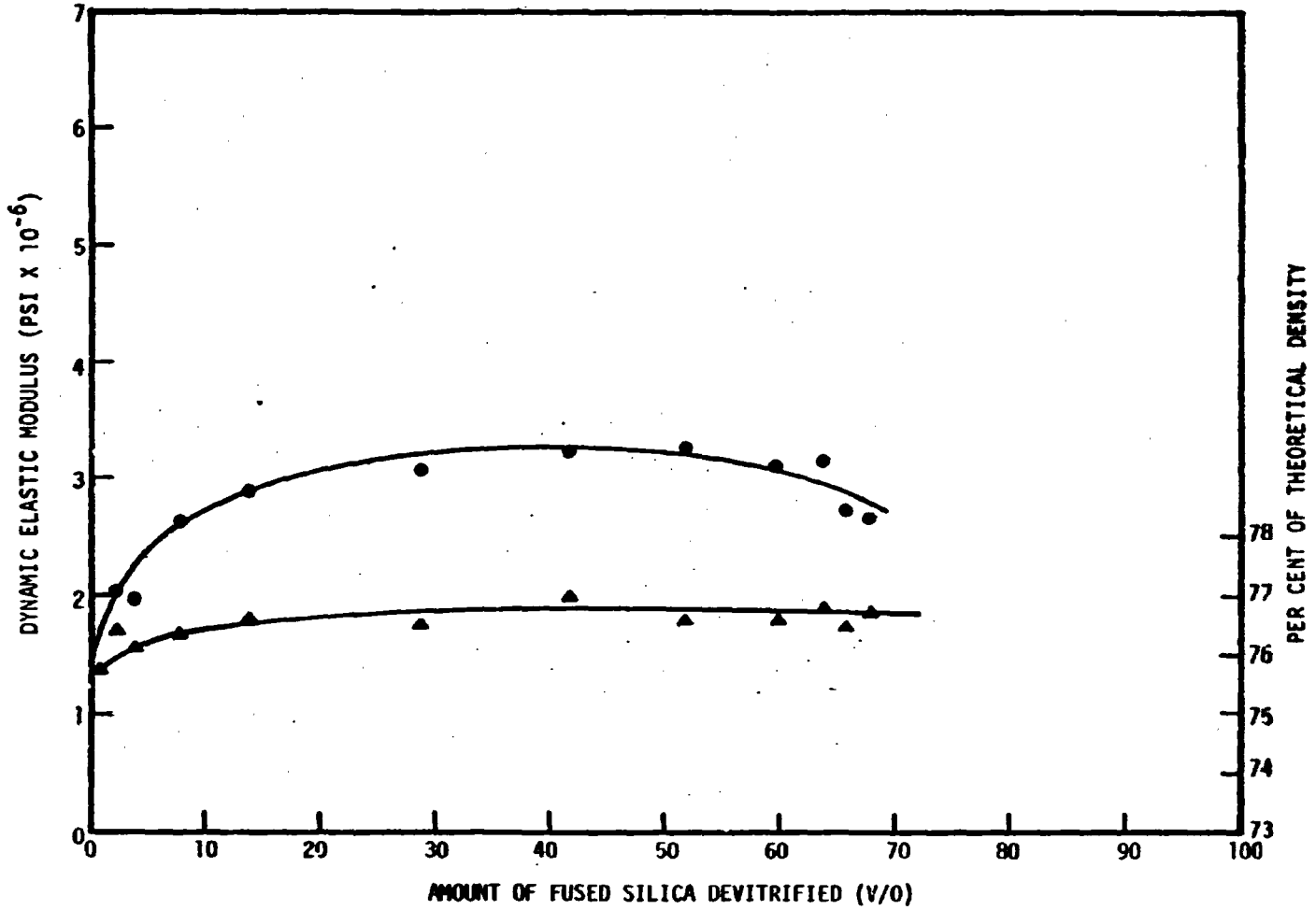


Figure 23. Dynamic Elastic Modulus of 1:1 Alumina-Fused Silica Composite as a Function of Density and Amount of Fused Silica Devitrified.

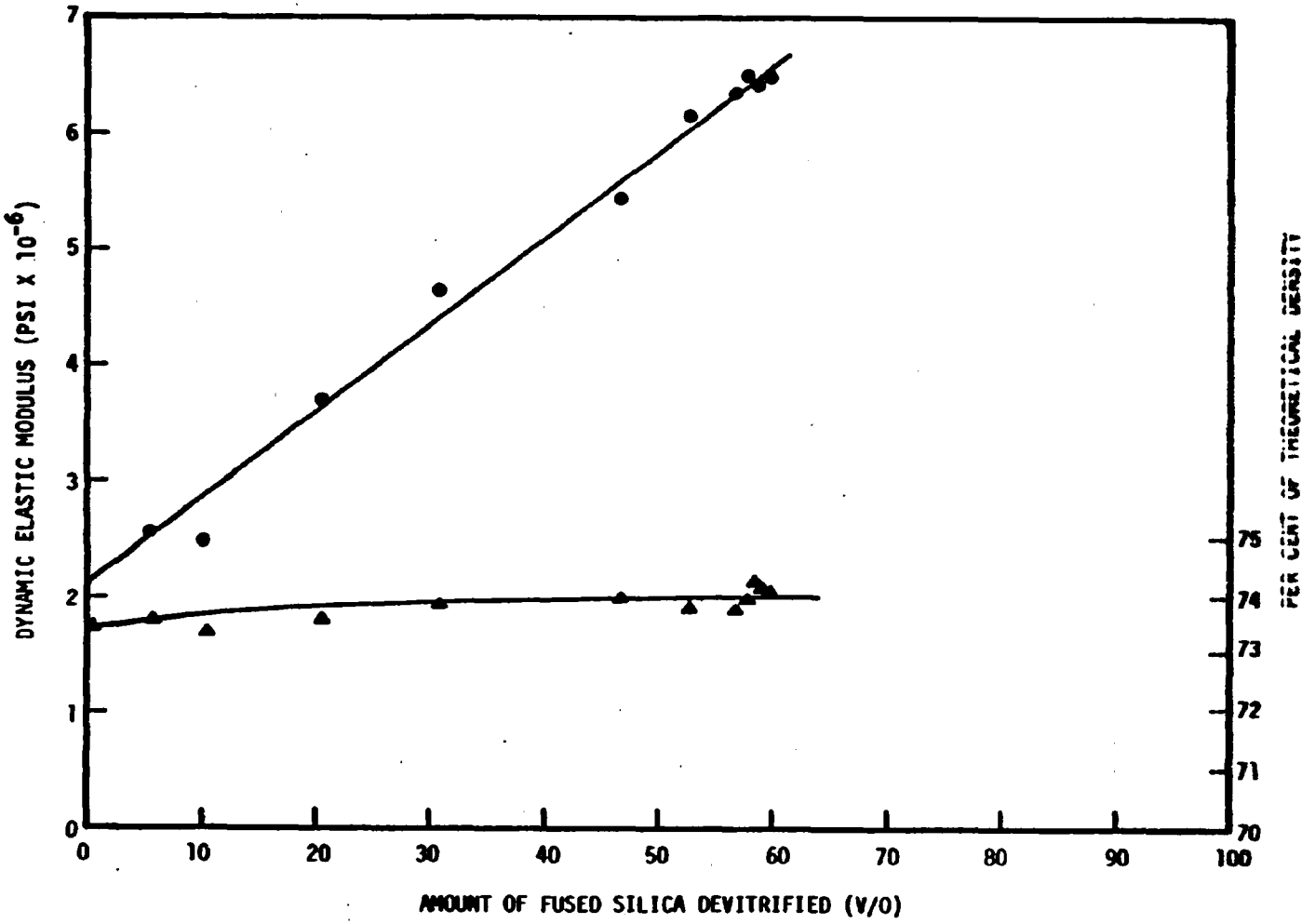


Figure 24. Dynamic Elastic Modulus of 3:1 Alumina-Fused Silica Composite as a Function of Density and Amount of Fused Silica Devitrified.

modulus in the 100 per cent fused silica specimens (see Figures 20 and 21). The specimens were slow-cooled in the furnace to prevent thermal shock of the 100 per cent alumina. Determinations of the cristobalite content, porosity, dynamic elastic modulus by sonic resonance 12/, and modulus of rupture in quarter point loading were made on each set of specimens. These data are presented in Table XV and Figures 25 and 26.

TABLE XV

PROPERTIES OF SLIP-CAST ALUMINA-FUSED SILICA COMPOSITES

| Weight Ratio of Alumina to Fused Silica | Modulus of Rupture ($lb/in^2$) | Elastic Modulus ($10^6$ $lb/in^2$) | Porosity (v/o) | Per Cent of Fused Silica Devitrified (v/o) |
|---|---|---|---|---|
| 0:1 | 4056 ± 414 | 4.58 ± 0.05 | 12.44 ± 0.47 | 8.4 ± 0.8 |
| 1:3 | 1355 ± 319 | 2.36 ± 0.18 | 21.41 ± 0.38 | 40.5 ± 1.1 |
| 1:1 | 3076 ± 108 | 3.69 ± 0.05 | 24.49 ± 0.40 | 42.1 ± 1.0 |
| 3:1 | 7511 ± 701 | 8.94 ± 0.11 | 27.04 ± 0.43 | 39.8 ± 1.4 |
| 1:0 | 8122 ± 413 | 10.6 ± 0.06 | 31.31 ± 0.17 | --- |

Confidence intervals are at 95 per cent level.

## 2. Fused Silica Grinding

Indications from present experimental work at Georgia Tech are that the full strength potential of slip-cast fused silica is not being realized*.

*Comparison of strength measurements and particle distributions from concurrent research programs at the Engineering Experiment Station of the Georgia Institute of Technology under Contracts DA-01-021-AMC-14464(Z) and AF 33(615)-3445 with results under this program.

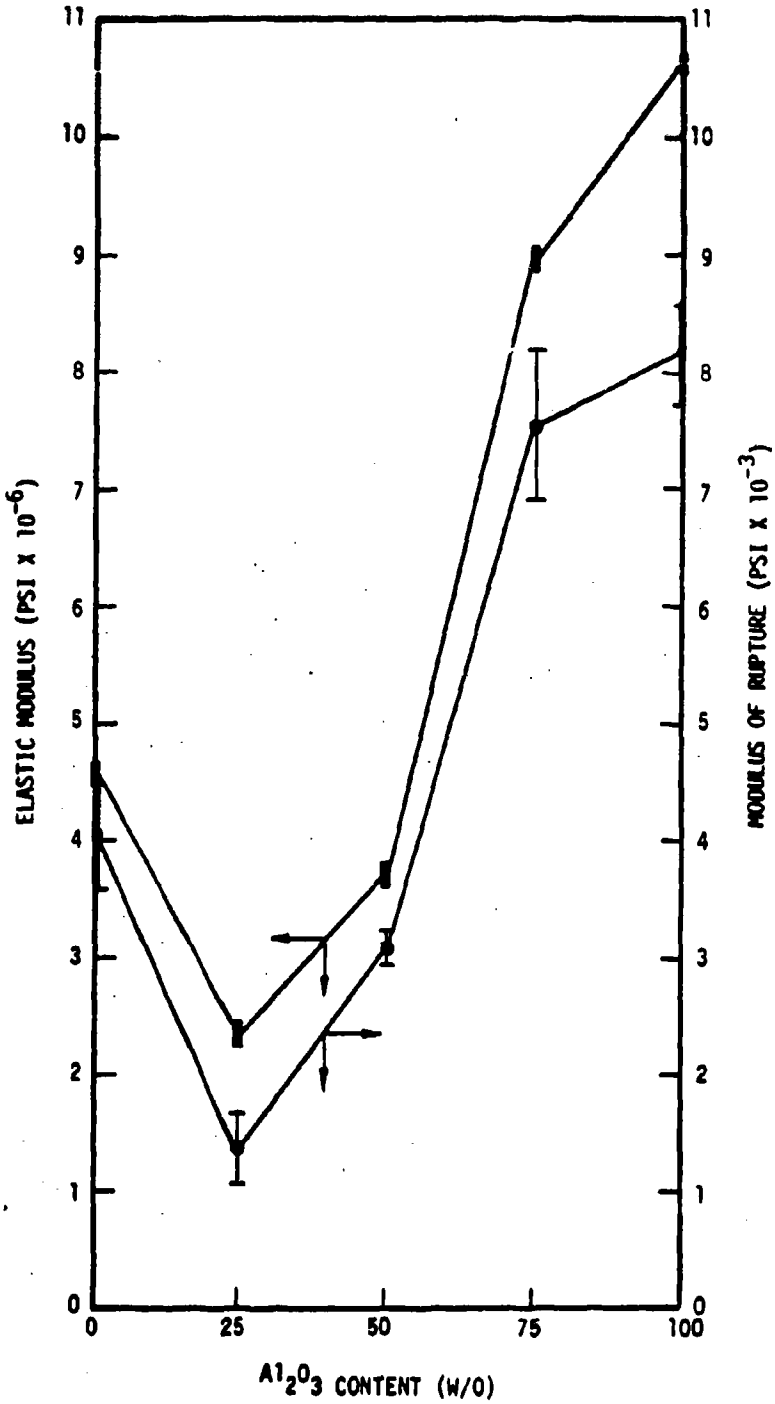


Figure 25. Variation of Modulus of Rupture and Dynamic Elastic Modulus with Alumina Content for Slip-Cast Alumina-Fused Silica Composites.

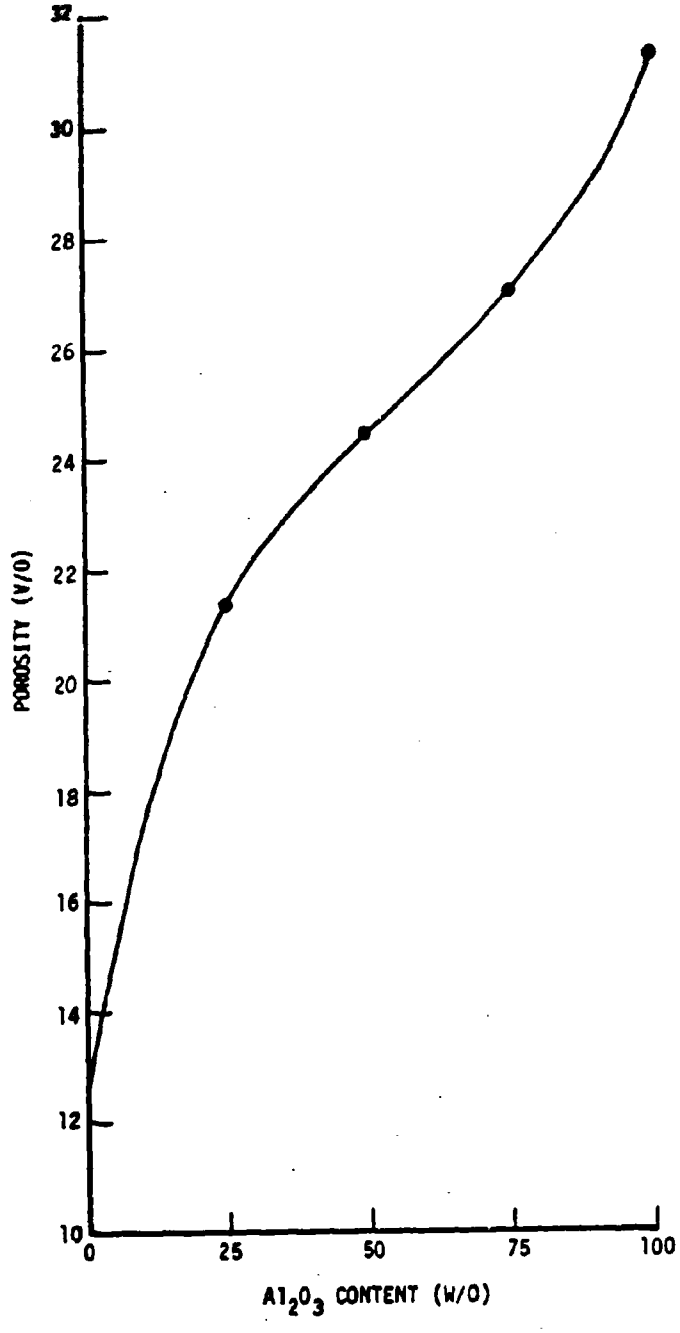


Figure 26. Variation of Porosity with Alumina Content for Slip-Cast Alumina-Fused Silica Composites.

This is thought to be due, in part, to the fact that the optimum or limiting particle size distribution of the fused silica slip has never been quantitatively established.

A program was initiated in an attempt to relate, quantitatively, the strength (specifically modulus of rupture) to particle size distribution with constant cristobalite content. The initial work was restricted to the grinding of "as received" fused silica slip in alumina ball mills with alumina cylinders. No attempt was made in the investigations to influence the rheology of the particular "grinds" by the addition of electrolytes; the criterion for "slip acceptance" was "castability."

It was first necessary to determine the grinding time limit for the particular batch of "as received" fused silica slip used in these investigations. Therefore, batches of slip were ground in 1 gallon grinding mills for various times. After each grinding period the viscosity and weight per cent solids were measured. The particle size distributions of these "grinds" were determined on a mass and count basis and are shown in Figures 27 and 28, respectively. The grinding was accomplished with strict control of grinding media weight, slip weight, and mill speed. The results of viscosity determinations on the "grinds" are presented in Figure 29. The weight per cent solids was found to remain constant within experimental measurement error.

To determine slip "castability," bars 3/4-inch diameter by 6 inches long were slip-cast from each grind and dried under the same conditions. The test bars from the 120 hour and 144 hour "grinds" cracked with drying. Thus, from this standpoint, these "grinds" were not acceptable. The fact that the test bars from the 120 and 144 hour "grinds" cracked on drying was not surprising

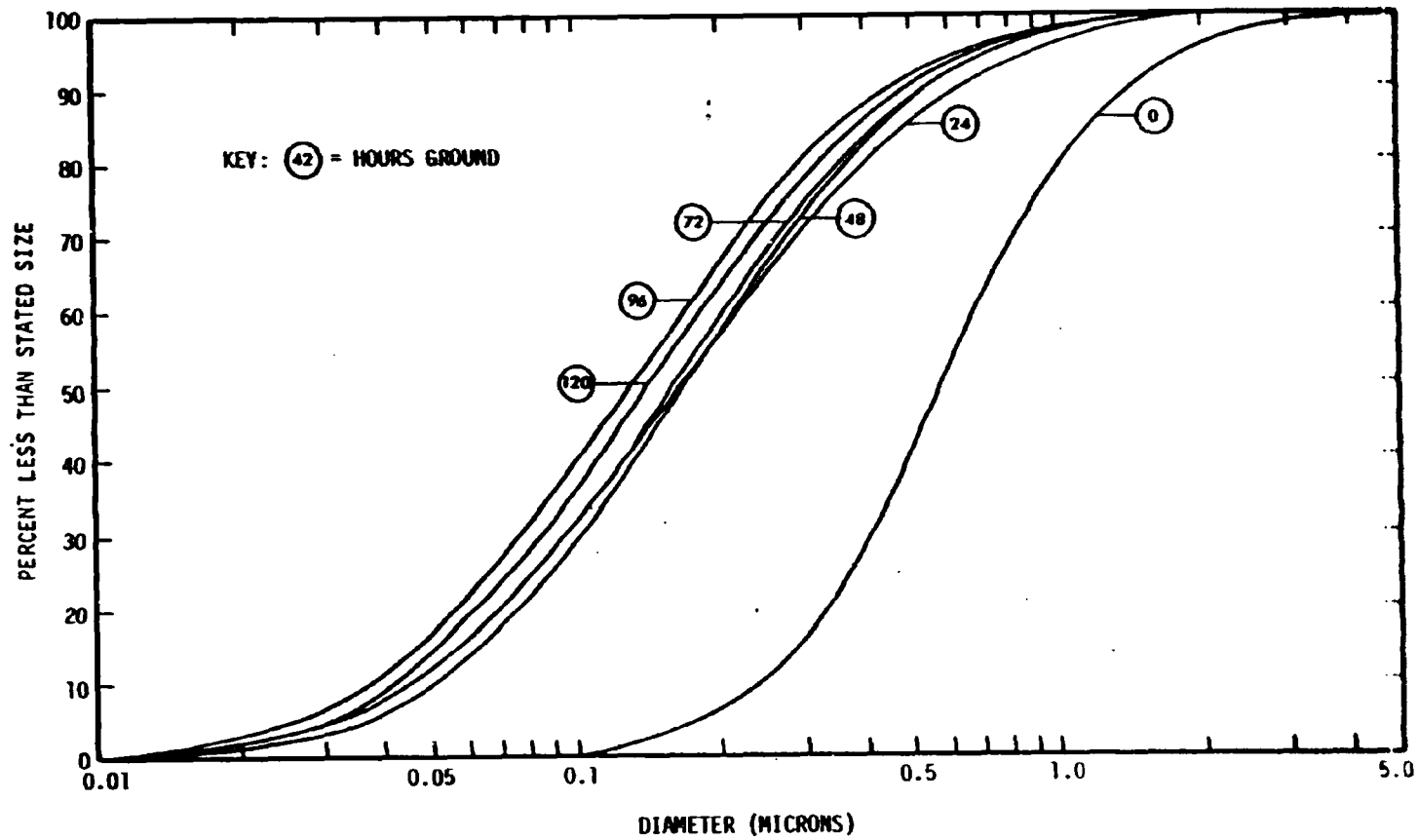


Figure 27. Count Basis Distribution of Particle Sizes of Various Fused Silica Slip Grinds.

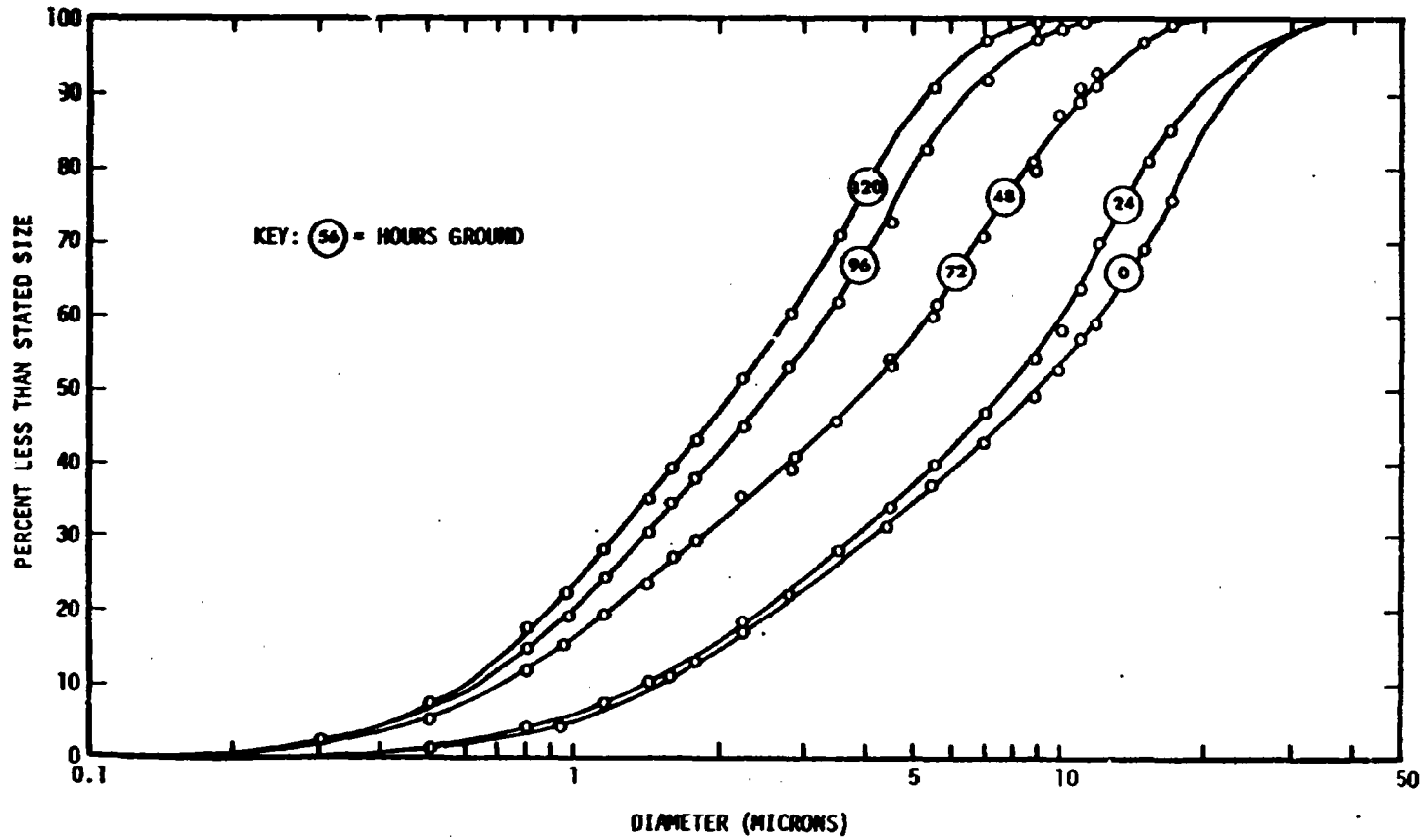


Figure 28. Mass Basis Distribution of Particle Sizes of Various Fused Silica Slip Grinds.

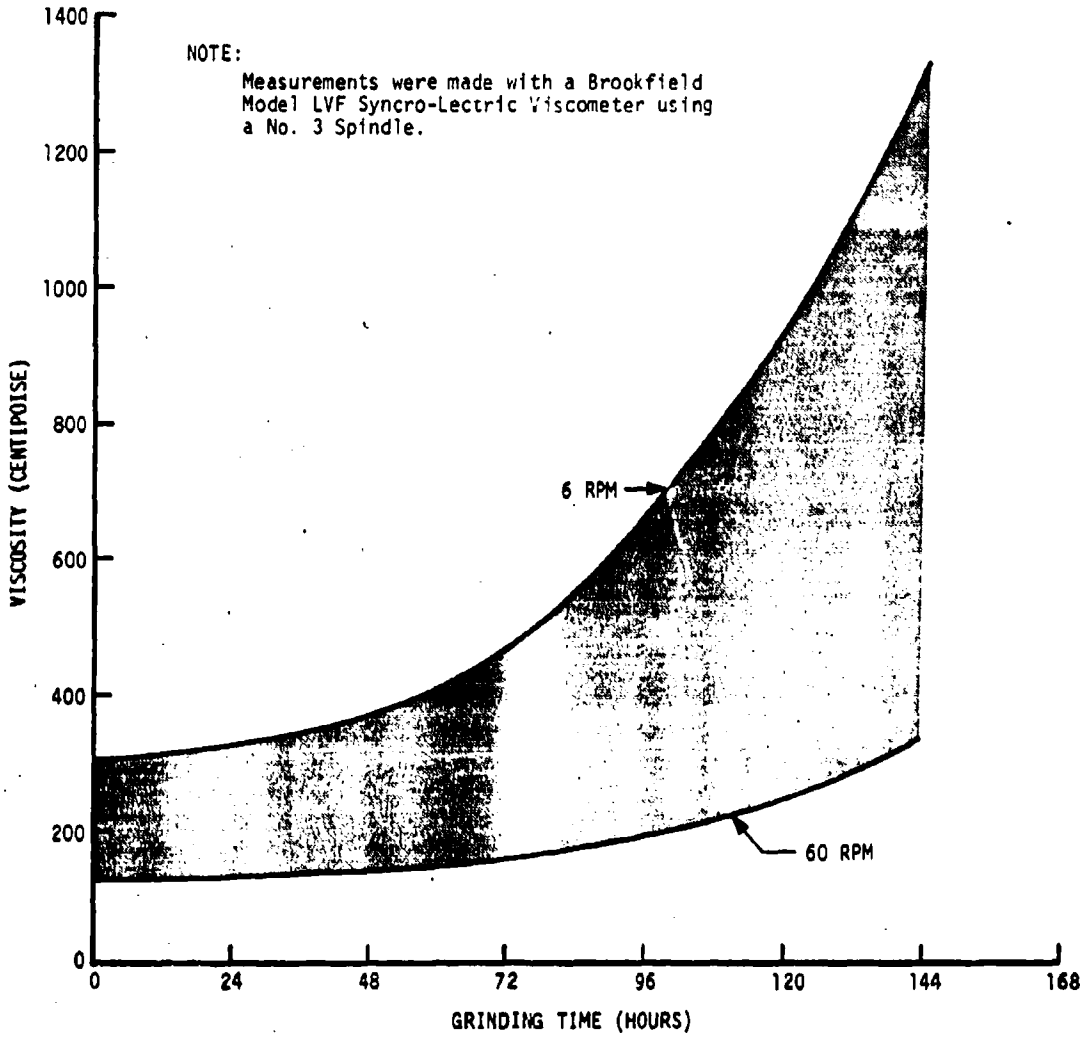


Figure 29. Fused Silica Slip Viscosity as a Function of Grinding Time.

since these "grinds" tended towards gellation as shown by the spread in the viscosity data presented in Figure 29.

Since the criterion of testing with constant cristobalite content was established, a specimen from each batch was sintered (in a well characterized furnace for a predetermined time-at-temperature which gives the maximum value of the dynamic elastic modulus for "as received" slip-cast fused silica) to ascertain the influence of grinding on cristobalite growth during sintering. The results of this experiment are presented in Table XVI. It is apparent from these data that the grinding does not affect the cristobalite growth significantly. Therefore, all test specimens of subsequent experimental specimens were sintered simultaneously.

Ten test bars (3/4-inch diameter by 6-inch long) from each grind were cast in new plaster molds. All molds had been fabricated from the same batch of plaster; dried to constant weight in a 110° F dryer and sealed in polyethylene bags until used to provide a uniform casting surface for the various "grinds." The bars were dried at 110° F and 350° F and measurements of dried porosity, bulk density, and theoretical density were made. These data are presented in Table XVII. The test bars were sintered following the extended time-temperature schedule established for the slip-cast fused silica radomes evaluated at the Ordnance Aerophysics Laboratory. After sintering, measurements of porosity, bulk density, theoretical density, elastic modulus (sonic method 12/) and modulus of rupture were made. These data are presented in Tables XVIII and XIX.

It was apparent from the particle size distributions in Figures 27 and 28 that a uniform time-particle size reduction relationship was not established using individual 1 gallon grinding mills. Also, an adequate quantity of slip

TABLE XVI

CRISTOBALITE CONTENT, DYNAMIC ELASTIC MODULUS, POROSITY, AND MODULUS OF RUPTURE OF SPECIMENS PREPARED FROM GROUND "AS RECEIVED" FUSED SILICA SLIP

| Grinding Time (hr) | Cristobalite Content (v/o) | Dynamic Elastic Modulus ($lb/in^2$) | Porosity (v/o) | Modulus of Rupture ($lb/in^2$) |
|---|---|---|---|---|
| "As received" | 9.2 ± 0.3[a] | $4.57 \times 10^6$ | 12.99 | 2,634[b] |
| 24 | 8.9 ± 0.3 | $5.22 \times 10^6$ | 12.48 | 1,239[b]<br>2,451[c] |
| 48 | 9.4 ± 0.7 | $6.66 \times 10^6$ | 10.15 | 2,215[b]<br>3,655[c] |
| 72 | 9.0 ± 0.6 | $6.62 \times 10^6$ | 10.44 | 4,158[b]<br>5,299[c] |
| 96 | 8.0 ± 0.5 | $6.76 \times 10^6$ | 10.12 | 1,848[b]<br>4,362[c] |

[a] 95% Confidence Interval.

[b] Four point loading, 4-inch lower span, 2-inch upper span.

[c] Four point loading, 2-inch lower span, 1-inch upper span.

to fabricate a small radome shape for evaluation of casting characteristics can not be obtained with a 1 gallon mill. Therefore, a grinding study was conducted to obtain (1) a uniform picture of the particle size reduction as a function of time, and (2) a quantity of ground material sufficient to fabricate a small ogival radome shape; approximately 5-1/2-inch base diameter by 16-inch long with a wall thickness of about 0.3-inch. This was accomplished in a larger grinding mill which would provide about 3 gallons of slip with one charge. The "as received" slip was ground for 83 hours; specimens were

TABLE XVII

POROSITY AND THEORETICAL DENSITY OF DRIED TEST BARS FABRICATED FROM GROUND "AS RECEIVED" FUSED SILICA SLIP

| Grinding Time (hr) | Porosity (v/o) | Theoretical Density ($gm/cm^3$) |
|---|---|---|
| "As Received" | 17.64 ± 0.15* | 2.256 ± 0.012* |
| 24 | 19.80 ± 0.06 | 2.275 ± 0.032 |
| 48 | 20.62 ± 1.67 | 2.318 ± 0.009 |
| 72 | 20.81 ± 0.45 | 2.306 ± 0.020 |
| 96 | 20.96 ± 0.52 | 2.313 ± 0.013 |

*95% Confidence Interval.

TABLE XVIII

POROSITY, THEORETICAL DENSITY, AND CRISTOBALITE CONTENT OF SINTERED TEST BARS FABRICATED FROM GROUND "AS RECEIVED" FUSED SILICA SLIP

| Grinding Time (hr) | Porosity (v/o) | Theoretical Density ($gm/cm^3$) | Cristobalite Content (v/o) |
|---|---|---|---|
| "As Received" | 12.31 ± 0.17* | 2.22 ± 0.01* | 6.7 ± 0.5* |
| 24 | 12.10 ± 0.31 | 2.23 ± 0.01 | 6.3 ± 0.7 |
| 48 | 9.69 ± 0.25 | 2.22 ± 0.01 | 5.5 ± 0.4 |
| 72 | 9.93 ± 0.18 | 2.22 ± 0.01 | 6.8 ± 0.9 |
| 96 | 9.69 ± 0.24 | 2.22 ± 0.01 | 5.6 ± 0.3 |

*95% Confidence Interval.

TABLE XIX

ELASTIC MODULUS, MODULUS OF RUPTURE, AND COMPUTED CRITICAL STRAIN FOR SINTERED TEST BARS FABRICATED FROM GROUND "AS RECEIVED" FUSED SILICA SLIP

| Grinding Time (hr) | Modulus of Rupture[b] ($lb/in^2$) | Elastic Modulus[a] ($10^6$ $lb/in^2$) | Critical Stain[c] ($10^{-3}$ in/in) |
|---|---|---|---|
| "As Received" | 2847 ± 388* | 5.12 ± 0.17* | 0.56 ± 0.08* |
| 24 | 2029 ± 1412 | 5.24 ± 0.84 | 0.36 ± 0.22 |
| 48 | 4243 ± 679 | 7.00 ± 0.07 | 0.61 ± 0.13 |
| 72 | 4356 ± 949 | 6.89 ± 0.06 | 0.63 ± 0.13 |
| 96 | 4216 ± 1072 | 7.03 ± 0.09 | 0.61 ± 0.16 |

[a]Sonic method.

[b]Four point load, 4-inch lower span, 2-inch upper span.

[c]Computed from $\sigma = E\,\epsilon$, where $\sigma$ = Modulus of Rupture, E = Elastic Modulus, and $\epsilon$ = Critical Strain.

*95% Confidence Interval.

extracted for particle size analysis at 24 hour intervals. The measured particle distributions for this grind are presented in Figures 30 and 31. Attempts to fabricate the small radome shape using slip ground for 48 and 83 hours have been unsuccessful due to cracking and breaking up of the castings during drying. This appears to be the result of the presence of a thicker immobile water layer separating the finer particles which caused greater differential drying strain (due to water concentration gradients) and failure during drying. No effort was made to modify the drying procedure to minimize

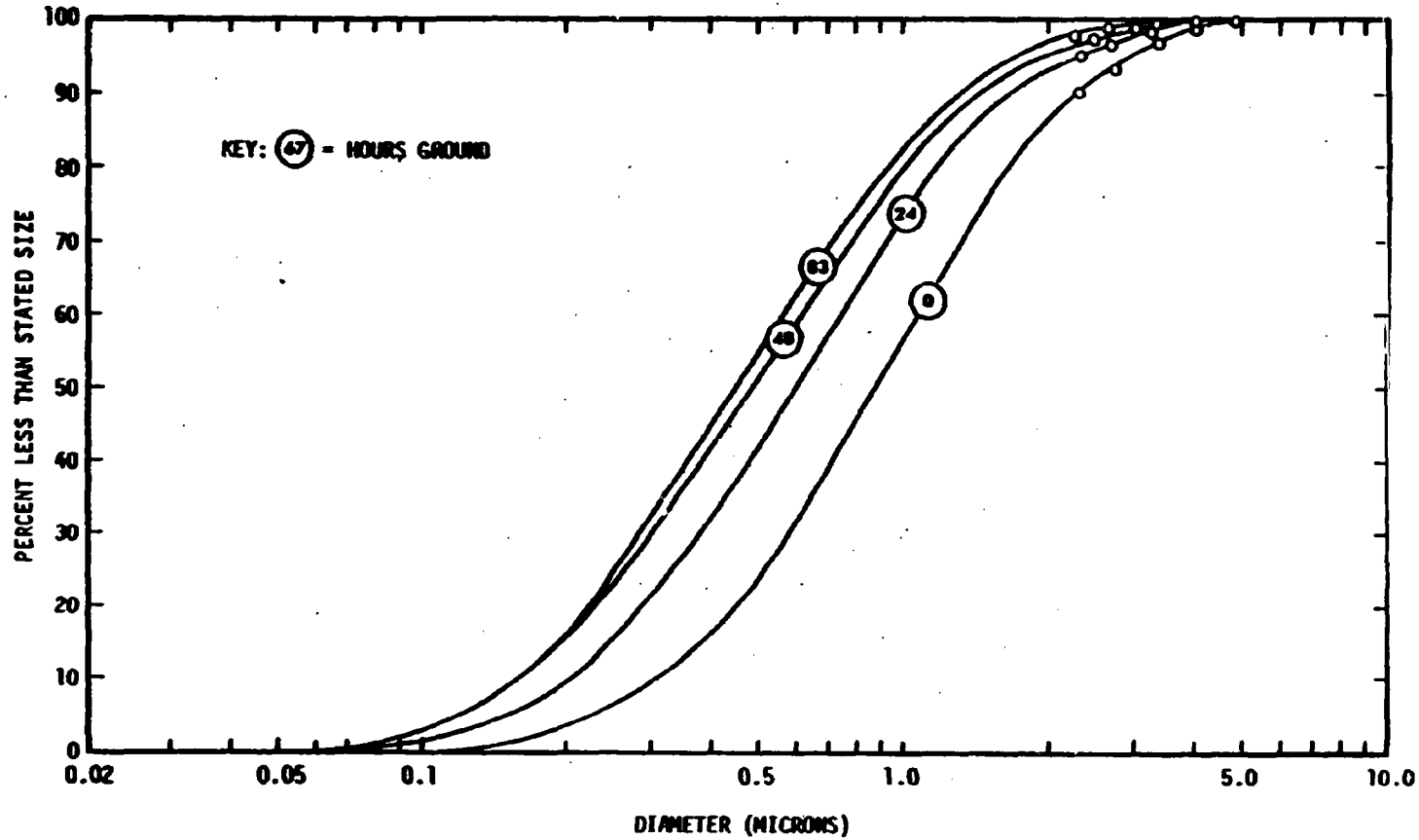


Figure 30. Count Basis Distribution of Particle Sizes of Fused Silica Slip Grinds for Particle Size Reduction-Time Studies.

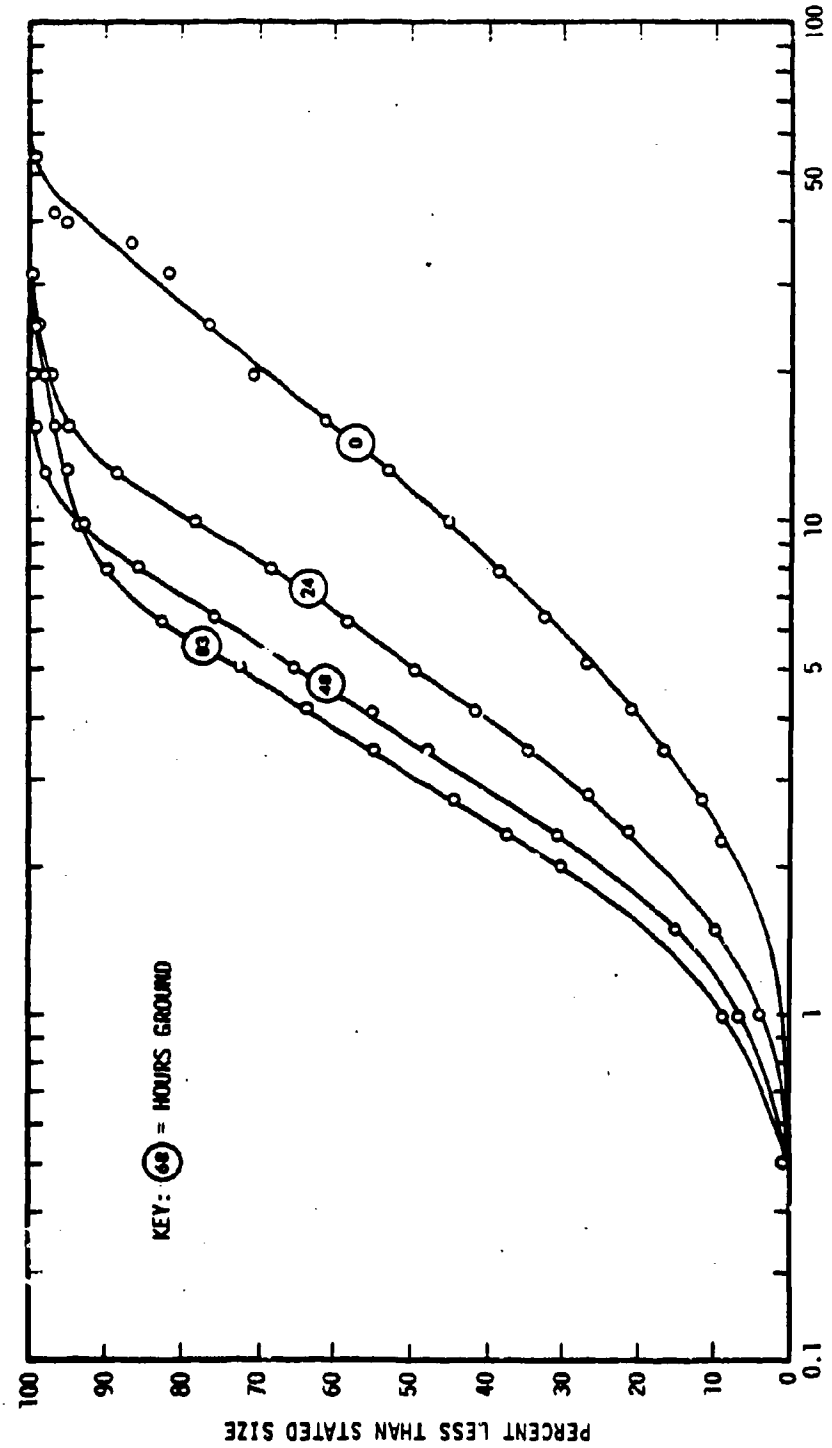


Figure 31. Mass Basis Distribution of Particle Sizes of Fused Silica Slip Grinds for Particle Size Reduction-Time Studies.

the drying strains and eliminate the drying failures. This was not considered to be of immediate significance since observations on the critical failure strain of sintered slip-cast fused silica had shown a wide variation and appears to require extended effort to evaluate the causes. The importance of careful assessment of the influence of the fused silica slip particle distribution was demonstrated in the attempts to slip-cast the small radome shapes with the "ground" fused silica slip. In each case the wall thickness of the cast radome was virtually constant from base-to-tip (less than 5 mils difference) as opposed to a variation of more than 20 mils using a nominal "as received" fused silica slip. Further, the internal tip region was sharp and well defined and no evidence of settling was present.

The data in Table XIX was of particular interest because the uniformity of the computed critical strain values (except for the 24 hour grind) suggested the origin of failure was virtually identical in each case; that is, each group of specimens had the same critical failure strain and probably very similar flaw size and distribution characteristics. Data that was obtained on other experimental programs with slip-cast fused silica gave computed critical strain values of very near $1 \times 10^{-3}$ in/in. The anomaly in behavior ($0.56 \times 10^{-3}$ in/in critical strain vs $1 \times 10^{-3}$ in/in critical strain) was thought to be the result of surface degradation caused by interaction with the plaster mold surface during the slip-casting (residual contamination promoting local cristobalite formation during sintering) and consequently, surface flaws which caused failure at a lower stress level. A brief experiment was conducted to provide some estimate of the effect on subsequent castings made in a particular mold, and the effect when graphite is used as a parting film. The molds that were

used to fabricate the "as received" bars of Table XIX were used to fabricate two groups of test bars from the same fused silica slip; one group cast directly in the molds and one group cast using a graphite parting film*. The bars were dried and sintered following the same procedures used to process the test bars of Table XVII. The modulus of rupture and apparent failure strain for these test specimens are compared with the data from the "as received" bars (Table XIX) in Table XX.

TABLE XX

COMPARISON OF MODULUS OF RUPTURE AND CRITICAL STRAIN DATA ON SLIP-CAST FUSED SILICA SPECIMENS FROM NEW, USED (ONE TIME) AND GRAPHITED PLASTER MOLDS

| Mold Condition | MR ($lb/in^2$) | E ($10^6$ $lb/in^2$) | $\epsilon$ ($10^{-3}$ in/in) | Cristobalite (v/o) |
|---|---|---|---|---|
| New | 2847 ± 388* | 5.12 ± 0.17* | 0.56 ± 0.08* | 6.0 ± 0.5* |
| Used | 3755 ± 625 | 5.01 ± 0.07 | 0.75 ± 0.14 | 5.4 ± 0.4 |
| Graphited[a] | 4334 ± 493 | 4.71 ± 0.14 | 0.92 ± 0.13 | 5.4 ± 0.5 |

[a]These molds were ones used to fabricate the specimens under "new" mold conditions.

*95% Confidence Interval.

The results of this brief investigation appear to be extremely revealing. That is, the apparent failure strain of the test bars suggests that the second castings from plaster molds will be stronger than the first castings and that using a graphite parting film will improve the material strength to a great extent over that obtained in new plaster molds with no graphite parting film.

*Graphite film deposited from a 0.01 w/o dispersion of milled Dixon's Micro Fyne Graphite.

The influence of the plaster mold on the strength of subsequent fused silica castings and the effect of using graphite parting films will be examined thoroughly in the program to be continued next year.

### 3. Metal Films

An investigation was conducted with the objective of developing techniques for depositing stable, metal films on slip-cast fused silica substrates. There are a number of applications for such films on slip-cast fused silica. Among them are thermal sensors and antennas that are integral with a radome.

There are a number of potential techniques for depositing metal films on ceramic substrates; (1) evaporation or sputtering, (2) electrostatic or electrophoretic deposition, (3) painting or screen printing, (4) chemical vapor deposition. Of these techniques, painting or silk screen printing is the simplest and most adaptable. Chemical vapor deposition appears to be a promising technique, but it is a relatively complex process. Evaporation and sputtering provide "line-of-sight" deposition, and, therefore, are not well suited to coating rough, porous surfaces. Also, evaporation and sputtering are not easily adapted to large specimens. Electrostatic and electrophoretic processes are complex and poorly characterized and usually produce films with relatively poor mechanical adherence.

Thick metal films* can be deposited on ceramic substrates, by painting or screen printing, through the use of organometallic compounds. Continuous,

*In the previous descriptions of this research (Quarterly Progress Reports No. 13, 14, and 15) the metal films produced by the screen printing process were described as "thin." However, from the standpoint of electronics technology it is common practice to describe such films as "thick films," in order to distinguish them from vapor deposited or sputtered films whose thicknesses are an order of magnitude less than screen printed films.

metal films of gold, platinum, silver, rhodium, palladium, ruthenium, and iridium can be obtained from organometallic compounds. The organometallic, after deposition, is fired in an oxidizing atmosphere to remove the organic matter and form the metal film. The painting of these compounds to produce dimensionally precise films has two drawbacks: (1) painting usually does not produce a sufficiently uniform film thickness, and (2) with porous, or very rough, surfaces a dimensionally precise film usually can not be obtained due to capillary action and the relative fluidity of the painting compound. This was found to be the case with slip-cast fused silica in preliminary experimentation. Screen printing, of course, has the advantage of providing an accurate pattern to begin with, and the squeegee technique used in screen printing can produce film thicknesses that are uniform to within ± 10 per cent. Also, the much greater viscosity of the pastes used in screen printing can mitigate the spreading of the film by the capillary action of a rough surface. Screen printing was selected as the deposition technique to be examined.

Platinum was the metal studied in this investigation. Several different squeegee pastes of platinum-organics are available, and the melting point of platinum is sufficiently high that it could be used in practical applications of thick metal films on slip-cast fused silica. Also, the temperature coefficient of resistance of platinum is very attractive for thermal sensor applications.

Nylon screens with a mesh size of 283 were used in all the work reported here. The screen pattern selected initially is shown in Figure 32. This pattern provided a good test for definition, size limitations, etc. The screens were mounted on frameworks designed to provide reproducible substrate location and substrate-to-screen clearances.

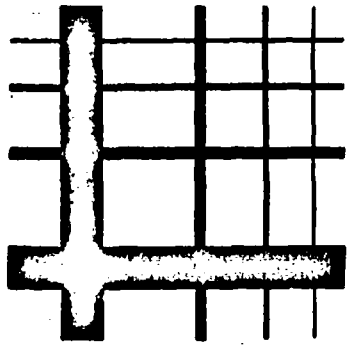

Figure 32. Pattern for Definition Test in Screen Printing.

The substrates used in the initial evaluation of the screen printing technique were slip-cast fused silica disks 3 inches in diameter and 1/4-inch thick. The disks after casting were sliced along a chord 1/4-inch from the circumference. The resulting flat edge was an aid in locating the substrate with respect to the pattern on the screens. The glazed substrates used in this study were coated with a spodumene glaze that had been previously developed specifically for use on fused silica 3/.

Four platinum screening pastes obtained from Englehard Industries, Newark, New Jersey were examined. The compositions of these four pastes are listed in Table XXI. The listing in Table XXI is in the order of decreasing apparent viscosity of the pastes.

TABLE XXI

COMPOSITION OF PLATINUM SCREENING PASTES

| Paste Identification Number* | Platinum Content (w/o) | Contains Ceramic Flux |
|---|---|---|
| 7724 | 35.0 | no |
| 7449 | 65.5 | yes |
| 8077 | 50.0 | yes |
| 7450 | 35.0 | yes |

*Listed in decreasing apparent viscosity.

Each of the above pastes were screened onto slip-cast fused silica substrates, both glazed and unglazed, using the screen pattern shown in Figure 32. The nature of the platinum films deposited were evaluated in terms of the following variables:

(1) nature of the screening paste

(2) distance between screen and substrate during screening

(3) condition of the slip-cast fused silica substrate (i.e. glazed unglazed)

Screen printings were made onto both glazed and unglazed slip-cast fused silica substrates, using screen-to-substrate distances of zero and 0.020-inch. The screened patterns were examined visually, and micrographs prepared, before and after firing. The screened specimens were fired according to the following procedure.

PROCEDURE FOR FIRING
PLATINUM PASTE SCREEN PRINTINGS

1. Dry for 20 hours at 115° C.
2. Fired from 260° C to 540° C with the kiln door half open to assure an adequate oxygen supply (approximate time 3 hours).
3. Fire from 540° C to 815° C with the kiln door closed (approximate time 2-1/2 hours).
4. Hold at 815° C for 20 minutes.
5. Cool in the kiln to 260° C and then quench at room temperature.

The results of this study are contained in the micrographs presented in Figures 33 to 40. These micrographs were made at an arbitrary location on a line of the screened pattern. The micrographs were made in a manner such that

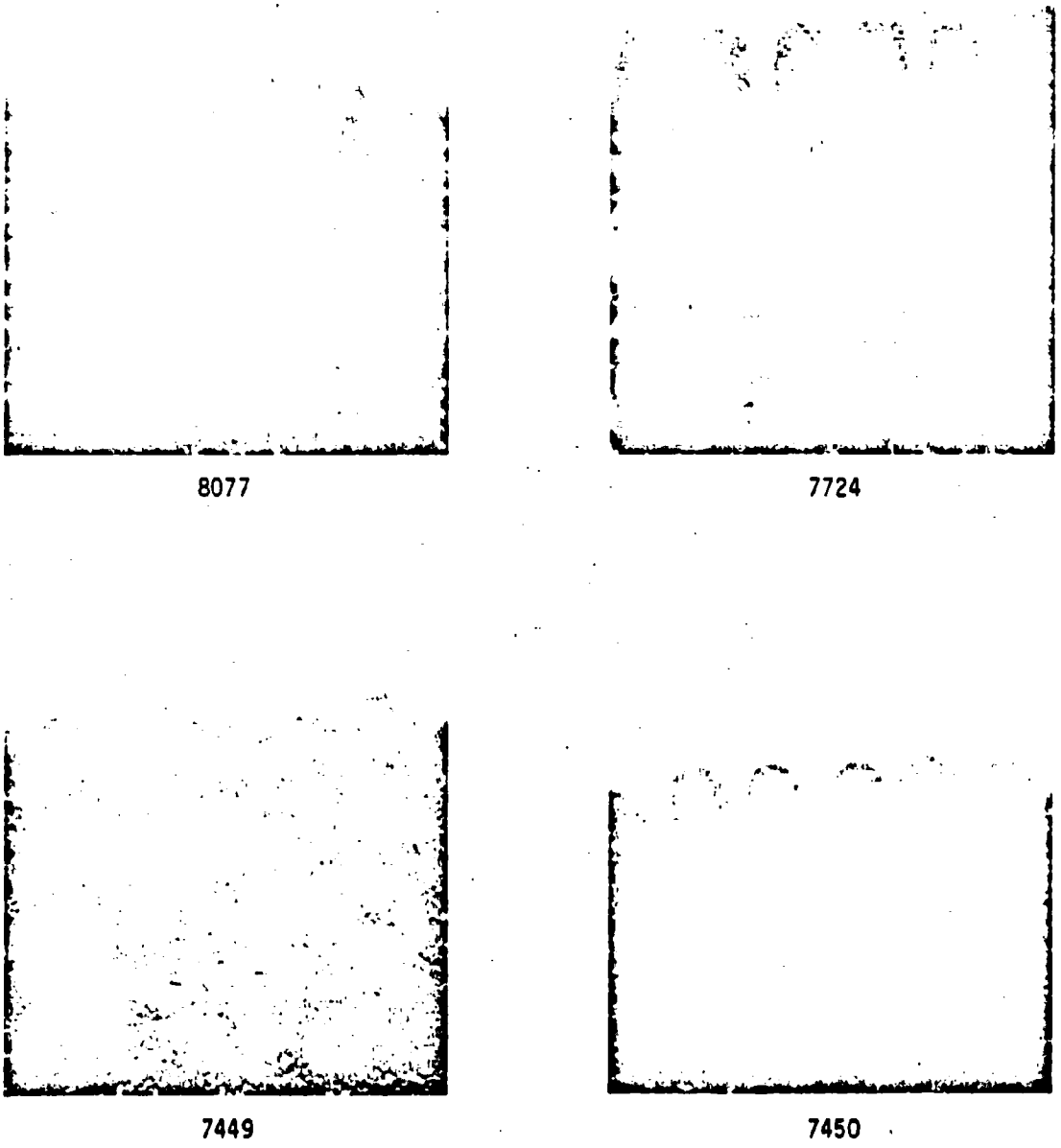


Figure 33. Micrographs of Platinum Pastes Screened Onto Unglazed Substrates with No Screen-To-Substrate Clearance (Before Firing).

8077

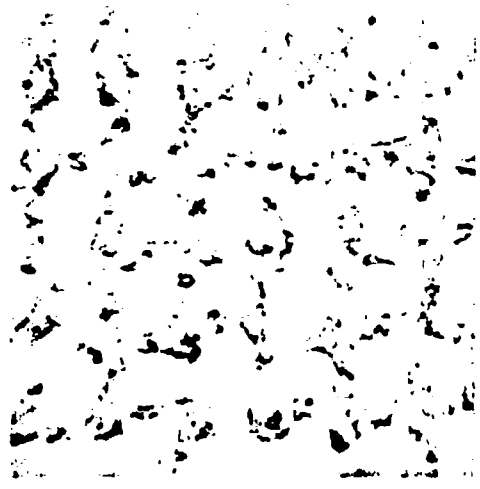

7724

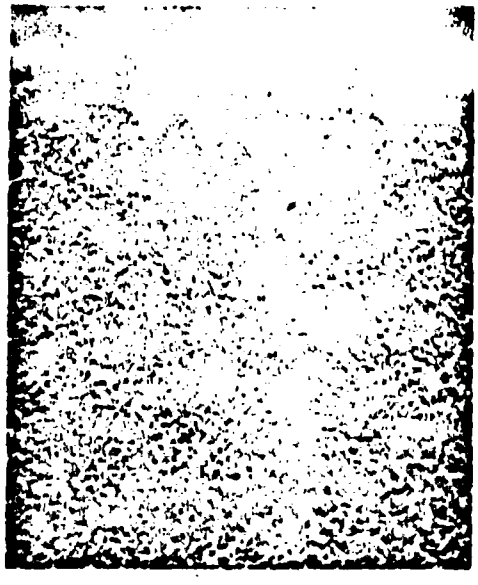

7449

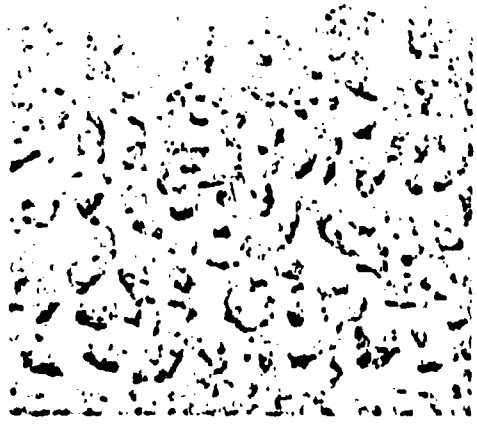

7450

Figure 34. Micrographs of Platinum Pastes Screened Onto Unglazed Substrates with No Screen-To-Substrate Clearance (After Firing).

8077

7724

7449

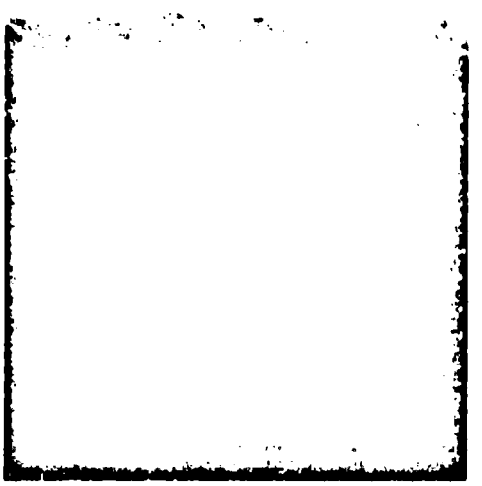

7450

Figure 35. Micrographs of Platinum Pastes Screened Onto Unglazed Substrates with 0.020-Inch Screen-To-Substrate Clearance (Before Firing).

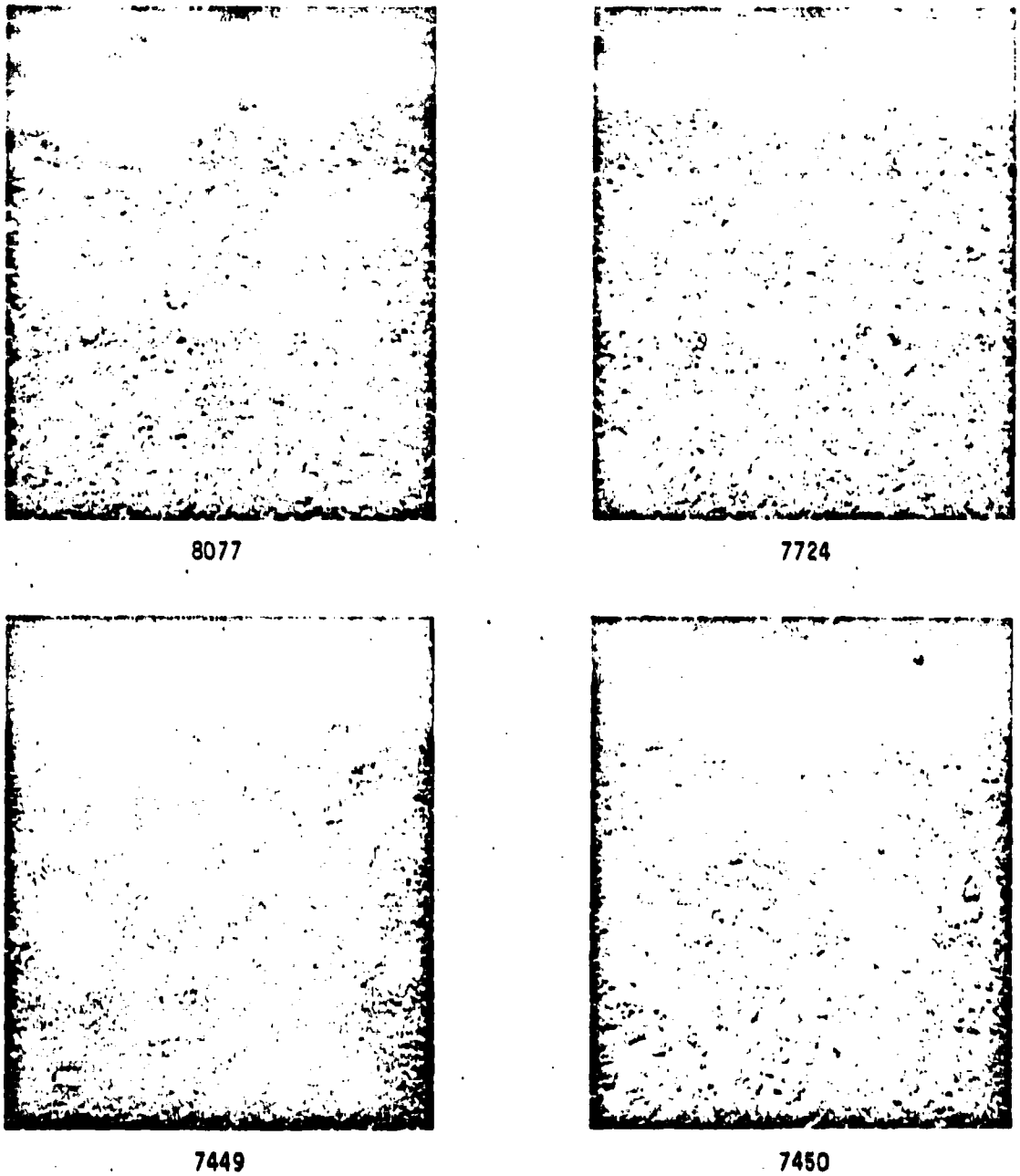


Figure 36. Micrographs of Platinum Pastes Screened Onto Unglazed Substrates with 0.020-Inch Screen-To-Substrate Clearance (After Firing).

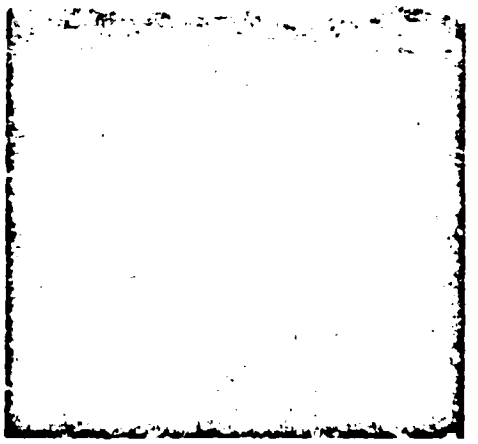

8077

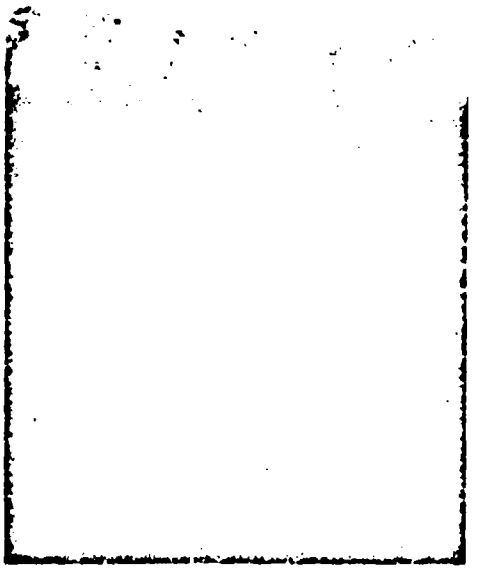

7724

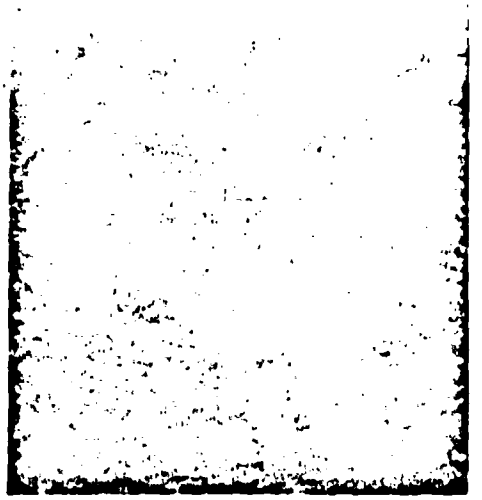

7449

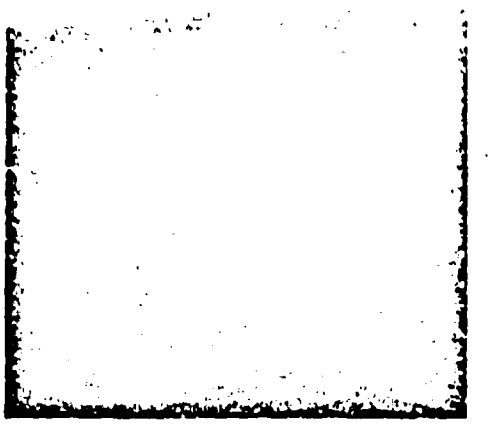

7450

Figure 37. Micrographs of Platinum Pastes Screened Onto Glazed Substrates with No Screen-To-Substrate Clearance (Before Firing).

8077

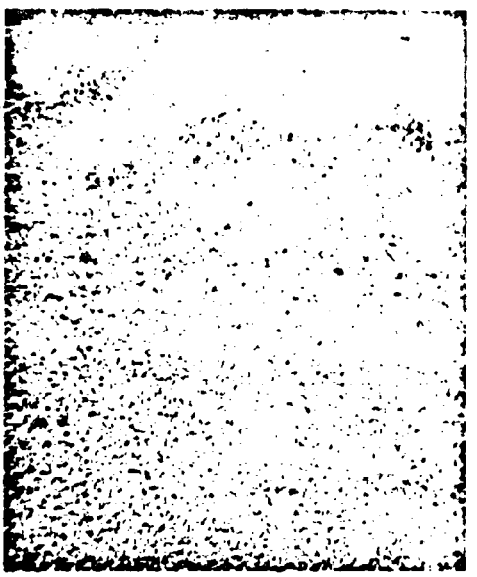

7724

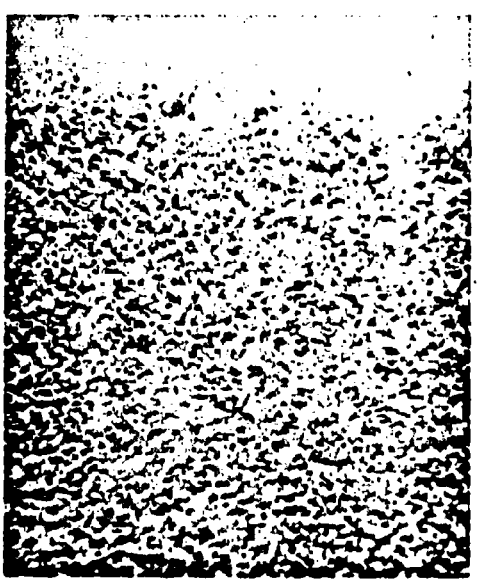

7449

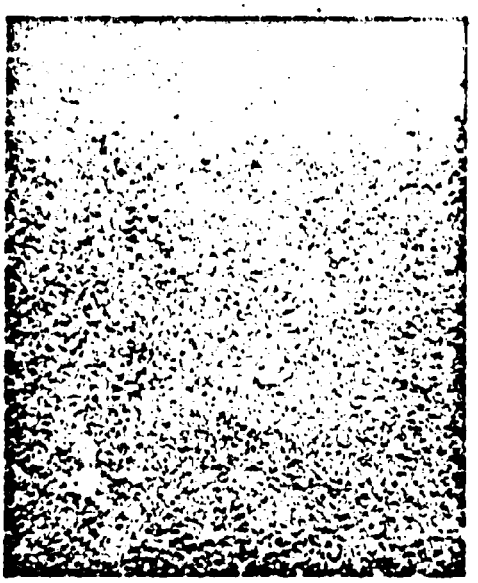

7450

Figure 38. Micrographs of Platinum Pastes Screened Onto Glazed Substrates with No Screen-To-Substrate Clearance (After Firing).

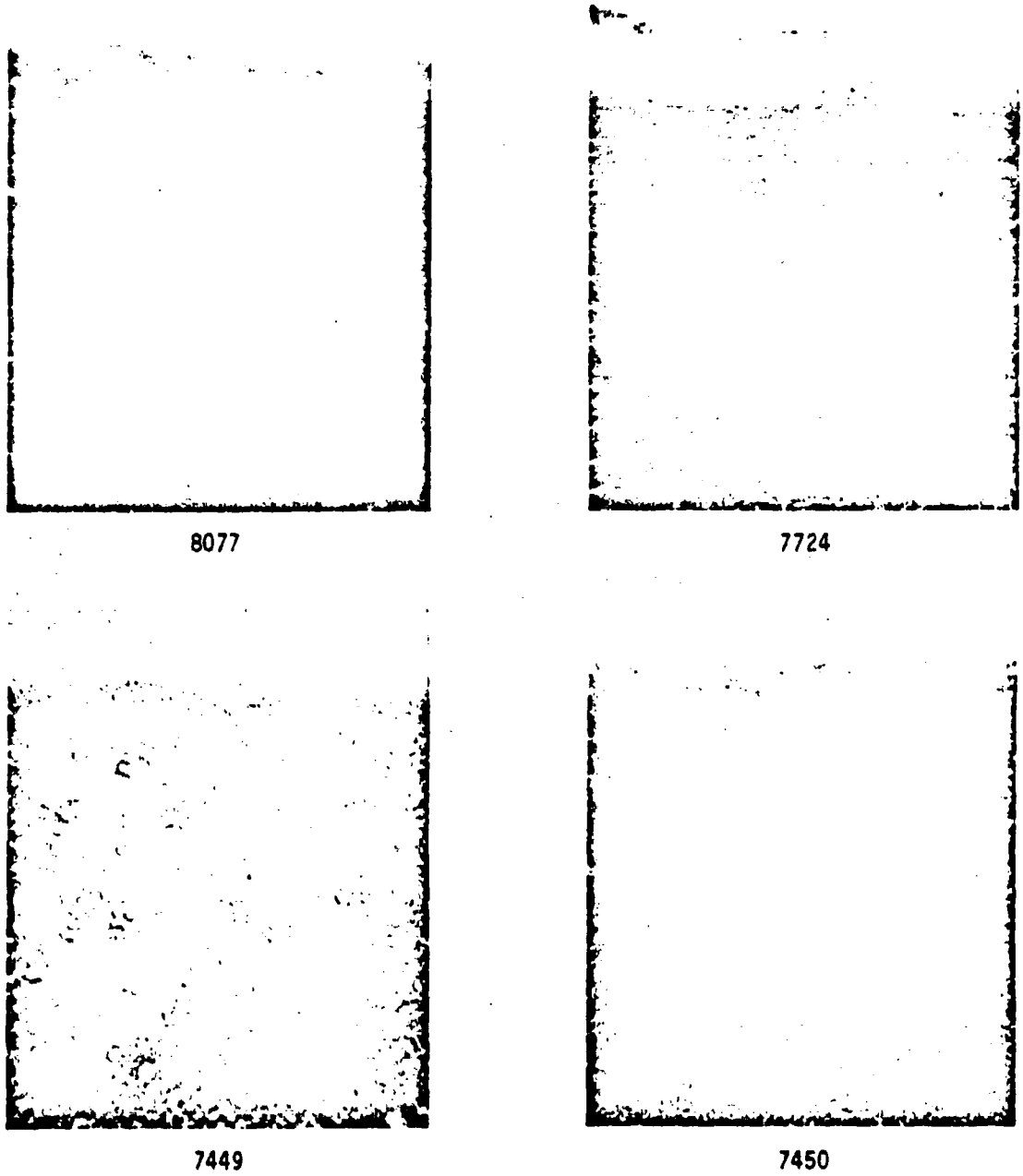


Figure 39. Micrographs of Platinum Pastes Screened Onto Glazed Substrates with 0.020-Inch Screen-To-Substrate Clearance (Before Firing).

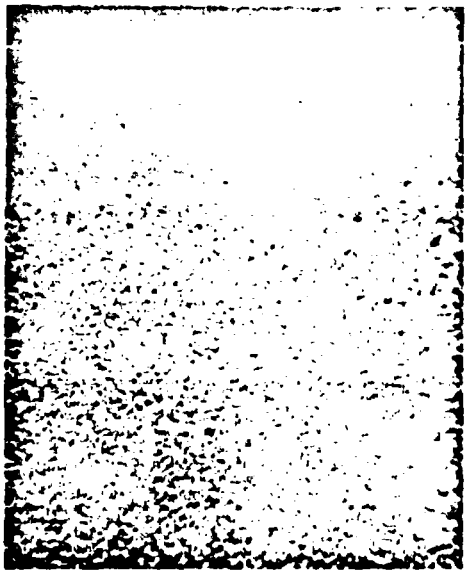

8077

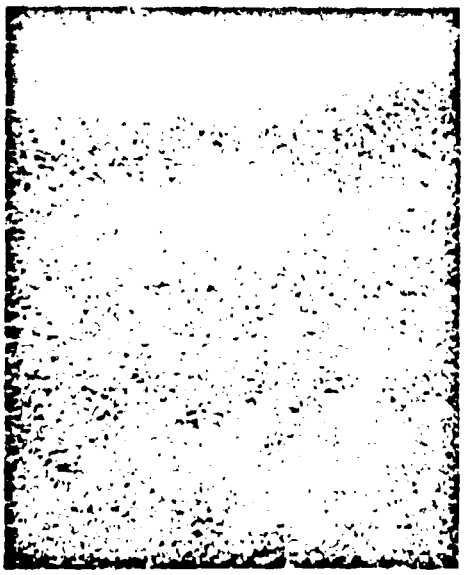

7724

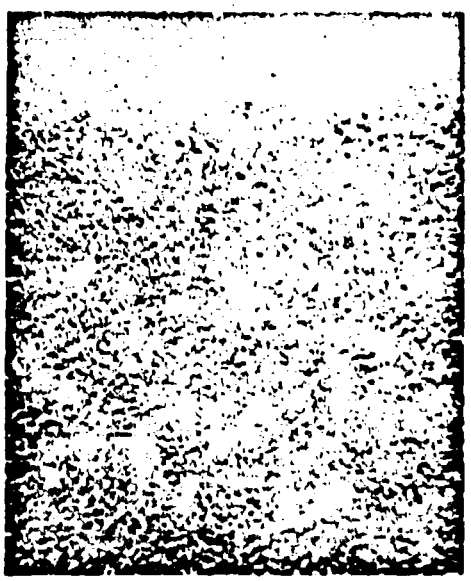

7449

7450

Figure 40. Micrographs of Platinum Pastes Screened Onto Glazed Substrates with 0.020-Inch Screen-To-Substrate Clearance (After Firing).

a portion of the screened line, the edge of the line and a portion of the substrate are shown.

The electrical characteristics of the screen-printed films were then examined. A set of parallel elements, or lines, of the screen-printed pattern (see Figure 32) were isolated electrically by removing the perpendicular elements. These connecting elements were removed by mechanical abrasion. A set of parallel elements was isolated electrically for specimens prepared with each of the four pastes on both glazed and unglazed substrates. The electrical resistance of the isolated elements, 1/4, 1/16, 1/32, and 1/64-inch in width were then determined with a Wheatstone bridge. Electrical contact was made with probes presed against the films. The resistance measured was corrected for contact resistance and the resistance of the wires connecting the probes to the Wheatstone bridge.

Resistance measurements were made along the length of each element, using probe spacings of 0.20, 0.35, 0.50, 1.0, and 2.0 inches. The latter spacing gave a measure of the resistance of an entire element, since each element was 2 inches long.

Film resistivities were computed from the measured resistances and the nominal values of width and length. That is,

$$\text{film resistivity} = \frac{Rw}{\ell}$$

where $R$ is the resistance of an element, or portion of an element, of width $w$ and length $\ell$. The film resistivity is the resistance of unit length and width of a film (i.e. a unit square), and its value depends on the specific resistivity of the platinum and the film thickness. The film resistivities

can be used to obtain an indication of element uniformity, both for a given element and from element to element. This was accomplished in the following manner. The five separate measurements of film resistivity for a given element were used to obtain a mean value for the element and a confidence interval at the 95 per cent level. The confidence interval provides an indication of element uniformity from element to element, prepared under a particular set of conditions (i.e. paste, screen-to-substrate clearance, and substrate condition) can be obtained, and the effect of element width can be determined.

A summary of the resistivity measurements for the thin platinum films, prepared by screening single applications of each of the pastes on glazed and unglazed substrates, is presented in Table XXII. In some cases measurable resistances would be found for an element over some of the smaller probe-to-probe distances, but not over the larger, or largest, distances. In these latter cases the resistances were in excess of $10^7$ ohms and this was taken as a clear indication that the film was not electrically continuous over the entire gage length. Therefore, the film resistivity over this length, or lengths, was taken as infinite (which for all practical purposes it was) and this was included in the computation of the mean film resistivity of an element. This resulted, of course, in failure to obtain a finite value for the average film resistivity and such a result is so indicated in Table XXII.

The apparatus for screen-printing the specimens was designed so that a specimen could be removed from underneath the screen, and subsequently reinserted and relocated precisely. This feature was utilized in studying the effect of multiple coatings on the uniformity of the screened films. Paste number 7449 was screened onto glazed and unglazed substrates with an initial

TABLE XXII

SUMMARY OF THE ELECTRICAL CHARACTERISTICS OF SCREEN-PRINTED, PLATINUM FILMS ON SLIP-CAST FUSED SILICA

| Platinum Paste No. | Screen-To-Substrate Clearance (in.) | Element Width (in.) | Film Resistivity[1] (ohms/square) unglazed substrate | glazed substrate |
|---|---|---|---|---|
| 8077 | zero | 1/4 | ∞ | 5.27 ± 1.13 |
| | | 1/16 | ∞ | 5.47 ± 0.68 |
| | | 1/32 | ∞ | 5.26 ± 0.63 |
| | | 1/64 | ∞ | ∞ |
| 7724 | zero | 1/4 | ∞ | 22.9 ± 1.13 |
| | | 1/16 | ∞ | ∞ |
| | | 1/32 | ∞ | ∞ |
| | | 1/64 | ∞ | ∞ |
| 7449 | zero | 1/4 | 0.76 ± 0.23 | 1.35 ± 0.25 |
| | | 1/16 | 0.75 ± 0.10 | 1.08 ± 0.22 |
| | | 1/32 | 0.73 ± 0.12 | 1.17 ± 0.22 |
| | | 1/64 | ∞ | ∞ |
| 7450 | zero | 1/4 | ∞ | 1.64 ± 0.50 |
| | | 1/16 | ∞ | 1.09 ± 0.22 |
| | | 1/32 | ∞ | 1.42 ± 0.23 |
| | | 1/64 | ∞ | 1.89 ± 0.84 |
| 8077 | 0.020 | 1/4 | ∞ | 3.01 ± 1.23 |
| | | 1/16 | ∞ | 5.34 ± 2.96 |
| | | 1/32 | ∞ | 4.31 ± 2.48 |
| | | 1/64 | ∞ | ∞ |
| 7724 | 0.020 | 1/4 | ∞ | ∞ |
| | | 1/16 | ∞ | ∞ |
| | | 1/32 | ∞ | ∞ |
| | | 1/64 | ∞ | ∞ |

[1]Elements whose resistivities are indicated by the symbol, ∞, had a total element resistance in excess of $10^7$ ohms, which was taken as evidence that the elements were not electrically continuous over their entire lengths.

(Continued)

TABLE XXII (Continued)

SUMMARY OF THE ELECTRICAL CHARACTERISTICS OF SCREEN-PRINTED, PLATINUM FILMS ON SLIP-CAST FUSED SILICA

| Platinum Paste No. | Screen-To-Substrate Clearance (in.) | Element Width (in.) | Film Resistivity[1] (ohms/square) | |
|---|---|---|---|---|
| | | | unglazed substrate | glazed substrate |
| 7449 | 0.020 | 1/4 | 3.63 ± 0.57 | 1.67 ± 0.19 |
| | | 1/16 | 2.30 ± 0.23 | 1.33 ± 0.19 |
| | | 1/32 | 2.25 ± 0.46 | 1.42 ± 0.39 |
| | | 1/64 | ∞ | ∞ |
| 7450 | 0.020 | 1/4 | ∞ | 3.57 ± 1.86 |
| | | 1/16 | ∞ | ∞ |
| | | 1/32 | ∞ | ∞ |
| | | 1/64 | ∞ | ∞ |

[1]Elements whose resistivities are indicated by the symbol, ∞, had a total element resistance in excess of $10^7$ ohms, which was taken as evidence that the elements were not electrically continuous over their entire lengths.

screen-to-substrate clearance of 0.020-inch. The specimens were fired in the usual manner, another coating screened onto the fired film and this fresh coating fired, etc. The initial screen-to-substrate clearance was not changed during the multiple coating process. The film resistivity of the elements was determined for each specimen as before. These results are presented in Table XXIII.

The electrical stability of the screen-printed platinum films in a thermal environment was investigated. A single platinum element 1/32-inch wide and 5 inches long was screen-printed onto an unglazed substrate. Paste number 7449 was used and the film was produced from a single coating. This substrate had

TABLE XXIII

SUMMARY OF RESULTS OBTAINED BY MULTIPLE COATING SLIP-CAST FUSED SILICA WITH PLATINUM PASTE #7449

| Number of Screened Coats | Element Width (in.) | Film Resistivity[1] (ohms/square) | |
|---|---|---|---|
| | | unglazed substrate | glazed substrate |
| one | 1/4 | 3.63 ± 0.57 | 1.67 ± 0.19 |
| | 1/16 | 2.30 ± 0.23 | 1.33 ± 0.19 |
| | 1/32 | 2.25 ± 0.46 | 1.42 ± 0.39 |
| | 1/64 | ∞ | ∞ |
| two | 1/4 | 0.219 ± 0.048 | 0.168 ± 0.050 |
| | 1/16 | 0.180 ± 0.027 | 0.139 ± 0.018 |
| | 1/32 | 0.154 ± 0.021 | 0.132 ± 0.019 |
| | 1/64 | 0.167 ± 0.023 | 0.171 ± 0.042 |
| three | 1/4 | 0.108 ± 0.014 | 0.069 ± 0.017 |
| | 1/16 | 0.094 ± 0.023 | 0.061 ± 0.006 |
| | 1/32 | 0.093 ± 0.015 | 0.060 ± 0.014 |
| | 1/64 | 0.111 ± 0.018 | 0.081 ± 0.033 |

[1]Elements whose resistivities are indicated by the symbol, ∞, had a total element resistance in excess of $10^7$ ohms, which was taken as evidence that the elements were not electrically continuous over their entire lengths.

the ends of platinum lead wires imbedded in such a manner that approximately 1/4-inch of each wire was parallel to the surface and a portion of the diameter of the wire was above the level of the substrate surface. These ends were located so that one was at each terminus of the screen-printed platinum film. The remainder of each lead wire was brought through the substrate and exited from the surface opposite to that carrying the platinum film. After firing of the screen-printed film (according to the procedure presented earlier) the

electrical contact between the ends of the lead wires and the film was checked and found to be satisfactory. The resistance of the film was measured, at room temperature, using a Wheatstone bridge and the specimen was placed in an electric furnace. A $Pt;Pt_{87}Rh_{13}$ thermocouple was placed in contact with the specimen and the entire assembly was shielded from any direct radiation from the furnace heating elements. The temperature of the furnace was raised incrementally and the temperature measured with the thermocouple. After thermal equilibration at each level the resistance of the platinum film was determined with a Wheatstone bridge. At a temperature of approximately 900° C there was evidence of a change in the film's characteristics; the film's resistance began to decrease with increasing temperature. The furnace temperature was then reduced in several steps, with measurement of the film's resistance, to confirm that the film had indeed changed its characteristics. These data are presented in Figure 41.

Since there was evidence that the platinum film had begun to sinter at about 900° C, the film was brought to 1200° C and maintained at this temperature for approximately 18 hours. The resistance of the film as a function of temperature was determined once more. These data are presented in Figure 42. A comparison of these data with the data of Figure 41 indicated that the additional sintering at the higher temperature had removed the hysteresis effect observed originally.

It appeared that a film fired at 815° C, as outlined in the original film preparation procedure, would undergo a decrease in resistance when the film was heated to above this temperature. To confirm this observation, a second platinum film was prepared as an experimental thermal sensor. This film was of

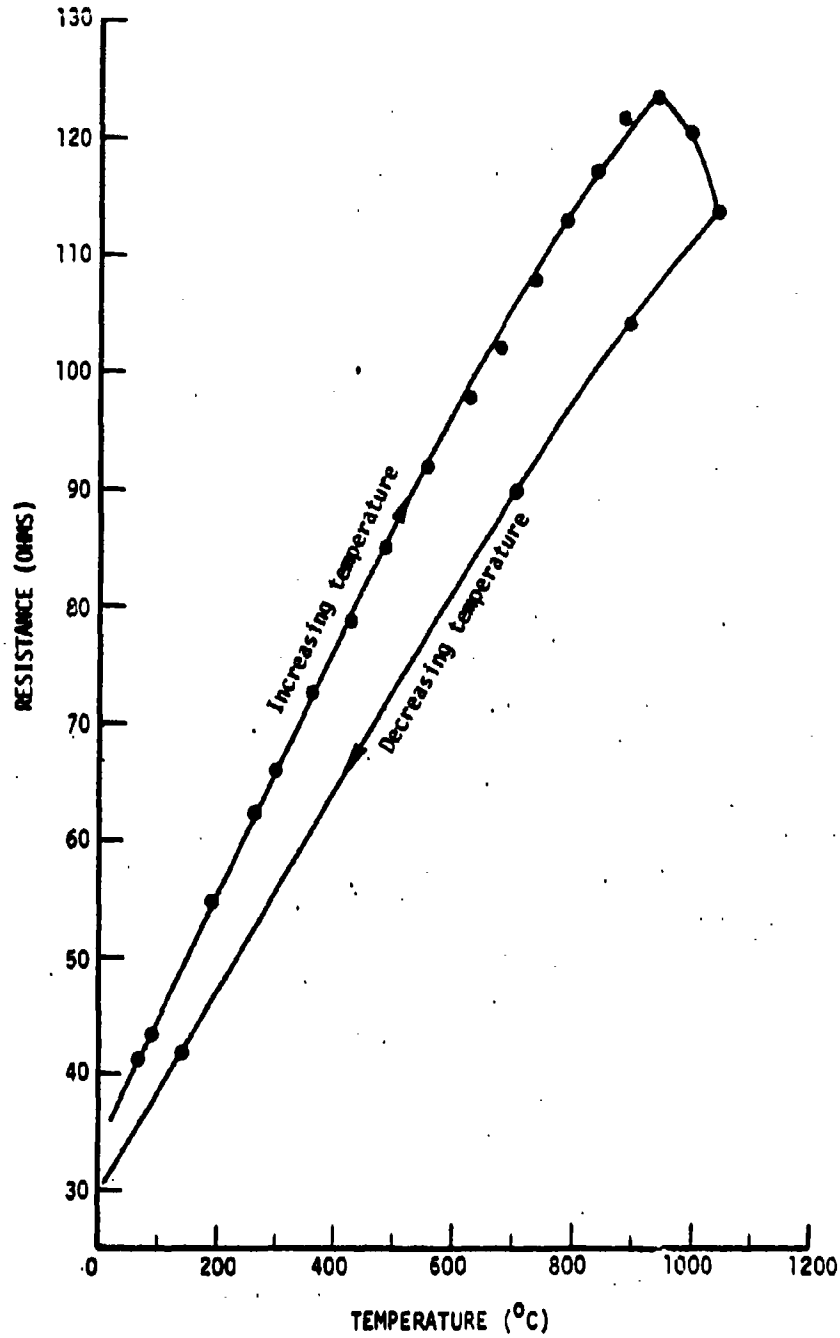


Figure 41. Change in Resistance with Temperature for a Platinum Film Prepared at 815° C.

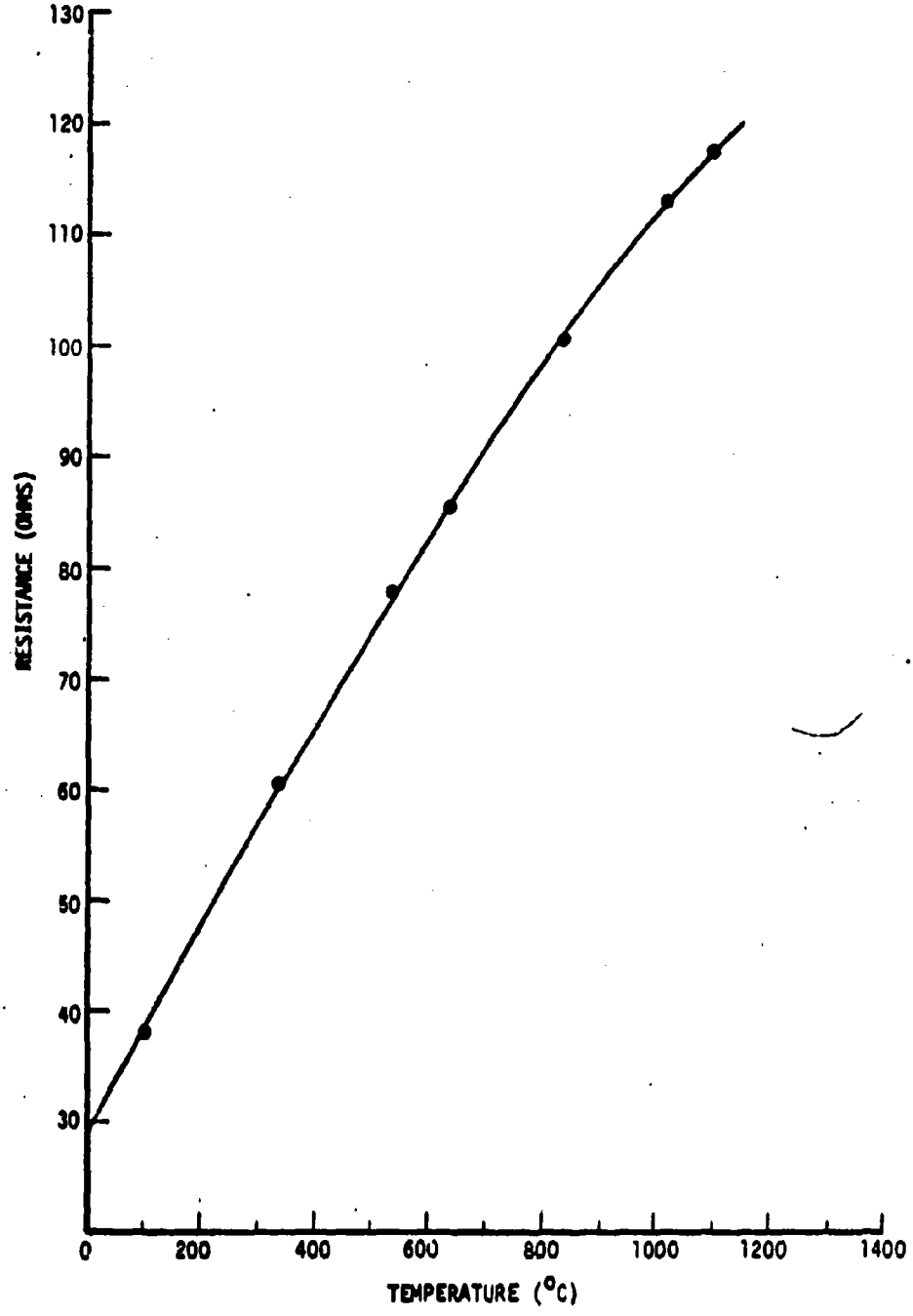


Figure 42. Change in Resistance with Temperature for a Platinum Film Fired at 1200° C for Approximately 18 Hours.

much greater length than the first, and was of the configuration shown in Figure 43. This film was screened onto an unglazed fused silica substrate as before and fired according to the usual procedure (i.e. at a temperature of 815° C). Platinum lead wires were also attached to this film by imbedding them, in the substrate, under the wide portions of the film that are shown in Figure 43. The substrate was placed in contact with the thermocouple used before and the specimen heated to 1250° C as before. The temperature-resistance data obtained with this sensor are presented in Figure 44.

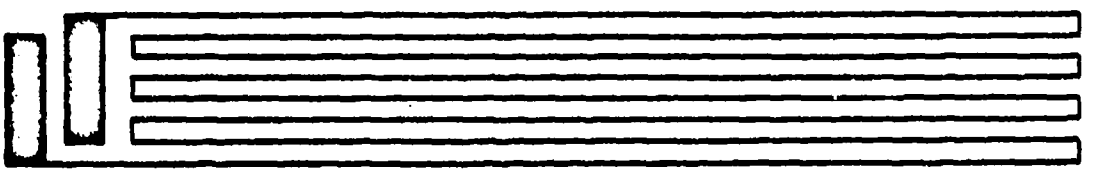

Figure 43. Pattern for Screen-Printed Thermal Sensor

After obtaining the data presented in Figure 44 the film was maintained at 1250° C for about 2 hours. Following this heat treatment the resistance of the sensor was again determined from room temperature to 1250° C. These data are shown in Figure 45. Again the decrease in resistance above 900° C disappeared.

An analysis of the resistance versus temperature data for the two platinum films after being sintered at approximately 1200° C showed that their resistivities at temperature relative to their resistivity at 0° C was the same. These data are presented in Figure 46 along with similar data for bulk platinum 13/ for comparison.

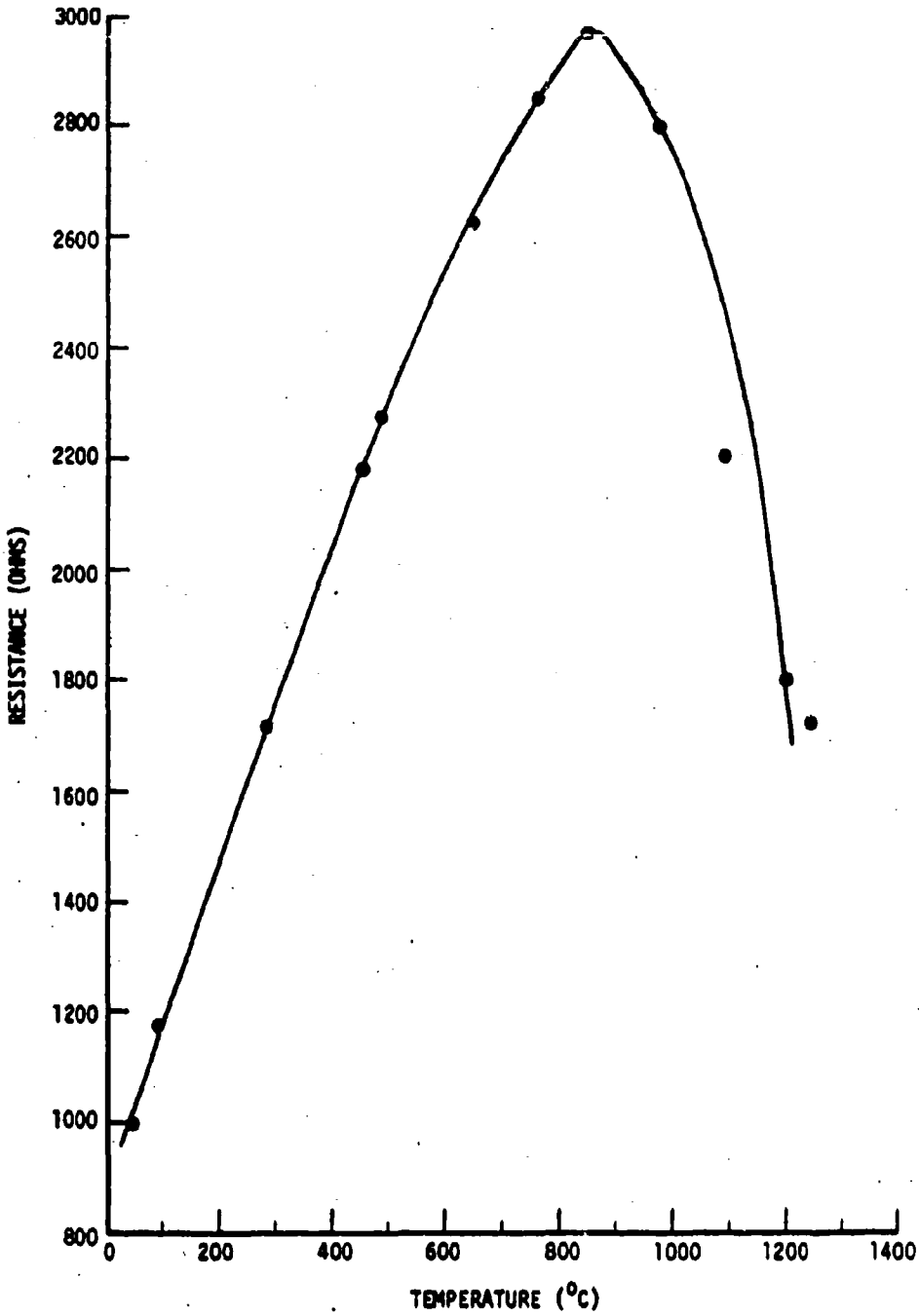


Figure 44. Change in Resistance with Temperature for an Experimental Thermal Sensor Prepared at 815° C.

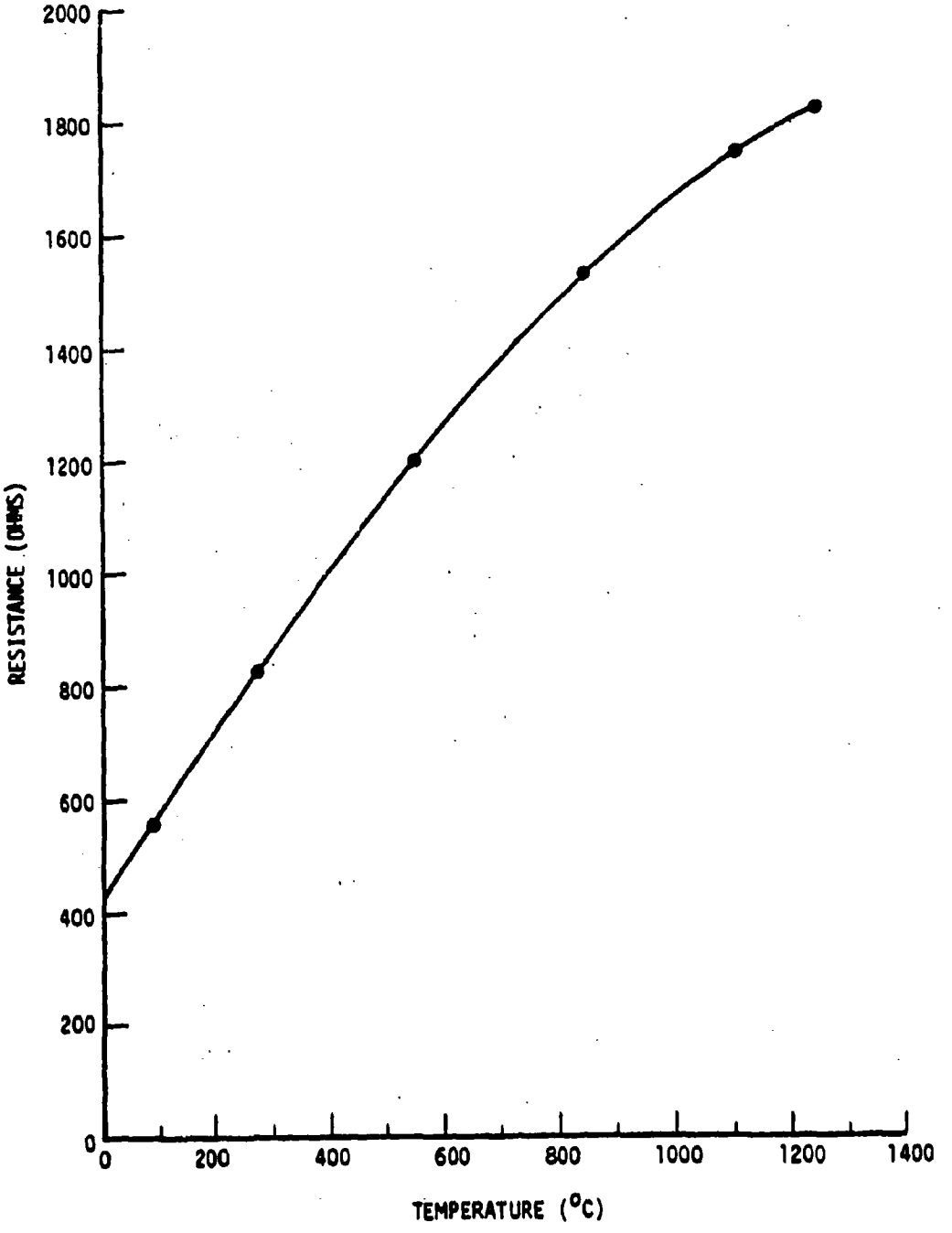


Figure 45. Change in Resistance with Temperature for an Experimental Thermal Sensor Fired to 1250° C for 2 Hours.

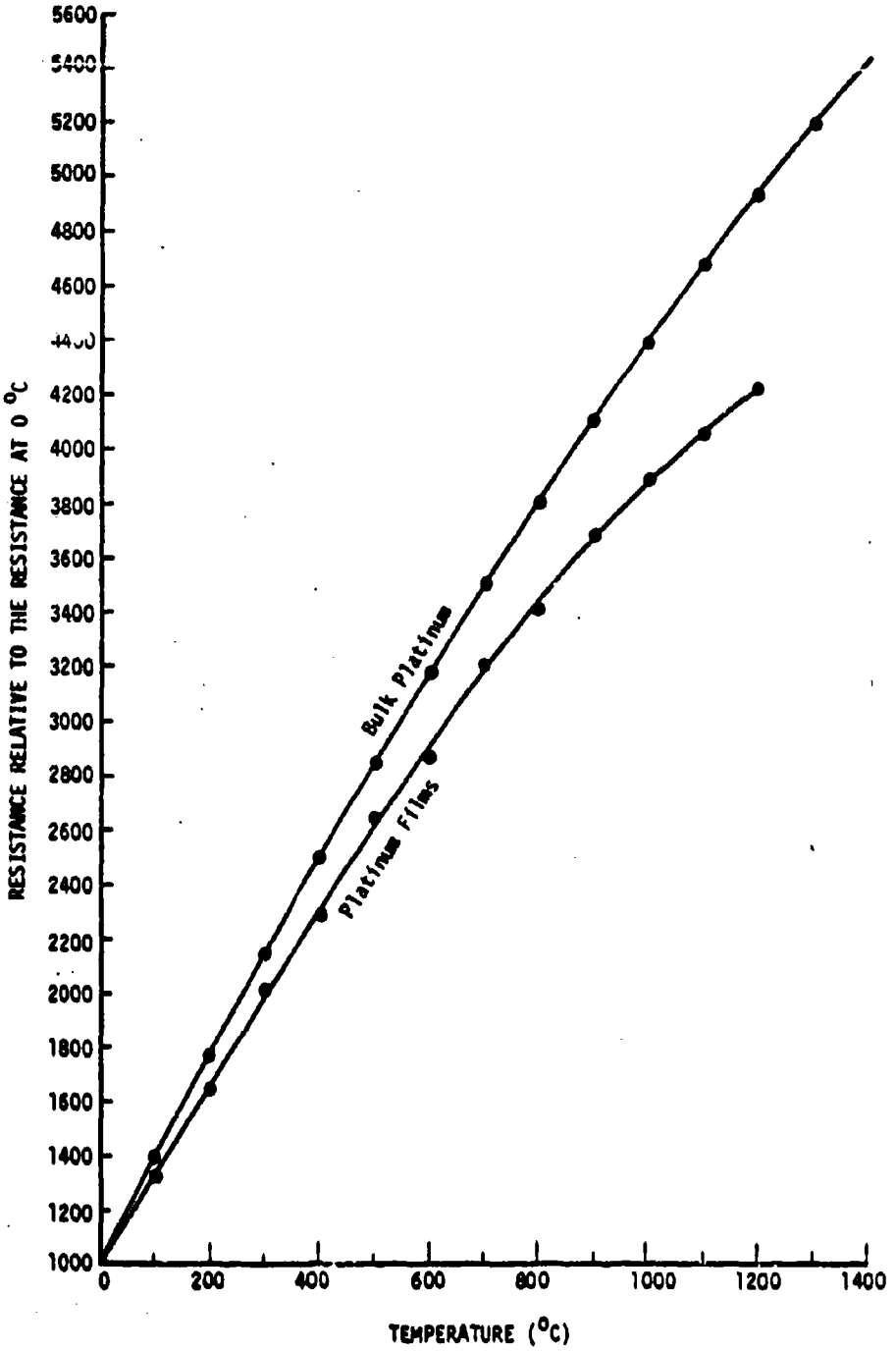


Figure 46. Relative Resistance vs Temperature for Bulk Platinum and Platinum Films.

The mechanical stability of the screen-printed platinum films in a thermal environment was evaluated qualitatively. A typical specimen, an unglazed substrate with a single-coat film, was exposed to the flame of an oxy-acetylene torch with the flame impinging directly onto the face of the specimen carrying the platinum film. In a matter of seconds the platinum elements became molten and the platinum ran off because the specimen face was vertical. However, there was no indication, prior to melting of the platinum, of failure of the bond between the platinum elements and the substrate. In a similar test on a similar specimen, the oxy-acetylene flame was made to impinge on the backside of the substrate. In a few minutes the flame had created a depression in the substrate, through the softening and flowing of the fused silica, that extended very nearly to the surface carrying the platinum film. The fused silica remaining between the bottom of this depression and the opposite surface had even become translucent, rather than opaque, due to the softening of the fused silica. However, there was no visible evidence of degradation of the platinum film, nor was there any apparent loss of adhesion between the film and the substrate.

4. Felted Ceramics

Preparation of felted ceramic composites was continued from the previous year and was channeled into two phases: (1) the development of a low sintering temperature (1850° F), high transverse strength (1300 to 1500 psi) felted ceramic composite, and (2) the development of refractory felted ceramic composites.

Attempts to obtain satisfactory transverse strengths with kaolin wool-alumina particulate material felted ceramic composites were unsuccessful in the previous year's work. This failure was due to the devitrification of the

kaolin wool fiber as a result of the high sintering temperature needed for the alumina particulate. The addition of sintering aids such as calcia and magnesia to the felting slurry did not alleviate this problem. In fact, these additions may have accelerated the devitrification rate of the kaolin wool fiber. Therefore, the kaolin wool-alumina felted system was temporarily dropped from consideration.

In previous work for an industrial sponsor and under Contract NOw-63-0[illegible]3-[illegible] ball clay-mineral wool boards were produced with a nominal sintered density of 75 lb/ft$^3$ and transverse strengths of 1200 to 1400 psi 1/. Although these boards did not have the desired refractory properties, the transverse strength was sufficient for the boards to serve as a model matrix system. Therefore, a series of the boards were fabricated, from the composition listed below:

| | |
|---|---|
| Tenn.-Ky. L-1 Ball Clay | 1250 gm |
| U. S. Gypsum Mineral Wool | 1250 gm |
| Separan AP-30 Flocculant | 0.24 gm |

With the exceptions that 0.24 gm of Separan AP-30 was mixed in 3 liters of water and that no starch solution was used and the total water volume was 30 gallons, the procedure for mixing the slurry was the same as reported for "Standard" boards in Summary Report No. 3 1/. After felting, the boards were pressed under a load of 420 psi to a nominal thickness of 3/4-inch. The boards were then dried at 130° F for 16 hours and 220° F for 24 hours. The dry bulk density of 8 boards was 70 $\pm$ 3 lb/ft$^3$ with 95 per cent confidence.

The above boards were "quick-fired" in a capped fused silica foam (25 lb/ft$^3$) sagger. The 12 x 12-inch felted boards were centered in the sagger's 15 x 15 x 1-inch cavity and fired at a furnace temperature of 1850° F for 3 hours and then cooled in the sagger to room temperature. Bulk density

for 7 boards was 71 ± 6 lb/ft$^3$ at the 95 per cent confidence level. Three point loading modulus of rupture values of 20 specimens cut from these boards was 816 ± 176 psi with 95 per cent confidence. This strength was considerably lower than the 1200 psi previously obtained with the ball clay-slag wool boards of this density 1/. It was thought that the 3 hour heating cycle might not have provided sufficient time for the felted board inside the sagger to reach the 1850° F sintering temperature. Therefore, a thermocouple was passed through the side of the sagger with the tip located directly above the center of a 12 x 12-inch felted board, and a time-temperature recording was initiated upon insertion of the sagger into the furnace. Figure 47 shows the heating and cooling rate for a board heated in the sagger for 3 hours. The maximum temperature obtained was 1695° F. The cooling portion of the curve is from the time the sagger was removed from the furnace.

When the heating cycle was extended to 4 hours, a maximum temperature of 1820° F as indicated by the thermocouple inside the sagger was obtained. Therefore, a board was fired using the extended 4 hour cycle and held for 2 hours. The thermocouple response pattern for this firing is shown in Figure 48. The fired modulus of rupture, based on 5 specimens, was 658 ± 253 psi with 95 per cent confidence. The large interval was attributed to a poor felted structure for this particular board. The bulk density of 4 of the bars varied from 68 to 87 lb/ft$^3$ with the average being 74 lb/ft$^3$, as determined by water absorption. Data obtained on an identical board sintered for 4 hours and 25 minutes gave an average bulk density of 85 lb/ft$^3$ with variation from 83 to 87 lb/ft$^3$. The average modulus of rupture of the latter board was 878 ± 70 lb/ft$^3$ at the 95 per cent confidence level.

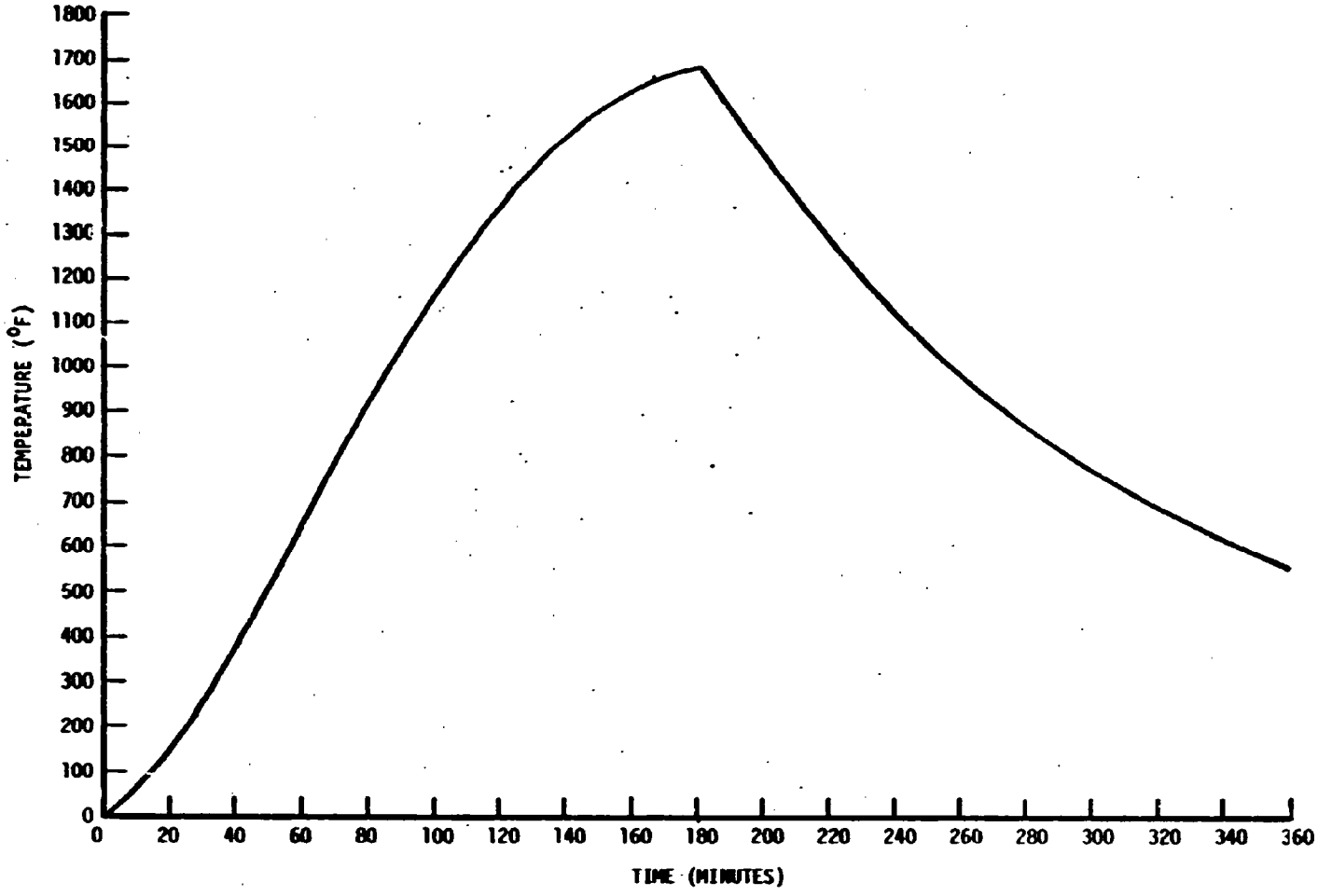


Figure 47. Time-Temperature for Felted Boards Heated in Fused Silica Foam Saggers - 3 Hours in 1850° F Furnace.

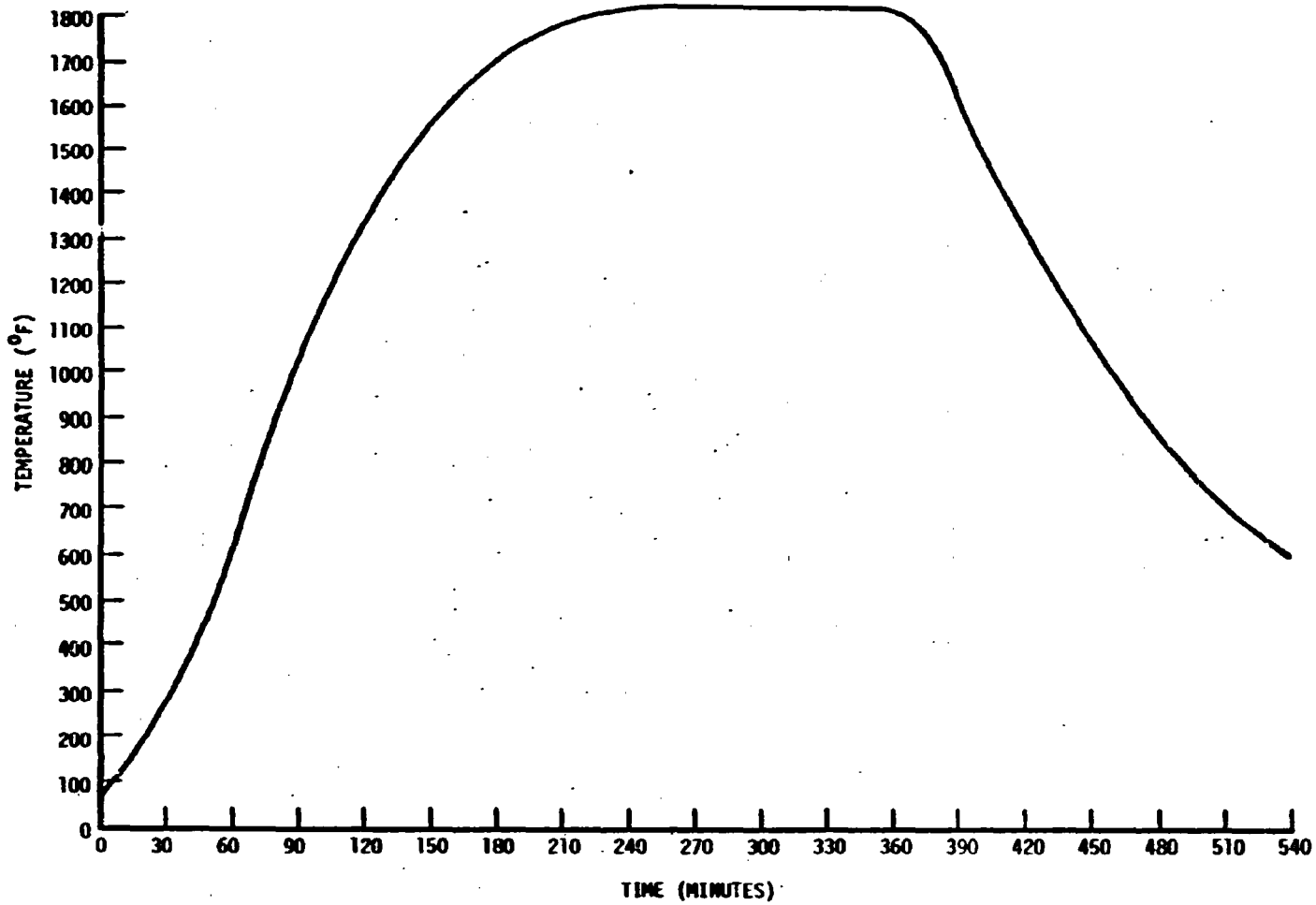


Figure 48. Time-Temperature for Felted Boards Heated in Fused Silica Foam Saggers - 6 Hours in 1850° F Furnace.

Figure 49 is a plot of the bulk density of four individual modulus of rupture bars plotted against the individual modulus of rupture values for each bar for the 6 and the 4-1/2 hour sinterings.

Additional ball clay-mineral wool felted ceramic composites were prepared after the procedure for chopping the mineral wool was altered slightly to rid the felts of glass shot. In the new procedure the mineral wool was chopped in a 25 gram batch with 500 milliliters of water using a 1-quart, high speed blender for 60 seconds. The resultant blend was then immediately transferred to a stainless steel beaker containing 2500 milliliters of water to disperse the chopped fiber and allow the glass shot to settle out. The blended fiber was then decanted onto a 35 mesh screen.

After felting each board, attempts were made to press it to a final nominal thickness of 3/4-inch. The compacting pressure required to reach this thickness varied from board to board and is shown in Table XXIV. The boards were then "quick-fired" in the capped fused silica foam sagger. Three 12-inch square boards, numbers S-15, S-16, and S-17 were fired in the sagger by placing the sagger in the furnace for 308, 360, and 465 minutes respectively. Upon removal from the furnace the boards were allowed to cool to room temperature inside the sagger. The modulus of rupture, bulk density, and compressive strength of the boards are listed in Table XXIV. The modulus of rupture was determined for 1-inch wide bars sawed from the boards using three point-center loading-on a 4-inch span and a loading rate of 600 lb/min. The compressive strength was determined on sections 1 x 1 x 3/4-inch cut from the boards and compressively loaded at a rate of 600 lb/min both perpendicular to and parallel to the felting plane. The bulk density was determined by water displacement.

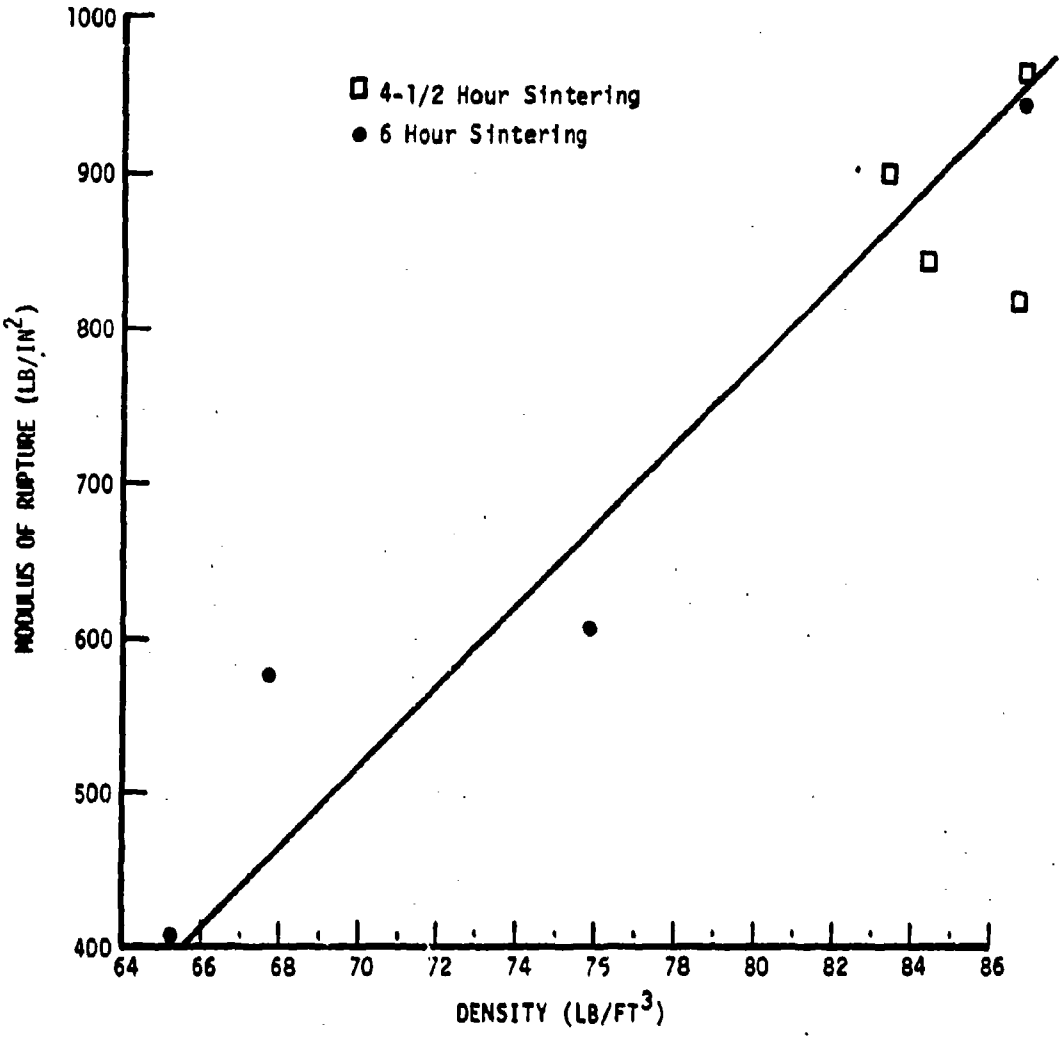


Figure 49. Effect of Bulk Density on Modulus of Rupture for Slag Wool-Ball Clay Felted Boards.

TABLE XXIV

DRY AND FIRED PROPERTIES OF BALL CLAY MINERAL WOOL FELTED BOARDS

| Board Number | Clay Type | Drain Time (sec) | Compact Pressure (psi) | Dry Bulk Density (a) (pcf) | Time in Furnace (min) | Fired Bulk Density (b) (pcf) | Modulus of Rupture (psi) | Compressive Strength ⊥ (psi) | Compressive Strength ∥ (psi) |
|---|---|---|---|---|---|---|---|---|---|
| S-15 | L-1 | 381 | 278 | 81 | 308 | 81.93 ± 1.85 | 1131 ± 65 | 873 ± 393 | 4393 (c) |
| S-16 | L-1 | 297 | 264 | 65 | 360 | 69.11 ± 1.42 | 1012 ± 202 | 394 ± 88 | 2044 (c) |
| S-17 | L-1 | 417 | 236 | 79 | 465 | 73.09 ± 3.16 | 1094 ± 126 | 896 ± 339 | 3889 ± 587 |
| S-18 | T-1 | 1425 | 222 | 75 | 465 | 72.13 ± 217 | 1383 ± 140 | 1335 ± 528 | 4237 ± 1120 |
| S-19 | T-1 | 1315 | 236 | 74 | 480 | 79.02 ± 4.45 | 1521 ± 135 | 1512 ± 426 | 6149 ± 1374 |
| S-20 | T-5 | 1021 | 278 | 73 | 465 | 79.12 ± 4.96 | 1157 ± 157 | 1150 ± 605 | 4388 ± 1849 |
| S-21 | T-5 | 1265 | 278 | 78 | 430 | 80.16 ± 4.04 | 1117 ± 55 | 934 ± 506 | 4188 ± 951 |
| S-23 | T-5 | 996 | 278 | 75 | 465 | 81.04 ± 1.07 | 1258 ± 262 | 1481 ± 410 | 4493 ± 910 |

Note: 95% Confidence Limits
(a) Calculated from measured volume and weight
(b) Calculated from water absorption data on MR basis
(c) Average of 2 specimens no confidence limits

(⊥) Loaded perpendicular to felting plane
(∥) Loaded parallel to felting plane.

Additional boards were prepared using the same procedures and materials as for the previous boards except Kentucky-Tennessee ball clays T-1 and T-5 were used in place of ball clay L-1. A large difference in drain time was noted for these clays as compared with the drain time using clay L-1. This difference can be explained by the difference in particle size of the three clays as shown in Figure 30.

Boards prepared with clays T-1 and T-5 were fired in the same manner as the previous boards and were subjected to the same tests. These results are also listed in Table XXIV.

High temperature ceramic fibers, suitable for incorporation in an embedded ablative system based on a ceramic felt, were examined. Fused silica, boron nitride, zirconia, magnesia, and silicon carbide coated graphite fibers were selected for study. The zirconia and magnesia fibers were selected for their high allowable operating temperature. The graphite and boron nitride fibers were selected for their promise as improved reinforcement agents for the conventional charring ablators. The silica fibers are considered to be a standard reinforcement for the conventional charring ablators. All five fibers are commercially available. The silica, boron nitride, zirconia, and magnesia fibers were supplied essentially in the form of a mat, while the graphite fibers were supplied in the form of a multi-end roving. The magnesia fibers were supplied in a hydrated form; they showed a 26.7 per cent weight loss when heated to 2000° F. The silicon carbide coated graphite fibers were, reportedly, 30 w/o silicon carbide.

Felts were successfully prepared from each of the five high temperature fibrous materials according to the following scheme:

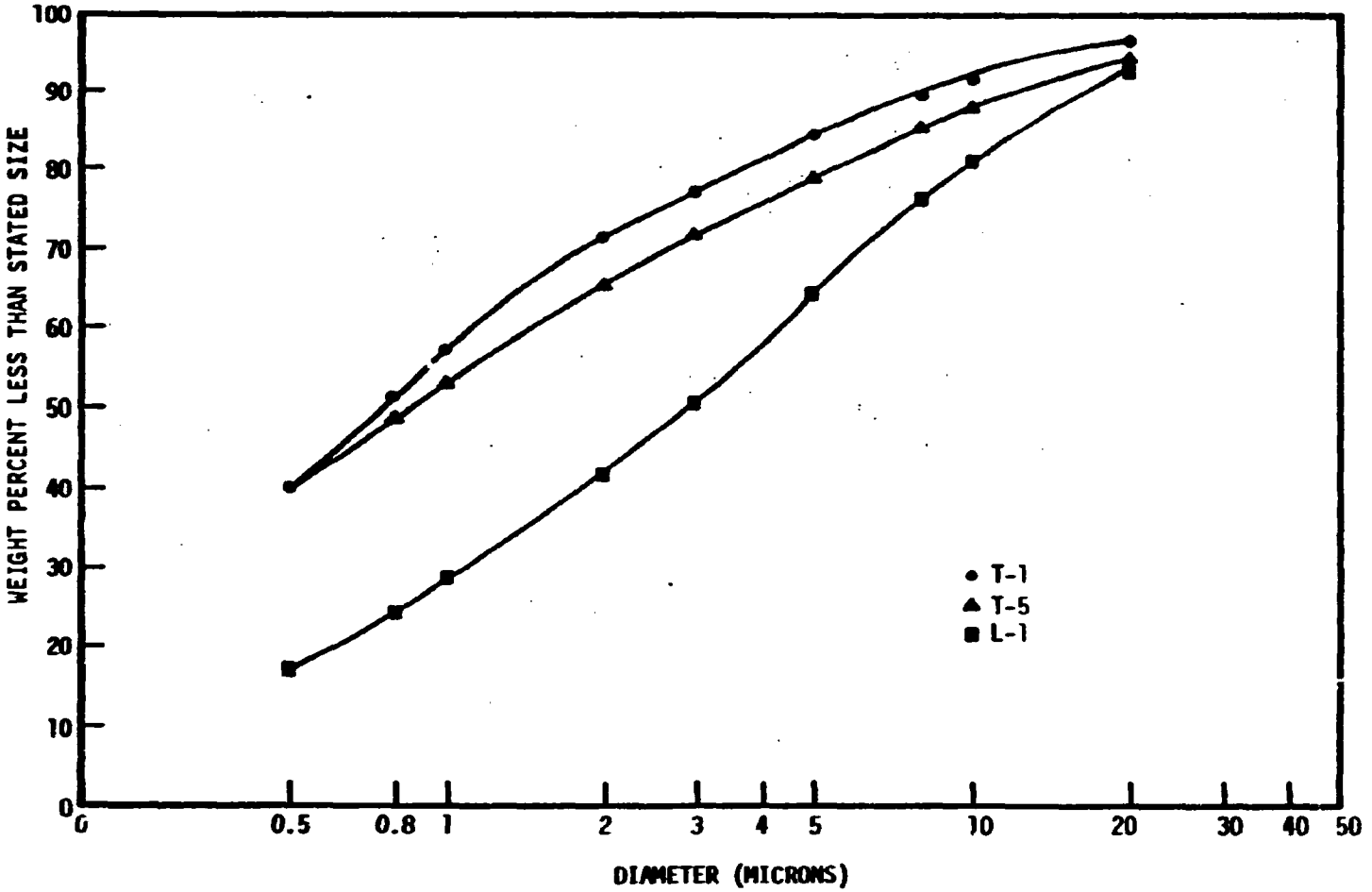


Figure 50. Distributions of Particle Sizes of Clays Used in Mineral Wool-Ball Clay Felts.

a. Fibers, in the amount required to produce a felt with 90% pores, were added to 800 milliliters of water.

b. The fibers were chopped by blending the mix in a Waring Blendor® until they no longer required excessive pressure for compaction.

c. Ten grams of starch were added as a binder, and the mixture was diluted to 2 liters.

d. The slurry was heated to 160° F and mixed with a Lightnin® (Model L) mixer for approximately 30 minutes.

e. The slurry was filtered through a screen, and, after settling, the residue was squeezed down to a 1/2-inch thickness, while being restrained laterally, to yield the felt.

The felts were nominally 4 inches in diameter.

The blending time was found to be critical and had to be determined by trial and error for each material. Overblending resulted in weak felts. However, when the fibers were too long, a sizeable pressure (500 psi, or more) was required for compaction and it was then difficult to achieve a uniform felt. For uniform felts that would retain their shape, very low pressure compaction was required. The blending times used were: 7 seconds with the fused silica fibers, 5 minutes with the boron nitride fibers, and 12-1/2 minutes with the silicon carbide coated graphite fibers. The silicon carbide coated graphite roving was chopped into one inch lengths before blending. The magnesia fibers and the zirconia fibers did not require preliminary chopping.

During earlier work this year 5 grams of starch were used, instead of 10 grams, but the 10 gram addition gave a felt that was somewhat sturdier, and the 10 gram addition was established as the standard. The use of 30 grams of starch or the use of gum arabic in place of the 10 grams of starch was found to give no real improvement.

The structures of the felts are shown in Figures 51 and 52. Figure 51 also shows the structure of a silica felt based on a 50-50 mixture of fused silica fibers and fused silica slip. Indications are that only a small fraction of the slip particles were retained on the screen and in the felt and that the slip particles induced abrasive damage to the fibers.

Full x-ray diffraction traces were run on all five high temperature fibers to yield, together with the 100X photomicrographs shown in Figures 51 and 52, characterization of the felt boards. In the fused silica fibers, no crystalline phases of silica were detected; only the amorphous hump, typical for thermally fused silica, was observed. The diffraction trace on the boron nitride fiber served only to confirm the work reported by Economy 14/. With the magnesia fibers only $Mg(OH)_2$ was indicated before heat treatment and only MgO after firing at 2000° F. The diffraction trace on the silicon carbide coated graphite was characteristic of a beta silicon carbide trace superimposed on a graphite trace. The zirconia fibers appeared as a tetragonal system.

Attempts were made to strengthen the magnesia, zirconia, and silica felts with heat treatment but the results were discouraging. The magnesia felts remained soft and relatively weak after 3 hours at 2700° F. Silica felts, both with and without the addition of the silica slip, failed to be appreciably strengthened by heat treatment. It appeared that sintering was as harmful to the felts (due to structural disruption) as it was helpful (due to increased

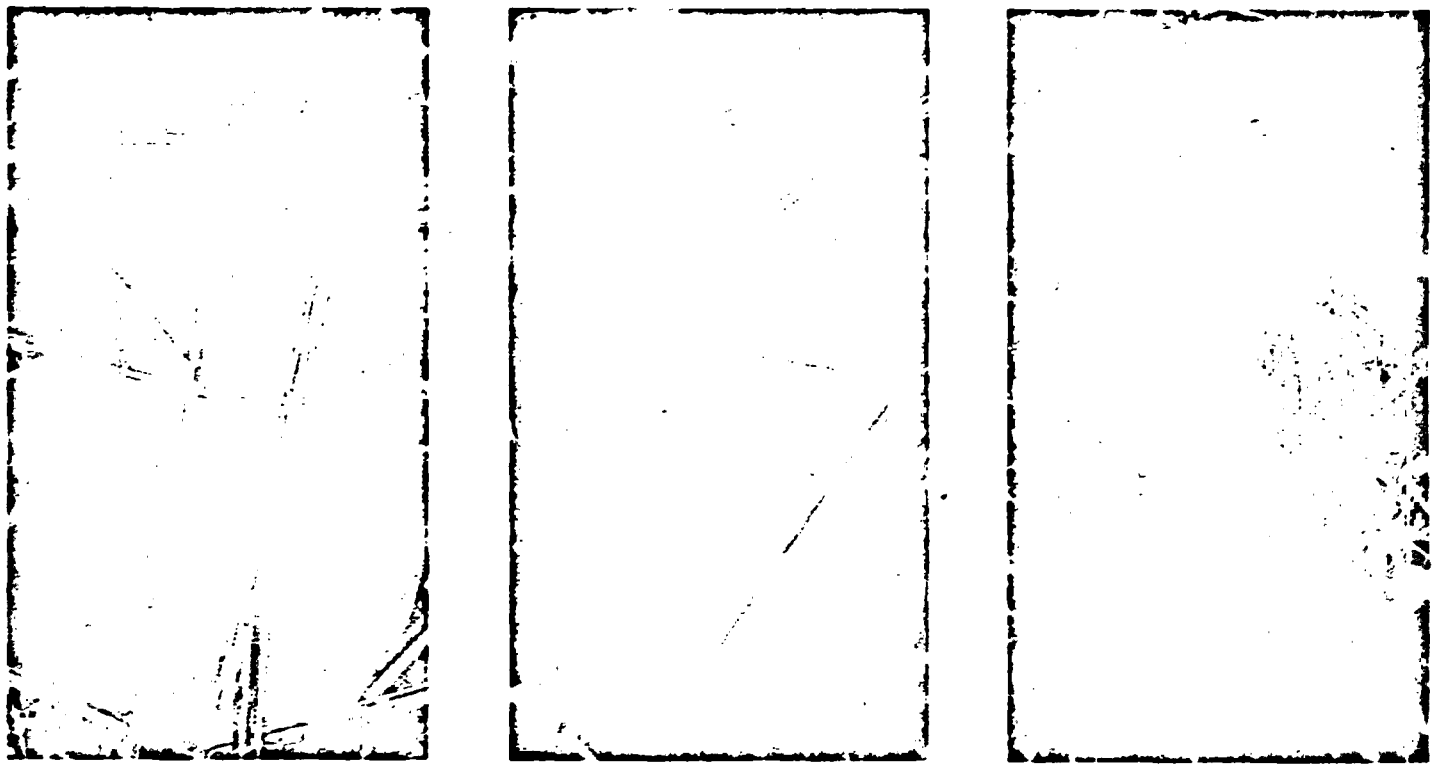

FUSED SILICA FELT
(100 X)

FUSED SILICA FELT WITH
FUSED SILICA SLIP
(100 X)

BORON NITRIDE FELT
(100 X)

Figure 51. Surfaces of Dry Felts of Fused Silica and Boron Nitride (100X).

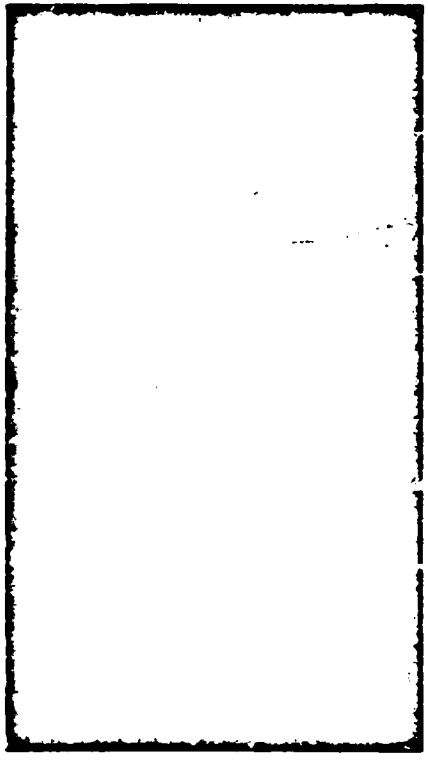

ZIRCONIA FELT
(100 X)

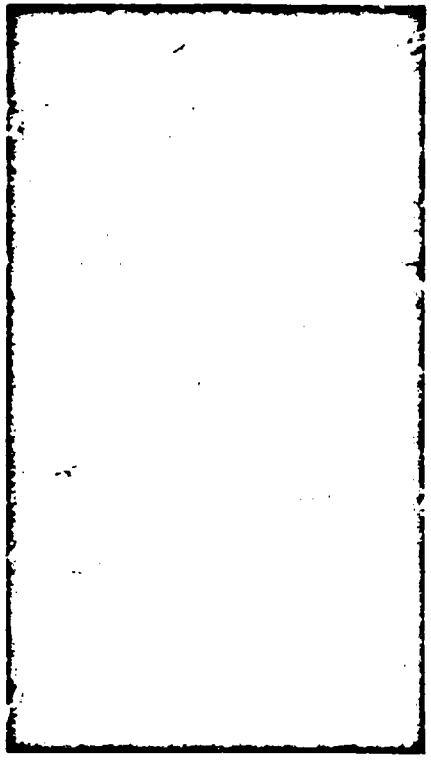

MAGNESIA FELT
(100 X)

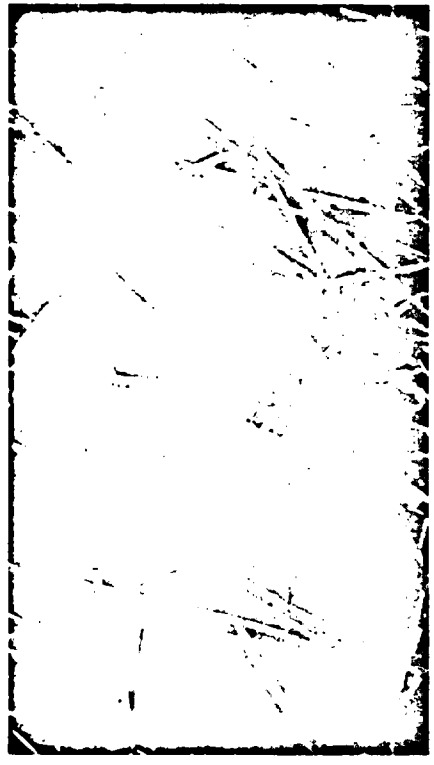

SILICON-CARBIDE-COATED-
GRAPHITE FELT
(100 X)

Figure 52. Surfaces of Dry Felts of Zirconia, Magnesia, and Silicon Carbide Coated Graphite (100X).

contact areas between fiber junctions). The firing schedules for the silica felts and the associated cristobalite contents are listed in Table XXV. All firings were made in electric kilns.

TABLE XXV

FIRING SCHEDULES AND ASSOCIATED CRISTOBALITE CONTENTS FOR THE FUSED SILICA FELTS

| | Volume Per Cent Cristobalite | |
|---|---|---|
| Firing Schedule | Silica Felt Without Silica Slip | Silica Felt With Silica Slip |
| 2200° F - 3 hr | 0.0 to 2.2 | --- |
| 2300° F - 2 hr | 1.0 to 1.4 | 1.0 to 1.3 |
| 2400° F - 3 hr | 0.8 to 1.5 | 8.6 to 10.6 |
| ≈2700° F - 3 hr | ≈100 | 72.0 to 77.4 |

With the zirconia felts firing shrinkage was a problem. The fibers were found to shrink approximately 13 per cent after 8 hours at 2200° F and approximately 14.5 per cent after 5 hours at 2500° F. After 3 hours at 2700° F the shrinkage was about 35 per cent. When the felts were prepared from fibers prefired at 2500° F, the shrinkage after the 2700° F - 3 hour firing was reduced to approximately 16 per cent. It first appeared that prefiring at higher temperatures would be beneficial. However, the zirconia fibers were found quite brittle after prefirings as low as 2600° F.

Attempts were made to prepare zirconia fiber-zirconia particulate felted composites. However, the temperatures required to sinter the compact caused extreme grain growth in the polycrystalline fiber resulting in very weak compacts.

Since the five high temperature ceramic felts were to be impregnated with ablative materials before testing, it was thought that reasonable results could be obtained under the program without prestrengthening of the felts. Therefore, further attempts to strengthen the boards was not justified, and, accordingly, this effort was set aside in favor of the experimental work described in C. Composite Thermal Protection Systems.

## C. Composite Thermal Protection Systems

A literature search was made to assess the state-of-the-art of heat shields. Emphasis was placed on short-term exposures to moderate to high heat fluxes, and interest was focused primarily on materials selection, processing techniques, attachment methods, design guides, testing methods, and refurbishment. The search led to the collection and review of more than 600 primary sources on thermal protection. The selection of literature was based on information provided by seven abstracting services, which included STAR, TAB, IAA, and U. S. Government Reports, and information provided by the Air Force Materials Laboratory 15/. Preliminary reports on the state-of-the-art were included in Quarterly Report No. 13 and Quarterly Report No. 14, and a preliminary bibliography on heat shields was given in Quarterly Report No. 13. The complete statement of the state-of-the-art is given as Appendix VI of this report, and the completed bibliography on heat shields is included in this report.

### 1. Charring Ablators

The results of the literature search indicated that charring ablators are the most important heat-protection materials in use today. Typically, these materials consist of a thermosetting resin reinforced with organic and/or inorganic fillers such as rayon, quartz or graphite fibers, and they offer a particularly advantageous combination of properties for heat shield applications, especially when a moderate to high heat flux and a relatively short-time exposure is the concern.

The availability of charring ablative materials was determined. These materials were found to be readily available, nonstrategic, and inexpensive.

Among the charring materials currently marketed as standard ablators those based on the phenolic compounds appear to be the most effective.

A particular phenolic was selected for use in the experimental work because it was readily available, relatively easy to process, and widely accepted. This material served, more or less, as a standard charring ablator during the program and was examined experimentally both as a charring ablator and as a major constituent in the embedded ablative systems which are discussed below. Also, two silicone-base ablators, suitable for troweling, were obtained and examined as sacrificial coatings for thermal protection systems. The evaluations were made in the Georgia Tech oxy-hydrogen rocket motor facility. As a basis for comparison, samples of a standard ablator obtained from NASA were also evaluated using the same facility. The results of these evaluations are given, together with test results on composite systems, below.

## 2. Embedded Ablators

The results of the literature search on thermal protection systems indicated that the embedded ablator holds the promise of providing a practical solution to the problem of thermal protection against a moderate to high heat flux and relatively short-term exposure where weight requirements are strict and where a charring ablator alone is not suitable because of dimensional stability requirements and/or because of wake contamination considerations. Candidate matrix materials for embedded ablative systems are ceramic foams and felts.

The availability of high-temperature ceramic foams was determined. Zirconia foams are available from a number of commercial sources, magnesia

foams are available from a few sources, and thoria foam is available from at least one commercial source. One source offered to supply the project with a 100-cubic inch sample of hafnia foam at a cost of one thousand dollars. The offer was rejected in view of the high cost and poor characterization of the sample.

In general, the available high temperature foams lack definition and proper characterization. Among the high temperature foams currently marketed as standard items the zirconia foams are the most uniform and reliable. Zirconia foams have been under development for several years by a number of laboratories. A 100-cubic inch sample of a high quality zirconia foam was placed on order early in the contract year, but unfortunately, the vendor reported several delays, and the order was cancelled when it was learned that the order could not be filled during the year. Plans were to determine the benefit that could be derived by embedding Teflon® in the zirconia, as it was anticipated that the zirconia would provide a hot reaction zone for the transpiring gaseous products. Fused silica foam was used in place of the zirconia foam since the zirconia sample could not be received in time. The assessment was made by testing in the Georgia Tech oxy-hydrogen rocket motor facility, the silica foam and the Teflon® both alone and when combined.

The availability of high temperature ceramic fibers, suitable for incorporation in an embedded ablative system based on a ceramic felt, was determined and fused silica, boron nitride, silicon carbide coated graphite, zirconia, and magnesia fibers were selected for use in an experimental program. These five high-temperature fibers were fashioned into felts, as described earlier in Section B.4. Felted Ceramics, and the felts were impregnated with phenolic and evaluated in the Georgia Tech oxy-hydrogen rocket motor facility.

As a basis for comparison samples of a standard ablator obtained from NASA were also evaluated in the Georgia Tech oxy-hydrogen rocket motor facility.

The descriptions of the materials used in the experimental program on composite thermal protection systems are given in Table XXVI. Based on these materials, 13 test samples were prepared, in duplicate. The descriptions of the test samples are given in Table XXVII.

The test samples were evaluated in the Georgia Tech oxy-hydrogen rocket motor facility 16/. One sample of each description was held normal to the hot stream at a station 8.9 inches from the nozzle exit; the other samples were subjected to the normal impingement of the hot gases at a position 6 inches from the nozzle exit. The cold-wall heat-flux for the two conditions were 450 and 1500 $Btu/ft^2$-sec 16/. All samples were tested for 60 seconds or until burnout. The samples were measured before and after testing to determine ablation and mass loss rates, and the frontside and backside temperatures were monitored during the runs. The frontside temperatures were determined using an optical pyrometer; surface thermocouples were used to measure backside temperature.

Test results are given in Figures 53, 54, and 55 and in Table XXVIII. Figures 53, 54, and 55 give the ablation and mass loss rates, while Table XXVIII lists data pertinent to the characterization of the samples together with frontside and backside temperature data.

TABLE XXVI

DESCRIPTIONS OF MATERIALS USED IN COMPOSITE THERMAL PROTECTION SYSTEM INVESTIGATIONS

| Materials | Description |
|---|---|
| Ceramic Felts | Felts of fused silica, boron nitride, hydrated magnesia, zirconia, and 30% silicon carbide coated graphite; nominally 4-inch in diameter, 1/2-inch thick and 10% dense. |
| Standard Ablator | Samples, nominally 4 x 4 x 0.6-inch, of an ablative material reinforced with asbestos and 10% pyrex obtained from NASA. |
| Fused $SiO_2$ Foam | Samples, nominally 4-inch in diameter and 1/2-inch thick, of 25 $lb/ft^3$ fused silica foam. |
| Phenolic | Resinox® SC-1008, a high heat resistant phenolic varnish, supplied by Monsanto. Recommended cure procedure: pressure contact at 325° F for 1 to 3 minutes. |
| Teflon® | Teflon® 30 Dispersion, an aqueous dispersion of 60% Teflon® resin and a wetting agent. Recommended heat treatment: 300° F for water removal 500° - 600° F to volatilize wetting agent, 750° - 900° F to sinter the Teflon® resin. Also, samples, nominally 4 x 2 x 1/2-inch, of TFE Teflon® sheet. |
| Wetting Agent | Triton® X-100, alkyl phenoxy polyethoxy ethanol, supplied by Rohm and Haas Co., Philadelphia, a non-ionic wetting agent. Recommended use: dissolve in warm water and use in very low concentrations to improve the wetting characteristics of Teflon® 30 Dispersion |

(Continued)

TABLE XXVI (Continued)

DESCRIPTIONS OF MATERIALS USED IN COMPOSITE THERMAL PROTECTION SYSTEM INVESTIGATIONS

| Materials | Description |
|---|---|
| Dow 325 Ablative | Dow Corning® 325 ablative material, a silicone rubber, which can be trowelled into place and cured at room or slightly elevated temperature, upon addition of a special catalyst. |
| GE TBS-757A | General Electric's TBS-757A foam thermal barrier, a methyl-phenyl silicone rubber compound, which can be trowelled in place and cured at room or slightly elevated temperature, upon addition of General Electric's TBS-757B curing agent. |

TABLE XXVII

DESCRIPTION OF THERMAL-PROTECTION TEST-SAMPLES

| Sample | Description |
|---|---|
| Phenolic | Resinox® SC-1008 cured at 200° F for 24 hours, nominally 4-inch in diameter and 1/2-inch thick. |
| Phenolic - SiC Coated Graphite Felt<br>Phenolic - BN Felt<br>Phenolic - Fused $SiO_2$ Felt<br>Phenolic - $ZrO_2$ Felt<br>Phenolic - $Mg(OH)_2$ Felt<br>Phenolic - Fused $SiO_2$ Foam | Ceramic felts, nominally 1/2-inch thick with 90% pores, and 25 lb/ft$^3$ fused silica foam, nominally 0.4-inch thick, vacuum impregnated with Resinox® SC-1008 and contact cured at 325° F. |

(Continued)

TABLE XXVII (Continued)

DESCRIPTION OF THERMAL-PROTECTION TEST-SAMPLES

| Sample | Description |
|---|---|
| Standard Ablator | Ablative material, nominally 0.6-inch thick, reinforced with asbestos and 10% pyrex, as received from NASA. |
| Teflon® | TFE Teflon® sheet, nominally 1/2-inch thick, as received. |
| Teflon® - Fused $SiO_2$ Foam | 25 lb/ft$^3$ fused silica foam, nominally 1/2-inch thick, vacuum impregnated twice with Teflon® 30 Dispersion with 100 ppm Triton® X-100 and heated at 300° F, 15 minutes, 580° F - 2 hours, and 825° F - 2 hours after each impregnation step. |
| Fused $SiO_2$ Foam | 25 lb/ft$^3$ fused silica foam, nominally 1/2-inch thick, as received. |
| Fused $SiO_2$ Foam - Dow 325 Ablative | 25 lb/ft$^3$ fused silica foam, nominally 1/2-inch thick, with a surface layer of Dow Corning® 325 ablative material about 1/5-inch thick trowelled in place and cured at 300° F for 15 minutes. |
| Fused $SiO_2$ Foam - GE TBS-757A | 25 lb/ft$^3$ fused silica foam, nominally 1/2-inch thick, with a surface layer of General Electric's TBS-757A foam thermal barrier about 1/10-inch thick trowelled in place and cured at 300° F for 5 minutes. |

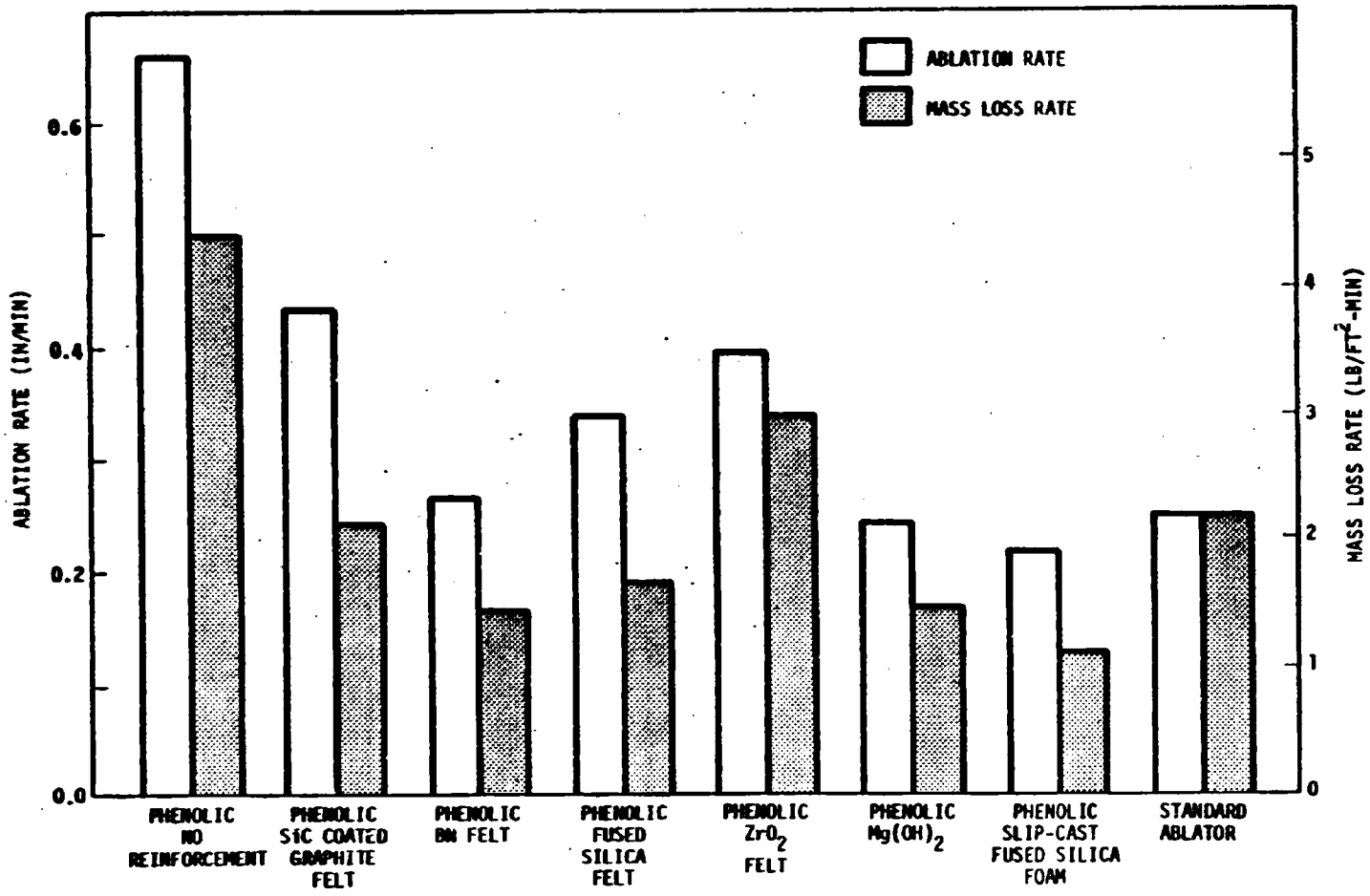


Figure 53. Comparison of Thermal Performance of Embedded Ablators with Standard Ablator at a Heat Flux of 450 Btu/ft$^2$-sec.

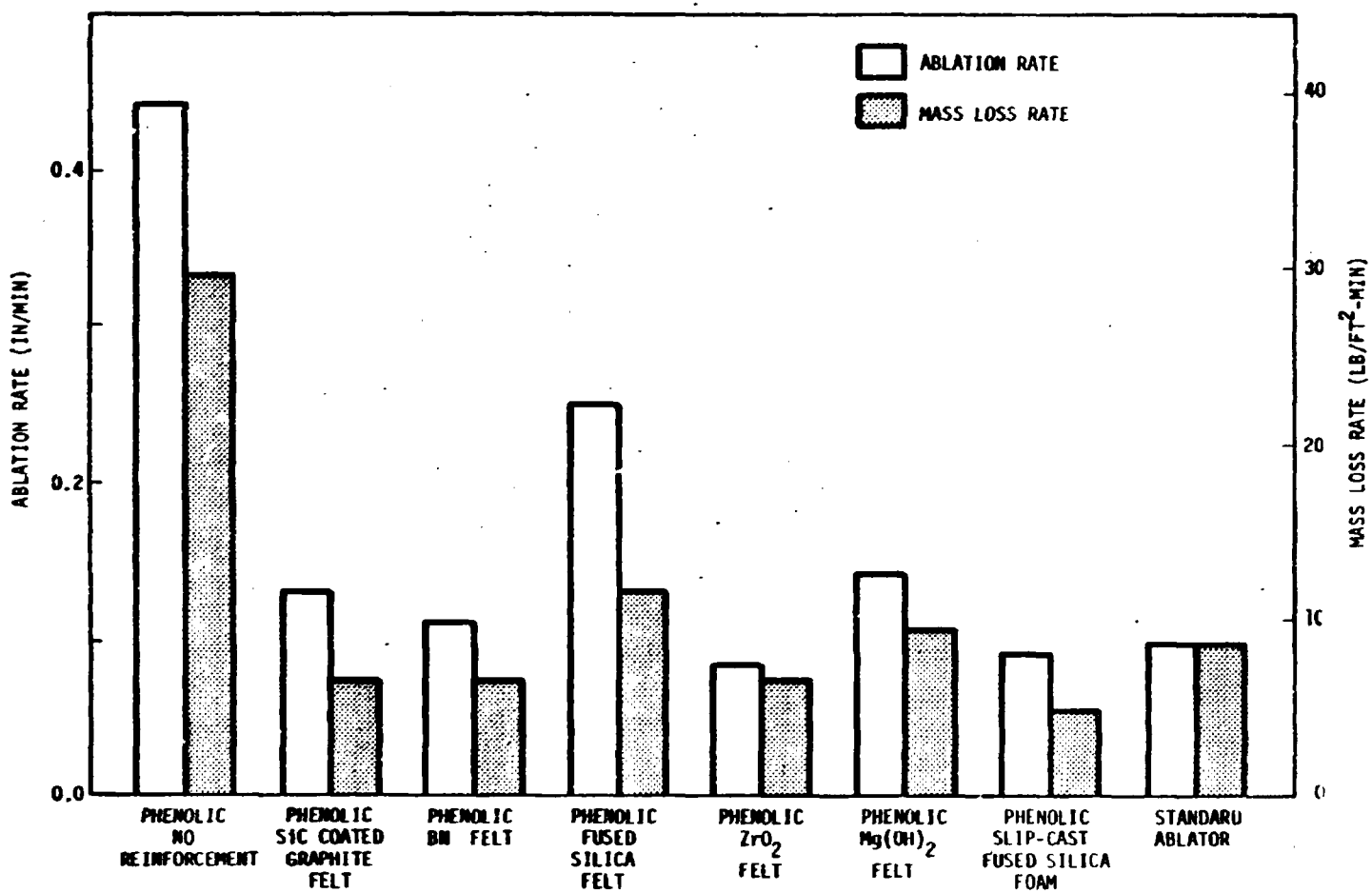


Figure 54. Comparison of Thermal Performance of Embedded Ablators with Standard Ablator at a Heat Flux of 1500 Btu/ft$^2$-sec.

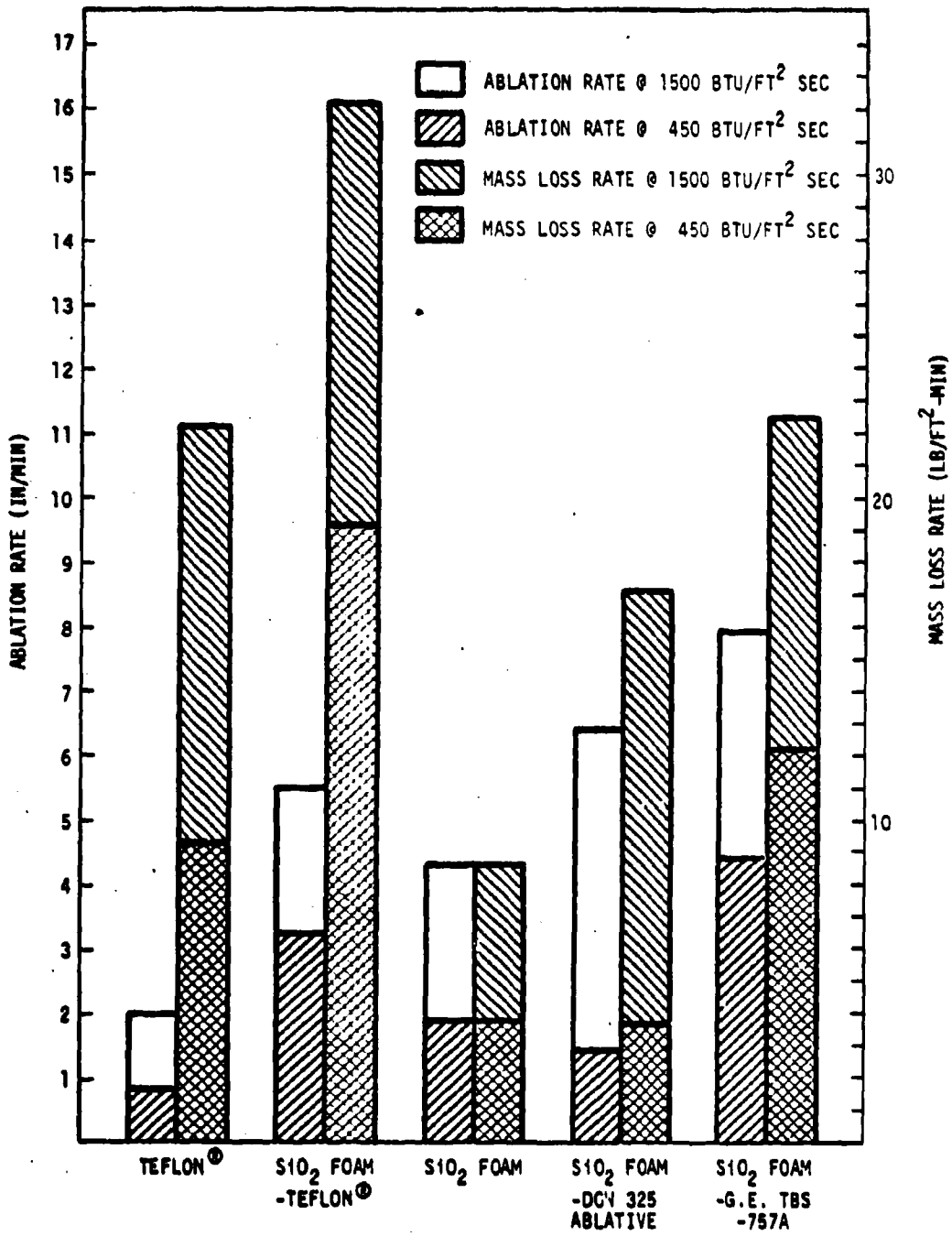


**Figure 55.** Performance of Embedded Ablators Evaluated in Oxy-Hydrogen Rocket Motor Facility at Georgia Tech.

TABLE XXVIII

PHYSICAL PROPERTIES OF THERMAL-PROTECTION TEST-SAMPLES AND FRONTSIDE AND BACKSIDE TEMPERATURES DURING EXPOSURE IN OXY-HYDROGEN ROCKET MOTOR FACILITY AT GEORGIA TECH

| Sample | Sample Thickness (in) | Bulk Density ($lb/ft^3$) | Porosity (%) | Max. Surface Temp. (°F) 450 $Btu/ft^2$-sec | Max. Surface Temp. (°F) 1500 $Btu/ft^2$-sec | Backside Temperature Data (seconds) 450 $Btu/ft^2$-sec: Time Below 100°F | Below 200°F | Duration of Run | 1500 $Btu/ft^2$-sec: Time Below 100°F | Below 200°F | Duration of Run |
|---|---|---|---|---|---|---|---|---|---|---|---|
| Phenolic | 0.38 | 80 | 0 | - | 3360 | 35 | 35 | 35 | 17 | 18 | 18 |
| Phenolic-SiC Coated Graphite Felt | 0.49 | 58 | 37 | 3260 | 3760 | 32 | 42 | 51 | 17 | 18 | 23 |
| Phenolic-HM Felt | 0.48 | 66 | 26 | 3130 | 3650 | 39 | 60 | 60 | 15 | 17 | 23 |
| Phenolic-Fused $SiO_2$ Felt | 0.50 | 60 | 39 | 3130 | - | 51 | 60 | 60 | 3 | 3 | 12 |
| Phenolic-$ZrO_2$ Felt | 0.46 | 90 | 23 | 3700 | 3720 | 48 | 48 | 50 | 32 | 35 | 35 |
| Phenolic-$Mg(OH)_2$ Felt | 0.49 | 74 | 37 | 3440 | - | 57 | 60 | 60 | 16 | 19 | 20 |
| Phenolic-Fused $SiO_2$ Foam | 0.52 | 59 | 49 | 3330 | 3430 | 24 | 43 | 60 | 13 | 22 | 37 |
| Standard Ablator | 0.64 | 107 | 0 | 2910 | 3430 | 60 | 60 | 60 | 37 | 40 | 42 |
| Teflon® | 0.50 | 135 | 0 | - | - | 31 | 32 | 36 | 10 | 11 | 15 |
| Teflon®-Fused $SiO_2$ Foam | 0.52 | 70 | 48 | 2600 | 2900 | 12 | 15 | 15 | 5 | 6 | 6 |
| Fused $SiO_2$ Foam | 0.52 | 25 | 84 | 2850 | 2850 | 3 | 10 | 10 | 1 | 2 | 5 |
| Fused $SiO_2$ Foam - Dow 325 Ablative | 0.68* | 34 | - | - | 2960 | 10 | 11 | 11 | - | - | 5 |
| Fused $SiO_2$ Foam - GE TBS-757A | 0.61** | 33 | - | 2900 | 3520 | 21 | 23 | 24 | 2 | 3 | 5 |

*0.50-inch thick foam with 0.18-inch thick silicone rubber coating.

**0.51-inch thick foam with 0.10-inch thick silicone rubber coating.

## IV. DISCUSSION

### A. Slip-Cast Fused Silica (SCFS) Radome Structures for Thermal Evaluation at General Dynamics/Pomona Ordnance Aerophysics Laboratory

#### 1. Test Program

The test program for 1966 was regarded as sufficiently broadbased to provide the maximum information that could be utilized for comparison with theoretical predictions of the SCFS response in the test environment. There were, however, areas where the performance of the instrumentation and/or hardware presented problems during the tests. In the case of the hardware there was some concern that the water cooled Invar attachment maintained the silica in that region at a lower average temperature than the remainder of the radome and introduced failure bending stresses in the radome at the attachment-radome fore juncture. This would be, in a sense, analogous to internal pressurization of the radome which would introduce discontinuity stresses at that location. It is thought that the failure of four of the test radomes was due to this effect. Another area that offered some difficulty was with the measurement of outer surface temperatures. The use of the 9000 Å wavelength pyrometers was hindered by a focal length requirement of 10-1/2 inches which placed them extremely close to the effluent hot stream and required secondary air cooling of the pyrometer lenses. It was hoped that the cast-in-wall thermocouples would provide secondary surface temperature readings for correlation with the readings from the spectral pyrometers. With these two surface temperature measuring methods it was anticipated that temperatures were obtained with an accuracy of $\pm$ 5 per cent.

The overall instrumentation was geared to "continuous correction" in the sense that all juncture points in the instrumentation scheme were temperature monitored with time for development of compensation base lines. Measures were taken to provide "clean" signals by appropriately shielding the instrumentation feed lines from test cell induced noise. The strain gage instrumentation of each test radome was temperature calibrated to 150° F equilibrium temperature in the laboratory prior to testing.

The reduction of the experimental data for correlation with the theoretical predictions of temperature and stress profiles has been undertaken by personnel of the Applied Physics Laboratory. This was not completed at the time of publishing this report. A preliminary report by APL is presented as Appendix III to this report. There are two very significant conclusions made in the preliminary APL report: (1) the test conditions in the Typhon combustor exhaust stream approximated a flight environment of Mach 8 at 50,000 feet and (2) the thermal shock associated with the material-environment interaction is comparable to that expected for a vehicle accelerating at greater than 100 g's.

No attempt was made to incorporate any of the experimental results into this report for two reasons: (1) the raw experimental data will be compiled in the near future by the Ordnance Aerophysics Laboratory, and (2) a report will be prepared and released in early 1967 by the Applied Physics Laboratory covering the data reduction and correlation with the theoretical analyses. The tests were not as successful as originally planned, but it is estimated that 65 to 70 per cent of the objectives were realized. A synopsis of each test is presented in Appendix IV.

2. QAL Test Radome Fabrication

It is apparent by comparing Figure 3 with Figure 4, that decreasing the time of casting from 63 minutes to 59 minutes did not decrease the cast wall thickness by 20 mils as would be expected from previous studies which have shown the cast wall thickness to be proportional to the square root of casting time. The data in Figures 3 and 4 is misleading, however, since the points shown are the average of two measurements and variation in wall thickness around a given circular cross-section has been observed to be greater than 20 mils.

The cristobalite data in Table V, at first glance, would seem to be contradictory since the radome (VK-5T) soaked at 2200° F for the longer time (75 minutes) appears to have less cristobalite. The difference is not practical and is the result of using a different x-ray cristobalite standard specimen for the data on radome VK-6T which, combined with not making several measurements, gave the apparently contradictory results. Subsequent analyses for cristobalite content were made on a sufficient number of specimens and with a "standard" such that the data provided statistical limits on the cristobalite content.

The modulus of rupture data in Table VI from specimens cut from radomes VK-5T and VK-6T are in the range that is expected with heat treated slip-cast fused silica containing the cristobalite content measured in these structures.

The roundness profiles obtained after heat treatment on radomes VK-5T and VK-6T suggested the resin bonded grain ring will not be beneficial in reducing the out-of-roundness magnitude of the slip-cast fused silica radome structures over that obtained with only the refractory felt support during heat treatment.

It appears the out-of-roundness approached a minimum value for that particular wall thickness and radome weight.

Long term observations on the strengths and cristobalite contents of slip-cast fused silica bodies had suggested that the strength should be related to the amount of cristobalite developed during sintering regardless of the time-temperature-atmosphere relationship used in the sintering process. This observation had apparently been confirmed by the work of Corbett, Sales, and Walton 11/, who determined the variation of the dynamic Young's modulus for SCFS as a function of cristobalite content and per cent of theoretical density. These data are reproduced in Figure 56. The dynamic measurement of Young's modulus is sensitive to the density of a specimen and to the presence of microcracks. In the absence of microcracks, the Young's modulus of SCFS should increase with an increase in density. As can be seen from Figure 56 the dynamic Young's modulus does increase with increasing density until a cristobalite content of 6 or 7 v/o has developed in the sintered specimens. From this point to a cristobalite content of about 14 to 15 v/o the dynamic Young's modulus was essentially constant even though the density of the specimens was increasing. Above a cristobalite content of about 15 v/o the dynamic Young's modulus of the specimens decreased even though the density continued to increase. The interpretation of these data by the investigators was, that the cristobalite which had formed during sintering led to the formation of microcracks and above a certain cristobalite concentration the degree of microcracking overcame the effect of densification on the dynamic Young's modulus. The specimens used in the measurements had been air quenched from the sintering temperature, and the large volume change associated with the conversion of $\beta$ to $\alpha$ cristobalite ($\approx$ 514° F) produced the apparent microcracking.

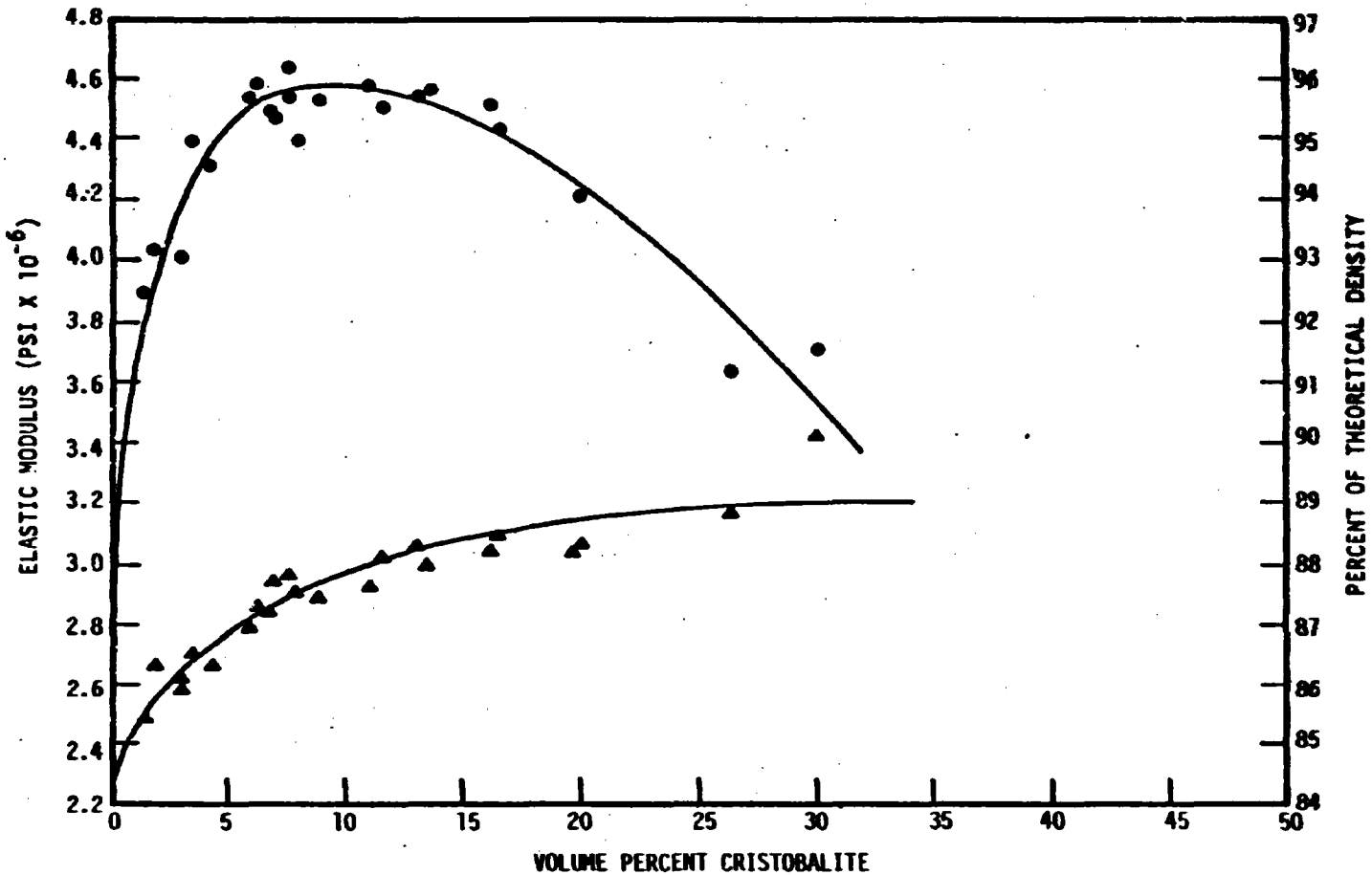


Figure 56. Dynamic Elastic Modulus of Slip-Cast Fused Silica as a Function of Density and Cristobalite Content (Reference 11, p 25).

During the sintering of a particulate compact, strength is developed through the formation of particle-to-particle contacts, or necks, and it is this same phenomena that is responsible for the increase in density and dynamic Young's modulus of such bodies. Also, the microcracks, which occur following the sintering of SCFS, will have a deleterious effect on the strength of the sintered body just as they do on the dynamic Young's modulus. Therefore, it can be inferred that the strength of SCFS should vary with the cristobalite content in the same manner that the dynamic Young's modulus varied with cristobalite content.

An examination of the data for strength and cristobalite content obtained on the test radomes, and presented in Table VII, does not reveal the relationship between strength and cristobalite content that would be expected on the basis of the preceding discussion. Furthermore, the strongest radome, HT-31, (mean strength 3905 psi) had a mean cristobalite content of only 4.6 v/o. If the strength values for these test radomes had been obtained from single test specimens the fluctuation of strength with cristobalite content could be attributed to presence of severe flaws in some of the test specimens. However, the mean strengths were determined from 10 or more test specimens from each radome and this should minimize the variation in observed strengths due to flaws. That the mean strengths for the individual test radomes are real and representative is supported by the correlation between the separate sets of samples from the 3.3-inch skirts and the radomes themselves (Table VIII).

As discussed above, a relationship between strength and cristobalite content is indicated from the work of Corbett et al. Since such a relationship apparently does not exist for the test radomes evaluated to date, additional microstructural variables that were held constant in one case and not in the

other are suspect. The evidence indicates that one variable was the amount of interparticle bonding, which was influenced by a difference in the distribution of particle sizes making up the SCFS bodies and the other, the impurity species and amount present. In the case of the work by Corbett, et al, one particular batch of slip was used to produce all of the samples and were all first casts of the slip. This would dictate that the distribution of particle sizes and the impurities should be the same in each of the samples used to obtain the data of Figure 56. In the case of the test radomes fabricated three batches of fused silica slip were used. These were designated OAL - 1, 2, and 3.

Figures 11 through 13 show the particle size distribution on a mass basis and on a count basis for four batches of fused silica slip obtained at separate times during this period. It is apparent that the mass basis distribution is nearly the same in each case, whereas the count basis distributions are grossly different. Therefore, if quality control is maintained on the basis of mass distributions no significant difference between the two batches of slip would be detected, and, if widely different properties of sintered shapes made from these slips occurred no evidence of any effect of particle distribution would be available. Thus, it now appears that quality control examination of fused silica slips used for hardware production should be made on a particle distribution count basis (this assumes investigations have already been conducted to determine the 'best' distribution). However, the sensitivity of the data to reduction techniques used for the Coulter Counter® leaves a great deal to be desired. The accepted procedure of reduction and interpretation of raw data from the Coulter Counter® requires an iterative procedure based on a variable assumed total number of particles to force the apparent particle distribution to conform to a log-normal distribution. This

is sensitive to the assumed additive increment of particle number used in the iterative procedure and can, unless a great deal of care is taken, introduce significant errors in the particle count distribution which makes comparison and correlation virtually impossible. The magnitude of the errors and the correlation behavior as it affects the data on fused silica slip is under investigation.

The effect on hardware fabrication caused by re-using fused silica slip that was excess to a "first" drain-casting (used to maintain a reservoir of slip) was not known when the fabrication of test radomes for the CAL tests was begun. Previous work [17] had suggested there was not a serious effect on particle distribution. That work, however, used mass particle distribution change as the criteria. Comparison on a particle number basis, however, reveals that there is a definite depletion of the finer particles as shown by comparing Figures 57 and 58 with Figures 59 and 60. The extent of removal is related to the ratio of the volume of solids removed to make the "first" casting to the volume of fused silica slip that made up the reservoir. Obvious techniques that would eliminate the necessity of large volumes of reservoir slip and thus the uncertainty of re-using the slip are precision casting (using a precision male mandrel) and the use of a displacement mandrel which would minimize the amount of slip that would have to be discarded if re-using constituted an impossibility to maintaining control of the hardware physical properties.

The investigation to determine the effect of water saturation and notching indicated that the computed failure stress for the hydrostatically tested radome was in line with the measured strength (modulus of rupture) of specimens cut from the radome. The computed failure stress of 1929 psi for the radome

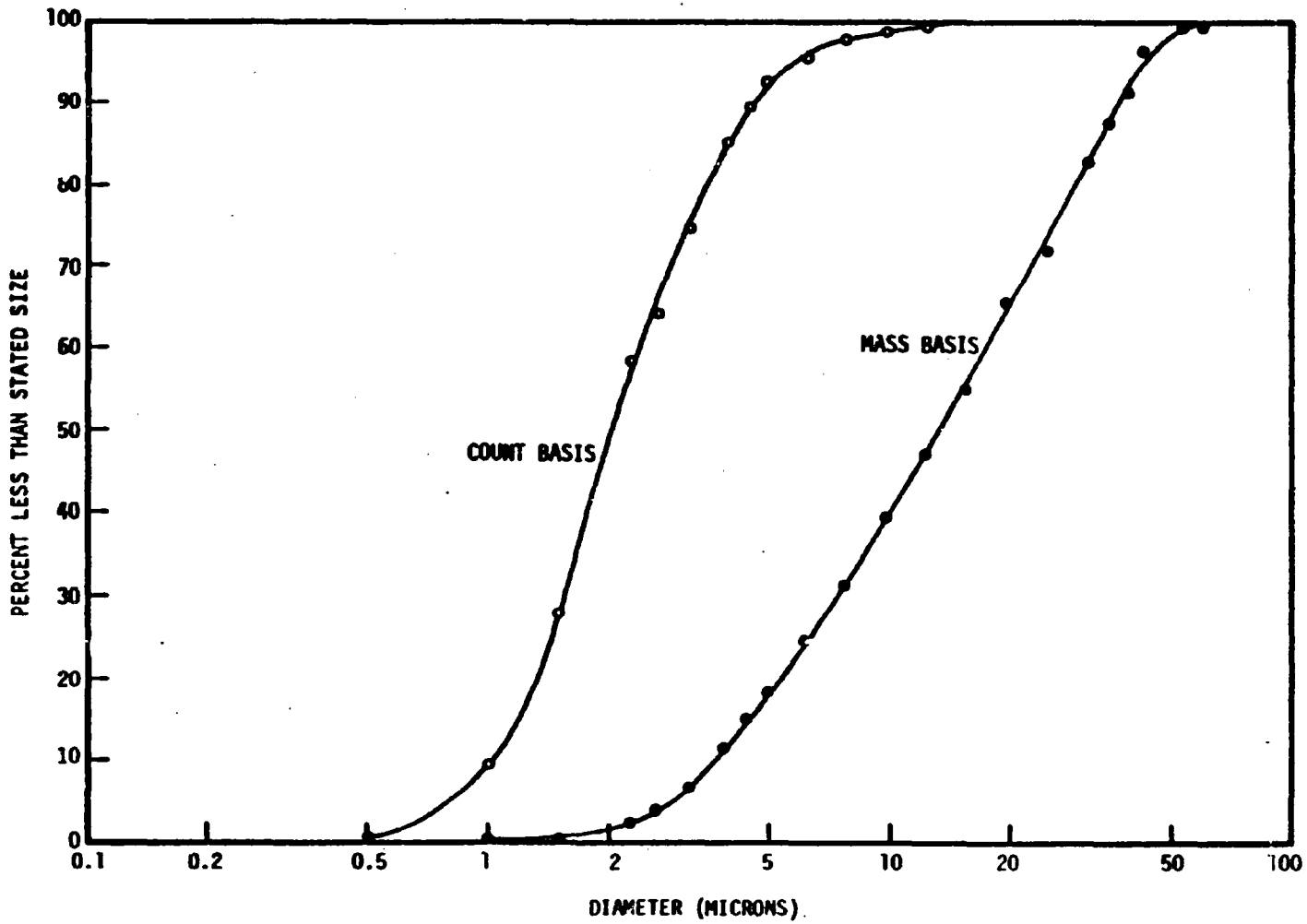


Figure 57. Count and Mass Basis Distributions of Particle Sizes in Fused Silica Slip Batch OAL-2.

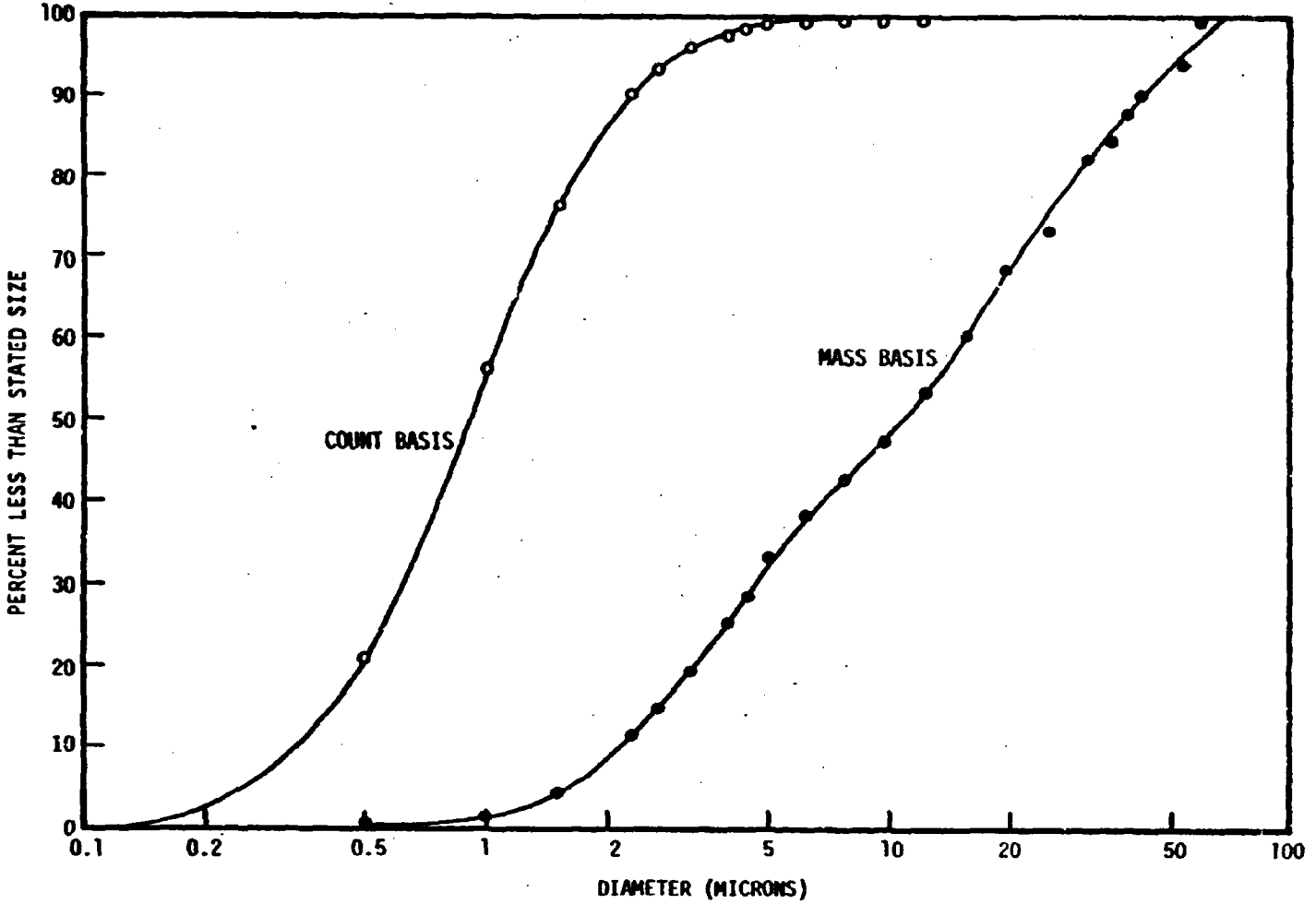


Figure 58. Count and Mass Basis Distributions of Particle Sizes in Fused Silica Slip Batch RE-1 (Reference 101).

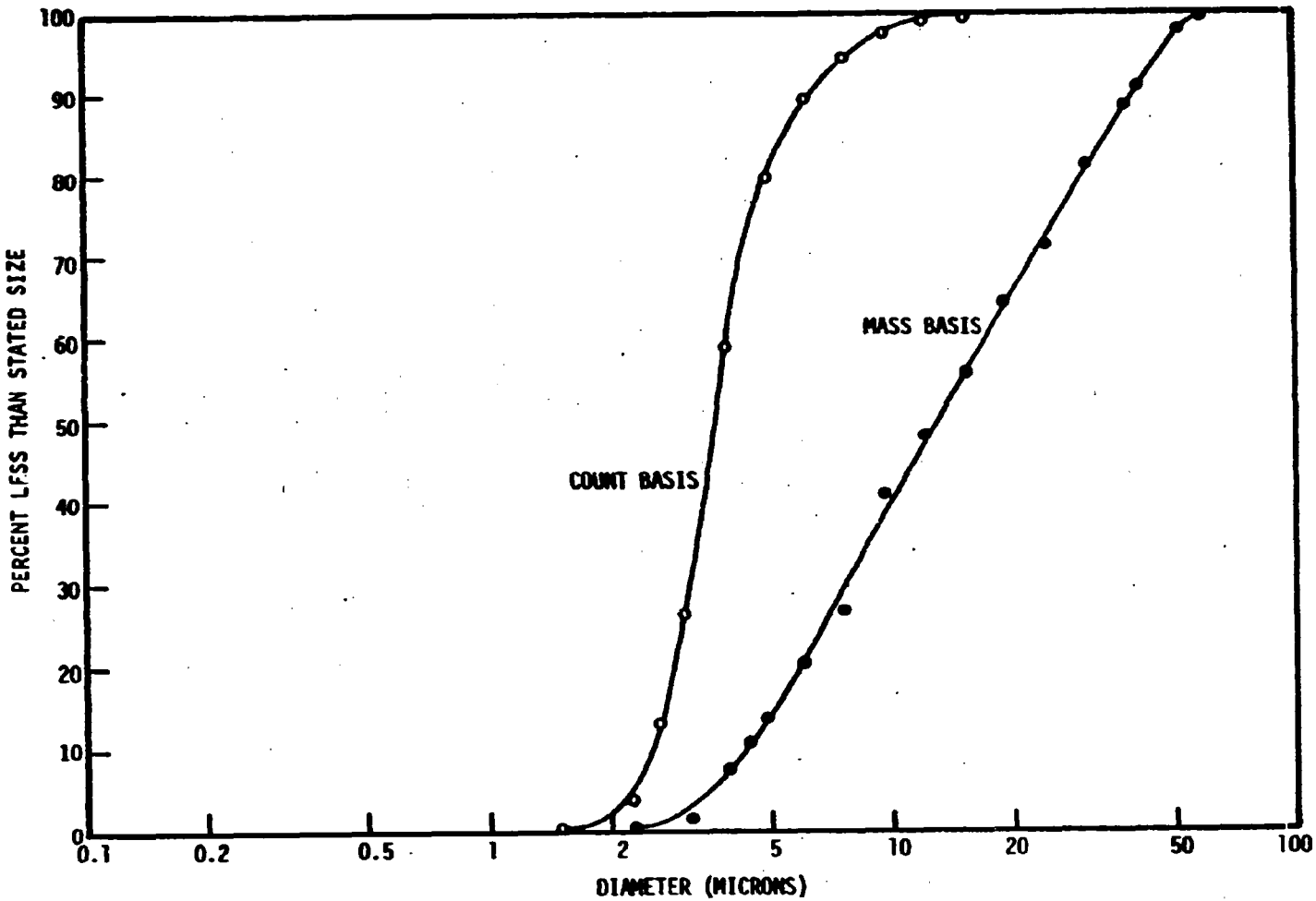


Figure 59. Count and Mass Basis Distributions of Particle Sizes in Fused Silica Slip Batch OAL-2 After One Casting.

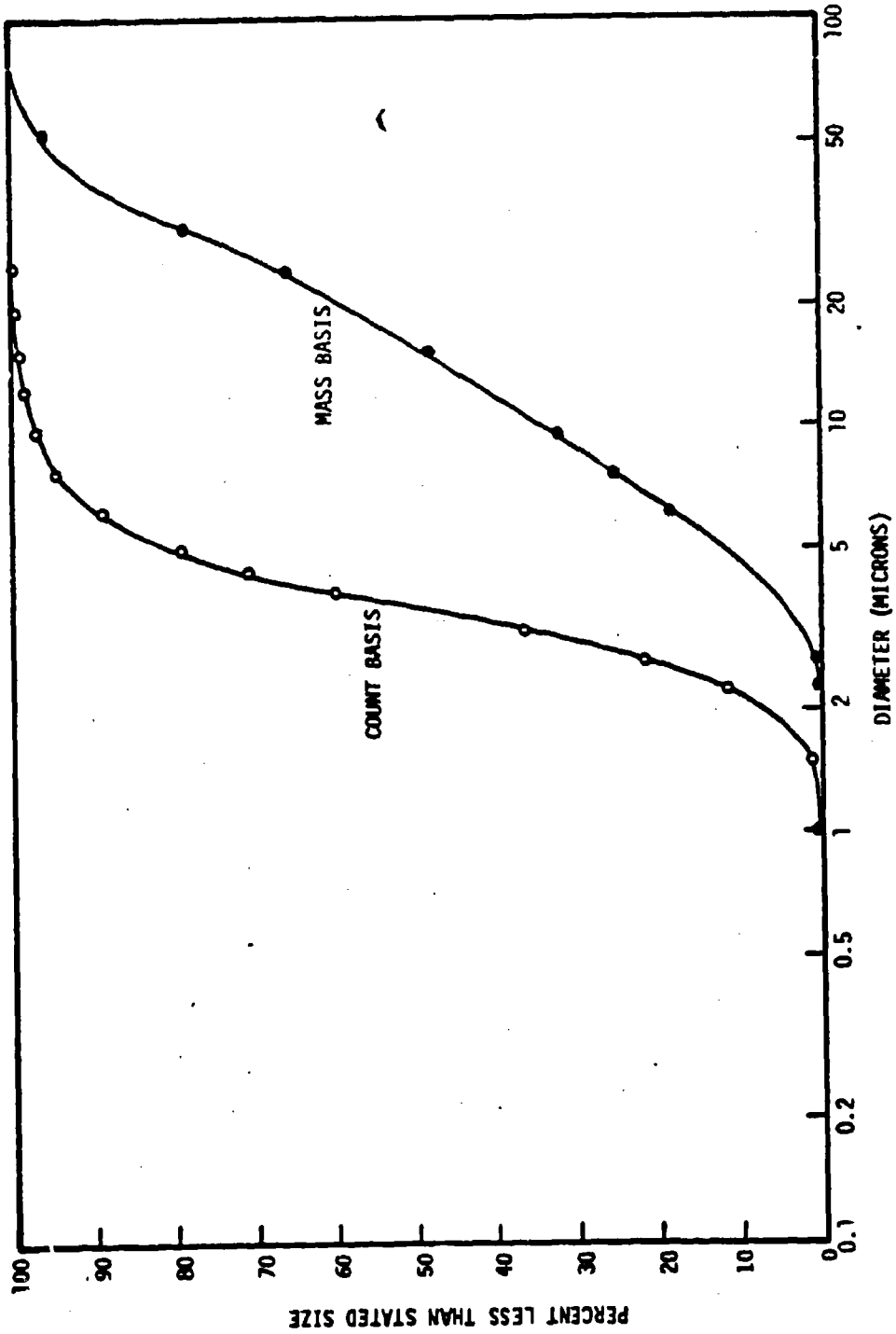


Figure 60. Count and Mass Basis Distributions of Particle Sizes in Fused Silica Slip Batch RE-1 After One Casting (Reference 101).

compared well with the modulus of rupture (2063 ± 103 psi) for the specimens that were wet and notched (Table X). The magnitude of the computed discontinuity stress at the junction of the radome and the forward surface of the attachment ring (1534 psi) precluded the continued use of the hydrostatic test as a proof test for the OAL test radomes and, as a result, the proof testing was accomplished using a cantilever test (Figure 10).

## B. Materials Development and Characterization

### 1. Slip-Cast Alumina-Fused Silica Composites

The solids concentration of the alumina slips, used in the study of alumina-fused silica composites, was selected after investigation of the rheological properties of alumina slips with various solids concentrations. The apparent viscosities of the alumina slips at various solids concentrations (Table XII) indicated that a concentration of 75 w/o alumina was too low. The slip had a very low viscosity and settled out very rapidly. These same data indicated that an alumina content of 85 w/o produced a slip that had a very high viscosity, and experience would indicate that it would have poor casting properties as a result. The slips containing 80 w/o and 82 w/o solids exhibited what is usually considered to be acceptable viscosities for casting slips (i.e. several hundred centipoise).

Since there was the possibility that the difference in concentration of the above slips had led to a difference in the degree of comminution, and that the difference in viscosities observed was influenced more by a difference in particle size than concentration, particle size analyses were performed on the 70 w/o and 82 w/o slips. These represented almost the entire range of concentration investigated. As can be seen from Figure 15, the difference in the

distributions of particle sizes was not great. Therefore, it was concluded that the principle effect was due to concentration.

There was not a significant difference in apparent viscosity on which to base a choice between the slip containing 80 w/o alumina and 82 w/o alumina. Therefore, the choice was in favor of the 82 w/o solids slip from the standpoint of convenience. Since the fused silica slip is normally produced at about 82 w/o solids, calculations of ratio and final solids concentrations for the mixed slips are simplified by having the slips at the same solids concentration.

The settling characteristics, and the apparent viscosity, of the alumina slip that had been milled for 48 hours dictated this as the choice for the best milling time. Since the fused silica slip has satisfactory casting behavior, it is logical to produce the alumina slip so that its settling time was certainly no greater. Also, from the standpoint of mixing the fused silica and alumina slips it would appear desirable to have about equal settling times for each solid constituent. As can be seen from the data of Table XIII, the apparent viscosity of the alumina slip increased significantly between 48 hours and 72 hours grinding time. The rather high apparent viscosity of the slips milled for longer than 48 hours would mitigate against their use even if there were no other reasons. The higher apparent viscosities of the slips milled for 72 and 96 hours are undoubtedly due to finer particle sizes in these slips.

From an examination of Figure 17 it can be seen that the minimum viscosity of the 82 w/o alumina slip occurs at an acid concentration of approximately 0.05 milliequivalents per gram of alumina. It can also be seen that due to the relative rates of change of pH with acid concentrations (Figure 16) and

viscosity with acid concentration (Figure 17) that the point of minimum viscosity can be located more precisely with a knowledge of the acid concentration than with measurement of pH. It is significant, however, that the acid concentration to produce minimum viscosity does correspond to a pH of about 4.0 which is in agreement with the findings of other investigators.

The aging properties of the slip produced in this work are significantly superior to those reported by other investigators. The relatively rapid changes in pH and viscosity observed during the first 24 hours following an acid addition apparently represent a necessary equilibrium period. Following this, however, the change in pH and viscosity of the slip with time are relatively insignificant up to a period of at least three weeks. Therefore, the slip can be said to be essentially stable over this period of time.

No problems were encountered in mixing the alumina and fused silica slips. The casting times of the alumina and alumina-fused silica slips were not significantly different from the casting time normally found with fused silica slip. The cast bodies also possessed green strengths equal to or greater than normally found for slip-cast fused silica.

It is apparent from an examination of Figure 20 that the presence of the alumina in the alumina-fused silica composites accelerated the rate of devitrification of the fused silica at 2200° F. However, as can be seen from an examination of Figures 21 through 24, the effect of devitrification of the fused silica, in the alumina-fused silica composites, is not as drastic as it is for the slip-cast fused silica alone. For example, the elastic modulus of the slip-cast fused silica specimens began to decrease after about 10 to 12 w/o of the fused silica had devitrified. This is in good agreement with similar data obtained in a previous program 11/. However, a decrease in elastic

modulus (attributed to microcracking as discussed in Section A-2) did not appear for the 1:3 alumina-fused silica specimens until 20 v/o of the fused silica present had devitrified. Likewise, over 50 v/o of the fused silica in the 1:1 alumina-fused silica composites had devitrified before a decrease in the elastic modulus was observed, and in the 3:1 alumina-fused silica composites no decrease was observed even after 60 v/o of the fused silica had devitrified.

An explanation of the failure of the elastic modulus of the 1:3 and 1:1 alumina-fused silica composites to exceed that obtained for the slip-cast fused silica alone can be obtained from an examination of the densification obtained with these various specimens. It would normally be expected that the addition of alumina, with its higher elastic modulus, to the fused silica would result in a higher elastic modulus for the composite then for the slip-cast fused silica alone. However, the density data reveals that the slip-cast fused silica had a lower initial porosity than any of the composite specimens, and that after sintering the slip-cast fused silica still had a considerably lower porosity. It is apparently this considerable difference in porosity that prevented the 1:3 and 1:1 alumina-fused silica composites from developing higher elastic moduli than the slip-cast fused silica. That porosity has a very significant effect on the elastic modulus of ceramics is well known. The 3:1 alumina-fused silica composite, of course, did develop a higher elastic modulus than the slip-cast fused silica. This composite behaved more like an alumina body. The elastic modulus of alumina even at 30 v/o porosity would be higher 18/ than the slip-cast fused silica with 13 to 14 v/o porosity.

It can be seen from a study of Figures 20 through 24 that the sintering times at 2200° F necessary to develop the optimum strength in the various

alumina-fused silica composites, the fused silica, and the alumina, are not the same. This, of course, necessitated a judicious choice in the conditions to be employed in sintering the various composites for a comparison of physical properties. One obvious choice was to sinter the specimens of each type of composite, or single component body, separately under the conditions necessary to produce optimum properties in that body. However, this was not considered to be realistic in view of the potential application of slip-cast alumina-fused silica mixtures. In practice, a single body such as a radome would probably contain a gradation of composition, say from the tip to the base, and it could not be sintered in a manner such that the optimum sintering conditions for each composition could be achieved. Therefore, it was decided to sinter all the compositions being studied under the same conditions of time and temperature, and compare the physical properties on this basis.

For the compositions of 0:1, 1:3, and 1:1 alumina-to-fused silica in the maxima in strength properties (as indicated by elastic modulus, Figures 21 through 23) were obviously limited by the amount of the fused silica devitrified. Also, the most drastic reduction in elastic modulus as a result of devitrification was with the straight fused silica body. Therefore, the sintering conditions necessary to develop maximum properties in the fused silica were chosen for sintering all the compositions being studied. From a study of the data contained in Figures 20 through 24 it was recognized that this would result in less than optimum strength properties in the 1:3 alumina-fused silica composite due to too much cristobalite, and in the 3:1 and 1:0 alumina-fused silica bodies due to insufficient sintering. Coincidentally, since the elastic modulus of the 1:1 composite did not vary significantly with cristobalite content over a wide range (Figure 23), this composite would

also be expected to have near optimum strength under the sintering conditions that would produce optimum strength in the fused silica.

It can be seen from the elastic modulus data contained in Table XV and Figures 25 and 26, that the excessive devitrification in the 1:3 alumina-fused silica composite did result in microcracking, as indicated by its less than optimum elastic modulus. The 1:1 composite, on the basis of elastic modulus, did appear to be optimally fired. It is readily apparent from the data of Table XV and Figures 25 and 26 that the addition of alumina to slip-cast fused silica in concentrations of up to 50 w/o does not result in improved mechanical properties. The data indicate that this is due to the increased porosities of these bodies* which are apparently the result of lower packing efficiency for the slip-cast alumina-fused silica composites as compared to slip-cast fused silica. However, even though the porosity is yet higher, the composite containing 75 w/o alumina has mechanical properties almost twice those of slip-cast fused silica.

While the 1:3 slip-cast alumina-fused silica composite does not have mechanical properties as great as the slip-cast alumina alone it did exhibit better thermal shock resistance. In an air-quench test from 2200° F to room temperature a cylindrical specimen of the slip-cast alumina failed catastrophically, while the 1:3, 1:1, and 3:1 composites only microcracked, as revealed by a 15 to 25 per cent reduction in their dynamic elastic moduli**. The slip-

*Even though the properties of the 1:3 composite were not the maximum attainable due to excessive devitrification, the data of Figure 22, coupled with the fact that the 1:1 composite apparently did have optimum mechanical properties, shows that even optimally fired the 1:3 composite would never have mechanical properties exceeding the optimum for slip-cast fused silica alone.

**This same behavior of microcracking on air quench is the explanation for the fact that the 1:1 and 3:1 composites developed significantly higher elastic moduli when furnace-cooled as compared to those presented in Figure 23 and 24.

cast fused silica specimen, of course, exhibited no evidence of deterioration due to the thermal shock.

## 2. Fused Silica Grinding

The data in Table XVI and XIX from the test specimens prepared from the ground fused silica slip is very encouraging when compared with the data from the "as received" fused silica slip specimens. The porosity of the sintered slip-cast fused silica is reduced by grinding and, as would be expected with a constant cristobalite content, the elastic modulus is increased accordingly. If "critical strain" criteria is applied, the strength should increase. That this is the case is demonstrated by the measured modulus of rupture values.

The low critical strain values for the test bars of Table XIX is apparently the result of test bar surface degradation caused by interaction with the plaster mold surface during the slip-casting. The degradation was apparently caused by local cristobalite formation on the test bar surface during sintering which lowered the failure stress level. That this was the case is illustrated by the data of Table XX. The critical strain level was significantly increased (thus higher strength) by the use of a graphite parting film on the plaster molds.

The importance of controlling the particle size of the fused silica slip was demonstrated by the increased strength of the test bars from the "ground" fused silica slip and by the uniform wall thickness and internal tip region definition obtained using the "ground" fused silica slip. These investigations and the results of using the graphite parting film, have suggested methods for greatly improving the strength and quality of slip-cast fused silica radomes using commercial fused silica slip. A third method of improving the sintered

fused silica would be by decreasing the cristobalite growth during sintering, thus allowing longer time-at-temperature for increased densification before a critical cristobalite level is reached. The importance of impurity control, as it influences cristobalite growth, has been demonstrated by the work of Harris, Gorton and Sales 19/. That work, with filament wound fused silica radomes, has shown that the impurity species and level of contamination greatly influences the cristobalite growth rate and the strength of the filament wound silica structures.

3. Metal Films

An examination of Figures 33, 35, 37, and 39 reveals that the nature of the slip-cast fused silica substrate (i.e. glazed or unglazed) has very little effect on the appearance of screen printed platinum films before firing. These same figures reveal more of an effect of varying the screen-to-substrate distance, although even this effect is not major. The absence of a screen-to-substrate clearance, when an unglazed substrate was used, does not appear, in general, to produce as sharply a defined edge on the screened films. This is particularly noticeable for pastes number 7724 and 7450. This lack of definition was apparently due to an enhanced capillary effect between the screen threads and the unglazed substrate, when the substrate and screen were in contact, causing the pastes to flow outward and forming a serrated edge on the film. Also, frequently with the more viscous pastes, a spotty film was produced when there was no screen-to-substrate clearance. This effect is shown in Figure 33 for paste number 7724. This was obviously caused by the highly viscous paste not being able to get under thread intersections.

An examination of Figures 34, 36, 38, and 40 does reveal an effect of the nature of the substrate (i.e. glazed or unglazed) on the condition of the

fired platinum films. There was a pronounced "crawling" of the fired films on the unglazed substrates, particularly for pastes 7724 and 7450. In the case of paste number 7724 this was probably due in part to the absence of a ceramic frit in the paste. It is possible that a low amount, or the nature, of frit in paste number 7450 accounted for the severe "crawling" of this film. In any event, the effect was minimized on a glazed substrate. As can be seen in Figures 34, 36, 38, and 40, all of the pastes, after firing, produced films of platinum agglomerates, rather than a continuous, unbroken film.

The results of the determination of the electrical characteristics of the screen-printed platinum films are in good agreement with the qualitative observations made on these films from microscopic examination. From a microstructural viewpoint it was concluded that paste number 7449 produced the most satisfactory film. From an examination of the electrical characteristics reported in Table XXII the same conclusion can be drawn. This paste is the only one of the four that produced any electrically continuous elements of 2-inch length on an unglazed slip-cast fused silica substrate. Also, it can be concluded that, in general, the uniformity of the films produced with this paste were better. The percentage confidence interval was lowest for films made with this paste, indicating a greater uniformity over a given element. Also, the mean film resistivities of the various elements produced with paste 7449 were more nearly the same value, indicating good uniformity from element to element. The principal shortcoming noted with this paste was an apparent inadequacy in producing a continuous film in the most narrow width, 1/64-inch. This, however, was overcome with the use of a multiple-coating technique as can be seen from the data of Table XXIII.

In general, it appears from the data of Table XXII that it was more difficult to produce electrically continuous films, with a single application of a paste, on unglazed substrates. The reason for this is not entirely clear. This may be a result of the fact that the surface roughness of the unglazed substrate was greater. A microscopic examination of single coat films showed them composed of essentially a single layer of platinum spheres. The fact that the unglazed slip-cast fused silica substrates had a greater surface roughness may have kept the platinum particles from lying in the same plane, on the surface, and thereby reduced the number of particle to particle contacts. Another possible explanation of the improved performance of the glazed surface may lie in a fluxing action of the spodumene glaze. This glaze may have acted very similar to the glass frits that are used, in some of the platinum pastes, to enhance the adhesion and integrity of the fired films. The question, however, appears to be only academic since, as can be seen from the data of Table XXIII, films with satisfactory integrity and uniformity could be produced on either unglazed or glazed substrates with thicker films obtained by multiple coating. The only difference noted from these results is that the glazed substrate did appear to produce films with slightly lower resistivities.

The electrical conductivity of platinum films produced with paste number 7449, particularly with multiple coating, are satisfactory for antenna applications. Also, the accuracy with which the screen printing process reproduces the intended pattern would appear to provide satisfactory dimensional control for the fabrication of antenna elements. The effects of such factors as the particulate nature of the films, and the serrated and beveled edges of the films can be evaluated only through experimentation with these films in an antenna application. In general, however, the screen printing process would

appear to be satisfactory for the deposition of antenna elements in the fabrication of integrated radome-antennas.

The behavior of the platinum films in a thermal environment appears satisfactory for integrated radome-antenna applications. The mechanical response test, even though qualitative, indicated no loss of film adherence when the film was protected from the heat source by the fused silica substrate. The condition where the fused silica was softened and eroded almost through to the platinum film is probably a more severe condition than would be encountered in a practical situation.

The study of the electrical stability of the screen-printed, platinum films in a thermal environment indicated satisfactory performance. The electrical continuity of the films was maintained up to the maximum test temperature. However, an examination of Figures 41, 42, 44, and 45 show that a uniform increase in the electrical resistivity of the platinum films with temperature can be expected only to the temperature at which they were fired during application. This is undoubtedly a sintering phenomena. When the films are raised in temperature above that used in their preparation additional sintering occurs and the electrical resistivity decreases. However, when the films have been fired at temperatures equal to, or greater than, the highest temperature to which resistivity measurements are to be made, the change in resistivity with temperature is a monotonically increasing function. As can be seen from Figure 46 the form of this function is not quite the same as is found for bulk platinum. The reason for this is not immediately obvious. However, it is probably a result of the fact that the film, which contracts more on cooling, than the fused silica substrate, is in a state of strain at room temperature. Upon heating this strain is relieved and a small, uniform,

decrease in resistance results. Therefore, the ratio of the resistance of the film at 1000° C, for example, to its resistance at room temperature would be less due to the absence of strain.

The fact that the temperature-resistance relationship for screened platinum films appears to be reproducible indicates that such films could be used as thermal sensors. By virtue of the fact that the films have low mass and are intimately bonded to the surface these sensors should be capable of providing rapid, accurate indications of surface temperature. The limitation of melting temperature of the platinum would undoubtedly preclude their use on the exterior surface of radomes under reentry conditions, but they could probably function quite satisfactorily as backside surface temperature indicators. The results of this study indicate that knowledge of the resistance of the film at, or near, room temperature and the temperature-resistance relationship given in Figure 46 is all that would be required to use the film as a thermal sensor. However, if the screened platinum film is used on a substrate other than fused silica, experiments should be conducted to ascertain whether or not the resistance-temperature function shown in Figure 46 describes the change in resistance with temperature of the film on the substrate of interest. Also, if the films were to be considered for use as thermal sensors under cyclic thermal conditions, experiments should be conducted to ascertain whether of not the reference point resistance changes during cycling. Results obtained during this study indicated that the change in resistance of a film became negligible after about two hours at continuous exposure to temperatures above the initial sintering temperature of the film. However, there were indications that the absolute value of resistance of the film at any temperature

did change with thermal cycling even though the relative resistance change with temperature (Figure 46) did not change with thermal cycling.

4. Felted Ceramics

By firing the experimental slag wool-clay boards in a fused silica foam sagger, it was found that one 12 x 12-inch board could be heat treated per day. Also, the use of the sagger eliminated the need for placing the board in a cold furnace, heating to firing temperature and then cooling the furnace back to room temperature. It can be seen in Figure 48 that the heating and cooling rates were sufficiently small to prevent thermal shock degradation of the felted board during the heating or cooling phases of the firing schedule.

The low strength obtained for the first boards fired in this manner was thought to be due to an inhomogeneous felted board. The large variations in fired density for individual modulus of rupture specimens reflected in Figure 49 support this conclusion.

By chopping the mineral wool fiber before adding it to the slurry a more homogeneous board was obtained and an improvement in strength was realized. While a modulus of rupture value of 378 $\pm$ 70 psi was obtained for the unchopped mineral wool - L-1 ball clay felted boards with an average density of 85 lb/ft$^3$, boards S-15, S-16, and S-17 (Table XXIV) made with chopped mineral wool and L-1 ball clay had a modulus of rupture of 1079 $\pm$ 65 psi when the density was only 74.3 $\pm$ 2.7 lb/ft$^3$. The chopping of the mineral wool fiber also resulted in a compact which required less pressure for compaction to the desired dry thickness of 3/4-inch.

In reference to Table XXIV, it should be noted that the density based on the simple measurement of the weight and characteristic dimensions of a test sample is not, in general, as precise as that obtained by water displacement.

Therefore, no significance is given to the indication in Table XXIV that some boards increased in density while others decreased in density upon firing.

The effect of the clay on the fired strength of the slag wool-clay boards can best be examined by considering strength to density ratios. For the L-1 clay this ratio was 14.5, for the T-5 clay the ratio was 14.6, and for the T-1 clay the ratio was 19.2.

The T-1 clay had the finest particle size distribution (Figure 50) of the three clays examined and this explains the long drain times encountered when this clay was used. The finer particles in this clay could also be considered partially responsible for the increased strength to density ratio of felts made with it. However, the particle size distribution of clay T-5 was closer to that of T-1 than to that of L-1 but did not result in an increased strength to density ratio. Alkali contents of T-1 and T-5 were similar and, therefore, there should not have been any difference in fluxing action between the two clays.

The amount of compression prior to firing appeared to be more important than the firing time from the standpoint of obtaining a mechanically strong slag wool-clay board.

The ease with which successful felts were prepared from fused silica, boron nitride, zirconia, magnesia, and silicon carbide coated graphite fibers added encouragement to the program. The felts were easily formed to a porosity of 80 to 90 per cent, and the pore structure appeared ideal for infiltration and transpiration.

While efforts to strengthen the felts through heat treatment met with little success, this does not preclude the possibility that the felts could be significantly strengthened through sintering. The extensive research

required to resolve this issue was simply beyond the scope of this program. Since the felts were to be impregnated with phenolic it was possible to obtain reasonable results under this program without prestrengthening the felts.

## C. Composite Thermal Protection Systems

### 1. Charring Ablators

While charring ablators are the most important heat protection materials in use today for moderate to high heat flux and relatively short-time exposures, they suffer from three major limitations. First, they cannot be used for applications, such as winged leading edges and small-angle nose cones, where dimensional stability is critical. Second, they are least effective when used in low-altitude flight situations where high oxygen concentrations and large shear forces are encountered, as their efficiency is markedly dependent upon char retention. Third, chars seriously attenuate electromagnetic signals.

### 2. Embedded Ablator

It is becoming more apparent that the future development of thermal protection systems must depart from the present choice of ablators, in a number of applications. However, as the departure is made two things must be kept foremost in mind. First, the composite approach appears most promising since single homogeneous materials generally perform adequately for only very short times. Second, the properties of a thermal protection system must be tailored to suit the particular environments to be encountered before efficient operation can be realized. Different sets of environmental parameters will require different component materials and, perhaps, different physical forms of construction. Thus, it becomes necessary to develop a variety of heat shield

materials to accommodate a wide spectrum of thermal environments, as, even today, different types of thermal protection are used on a single vehicle. It follows that the promise of a heat shield varies directly with its versatility.

The embedded ablator holds the promise of providing a practical solution to the problem of thermal protection against moderate to high heat flux and relatively short-time exposure in those situations where a charring ablator alone is not acceptable because of dimensional stability requirements and/or wake contamination considerations. The concept encompasses the composite system consisting of an ablative material embedded in a ceramic matrix. This composite approach shows considerable promise as a means of overcoming the brittle tendency of ceramic materials and achieving a high degree of shape stability. In addition, this type of composite construction is extremely versatile, as once a suitable matrix has been developed it can be infiltrated with a wide variety of ablative materials giving the designer a high degree of flexibility with a single matrix material. Also, graded heat shields can be prepared to accommodate the unusual thermal responses associated with advanced designs. For example, the impregnant can be graded in depth to reduce properties mismatch, or a single matrix component can be impregnated with high temperature ablator in the region of turbulent heating to ensure stability and with a low temperature sublimer in the region of laminar heating where vapor injection has a strong influence.

Candidate matrix materials for the impregnated-ceramic systems are ceramic foams and ceramic felts. Filament wound matrices are currently ruled out because of their low operating temperatures. The use of ceramic felts is a rather new concept and, thus, has received only limited attention. However, foamed ceramics have received considerable attention, and a number of the

requirements for foams and their associated impregnants have been cited. At the current state-of-the-art, impregnated foams offer the distinct advantage over charring ablators of high dimensional stability, but only at the expense of a lower heat dissipating efficiency; ceramic matrices with more uniform physical and mechanical properties and higher allowable operating temperatures must be developed before the full potential of the embedded ablator can be realized. These findings were derived from the literature search which was conducted for the purpose of assessing the state-of-the-art on heat shields.

The results obtained under this program clearly demonstrate that improved ablative performance can be realized through the use of highly refractory reinforcements which are already available commercially. Figures 53 and 54 which are normalized using a standard ablator obtained from NASA as a basis, show that several high-temperature fibers performed favorably from the standpoint of minimum-weight-design considerations. The performance of the systems based on the refractory fibers was also favorable from the standpoint of geometrical stability, which is especially encouraging since these systems contained only 10 v/o fibers as compared to the 50 v/o normally associated with this type of heat shield.

Figure 55, which is normalized using 25 $lb/ft^3$ fused silica foam as a basis, shows that no advantage was realized when Teflon® was embedded in the silica foam. This figure also shows that no benefit was derived from the use of the trowellable silicon materials as sacrifical surface layers.

Also, in this program, the embedded ablative concept based on ceramic felts has been shown to be feasible. Hopefully the embedded ablator will provide the following advantages over the charring ablator:

1. Increased efficiency because of the hot reaction zone provided for transpiring gaseous products by the matrix.

2. Increased char thickness due to diffusion barriers within the matrix.

3. Ultimately an increase in radiative cooling as matrix materials with higher service temperatures are developed.

4. Increase in dimensional stability.

5. Greater versatility.

6. Improved char retention in high-shear environments.

The use of a ceramic felt in an embedded ablator may offer the following advantages over the use of a ceramic foam:

1. The felt would have a completely open pore structure and would be more easily infiltrated, yet the pores in a felt are distinctly "interwoven" and could effectively retain an impregnant.

2. A felt may be more thermal shock resistant than a foam, owing to the distinct parallel structure. A felt may be more reliable mechanically for the same reason. Therefore, a modular design might not be a requirement when a felted matrix is employed.

3. The completely open porosity of a felt would aid in allowing gaseous decomposition products to escape without structural degradation. Thus, thermoplastic impregnants would be more

effective in a felted matrix than in a foamed matrix. In addition, a felt would provide a hot reaction zone with an extremely high surface area and would promote very close thermal equilibrium for any transpiring products. In particular, the clean ablators, or subliming ablators, might be much more effective when incorporated in a ceramic felt.

## APPENDIX I

### DIAMOND MACHINING OF SCFS RADOMES AND TEST CYLINDERS

The machining of SCFS requires the use of diamond tooling. The material can be rough machined using conventional carbide tooling but extreme tool wear occurs and surface finish cannot be controlled.

The major problem associated with diamond machining the material is developing methods of holding the part during the machining operation. In the case of the test cylinders made up during this period this was accomplished by epoxying the cylinders to discs of aluminum which could be chucked in a lathe. This sufficed for accomplishing the machining on the test cylinders since interest was focused on one end only; the other end was epoxied to the aluminum disk which was subsequently cut off.

In the case of the test radomes, however, this simple technique was not adequate since only one end (the base) could be interfered with and this obviously was the end that required machining. This posed the problem of developing a method of holding the radome during machining. Two methods were considered, viz: (1) precision female tooling, made of plaster using a sintered SCFS radome as the plaster molding-form, with steel supports; the radome being held in the tooling with axial loading through a rotating shaft inserted from the open base or by the application of a lower pressure (vacuum system) through the plaster and (2) by constructing a vacuum chuck from steel pipe which would incorporate support points for the radome near the tip and about half-way up the radome. Of the two methods, the second was considered to be the most reasonable from a standpoint of providing permanent tooling. The first method does, however, provide a means of using the basic support

tooling for any configuration (up to the size of the basic support tooling) that would require machining since only the plaster tooling would require replacement.

In the case here it was considered reasonable to make up the vacuum chuck as outlined in (2) above since the least cost and time would be involved and the configuration is the only one under consideration for this program effort. The vacuum chuck constructed is shown in Figure 61.

The machining of the SCFS test cylinders and radomes was accomplished using two diamond tools. A 4 :: 0.035 x 3/8 DIAR Std. D 60 150 MB 1/8 cut-off wheel was used to cut through the walls and a 4 x 0.187 x 3/8 DIAI Std. D 100 MB 1/8 wheel was used to machine the inner surface of the radomes and test cylinders for insertion of the attachments and simulated attachments respectively. A tool periphery speed of 5400 feet per minute was used for all work on the SCFS structures.

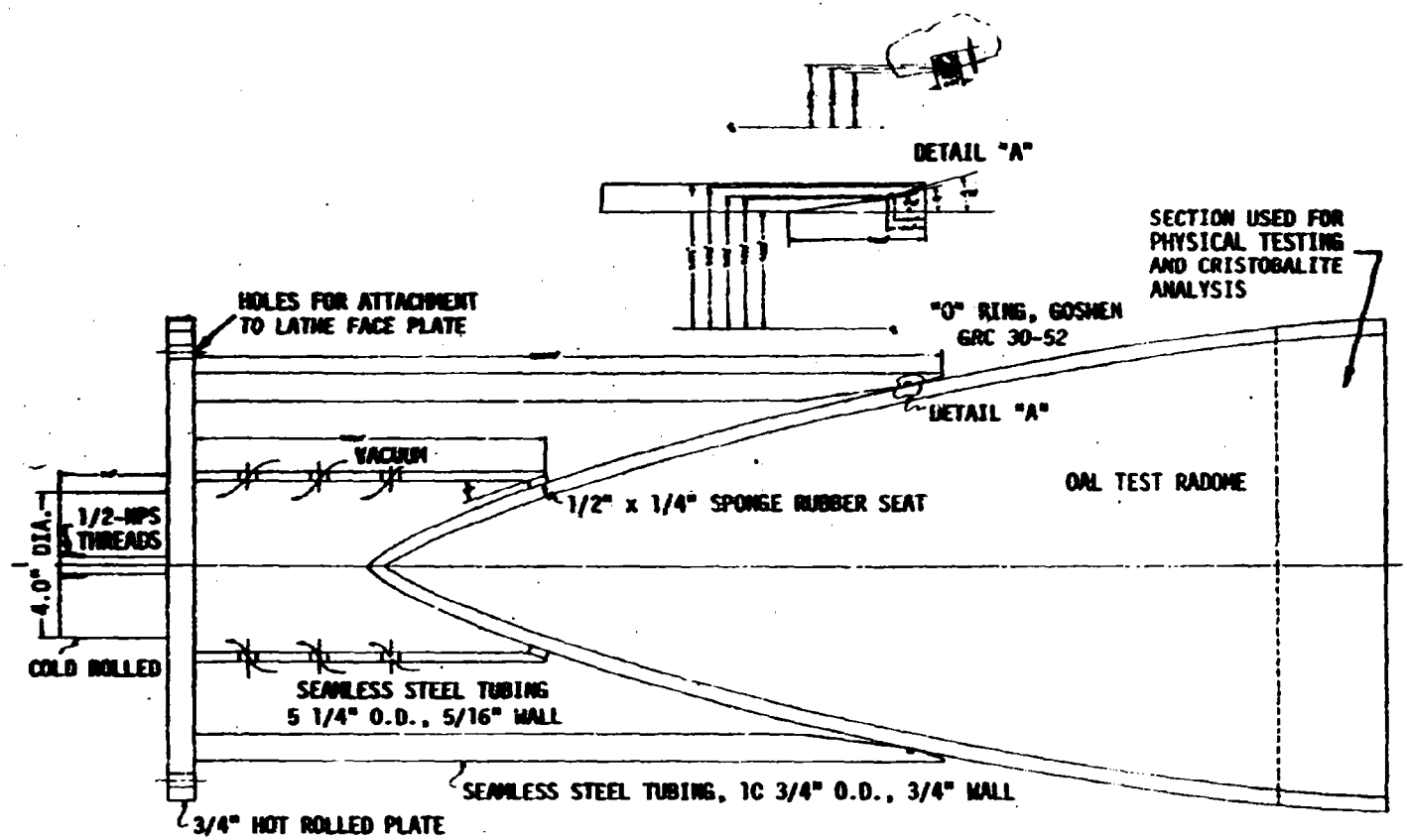


Figure 61. Drawing of Vacuum Chuck Constructed to Hold SCFS OAL Test Radomes During Diamond Machining.

## APPENDIX II

## ANALYSIS OF ATTACHMENT SYSTEM USED ON 1966 OAL TEST RADOMES

### Nomenclature

$a_h$ - Horizontal Acceleration (6.9 ft/sec$^2$)

$a_v$ - Vertical Acceleration (6.9 ft/sec$^2$)

$C_p$ - Pressure Coefficient

$D_i$ - Inside Diameter of Radome

$D_o$ - Outside Diameter of Radome

$E_a$ - Young's Modulus of Elasticity for Adhesive (3 x $10^5$ psi)

$E_i$ - Young's Modulus of Elasticity for Invar (20.5 x $10^6$ psi)

$E_s$ - Young's Modulus of Elasticity for Slip-Cast Fused Silica (4.5 x $10^6$ psi)

$F_{ID}$ - Inertia Force Downward

$F_{IR}$ - Inertia Force Rearward

$F_y$ - Vertical Aerodynamic Pressure Force

$g$ - Acceleration Due to Gravity (32.2 ft/sec$^2$)

$\gamma$ - Ratio of Specific Heats (1.4)

$\ell$ - Total Length of Radome (25.0")

$\ell_1$ - Distance from Base of Radome To Location of $F_y$

$\ell_2$ - Distance from Base of Radome to Inertia Center (6.25")

$M_\infty$ - Mach Number of Free Stream (2.2)

$M_I$ - Total Inertia Moment

$M_{I(cc)}$ - Inertia Moment Counterclockwise

$M_{I(cw)}$ - Inertia Moment Clockwise

$M_R$ - Resultant Moment due to Inertia and Aerodynamic Loading

$P_\ell$ - Local Static Pressure on Radome

$P_\infty$ - Free Stream Static Pressure

$q_\infty$ - Free Stream Dynamic Pressure

$R_i$ - Inside Radius of Radome

$\sigma_{avg}$ - Average Tensile Shear Stress in 901/B-1 Adhesive

$\sigma_{IC}$ - Compression Stress in Radome Wall Due to $F_{IR}$

$\sigma_{max}$ - Peak Tensile Shear Stress in 901/B-1 Adhesive

$t_a$ - Thickness of Adhesive (0.005")

$t_i$ - Thickness of Invar (0.080")

$t_s$ - Thickness of Radome

$\mu_\infty$ - Free Stream Velocity

W - Weight of Radome

x - Distance Along Centerline From Tip of Radome

y - Outside Radius of Radome for a Given Value of x

$y_o$ - Outside Radius of Radome At Base

The test radomes will experience loading from several mechanisms during the OAL tests. The major loading consideration will be a result of the aerodynamic forces acting on the test radomes during insertion into the Mach 2.2 effluent from the Typhon combustor. This will induce a significant downward force on the radome and a minor force in the rearward direction. Of secondary importance are the inertia forces which are induced by the Mauler sled acceleration of the test radome into the hot stream. The force systems are illustrated in Figure 62.

The effect of the forces on the radome can be determined by resolving the force systems into a bending moment which acts on the radome and develops

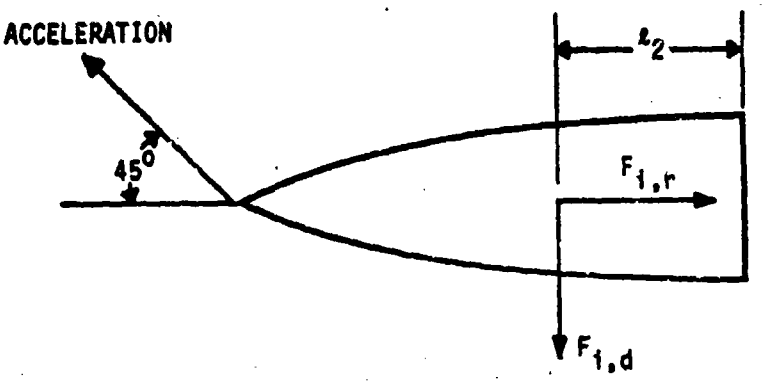


(a). INERTIA FORCES

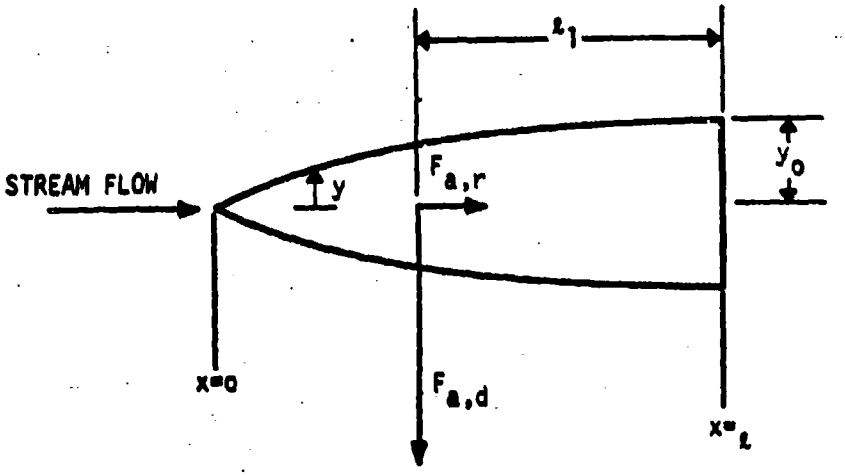


(b) AERODYNAMIC FORCES

Figure 62. Force Systems Acting on SCFB OAL Test Radomes.

the stress pattern in the radome wall. This bending moment is then used to compute the peak tensile shear stress in the attachment epoxy bond line using the Volkerson Equation 102/.

A. Inertia System

1. Clockwise Moment

$$F = Ma$$

$$F_{IR} = \frac{W}{g} a_h$$

$$\sigma_{IC} = \frac{4 W a_h}{\pi g (D_o^2 - D_i^2)}$$

The equivalent clockwise bending moment will be:

$$M_{I(cw)} = \frac{W a_h (D_o^2 + D_i^2)}{8 g (D_o + D_i)} \qquad (1)$$

2. Counterclockwise Moment

$$F = Ma$$

$$F_{ID} = \frac{W}{g} a_v$$

The equivalent counterclockwise bending moment will be:

$$M_{I(cc)} = \frac{W a_v \ell^2}{g} \qquad (2)$$

3. Combined Inertia Bending Moment

$$M_I = \frac{Wa_v \ell_2}{g} - \frac{Wa_h (D_o^2 + D_i^2)}{8 g (D_o + D_i)}$$

Since $a_v = a_h$

$$M_I = \frac{Wa}{g} \left[ \ell_2 - \frac{D_o^2 + D_i^2}{8 (D_o + D_i)} \right] \qquad (3)$$

$M_I = 78$ ft $lb_f$ (Counterclockwise)

B. Aerodynamic System

The moment acting on the radome was calculated assuming that the upper half was exposed to a pressure obtained from the Cp versus $\frac{x}{\ell}$ curve shown in Figure 63. The lower half of the radome was assumed to be exposed to the static pressure.

1. Counterclockwise Moment

The counterclockwise moment produced by the vertical components (Figure 62) of the surface pressure forces is

$$dM = (p_\ell - p_\infty) \; 2y \; dx \; (\ell - x) \qquad (4)$$

Now

$$(p_\ell - p_\infty) = C_p \, q_\infty \qquad (5)$$

where

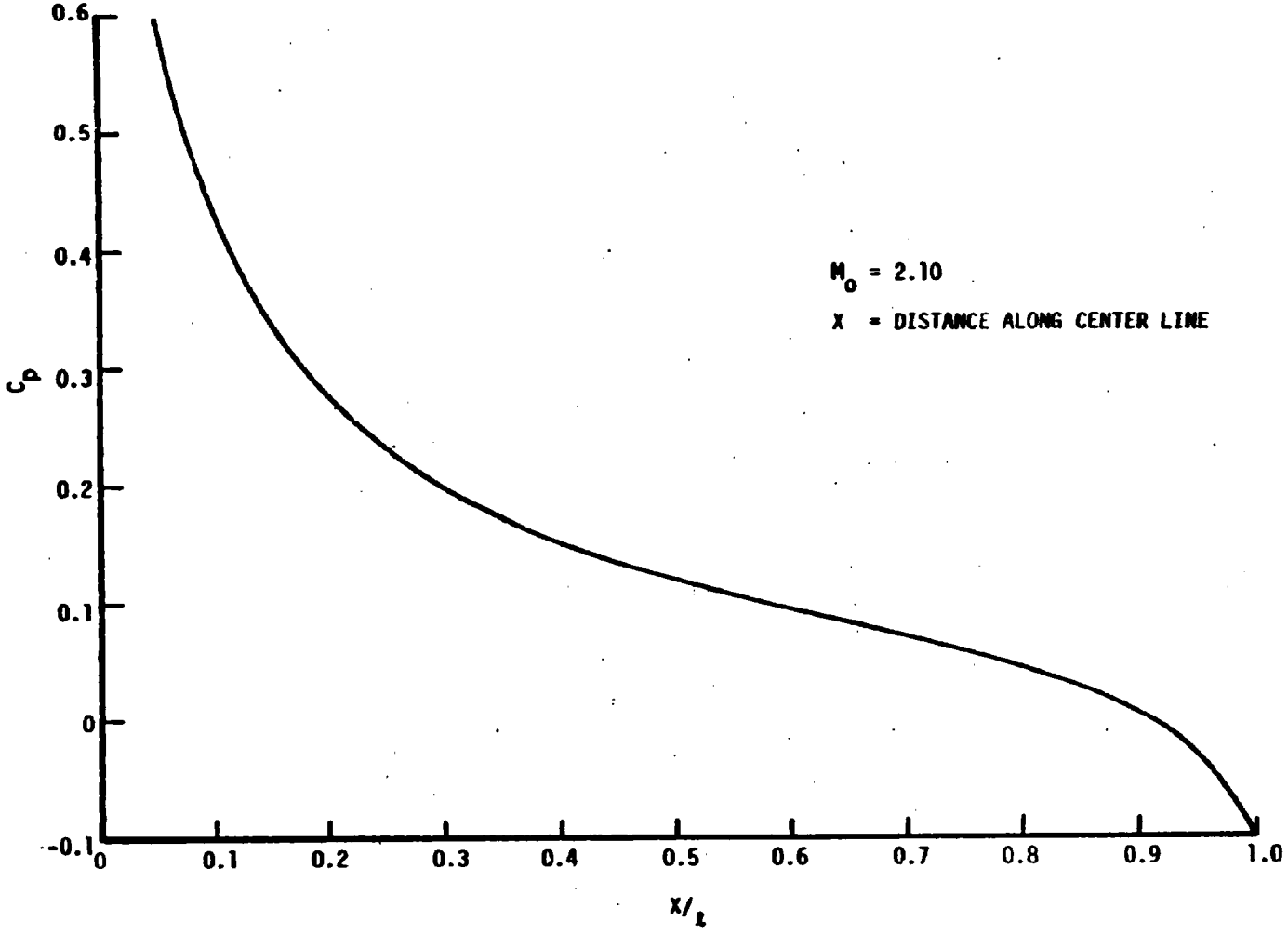


Figure 63. Pressure Coefficient Distribution for Von Karman Configuration OAL Test Radomes.

$$q_\infty = \frac{1}{2} \rho_\infty u_\infty^2 = \frac{1}{2} \gamma M_\infty^2 p_\infty \qquad (6)$$

Combining equations (4), (5), and (6) gives

$$dM = \gamma M_\infty^2 p_\infty y_o \ell^2 C_p \left(\frac{y}{y_o}\right) \left[1 - \frac{x}{\ell}\right] d\left(\frac{x}{\ell}\right) \qquad (7)$$

which becomes

$$M = y_o \ell^2 \gamma M_\infty^2 p_\infty \int_o^1 C_p \left(\frac{y}{y_o}\right) \left[1 - \frac{x}{\ell}\right] d\left(\frac{x}{\ell}\right) \qquad (8)$$

Now $C_p$ is given as a function of $\frac{x}{\ell}$ and $\frac{y}{y_o}$ is a function of $\frac{x}{\ell}$ for the particular radome being considered. Thus, $C_p \left(\frac{y}{y_o}\right) \left[1 - \frac{x}{\ell}\right]$ is a function of $\frac{x}{\ell}$.

Numerical integration of equation (8) gives

$$M = 0.0391 \; y_o \ell^2 \gamma M_\infty^2 p_\infty \qquad (9)$$

Substituting the values of $y_o$, $\ell$, $\gamma$ (= 1.40), $M_\infty$, and $p_\infty$ gives a value of M of 1186 ft.$lb_f$.

## 2. Clockwise Moment

The result represented by M in equation (9) above is not the net moment acting on the radome. The horizontal components of pressure produce a clockwise moment. This was calculated in a similar manner and yielded a value of 56 ft.$lb_f$.

3. Combined Aerodynamic Bending Moment

The combined bending moment is therefore:

$$M_a = 1186 - 56 = 1130 \text{ ft·lb}_f$$

which acts in a counterclockwise manner.

4. Vertical Force and Location

In a manner similar to that used in calculating the moment the net vertical force on the radome can be shown to be

$$F_y = \gamma M_\infty^2 p_\infty y_o \int_o^1 C_p \left(\frac{y}{y_o}\right) d\left(\frac{x}{l}\right) \qquad (10)$$

Numerical integration of the integral in equation (10) gives a value of $F_y$ of 940 $\text{lb}_f$. The location of this force would be $\frac{1186}{940}$ or

$$l = 1.26 \text{ feet}$$

C. Resultant Bending Moment

The resultant bending moment is therefore the algebraic sum of the individual moments due to inertia and aerodynamic loading and is:

$$M_R = 1130\ (12) + 78\ (12) \qquad (11)$$

$$M_R = 14{,}596 \text{ inch·lb}_f \text{ (Counterclockwise)}$$

D. 901/B-1 Adhesive Peak Tensile Shear Stress

The peak tensile shear stress in the 901/B-1 adhesive was computed using the Volkersen Equation 102/,

$$\sigma_{max} = \sigma_{avg} \left(\frac{\Delta}{W}\right)^{1/2} \cdot \frac{W-1+\cosh(\Delta W)^{1/2}}{\sinh(\Delta W)^{1/2}} \qquad (12)$$

$$\Delta = \frac{3 E_a \ell^2}{8 E_s t_s t_a}$$

$$W = \frac{E_i t_i + E_s t_s}{E_s t_s}$$

The value of $\sigma_{avg}$ is computed by

$$\sigma_{avg} = \frac{M}{2 \pi R_i^2 \ell} \qquad (13)$$

Combining Equations (12) and (13) and substituting equivalent relationships for $\Delta$ and $W$ in several terms -

$$\sigma_{max} = \frac{M_R}{2 \pi R_i^2 \ell} \left(\frac{3 E_a \ell^2}{8 t_a (E_i t_i + E_s t_s)}\right)^{1/2} \cdot \frac{\frac{E_i t_i + E_s t_s}{E_s t_s} - 1 + \cosh(\Delta W)^{1/2}}{\sinh(\Delta W)^{1/2}} \qquad (14)$$

It is apparent that the bond length $\ell$ is eliminated by cancellation from the first part of Equation (14) and therefore, the bond length $\ell$ enters into the computation of $\sigma_{max}$ only in the hyperbolic sine and cosine functions contained in the last term. It can be shown, for $\ell$ equal to 0.5-inch, that the expression

$$\frac{W - 1 + \cosh(\Delta W)^{1/2}}{\sinh(\Delta W)^{1/2}}$$

is equal to 1.17 and for the case here, $\ell$ = 1.75-inch, the expression is

very close to unity. Therefore, the peak tensile shear stress is determined by

$$\sigma_{max} = \frac{M}{2\pi R_i^2} \left( \frac{3 E_a}{8 t_a (E_i t_i + E_s t_s)} \right)^{1/2} \qquad (15)$$

For the case of the x-band radome attachment

$$\sigma_{max} = 166 \text{ lb}_f/\text{in}^2$$

APPENDIX III

ENGINEERING MEMO PAGE 1 OF 7

APPLIED PHYSICS LABORATORY

THE JOHNS HOPKINS UNIVERSITY

SILVER SPRING, MD.

TO A. J. Bell REF.NO. EM-4062 GROUP BBE

BY L. B. Weckesser DATE 8/18/66 APPROVED DATE 8/22/66

SUBJECT 1966 OAL Fused Silica Radome Tests - Preliminary Report

References:

(1) EM-4028, "Instrumentation and Data Reduction for OAL Fused Silica Radome Tests" by L. B. Weckesser and J. F. George, dated 3/2/66.

(2) GIT Report, "Thermal Evaluation of Slip Cast Fused Silica Radomes - Test Outline", dated 1966.

(3) EM-4024, "Estimates of Temperature and Thermal Stresses to be Encountered in the 1966 OAL Fused Silica Radome Tests" by R. P. Suess, dated 2/14/66.

(4) Paper Presented at the 8th Electromagnetic Window Symposium GIT, June 1966, "Radome for Hypersonic Interceptor" by R. O. Howell, Raytheon Co., MSD.

Free jet tests were conducted to evaluate the thermal shock capability of fused silica radomes at the Ordnance Aerophysics Laboratory during the period July 6 to July 18, 1966. The test procedure and the instrumentation of the radomes were presented in References (1) and (2). In general, all five radomes tested survived the maximum thermal stress to which they were subjected; however, only one radome remained intact through the tunnel shut-down period. A summary of the test results is presented in Table I.

The required wind tunnel flow conditions for those tests were: Mach 2.2, total temperature 4000°F and total pressure 140 psi. These conditions approximate a flight environment of Mach 8 at 50,000 ft; however, this does not define the thermal shock environment. Referring to Reference (3), the theoretical surface temperature history predicted was found comparable to data presented in Reference (4). In Reference (4) an analyses was made of a similar radome in which the sea level launch acceleration was in excess of 100g's. Thus it may be concluded that the thermal shock witnessed during these tests at OAL was comparable to that expected from a vehicle being accelerated at better than 100g's.

Prior to testing any of the radomes, an attempt was made to measure the total temperature of the air stream. The purpose of this effort was to provide a check on the theoretically predicted values to be made by OAL. (The methods of calculation used by OAL to predict total temperature are discussed later in this memorandum.) A specially prepared total temperature probe was used to make the measurements by injecting it into the stream after the flow was established. Figure 64 presents a general test arrangement photograph showing

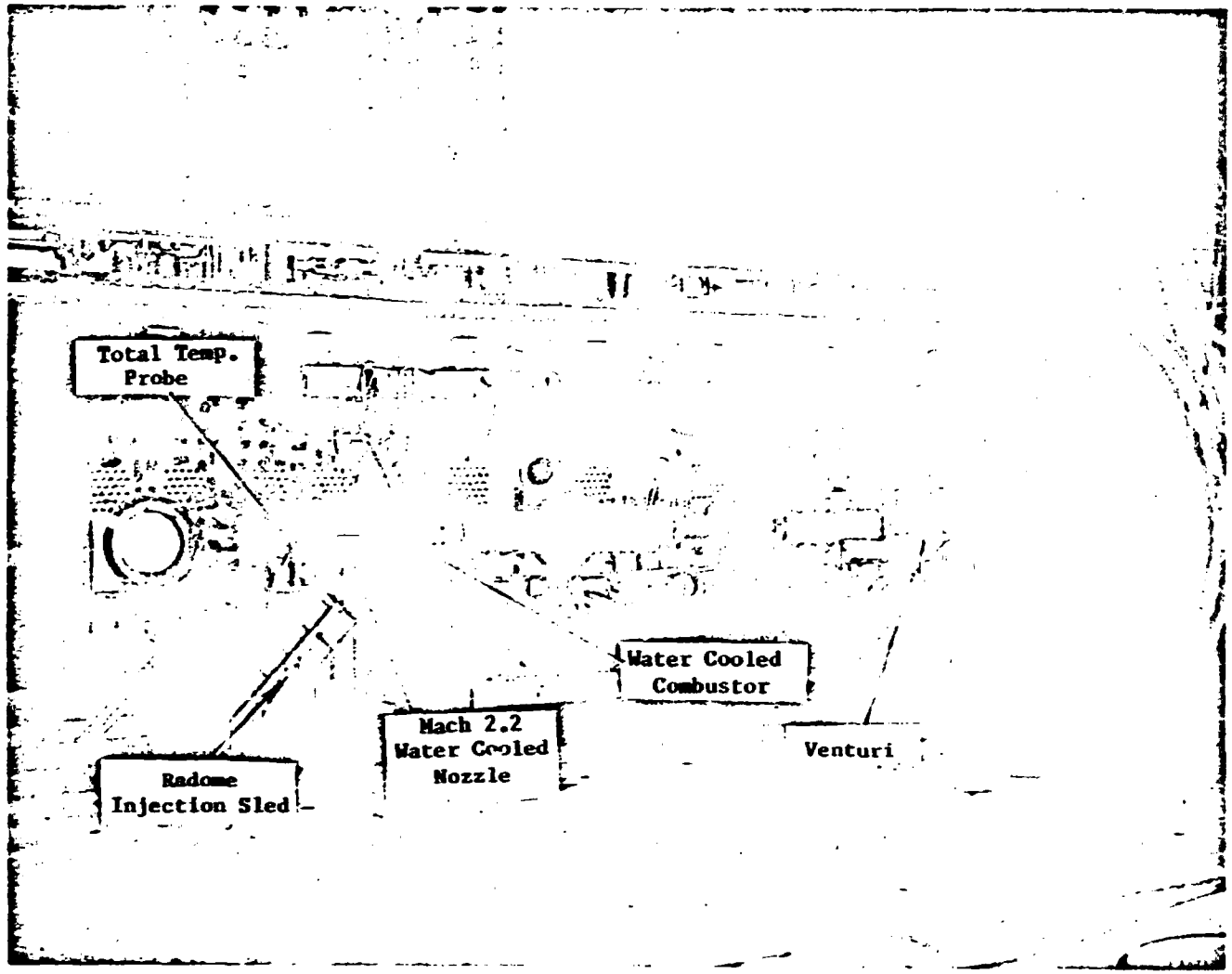


Figure 64. Test Arrangement Fused Silica Radome Tests.

various major components of the test. In this figure, the total temperature probe is mounted on the injection sled platform. To keep from destroying the probe, it was held in the stream for only 10 seconds. Because of its mass, the probe never stabilized at an equilibrium temperature and no method could be devised for extracting a total temperature from the transient data measured. Thus, the effort to verify the total temperature values determined by CAL was unsuccessful.

The methods used by CAL to determine total temperature are presented below:

I. Determination of TEX (Total temperature based on weight flow measurements)

TEX is computed by using the basic equation

$$W_g = \frac{A\ (P/P_t \hat{m})\ P_t}{\sqrt{T_T}}$$

which may be rewritten

$$TEX = \left[\frac{A\ (P/P_t\ \hat{m})\ P_t}{W_g}\right]^2$$

where:

$TEX = T_T$ = total temperature

$W_g = W_a + W_f$

$W_a$ = weight of air flow (obtained from venturi)

$W_f$ = weight of fuel flow

A = Area of nozzle throat

$(P/P_t\ \hat{m})$ = value obtained from Mach No. Tables for $\gamma = \frac{9}{7}$

$$(P/P_t\ \hat{m} = .51619 \text{ for } m = 1)$$

$P_t$ = pressure measured in the combustion chamber

II. Determination of TEXIDL (Total temperature based on combustor data)

During the development of the TYPHON LR combustor, data was accumulated which indicated the temperature rise of the air as a function of fuel flow and air flow. This data can be used in determining the total temperature, TEXIDL.

$$TEXIDL = T_{Tfc} + \Delta T_f$$

$T_{Tfc}$ = Total temperature measured at the combustor inlet

$\Delta T_f$ = Temperature rise in the combustor (obtained from combustor curves)

The values presented in Table XXIX are average values obtained as TEXIDL. Values of TEX were lower on runs 6167, 6169 and 6172 but were about equal on runs 6170 and 6171. Further evaluation of the test data will be required before complete confidence can be established in these total temperatures.

Mr. Nazzal of OAL made an analysis of a gas sample collected during each radome test and from these data he computed the ratio of specific heats (Gamma) as a function of temperature. The data he obtained for runs 6171 and 6172 compared with that for air are presented in Table XXX. As may be noted the values for air are quite close to those determined for the gas. Thus, it is felt that the gamma for air may be safely used in any theoretical studies which may be performed to determine aerodynamic heating to the radomes.

The test procedure employed for each radome test was as follows. The radome was wrapped with an insulating blanket which was held in place by a fiberglas cover. It was held below the air stream until the tunnel conditions had stabilized as much as possible (this required 80 to 90 sec.). At this time, the radome was injected into the air stream and held at zero angle of attack for the prescribed time. For the first test the radome was withdrawn from the stream, but on the subsequent tests the radome was held in the stream during tunnel shut-down.

Table XXIX essentially summarizes the entire series of radome tests. In this table the various radomes tested are defined along with the test conditions. Also presented are: the time to attain maximum stress as predicted theoretically by Reference (3), the time at test conditions, the time at which failure occurred and lastly, any significant comments. As may be noted, with exception of the last test the radomes all survived well past the time to maximum stress as predicted in Reference (3). Premature radome failure on run 6172 is attributed to the combustor burnout. When the radome broke during extraction of the sled from the stream on run 6167 it was theorized that the uneven loading during extraction caused the break. All remaining radomes were left in the stream and the flow slowly reduced after the test was complete. This was successful for test 6169 and the radome survived the shut-down period; however, during the remaining tests it was not successful. On run 6170 the radome appeared to explode just as the combustor fuel was completely turned off. Breakage occurred in the same period on run 6171. During run 6171 visual observation disclosed that the radome was stopped while half way in the stream for a period of approximately 3 seconds. At the beginning of this period the blanket blew off resulting in an uneven heating to the radome. At approximately 30 seconds the radome was noted to be cracked completely around its circumference just forward of the attach ring area. Surprisingly, the radome remained intact during the entire test until the combustor had been turned off. At this time there is no

explanation available as to why the radomes tested during runs 6167, 6170 and 6171 failed at the time of shut-down. It is unlikely that the cool-down caused the failure and presently thoughts are that the attach ring resulted in these failures; however, no definite information is available indicating where the source of failure was.

As may be noted, the test conditions were approximately those required; namely, 4000°F total temperature and 140 psia total pressure. A discrepancy exists however between the surface temperatures measured and those predicted. Reference (3) predicted the surface temperatures at the 4 inch location to be approximately 3000 to 3100°F. This compared with temperatures of 2300°F to 2700°F measured by the pyrometers and surface thermocouples. Further study of the data and theoretical predictions of surface temperature using the actual flow conditions may uncover an explanation for this discrepancy.

LBW:jmd
Distribution:
AJBell
RWBlevins
MHill
WCCaywood
JFGeorge
DCSperau
CAMurphy - GIT
JJeter - QAL
PDFisher - ORD 03211
WKBaker - ORD 03511
LBWeckesser
Archives (2)
EM File

TABLE XXIX

Fused Silica Radome Test Data

| OAL Run No. | Radome Description & avg. wall Thickness | Test Conditions Total Press. psia | Test Conditions Total Temp. °F | Time to max. stress sec. | Time at test conditions sec. | Time to failure sec. | Comments |
|---|---|---|---|---|---|---|---|
| 6167 | Plain Drain Cast X-Band $t_{ave}$ = 0.455" | 131 | 3800 | 32.5 | 60 | 67.1 | Radome survived until it was extracted from the stream at which time it broke. Instrumentation wires burned someting during the run. |
| 6169 | $Cr_2O_3$ Coated Drain Cast X-Band $t_{ave}$ = 0.466" | 136 | 3910 | 34 | 45 | | The radome was left in the air stream during combustor shut-down. Radome was undamaged. There was no visual ablation at the tip. There were several nicks on the radome surface which probably resulted from solid particles in the air stream |
| 6170 | Plain Precision Cast X-Band $t_{ave}$ = 0.372" | 137 | 3980 | 23 | 40 | 43.7 | Radome fabricated by GD/P Left in stream during shut-down. Just after the fuel to the combustor was turned off the radome appeared to explode. |
| 6171 | $Cr_2O_3$ Coated Drain Cast C-Band $t_{ave}$ = 0.764" | 138 | 4000 | 85 | 103 | 105 | Sled stopped for about 3 sec. when radome was half in stream (blanket blew off resulting in uneven heating). Radome cracked all the way around near the attach ring at about 30 sec., but it remained intact until combustor had been turned off. Air was still flowing when radome broke. |
| 6172 | Plain Drain Cast C-Band $t_{ave}$ = 0.723" | 140 | 4100 | 75 | 67.5 | 67.5 | Combustor burned out and broke radome. |

Note: The Mach No. for all tests was 2.2. All radomes were of the von Karman configuration and fitted with water cooled Invar attachment rings.

TABLE XXX

Gas Composition and Gamma
Fused Silica Radome Tests

Gas Composition

| Component | Run 6171 | Run 6172 |
|---|---|---|
| $H_2$ | 5.4 | 7.4 |
| $N_2$ | 65.8 | 64.6 |
| $H_2O$ | 11.3 | 10.6 |
| CO | 10.3 | 12.7 |
| $CO_2$ | 6.4 | 4.6 |
| A | 0.8 | 0.7 |
| $O_2$ | 0.0 | 0.0 |

Gamma for Products of Combustion and for air

| | 500°F | 1000°F | 1500°F | 2000°F | 2500°F | 3000°F | 3500°F | 4000°F | 4500°F |
|---|---|---|---|---|---|---|---|---|---|
| Run 6171 | 1.3611 | 1.3272 | 1.3064 | 1.2906 | 1.2780 | 1.2712 | 1.2661 | 1.2624 | 1.2594 |
| Run 6172 | 1.3672 | 1.3336 | 1.3131 | 1.2971 | 1.2861 | 1.2777 | 1.2723 | 1.2684 | 1.2653 |
| Air | 1.3809 | 1.3488 | 1.3302 | 1.3165 | 1.3068 | 1.2994 | 1.2940 | 1.2910 | 1.2872 |

## APPENDIX IV

## SYNOPSIS OF THERMAL TESTS ON SLIP-CAST FUSED SILICA RADOMES AT THE ORDNANCE AEROPHYSICS LABORATORY

### OAL Test 6167

Test Radome: SCFS drain cast, ≈ X-band thickness

The radome was covered with an insulation jacket consisting of Fiberfrax® encapsulated in cotton cloth and overwrapped (outer surface) with silica cloth. The composite jacket was taped (loosely) in place with glass tape. The radome was mounted on the injection sled in the retracted position; radome centerline to combustor centerline approximately 24 inches. Air flow through the combustor and cell suction were initiated. Air flow was stabilized and fuel (JP-5) was injected and ignited. Combined total pressure, gas analysis and total temperature rake inserted into stream and measurements made. At about the time the air flow was stabilized the insulation jacket blew off as a result of air recirculation in the cell. When the combustor was ignited the strain gage signals began to increase and at the point where the radome was injected into the stream the strain gage signals had maximized. The radome was immersed in the stream for 60 seconds. At the end of the 60 second immersion the sled was retracted. When this occurred the radome failed. The instrumentation lead-out housing was burned extensively during the test.

## OAL Test 6168

Test Radome: SCFS drain cast, ≈ X-band thickness, with $Cr_2O_3$ modified coating on forward region

The radome was covered with an insulation jacket, overwrapped with silica cloth and taped more substantially than for OAL Test 6167. The air flow was initiated, the combustor ignited and stabilized and the total pressure and gas analysis rake was inserted in the stream for ten seconds. At this point the strain gage signals (observed on visual read-out panel of computer data input system) began to rise rapidly. The engine was shut down to determine location of the signal interference (it was thought that this problem had been eliminated prior to the test by modifying the instrumentation lead-out system to prevent heating and burning). The only logical explanation for the strain gage signal increase was a recirculation of hot air into the rear of the radome mount around the exiting Invar attachment water leads. These were sealed as was the instrumentation output hole in the radome-mount transition plate. This was effective as observed in subsequent test 6169.

## OAL Test 6169

Test Radome: Same as Test 6168

The radome was examined for possible insulation loss during Test 6168, retaped, and the combustor ignited. Visual output monitoring of the strain-gage output showed no disturbances with the instrumentation. Test sequence switched from manual to automatic. Again the insulation jacket blew off the

test radome before the radome was inserted into the stream. The radome was immersed in the stream for 45 seconds. All instrumentation performed satisfactorily. At the end of the 45 second period the engine was shut down with the radome in the stream. The radome was recovered intact.

OAL Test 6170

Test Radome: SCFS precision cast, X-band thickness

The radome was mounted and the insulation jacket was taped tightly (much more so than in Tests 6167 and 6169). The combustor was ignited and stabilized. No disturbance of the strain gage instrumentation occurred. Test switched from manual to automatic. Radome went into stream perfectly; insulation jacket peeled off as radome entered stream. The test time was 40 seconds. As with Test 6169 the engine was shut down with the radome in the stream. The fuel flow was terminated and the air flow gradually decreased. The radome failed catastrophically as this was accomplished.

OAL Test 6171

Test Radome: SCFS drain cast, ≈ C-band thickness, with $Cr_2O_3$ modified coating on forward region

The radome was mounted, the insulation jacket was taped tightly, and the engine brought up to operating conditions. Test sequence was switched to automatic. Sled activated and moved towards stream. It stopped moving when radome was half-way into stream. Apparently the hydraulic accumulators were not up to maximum operating pressure. Insulation jacket stripped off as planned. There was a time lag of about 4 seconds before hydraulic system pressure was sufficient to move radome fully into stream. At approximately 40

seconds after the radome was immersed in the stream (total test time of 100 seconds) a circumferential crack appeared in the radome at a point corresponding (approximately) to the fore surface of the water cooled Invar attachment; the crack was apparently through the radome wall and completely circumferential. The radome remained in position (even with this severe failure) due to the symmetrical air load. However, as expected, the radome was blown away as the engine was being shut down.

## OAL Test 6172

Test Radome: SCFS drain cast, ≈ C-band thickness

The radome was mounted, the insulation jacket was taped on, and the engine brought up to operating conditions*. The insulation jacket was blown off before the radome was injected into the stream. At about 60 seconds after immersion into the stream the engine internal components failed causing the nozzle to burn out. The radome failed at this point and was blown from the attachment; it is suspected that the radome had cracked circumferentially as occurred in Test 6171.

*For this run it was requested that the stream temperature be increased by increasing the inlet air temperature 200° F.

## APPENDIX V

### INSTRUMENTATION FOR 1966 OAL SCFS RADOME TESTS

The instrumentation of the SCFS radomes for the 1966 OAL tests consisted of strain gages, thermocouples, and brightness pyrometers. The instrumentation was expected to provide information on the material response to the environment which would be used as a comparison to the analytically predicted material response.

Radomes 4 and 5 contained all instrumentation listed in Table XXXI. Radomes 1, 2, and 3 did not have the external surface thermocouples T-2, T-4, T-6, and T-8 (thus, T-11 through T-18 were not on these radomes either). For these radomes, the pyrometers were the only instruments available to define external surface temperature.

TABLE XXXI

COMPLETE INSTRUMENTATION LIST
OAL FUSED SILICA RADOME TESTS

| I.D. No. | Location | Type Wire | Maximum Temperature Expected (°F) Test 1 | Test 2 | Test 3 | Test 4 | Test 5 |
|---|---|---|---|---|---|---|---|
| T-1 | *On internal surface, 5.1 inches from tip (measured along center-line), on right side of radome looking forward. | Chromel vs Alumel | 800 | 800 | 300 | 300 | 00 |
| T-2 | **On external surface, opposite T-1. | See note** | 3100 | 3100 | 3100 | 3100 | 3100 |
| T-3 | *On internal surface, 5.1 inches from tip, on left side of radome looking forward. | Chromel vs Alumel | | | same as T-1 | | |
| T-4 | **On external surface, opposite T-3. | See note** | | | same as T-2 | | |
| T-5 | *On internal surface, 7.1 inches from tip, on right side of radome looking forward. | Chromel vs Alumel | | | same as T-1 | | |

*On radome 4 these end instruments were located on the top and bottom instead of right and left.

**These thermocouples were only on radomes 4 and 5. On radome 5 the thermocouple wire was 40% IR-60% Rh vs IR, but on radome 4 it was Pt vs Pt-13% Rh.

(Continued)

TABLE XXXI (Continued)

COMPLETE INSTRUMENTATION LIST
OAL FUSED SILICA RADOME TESTS

| I.D. No. | Location | Type Wire | Maximum Temperature Expected (°F) Test 1 | Test 2 | Test 3 | Test 4 | Test 5 |
|---|---|---|---|---|---|---|---|
| T-6 | **On external surface, opposite T-5. | See note** | | | same as T-2 | | |
| T-7 | *On internal surface, 7.1 inches from tip, on left side of radome looking forward. | Chromel vs Alumel | | | same as T-1 | | |
| T-8 | **On external surface, opposite T-7. | See note** | 200 | 200 | 150 | 150 | 200 |
| T-11 | On junction block connected to positive lead (40% Ir-60% Rh wire on radome 3 and Pt. wire on radome 4) of T-2. | Copper vs Constantan | 200 | 200 | 150 | 150 | 200 |
| T-12 | On junction block connected to negative lead (Ir wire on radome 3 and Pt-13% Rh wire on radome 4) of T-2. | Copper vs Constantan | 200 | 200 | 150 | 150 | 200 |

*On radome 4 these end instruments were located on the top and bottom instead of right and left.

**These thermocouples were only on radomes 4 and 5. On radome 5 the thremocouple wire was 40% IR-60% Rh vs IR, but on radome 4 it was Pt vs Pt-13% Rh.

(Continued)

TABLE XXXI (Continued)

COMPLETE INSTRUMENTATION LIST
OAL FUSED SILICA RADOME TESTS

| I.D. No. | Location | Type Wire | Maximum Temperature Expected (°F) Test 1 | Test 2 | Test 3 | Test 4 | Test 5 |
|---|---|---|---|---|---|---|---|
| T-13 | On junction block connected to positive lead of T-4. | Copper vs Constantan | 200 | 200 | 150 | 150 | 200 |
| T-14 | On junction block connected to negative lead of T-4 | Copper vs Constantan | 200 | 200 | 150 | 150 | 200 |
| T-15 | On junction block connected to positive lead of T-6. | Copper vs Constantan | 200 | 200 | 150 | 150 | 200 |
| T-16 | On junction block connected to negative lead of T-6. | Copper vs Constantan | 200 | 200 | 150 | 150 | 200 |
| T-17 | On junction block connected to positive lead of T-8. | Copper vs Constantan | 200 | 200 | 150 | 150 | 200 |
| T-18 | On junction block connected to negative lead of T-6. | Copper vs Constantan | 200 | 200 | 150 | 150 | 200 |
| T-19 | 1/8-inch from tip on the external surface. | Pyrometer | 3500 | 3700 | 3500 | 3700 | 3700 |
| T-20 | 1/2-inch from tip on the external surface. | Pyrometer | same as T-19 | | | | |

(Continued)

TABLE XXXI (Continued)

COMPLETE INSTRUMENTATION LIST
OAL FUSED SILICA RADOME TESTS

| I.D. No. | Location | Type Wire | Maximum Temperature Expected (°F) Test 1 | Test 2 | Test 3 | Test 4 | Test 5 |
|---|---|---|---|---|---|---|---|
| T-21 | F've inches from tip, on the external surface, on same spot as T-2. | Pyrometer | same as T-2 | | | | |
| T-22 | Seven inches from tip, on the external surface, on same spot as T-6. | Pyrometer | same as T-2 | | | | |
| S-1 | *Strain gage measuring meridional strain adjacent to T-1. | | | | | | |
| S-2 | *Strain gage measuring circumferential strain adjacent to T-1. | | Maximum change in output voltage at time of calculated maximum stress was 1500 micro volts (negative). | | | | |
| S-3 | *Strain gage measuring meridional strain adjacent to T-3 | | | | | | |
| S-4 | *Strain gage measuring circumferential strain adjacent to T-3. | | | | | | |
| S-5 | *Strain gage measuring meridional strain adjacent to T-5. | | | | | | |

*On radome 4 these end instruments were located on the top and bottom instead of right and left.

(Continued)

TABLE XXXI (Concluded)

COMPLETE INSTRUMENTATION LIST
OAL FUSED SILICA RADOME TESTS

| I.D. No. | Location | Type Wire | Maximum Temperature Expected (°F) Test 1 | Test 2 | Test 3 | Test 4 | Test 5 |
|---|---|---|---|---|---|---|---|
| S-6 | *Strain gage measuring circumferential strain adjacent to T-5. | Maximum change in output voltage at time of calculated maximum stress was 1500 micro volts (negative). | | | | | |
| S-7 | *Strain gage measuring meridional strain adjacent to T-7. | | | | | | |
| S-8 | *Strain gage measuring circumferential strain adjacent to T-7. | | | | | | |

*On radome 4 these end instruments were located on the top and bottom instead of right and left.

## APPENDIX VI

## A STATE-OF-THE-ART REPORT ON THE THERMAL PROTECTION OF HIGH-SPEED VEHICLES AGAINST MODERATE TO HIGH HEAT FLUXES, WITH EMPHASIS ON RELATIVELY SHORT-TERM EXPOSURES

### Types of Thermal Protection Considered

Since high-speed vehicles encounter thermal environments which are beyond the capabilities of the hot structure of the present or foreseeable future, some form of thermal protection is required for vehicle survival. Two basic types of thermal protection are considered promising: the radiative system and the absorbtive system.

### Thermal Protection by Radiation

Thermal protection by radiation is relatively simple and theoretically efficient but is limited to low aerodynamic heating rates, and thus to relatively low velocities, because of the service temperature limitations of the available skin materials. There are also attendant attachment and support problems with the radiative concept due to thermal mismatch between component materials. The radiative system is favored for long-time exposures to relatively low heating rates but is a much less efficient means of thermal protection than some of the absorbtive systems for short-time exposures to high heating rates. For example, the radiative concept is generally not employed on reentry vehicles with reentry times less than 15 minutes.

### Thermal Protection by Insulation

Insulation is considered as a special case of a radiative system in which heat dissipation at the hot surface is increased by means of an increased surface temperature. Insulation is defined as a material or state which tends

to thermally isolate components, and the Dewar-type of construction provides the most effective insulative system.

Thermal Protection by Absorbtion

Absorbtive systems provide thermal protection by the absorbtion (storage) of heat and are generally restricted to flight periods of relatively short duration. Absorbtive systems of interest are the heat sink, the ablative system, and the transpirationally cooled system.

Heat Sinks

A heat sink is a low-temperature, constant-weight system which absorbs heat by conduction from a hot surface. An effective heat sink requires a material with a high specific heat, a high thermal conductivity, and a high melting (softening) or sublimation temperature. Heat sinks are generally quite heavy because of the limited sensible heat of most materials, and their effectiveness is markedly reduced at high velocities.

Thermal Protection by Ablation

For high performance vehicles (total heat greater than 10,000 Btu/ft$^2$) the mass transfer approach (ablation or transpiration) appears inherently superior to all other thermal protection schemes, and for a number of missions involving hypervelocity flight through the atmosphere, only the ablating thermal protection system is currently practical.

Ablative systems represent the most promising absorptive system available today. Ablative heat shields are relatively easy to fabricate, and they are economical. Ablative heat shields are often the designer's choice because they are applicable to a number of vehicles and environments and because they offer the advantages of self-regulation, simplicity, and reliability.

Ablation cooling is suitable for heat pulses of moderate magnitude and intermediate duration and is very effective for extremely high heating rates of relatively short duration. To date, ablators have found applications in ballistic missiles, manned and unmanned entry vehicles, rocket systems, and recoverable research probes. For the future, ablative materials appear to be the most promising thermal protection materials for use on lifting aerospace-craft.

In practice, the ablation process is extremely complicated, and a variety of definitions of ablation have been cited:

1. The sacrifice of surface material for the protection of an underlying structure - mass traded for heat 20/.

2. A complex energy dissipative process which takes place when a coating is decomposed, burned off, or sacrificed - the process of removing the material by melting or vaporization 21/.

3. The orderly removal of material from a surface in a hyperthermal environment by interaction between the surface and the applied heat and velocity 22/.

4. The gradual, non-catastrophic loss of material through melting, vaporization, chemical decomposition, or chemical reaction with active boundary layer species, resulting when a relatively cool material receives energy from an environment at a higher temperature.

5. A self-cooling, mass transfer process which is initiated when a sufficient quantity of heat is absorbed by a material surface to cause varying amounts of melting, vaporization, sublimation, and depolymerization in which gaseous and solid products are formed 23/.

6. A self-controlled, uniform process of heat absorption in which the entire heat content of a material is used and in which air flow is utilized for the continuous removal of the resulting products 24/.

Recent reviews and/or bibliographies on ablation and ablative systems have been provided through the efforts of Hanna 21/, Israel and Nardo 25/, Keller, Kimmel, and Schwartz 26/, Schmidt 27,28/, Steg and Lew 29/, and Strauss 30/.

Ablative materials are unique in that they provide a relatively simple means for accommodating a wide range of temperature or heat flux conditions. They degrade in a self-regulating and orderly manner and do not require an accurate adjustment to a specific heat-flux rate. Changes in the environment are automatically matched by changes in the ablation rates of these materials, and their operating temperatures can remain practically constant. Ablative materials are readily available and are nonstrategic, their costs are relatively low, and, while the design of ablative materials is not a simple task, it involves less complexity than that associated with most other thermal protection schemes. Ablative materials can be made to possess low density, low thermal conductivity, and good mechanical strength.

A very desirable characteristic of the ablation process as a thermal protection method is its self-contained feature. Other cooling methods, such

as heat sinks and circulation of coolant, require extra weight and volume and are considerably more complicated.

Charring Ablators

Without exaggeration charring ablators are the most important heat-protection materials in use today; they are now extensively employed in the design of both ballistic and entry vehicles.

Typically, the charring ablators consist of a thermosetting resin (such as an epoxy or phenolic compound) reinforced with organic and/or inorganic fillers (such as nylon, quartz or graphite fibers) and offer a particularly advantageous combination of properties for heat shield applications. However, a heterogeneous or composite structure is generally required for ablative materials and the properties of an ablative thermal protection system must be tailored to suit the particular environment to be encountered before efficient operation can be ensured.

Charring plastics are very effective heat dissipators for high aerodynamic-heating-rate situations; their effective heats of ablation typically range from 2000 to 8000 Btu/lb. These materials owe their effectiveness to a multitude of heat and temperature regulating phenomena which occur simultaneously within the material and on or near its surface. These phenomena include thermal insulation, reradiation, endothermic decomposition, transpiration and boundary layer thickening. As the material degrades, it tends to form a porous carboniferous char which has a low thermal conductivity and consequently provides thermal insulation; thus the charring plastics possess the most important advantages of pyrolytic graphite without incurring the economic penalties and fabrication difficulties associated with the graphite. The char is capable of

attaining a high surface temperature and, owing to its high emissivity, can dissipate a large portion of the incident heat flux through the process of radiation. At the same time, the effective thermal conductivity of the char is reduced by the effect of the endothermic decomposition of gases which result from depolymerization beneath the surface. The char provides a hot reaction zone for the primary gaseous products and can promote near thermal equilibrium. The gaseous products leaving the char further contribute to thermal protection by thickening and cooling the boundary layer and thereby lessen the convective heating. Combustion of the gaseous products can limit the effectiveness of the ablator. However, exothermal reactions within the boundary layer do not greatly affect the mass and heat transfer at the hot surface 31/, and these reactions are bound to occur in the boundary layer, and not within the charred structure, if the heating rate is relatively high. If the combustion products have much lower molecular weights than the original gaseous products of the ablation, the combustion might actually improve the effectiveness of the ablator, by tending to further increase the thickness of the boundary layer.

Thus, charring ablative systems can be extremely efficient in comparison with other thermal protection schemes, with efficiencies to many thousand Btu/lb compared with approximately 1000 Btu/lb for heat sinks.

While charring ablators are the most important heat-protection materials in use today for moderate to high heat flux and relatively short-time exposure, these materials have three major limitations, namely:

1. Even the best performing charring ablators (i.e. the reinforced phenolics) present drastically altered surfaces after exposure.

2. The effectiveness of a charring ablator depends markedly upon the char thickness and its variation with time.

3. Chars seriously attenuate electromagnetic signals.

Each of these points warrants further consideration. First, the major obstacle for charring ablators is the requirement of shape integrity; dimensional stability during flight is not among the virtues of these materials. Being basically brittle in nature and subject to thermal shock and other failure mechanisms, a char is prone to spallation at unpredictable times and rates. Thus, unavoidable surface disuniformities are created in these materials, and rugged contours are formed which promote localized heating and catastrophic damage. Surface disuniformities are unavoidable even when the char is extremely strong since large shape changes are associated with the virgin material because of side heating and char growth. These considerations are of prime importance for applications, such as leading edges and small-angle nose cones, where changes in the aerodynamic contour greatly influence the performance of the vehicle.

Second, the performance of a charring ablator depends to a large measure on char retention. It is exceedingly important for the char layer to remain intact. When the char is lost, the ablative performance is not nearly as effective as it should be, and weight requirements are increased several times.

Char may be removed from the surface of an ablator by any number of competing mechanisms, as removal is effected by: vaporization, oxidation, aerodynamic shear forces, thermal stresses, the melting of inorganic fillers beneath the surface, and internal pressure due to gaseous products.

The effects of oxygen on chars has been studied rather extensively both theoretically and experimentally 32/. It has been found that char removal is greatly influenced by oxygen in the environment. Koubek, Hartmann and Caum 33/ studied typical organic ablators in an arc image furnace and found that most ablators were more efficient in argon than in air. Brooks, Swann, and Waklin 34/ found that char thickness is inversely related to the stream oxygen content. In one experiment where nylon phenolic was exposed to an arc, the overall loss of ablated material was nearly ten times greater in air than in nitrogen 35/.

Typical organic ablators have also been shown to be more efficient without shear forces than with shear forces acting on them 33/. In turbulent pipe arc plasma tests it has been noted that increased shear forces result in increased spallation and, in some cases, complete suppression of char layer formation was observed.

Summarily, then, the effectiveness of the charring ablator may be greatly diminished in low-altitude flight situations where it is difficult to retain a char due to the high oxygen concentrations and large aerodynamic shear forces.

Finally, charring ablators cannot be used for the protection of antenna since chars seriously attenuate electromagnetic signals.

Transpiration Cooling

The transpiration cooling concept is of considerable interest because it allows the surface temperature of a heat shield to be maintained at a safe and predetermined level by the adjustment of coolant flow and provides a constant surface contour. The method is extremely efficient, expecially when very high heating rates are encountered, and may be the only means to achieve thermal

protection when high heat flux rates are encountered for prolonged periods of time.

Many tests have confirmed the effectiveness of transpiration cooling under the conditions of high aerodynamic shear forces and thermal stresses which inhibit the development of a char layer in an ablative system. Unfortunately, however, a number of difficulties have been encountered in attempting to translate the concept from the laboratory to flight configurations. A complicated subsystem is required to store the coolant and to distribute the coolant in a preprogrammed fashion over substantial areas 36/, and the weight penalties for the pumping and distribution network are severe.

In the "ideal" transpirationally cooled system, the coolant would be stored behind insulation, as this should provide the lightest system. The storage of coolant throughout the thickness of an insulating barrier represents a practical adaptation of the "ideal" transpirationally cooled system and approximates the behavior of the charring ablator 37/. Advances in the development of "coolant packages," such as Vought Astronautics Thermosorb 38/, encourage the approach. Thermosorb is a high-water-content, semi-solid gel retained by an open cell sponge in a thermoplastic container which melts upon exposure to severe heating.

The feasibility of a water/stream transpirationally cooled system has been demonstrated with the "water-wall" type of construction described above for a total heat flux of 65 Btu/ft$^2$-sec (25 Btu/ft$^2$-sec absorbed) 39/. Readily available materials were used in the construction.

Much work remains towards the development of suitable transpirationally cooled systems. Porous surface materials with higher temperature capabilities and greater reliability are needed, and the pertinent mechanical properties of

the materials must be determined so that optimum designs can be realized __ . Fortunately, many recent advances have been made with metal-wire winding techniques, and porous members, which are stronger and more uniform than those made by the conventional powder-metal methods, are now available 22/.

At the present, transpiration cooling is most attractive when incorporated with other thermal protection techniques and restricted to small surface areas where very large heating rates must be accommodated without shape change 36,39/.

Composite Thermal Protection Systems

It is becoming more apparent that the future development of thermal protection systems must depart from the present choice of ablators, in a number of applications. However, as the departure is made two things must be kept foremost in mind. First, the composite approach appears most promising since single homogeneous materials generally perform adequately for only very short times. Second, the properties of a thermal protection system must be tailored to suit the particular environment to be encountered before efficient operation can be realized. Different sets of environmental parameters will require different component materials and, perhaps, different physical forms of construction. Thus, it becomes necessary to develop a variety of heat shield materials to accommodate a wide spectrum of thermal environments, as, even today, different types of thermal protection are used on a single vehicle. It follows, of course, that the promise of a heat shield varies directly with its versatility.

Embedded Ablators

For relatively short operation times, transpiration cooling may be provided by an oriented heterogeneous composite consisting of an ablative

material embedded in a refractory matrix. Such a system, which has been termed an "embedded ablator," combines the dimensional stability of an efficient heat sink and the heat dissipation ability of the ablation or transpiration process. In this type of system, material removal takes place within the interior of the component rather than at its surface; the refractory matrix provides for dimensional stability, and the ablative impregnant serves to reduce the temperature rise of the matrix so that it will not melt during service.

The embedded ablator holds the promise of providing a practical solution to the problem of thermal protection against a moderate to high heat flux and relatively short-time exposure in those situations where weight requirements are strict and where a charring ablator alone is not suitable because of dimensional stability requirements and/or because of wake contamination considerations. The embedded ablator approach shows considerable promise as a means of overcoming the brittle tendency of ceramic materials and represents a construction which is extremely versatile. Once a suitable matrix has been developed it can be infiltrated with a wide variety of ablative materials giving the designer a high degree of flexibility with a single matrix material. Also, graded heat shields can be prepared to accommodate the unusual thermal responses associated with advanced designs. For example, the impregnant can be graded in depth to reduce properties mismatch, or a single matrix component can be impregnated with high temperature ablator in the region of turbulent heating to ensure stability and with a low temperature sublimer in the region of laminar heating where vapor injection has a strong influence 41,42/.

It appears that the embedded ablator will provide the following advantages over the charring ablator:

1. Increased efficiency because of the hot reaction zone provided for transpiring gaseous products by the matrix.

2. Increased char thickness due to diffusion barriers within the matrix.

3. Ultimately an increase in radiative cooling as matrix materials with higher service temperatures are developed.

4. Increase in dimensional stability.

5. Decrease in wake contamination.

6. Decrease in electromagnetic signal attenuation.

7. Greater versatility.

8. Improved char retention in high-shear environments.

The following requirements have been cited for an impregnant in an embedded ablative system:

1. The impregnant must not induce mechanical stresses upon heating due to thermal expansion mismatches which would exceed the strength of the matrix. Thus, in the case of a charring impregnant a high temperature final or post cure is desirable, to allow the matrix and resin to come to a low stress level as close to the charring temperature as possible.

2. The impregnant must lend itself to reproducible infiltration, and the ablation products and the matrix material must be chemically compatible.

3. Good performance should be achieved using impregnants with a high degree of gasification and resins with a low pyrolysis temperature.

Matrix requirements, which have been cited, are as follows:

1. The matrix should have as high a strength-to-weight ratio as possible.

2. The thermal shock resistance should be good. While thermal stresses are reduced by the ablative action of the impregnant, they are not eliminated.

3. The matrix should have a high melting point; for exposures of about 500 $Btu/ft^2$-sec, temperature will probably be in the range of 4000° to 4500° F.

4. The matrix should have a low thermal conductivity and a high thermal stability.

5. The void system should be amenable to impregnation, and a fine pore size should be used to promote near thermal equilibrium of the transpiring gaseous products.

Candidate matrix materials for impregnated-ceramic systems are ceramic foams and ceramic felts; filament wound matrices are currently ruled out because of their low operating temperatures.

Foamed ceramics have already received considerable attention in regard to the embedded ablator concept. Impregnated ceramic foams have been utilized in applications to nozzles, baffles and cases for rocket motors, thrust chambers and blast tubes.

Resin-impregnated ceramic foams have been found to be less affected by the form of heat input than the low-temperature sublimers and to experience lower mass-loss rates than the charring ablators. In addition, resin impregnation increases the thermal shock resistance of ceramic foams and improves their mechanical strength [43]. Infiltrated samples have exhibited better compressive strengths, much higher flexural strengths, and greater resistance to impact [44]. Resin-impregnated ceramic foams combine the low thermal conductivity, high specific heat and boundary layer cooling effects of plastics with the heat resistance and thermal stability of ceramics and the radiation capabilities of a high temperature char.

At the current state-of-the-art, impregnated foams offer the distinct advantage over charring ablators of high dimensional stability, but only at the exprense of a lower heat dissipating efficiency. The impregnated ceramic systems require much more development before their full potential can be realized. In particular, there is a need for ceramic foams which can operate at higher temperature and thus provide radiation cooling on the same level as the charring ablator. Radiation cooling is expected to be very effective with impregnated ceramics. Because of the voids, the matrix would have a relatively high effective emittance. To take advantage of this characteristic, and thus allow the thermal efficiency to approach that of a charring ablator, ceramic matrices with higher use temperatures are required.

The major limitations of ceramic foams include:

1. Ceramic foams with more uniform physical and mechanical properties are needed.

2. Because of the low thermal conductivity of resin-impregnated ceramic foams, thermal stresses will be induced in the ceramic portion of the heat shield, and a modular design might be required 45/.

3. The high temperature ceramic foams may be difficult to machine 46/.

The principle ceramic foams investigated have been alumina, zirconia, silica, and silicon carbide foams. However, beryllia foam 47/ and foams of chemically bonded magnesia, titanium carbide, zirconium carbide and zirconium boride have also received some attention in regard to the embedded-ablator concept 48/. Impregnants have included phenolics, phenylsilanes, silicones, polyethylene, nylon, polystyrene, polypropylene and ammonium chloride. The thermoplastics have been reported to yield higher thermal efficiencies than thermosetting resins 43/. However, mixtures of thermoplastic and thermosetting resins might be required since thermoplastic impregnants tend to damage the matrix cell structure during heating due to swelling or rapid gas liberation 49/ and thermosetting resins may provide higher strengths 43/.

Promising foamed materials which are currently available include zirconia, magnesia, and thoria. However, only the zirconia has been extensively studied. Zirconia foams have been found to be quite strong with good structural integrity and good thermal stability; zirconia melts at 4870° F, and the available foam can be used at least to 4000° F. An impregnated magnesia foam has been tested in a plasma jet for 3 minutes at 500 Btu/ft$^2$-sec 50/; the composite performed very well. It has been suggested that thoria foams could be used to 5000° F 51/; however, high material costs and fabrication problems have apparently prevented the thermal evaluation of this material as a foam.

The use of ceramic felts is a rather new concept and, thus, has received only limited attention. However, the same advantages obtained with impregnated ceramic foams can be obtained with impregnated ceramic felts, and a ceramic felt may offer a number of advantages over a ceramic foam:

1. The felt would have a completely open pore structure and would be more easily infiltrated, yet the pores in a felt are distinctly "interwoven" and could effectively retain an impregnant.

2. A felt may be more thermal shock resistant than a foam, owing to the distinct parallel structure. A felt may be more reliable mechanically for the same reason. Therefore, a modular design might not be a requirement when a felted matrix is employed.

3. The completely open porosity of a felt would aid in allowing gaseous decomposition products to escape without structural degradation. Thus, thermoplastic impregnants would be more effective in a felted matrix than in a foamed matrix. In addition, a felt would provide a hot reaction zone with an extremely high surface area and would promote very close thermal equilibrium for any transpiring products. In particular, the clean ablators, or subliming ablators, would be much more effective when incorporated in a ceramic felt.

4. Ceramic felts should be easier to machine than ceramic foams.

Consideration of radiation cooling effects leads to the same requirements for the development of higher temperature ceramic felts as were described for

ceramic foams. In this regard, two of the most promising fibers available for the production of ceramic felts are zirconia fibers and a hydrous-magnesium oxide fiber called "TX*."

Zirconia fibers have been processed into paper, mat, and felt forms and used to reinforce phenolic plastics by Schwartz [52]. When samples were exposed to a simulated air arc plasma at 500 Btu/ft$^2$-sec cold wall heat flux for 24 seconds, the zirconia reinforcement proved to be superior to similar reinforcements of nylon, glass, or carbon, on the basis of both erosion and insulating capability, and the zirconia also provided a higher surface temperature (4400° F compared with 3900° F for glass reinforcements, 4150° F with the nylon, and 4310° F with the carbon).

The fiber "TX" is a naturally occurring fiber which provides a nonwoven mat with a random fiber distribution. The fiber has approximately 13 per cent combined water so that it can function partially as a transpiration cooling device. The material can be transformed to magnesium oxide by dehydration and may have a use temperature as high as 5000° F [53]. Farmer [54] has strongly recommended the study of the "TX" fibers, and Schmidt [55] has presented recent data which indicate that magnesia fibers could provide even better insulating characteristics than zirconia fibers when used as the reinforcement in a charring ablative system.

Other ceramic fibers available for the production of ceramic felts include boron nitride, fused silica, silicon carbide coated graphite, and sapphire fibers [56]. Metal fibers might also be considered for the production of felts for an embedded ablative system; such felts show considerable promise of

*Johns-Manville Corp., Manville, N. J.

allowing mechanical stability to be maintained even when penetrated by foreign objects, as the "stopping power" of a metal fiber is exceptional 57/. Boron fibers have been considered as the reinforcement in an ablative composite, but the results of tests at 500 Btu/ft$^2$-sec 58/ have discouraged their use in an embedded ablator.

It is recognized that the orientation of the reinforcement can greatly affect the performance of an ablator 59/. For example, ablative systems would be expected to show a tendency toward a low thermal conductivity, delamination, and surface spalling due to gas entrapment when the reinforcement is parallel to the surface; while the arrangement of reinforcement perpendicular to the surface should promote a system which has a higher thermal conductivity but one which is less prone to delamination during flight. It is also recognized that the form of the reinforcement can be very important and, in some cases, can have an effect which overrides the influence of orientation. In this regard it is thought that a felt can provide an orientation (and represents a form) which is consistent with good ablator design.

Subliming Ablators

Low-temperature, or subliming, ablators are suitable for high-laminar-heating-rate environments where high mass transfer cooling by vapor injection into the boundary layer is effective. However, turbulent heating and gas-layer radiation markedly increase the weight loss of these low-temperature materials. Also, heats of sublimation are generally low, and a subliming ablator would be expected to be highly effective only if its sublimation temperature were high so that a significant amount of heat could be absorbed as sensible heat of the subliming material 22/. However, the heat absorbing capability of a subliming ablator could be improved by embedding the ablator

in a matrix constructed of a material with an operating temperature higher than the sublimation temperature of the ablator. In this case the matrix would provide a hot zone, and the sensible heat of the effluent material could be utilized. It has been demonstrated that a subliming ablator is less affected by the form of heat input when incorporated in this type of system.

Recently it has been demonstrated that oxides such as magnesia, thoria, and hafnia and oxide-forming materials such as hafnium carbide may sublime rather than melt under certain conditions of elevated temperature and moderate pressure. The complete conversion of these solids to gaseous products enhances their heat protective capability and results in better dimensional stability 27/.

New Material Developments

Among the c' ring materials commercially available those based on the phenolic compounds appear most effective. The phenolic resins give a high yield of char upon pyrolysis, but only with fabrication difficulties when large parts are required. It is reported, however, that a high char yield can be obtained with epoxy or epoxy-novalac resins which can be fabricated into large parts more easily and with less expensive equipment 60/. Polyborophane resins, a class of semi-inorganic resins, have been studied because they yield a low-carbon, oxidation-resistant residue upon pyrolysis 61/.

Finely divided powders have been added to ablative plastics to improve their molding characteristics and to reduce the cost of molded parts 27/. Also, it has been suggested that the addition of certain particulate fillers can greatly enhance char yield when the filler is uniformly dispersed and a method of achieving the necessary dispersion based on certain mold rotations has been demonstrated 60/. Special purpose fillers which have been incorporated

into ablative plastic composites include cobalt oxide, boron carbide, vanadium pentoxide, molybdenum diboride and titanium diboride 26/. Flakes 62/ and hollow microspheres 63/ have been considered as radiation barriers for thermal protection systems, and special "chemical techniques" have been used to introduce radiation barriers into a heat shield 64,65,66/. Special purpose reinforcing agents incorporated into ablative plastic composites include zirconia foil 26/ and hollow glass fibers 67/. The hollow fibers were reported to have superior mechanical strength, mechanical rigidity, thermal insulation value, and electrical transparency.

In some situations where relatively low heating rates are first encountered the chars formed during ablation have exhibited poor structures, which tend to crack and spall during use and to induce delamination. By carbonizing a plastic (using a pyrolysis procedure) prior to its use an an ablator it has been found that many structural deficiencies can be eliminated 52/. Under controlled conditions the carbonized material can still perform its binder function and gives a structure with a promising strength-to-weight ratio and high-temperature stability 68/. However, charring at a high temperature may increase the thermal conductivity of the char 69/.

Mountvala, Nakamura, and Rechter 70/ have made a survey of commerically available materials for heat shields, and Raech 71/ has reported electrical properties for a number of resin-laminates over a wide range of frequencies and temperatures.

## Fabrication Methods

Improved resin impregnation techniques which have been considered for the production of composite thermal protection systems include:

1. spatula coating, dip coating, wet layup and vacuum impregnation 26/

2. dry powder layup and slip-casting 56/

3. centrifugal casting, mat processing and normal casting around prepositioned fibers 72/

Attachment

While attachment methods have probably limited the use of ablative systems, there are indications that either mechanical fastener or bonding techniques are adequate for these systems 73/. Chemical bonding has been the rule for ablator attachment, but mechanical methods have had greater application with materials, such as Teflon®, which exhibit poor adhesion characteristics. The nitril-modified, epoxy-type prepolymer has been suggested as the base for thermal protection systems, as it has been reported to provide excellent adhesion to the metals and plastics currently used in missile fabrication 74/.

When high-speed collisions with foreign particles are of concern, the mechanical fastening of heat shields may be required. The intense shock waves produced by high-speed impacts have been found to promote unbonding in the mechanically stressed regions of ablative heat shields 75/.

Testing

The best laboratory facility available for the evaluation of thermal protection systems appears to be the arc-heated air-jet which is capable of stagnation enthalpies comparable to flight velocities in the range 15,000 - 25,000 ft/sec and capable of achieving heat transfer rates and pressure levels

appropriate for reentry. The power requirements for such a facility is in the megawatt range 76/.

Composite thermal protection systems have been subjected to heat fluxes up to 5280 Btu/ft$^2$-sec and shear stresses up to 60 lb/ft$^2$ in experimental evaluation programs 77/.

The application of test-facility data to predict ablative performance in flight has been discussed by Wick 78/.

Theoretical Work

The ablation process has been treated theoretically by Adams and Scala 74/, Freedman 79/, Hidalgo and Kadanoff 30/, Hurwicz and Fledderman 81/, Hurwicz, Mascula, and Levin 82/, Johnson 83/, McFarland and Joerg 84/, Reinikka and Wells 85/, and Warmbrod 86/, and theoretical reviews have been presented by Economos 31/ and Gerard 87/. Hildalgo and Kadanoff 80/ have compared the theory of ablation with flight data, while Johnson 83/ has compared data from flight tests, plasma tunnel tests and analytical predictions. Capey 88/ has derived a figure of merit for ablative materials.

The internal ablation process has been treated theoretically by Grosh 74/, Vassallo 89,90/, and by Vassallo, Gamnitz and Kirchner 91,92/.

A number of investigators have considered thermal protection systems from the standpoint of analysis 93,94,82,95,96,97,69,85,98,99,100/. Hurwicz and Brown 94/ have accomplished a computer program for the transient analysis of an ablator, and Lafazan and Welsh 96/ have presented a complete analysis and an illustrative example of the ablation process.

Pears and Shoffner 69/ have provided graphs which indicate the dependence of the transient ablation process on material properties such as thermal

expansion, thermal conductivity, mechanical strength, emissivity and heat capacity. Reinikka and Wells 85/ have presented design charts for thermal protection weights when micro-ballooned phenolic nylon is used, and Shapland 98/ has extended a model describing the degradation of nylon-phenolic to the range of interest for the MMERM vehicle.

Strauss 99/ developed a simplified digital analysis for an ablator by assuming a unique pyrolysis temperature and obtained good agreement with data from arc-plasma tests. Swann and Pittman 100/ analyzed the ablation process by finite difference techniques using three layers, the first two with moving boundaries, and obtained good agreement with an exact solution; in this work a number of options were introduced which successfully reduced computer time.

System selection charts for thermal protection have been presented by Heldenfels 93/, Hurwize, Mascula, and Levin 82/ and Steurer 24/. In the work of Hurwize, Mascula, and Levin graphs and tables are given which indicate the values of significant parameters necessary to achieve "reasonable unit weights" (4 to 8 $lb/ft^2$), and the values are compared with typical material properties, on the basis of structural design. Various vehicle parts (including a nose cap, a wing leading edge, and a fuselage) and various thermal protection schemes (radiation, heat sinks, ablation, ablation-radiation, transpiration and insulation) are considered in the design selection.

Schmidt 27/ has considered the model simplifications that have been employed in the analysis of the ablation process.

## REFERENCES


1. N. E. Poulos, J. N. Harris, C. A. Murphy, et al., "Ceramic Systems for Missile Structural Applications," Contract NOw-63-0143-d, Georgia Institute of Technology, Summary Reports No. 2, 31 October 1964 and No. 3, 31 October 1965.

2. R. P. Suess, "Estimates of Temperature and Thermal Stresses to be Encountered in the 1966 OAL Fused Silica Radome Tests," Engineering Memo (Ref. No. EM-4024), Applied Physics Laboratory, The Johns Hopkins University, Silver Spring, Maryland, 21 February 1966.

3. N. E. Poulos, C. A. Murphy and J. N. Harris, "Design and Development of an Electromagnetic Window for Air Lift Reentry Vehicles," Contract AF-33(657)-11504, Georgia Institute of Technology, Technical Report AFAL-TR-66-3-, March 1966.

4. "Design/Development Slip-Cast Fused Silica Radome Assembly," Contract NOw-64-0505-di, Technical Report CR 223-080-004, September 1965.

5. R. J. Roark, Formulas for Stress and Strain, p 275, (McGraw-Hill Book Co., Inc., New York), 1954.

6. W. E. Hauth, Jr., "Slip-Casting of Aluminum Oxide," J. Am. Ceram. Soc. 32, 394-98 (1949).

7. W. Watt and J. P. Roberts, "The Preparation of Alumina Bodies by the Slip-Casting Method," Metallurgia 43, 307-8 (1951).

8. P. Boland, "Strength of Slip-Cast Fused Alumina Fired Near or Below the Tammann Temperature," paper presented at 66th Annual Meeting of the American Ceramic Society, Chicago, Ill., April 1964.

9. P. Howard and A. L. Roberts, "A Study of Alumina Suspensions," Part II, Trans. Brit. Ceram. Soc. 52, 386-403 (1953); Part III, Ibid., 53, 271-291 (1954).

10. V. A. Chase, R. L. Van Auken and R. F. Greene, "Fabrication Techniques for Light Weight Hyper-Environment E-M Windows," Interim Engineering Report No. 2, Project No. 4161, Brunswick Corporation, Marion, Virginia, 1965.

11. W. J. Corbett, A. T. Sales and J. D. Walton, Jr., "Improving the Mechanical Properties of Slip-Cast Fused Silica by Fibrous Reinforcement," Sandia Corporation Contract No. 16-2092, Georgia Institute of Technology, Final Report, 6 August 1965.

12. S. Spinner and W. E. Tefft, "A Method for Determining Mechanical Resonance Frequencies and for Calculating Elastic Moduli From These Frequencies," A.S.T.M. Proc. 61, 1221-1238 (1961).


(Continued)

13. Temperature - Its Measurement and Control in Science and Industry, Vol. 3, pt. 2, p 88, A. I. Dahl, ed. (Reinhold Publishing Corporation, New York), 1962.

14. J. Economy, "Boron Nitride Fibers," presented at the Engineering Institute on Fiber Composite Materials, University of Wisconsin, 8 October 1965.

15. D. L. Schmidt, Technical Manager, Ablation Materials, Nonmetallic Materials Division, Air Force Materials Laboratory, Wright-Patterson Air Force Base, Ohio, private communique and "AFML (MANC) Bibliography of Ablative Plastics Research," (1966).

16. C. R. Mason, J. D. Walton, Jr., M. D. Bowen and W. T. Teague, "Investigation of High Temperature Resistant Materials," Contract No. NOrd-15701, Georgia Institute of Technology, Summary Report No. 3, 31 October 1959.

17. N. E. Poulos, et al., "High Temperature Ceramic Structures," Contract No. NOrd-15701, Georgia Institute of Technology Final Report, 31 October 1962.

18. F. P. Knudsen, "Effect of Porosity on Young's Modulus of Alumina," J. Am. Ceram. Soc. 45, 94-95 (1962).

19. J. N. Harris, C. W. Gorton, A. T. Sales, "Filament Wound Silica Radome Techniques," Contract AF-33(615)-3330, Georgia Institute of Technology, Interim Technical Report No. 4, 15 November 1966.

20. I. J. Gruntfest, "The Outlook for Ablating Heat Protection Systems," pp 1-6 of "Aerodynamically Heated Structures," Prentice-Hall, Inc. (Englewood Cliffs, N. J. 1962).

21. P. A. C. Hanna, "A Survey and Evaluation of Ablation Phenomena," ERR-PO-138 (Jan. 1964).

22. H. A. King, "Materials and Techniques for Thermal Transfer and Accommodation," pp 202-34 of "Proceedings of an International Symposium on High Temperature Technology, Asilomar Conference Grounds, California, October 6-9, 1959," McGraw-Hill Book Company, Inc. (New York 1960).

23. T. L. Norin, "The Measured Electrical Characteristics of Several Ablative and Some Non-Ablative High Temperature Radome Materials," Proceedings of the OSU-RTD Symposium on Electromagnetic Windows," Vol. I, 2-4 June 1964.

24. W. H. Steurer, "Materials for Thermal Protection," pp 94-121 of "Materials for Missiles and Spacecraft," McGraw-Hill Book Co., Inc. (New York 1963).

(Continued)

25. M. H. Israel and S. V. Nardo, "An Annotated Bibliography on Ablation and Related Topics," PIBAL-686 AD-603 139 (May 1964).

26. L. B. Keller, B. G. Kimmel and G. Schwartz, "New Ablative Plastics and Composites, Their Formulation and Processing," AD 454 497 (June 1964).

27. D. L. Schmidt, "Ablative Materials," pp 23-78 of "Air Force Materials Symposium/1965, 9, 10, 11 June - Technical Papers," AFML-TR-65-29 (May 1965).

28. D. L. Schmidt, "Ablative Materials," pp 775-815 of "Materials Symposium 13-15 September 1961, Hotel Westward Ho, Phoenix, Arizona," ASD-TR-61-322, AD-264 193 (July 1961).

29. L. Steg and H. Lew, "Hypersonic Ablation," AD 275-292 (May 1962).

30. E. L. Strauss, "The Historical Background of Reinforced Plastics in Aerospace Vehicles," Chemical Engineering Progress 59, Symposium Series No. 40, 1-8 (1963).

31. Constantino Economos, "Results of Ablation Tests on Several Plastic Models in a Hypersonic Wind Tunnel," WADD-TN-60-273 (July 1961).

32. R. T. Swann, M. B. Dow and S. S. Thompkins, "Analysis of the Effects of Environmental Conditions on the Performance of Charring Ablators," pp 259-69 of "American Institute of Aeronautics and Astronautics, Entry Technology Conference, Williamsburg and Hampton, Va., Oct. 12-14, 1964."

33. F. J. Koubek, B. T. Hartmann and D. M. Caum, "High Temperature Resistant Materials for Missile Propulsion Systems," Summary Report, 30 June 1963 - 30 June 1964, NOLTR-64-207, AD-612504 (Feb. 1965).

34. W. A. Brooks, Jr., R. T. Swann and K. L. Wadlin, "Thermal Protection for Spacecraft Entering at Escape Velocity," SAE Preprint 513F (April 1962).

35. L. E. McAllister, J. C. Bolger, E. L. McCaffery, A. C. Walker, Jr. and F. W. Ward, "Behavior of Pure and Reinforced Charring Polymers During Ablation Under Hypervelocity Re-Entry Conditions. Appendix A - Calculation of Elimination to Cleavage Ratio for Char Protection. Appendix B - X-Ray Diffraction Theory for Random Layer Lattices as Applied to the Structure of Graphite," pp 17-32 of "Applications of Plastics Materials in Aerospace," Chemical Engineering Progress 59, Symposium Series, No. 40, American Institute of Chemical Engineers (New York 1963).

36. J. A. Collins, C. Toscano, D. Moodie and W. Wolz, "Transient Behavior of Composite Thermal Protection Systems" presented at the American Rocket Society Lifting Reentry Vehicles: Structures, Materials and Design Conference, Palm Springs, California, April 4-6, 1961.

(Continued)

37. R. A. Anderson, "Thermal Protection Systems and Structures for Re-entry Vehicles," pp 207-30 of "Virginia Polytechnic Inst., Blacksburg. Re-entry Dynamics, Part II. Proc. of the Conf. on Physics of the Solar System and Re-entry Dynamics," July 31 to Aug. 11, 1961.

38. J. H. Bridges and F. D. Richmond, "Design Considerations for a Re-entry Vehicle Thermal Protection System," pp 761-82 of "Technology of Lunar Exploration. Progress in Astronautics and Aeronautics. Vol. 10," C. I. Cummings and H. R. Lawrence, ed., Academic Press, Inc. (New York 1963).

39. R. W. Evans, F. J. Crossland and W. A. Baginski, "Development of Practical Water/Steam Transpiration Cooled Systems," presented at the AIAA 2nd Annual Meeting, San Francisco, Calif., July 26-29, 1965.

40. J. S. Islinger, "The Structural/Material Considerations for Transpiration Cooling Systems," SAMPE Journal 2, 30-33 (Aub./Sept. 1966).

41. E. W. Adams, "Analysis of Quartz and Teflon Shields for a Particular Re-entry Mission," pp 222-36 of "Proceedings of the 1961 Heat Transfer and Fluid Mechanics Institute," Stanford University Press (Stanford, Calif. 1961).

42. M. C. Adams and E. Scala, "Ceramic Heat Shielding for ICBM Re-entry Vehicle," Ceramic Ind. 74, 128-33 (April 1960).

43. E. L. Strauss, "The Application of Resin-Impregnated Porous Ceramics to Re-entry Vehicle Heat Shields," pp 7-27 of "Aerodynamic Heated Structures," Prentice-Hall, Inc. (Englewood Cliffs, N. J. 1962).

44. S. Goldfein, "Infiltration of Porous Ceramic Materials with Plastics," Army Engineer Research and Development Laboratories, Rep.-1780-TR, AD-445878 (Jul. 1964).

45. N. Bilow, R. Akawie and A. Tuckerman, "Synthesis of New Plastics and Plastic Composites for Rocket Nozzles," AD 445927 (1962).

46. N. Bilow and L. Miller, "Synthesis of New Ablative Plastics for Rocket Nozzles, Part II, (Jan. 1964).

47. Anon., "Honeycombs Bid for High Temperature Use," Chem. Eng. News 40, 44 (July 23, 1962).

48. M. A. Schwartz and T. A. Greening, "Impregnated Foam Ceramic Insulating Materials," a 33 page paper in "National SAMPE Symposium on Insulation Materials and Processes for Aerospace and Hydrospace Applications, 8th, San Francisco, Calif., May 25-28, 1965."

(Continued)

REFERENCES (Continued)

49. E. L. Strauss, "Studies of Advanced Refractory Composites Concepts for Structural and Heat Shield Applications," Martin Report RM-191 (March 1965).

50. F. N. Breslich, Jr. and L. M. Stejskal, "Evaluation of Impregnated Porous Refractory Oxide Composites," ML-TDR-64-185 (May 1964).

51. W. H. Dukes and F. M. Anthony, "Thermal Protection of Lifting Re-entry Vehicles," Aerospace Eng. 22, 108-24 (Jan. 1963).

52. H. S. Schwartz, "New Materials and Physical Constructions for Ablative Use," pp 447-69 of "High Temperature Technology: International Union of Pure and Applied Chemistry, Commission on High Temperatures and Refractories, International Symposium, Pacific Grove, Calif., September 8-11, 1963, Proceedings," Butterworth and Co., Ltd. (London 1964).

53. S. B. Spencer and W. O. Jackson, "A New Fiber for Reinforced Plastic Aerospace Applications," pp 55-63 of "Plastics and Adhesives in the Space Age; Regional Technical Conference, Garden City, N. Y., May 13, 14, 1964, Technical Papers," Society of Plastics Engineers, Inc. (New York 1964).

54. R. W. Farmer, "Air Aging of Inorganic Fibrous Insulations," ML-TDR-64-137 (June 1964).

55. D. L. Schmidt, "New Ablative Plastics and Composite Materials," SAMPE Journal 2, 10-18 (February/March 1966).

56. B. G. Kimmel and G. Schwartz, "New Ablative Plastics and Composites, Their Formulation and Processing," AFML-TR-66-75 (April 1966).

57. F. J. Zimmerman, "Fiber Metals for Meteoroid Protection," presented at the AIAA Fifth Annual Structures and Materials Conference, Palm Springs, Calif., April 1-3, 1964.

58. S. A. Marolo, "Ablative Characterization of Boron Filament Reinforced Plastic Composites - Part I. Preliminary Screening in an Air Arc Environment," AFML-TR-65-348 (Dec. 1965).

59. R. Achard, "General Application of Ablators in Flight Structures," presented to the American Ceramic Society meeting at French Lick, Indiana, September 1964.

60. R. L. Hough, "Ablative Plastics Containing Highly Uniform Concentrations of Particulate Refractory Material," AFML-TR-65-273 (December 1965).

61. C. O. Wilson, Jr. and F. X. Maggio, "Polyborophane Resin Laminates," ML-TDR-64-183, Part II (July 1965).

(Continued)

62. Hal-Curtis Flesher and W. J. Hanav. "Reflective Metallic Flakes in Ablative Plastics," Society of the Plastics Industry, pp 17-F-1 to 17-F-5 (1965).

63. K. H. Styhr, Jr., P. S. Hessinger and Eugene Ryshkewitch, "Research on Low Density Thermal Insulation Materials for Use Above 3000° F," Third Quarterly Status Report for the Period October 1 to December 31, 1962, prepared under NASA Contract NASr-99 (1962).

64. K. H. Styhr, "Research on Low Density Thermal Insulation Materials for Use above 3000° F," NASA-CR-57727 (1964).

65. Ibid., NASA-CR-59210 (1964).

66. Ibid., NASA-CR-60542 (1964).

67. Z. Hashin, et al., "Hollow Glass Fiber Reinforced Laminates," AD 451684 (Final Report 15 June 1963 - 15 August 1964).

68. B. A. Forcht, I. E. Harder and R. K. Carlson, "Reinforced Pyrolyzed Plastics," LTV Aerospace Corp. Report (April 1965).

69. C. D. Pears and J. E. Shoffner, "The Thermal Response of Ablative Materials," a 28 page paper in "National SAMPE Symposium on Insulation-Materials and Processes for Aerospace and Hydrospace Applications, 8th, San Francisco, Calif., May 25-28, 1965."

70. A. J. Mountvala, H. H. Nakamura and H. L. Rechter, "Development of Lightweight Thermal Insulation Materials for Rigid Heat Shields," NASA-CR-68709 (25 June 1965).

71. Harry Raech, Jr., "Prepreg Materials for High Performance Dielectric Applications," pp 11-A-1 to 11-A-6 in "SPI Reinforced Plastics Division, Anniversary Technical Conference, 20th, Chicago, Ill., February 2-4, 1965, Proceedings."

72. R. L. Sharkitt, P. S. Hessinger and Eugene Ryshkewitch, "High-Temperature Resistant Beryllia Fiber-Reinforced Structural Composites," ASD-TDR-62-632. Part II (July 1963).

73. General Dynamics/Fort Worth, "Developments in Thermal-Structural Composites at General Dynamics/Fort Worth," AD-438471 (15 April 1964).

74. R. J. Grosh, "Transient Temperature in a Semi-Infinite Porous Solid with Phase Change and Transpiration Effects," WADD TR 60-105 (1960).

75. J. L. Summers, "Evaluation of the Impact Performance of Realistic Space Structures," NASA-TM-X-51620 (1964).

(Continued)

76. M. C. Adams and E. Scala, "The Interaction of High Temperature Air with Materials During Re-entry," pp 54-60 of "International Symposium on High Temperature Technology, Asilomar, California, 1959 Proceedings," McGraw-Hill (New York 1960).

77. B. J. Mitchel, "Ablative Plastics Characterization," AFML-TR-65-156, Part II. (June 1966).

78. B. H. Wick, "Ablation Characteristics and Their Evaluation by Means of Arc Jets and Arc Radiation Sources," presented at the 7th International Aeronautical Congress on the Problems of Structures of Aviation and Engineering, Paris, France, 14-16 June 1965.

79. S. J. Freedman, "Ablation," Chapter t of "Developments in Heat Transfer," W. M. Rohenow, ed., The M. I. T. Press (Cambridge, Mass. 1964).

80. Henry Hidalgo and L. P. Kadanoff, "Comparison Between Theory and Flight Ablation Data," AIAA Journal 1, 41-45 (Jan. 1963).

81. H. Hurwicz and R. G. Fledderman, "Computer Simulation of Transient Ablation and Heat Conduction Phenomena at a Vaporizing Surface," American Rocket Society Space Flight Report to the Nation/New York Coliseum, October 9-15, 1961.

82. H. Hurwicz, R. E. Mascula and L. Levin, "Glide Re-entry Vehicle Thermal Protection," pp 15-35 in "aerospace Forum, 2nd Session, Proceedings. New York, Institute of the Aerospace Sciences, SMF Fund Paper FF-35, 1963."

83. R. H. Johnson, "Advanced X-15A-2 Ablation System Design, Tests, and Analysis," North American Aviation Report NA 64-177 (14 Feb. 1964).

84. B. L. McFarland and P. Joerg, "A Theory for the Ablation of Heterogeneous Materials," presented at the AIChE National Meeting in New Orleans, March 10, 1963.

85. E. A. Reinikka and P. B. Wells, "Charring Ablators in Lifting Reentry," AIAA Summer Meeting, Los Angeles, Calif., June 17-20, 1963.

86. J. D. Warmbrod, "Calculated Results for the Transient Heating and Melting Process of Glass Shields with Various Material Properties at the Stagnation Point of a Re-entering ICBM," NASA-TN-D-1643 (May 1963).

87. George Gerard, "Optimum Structural Design Concepts for Aerospace Vehicles: Bibliography and Assessment," AFFDL-TR-65-9 (June 1965).

88. E. C. Capey, "Theoretical Evaluation and Minimum Weight Design of Thermal Protection," Royal Aircraft Establishment (England) Technical Report 65041 (Mar. 1965).

(Continued)

89. F. A. Vassallo, "Internally Ablating Composites," ASD-TR-60-697 (April 1961).

90. F. A. Vassallo, "Dimensional Stability Together with Ablation," SAE Preprint 354B (April 1961).

91. F. A. Vassallo, H. G. Camnitz and H. P. Kirchner, "Study of Thermal Radiation Within Solids and Study of Internally Ablating Composites," AD 251332 (May 1961).

92. Ibid, "Part II, Vol. I: Internally Ablating Composites," AD 259948 (Sept. 1961).

93. R. R. Heldenfels, "Structures for Manned Entry Vehicles," pp 197-217 of "Aerodynamically Heated Structures," Prentice-Hall, Inc. (Englewood Cliffs, N. J., 1962).

94. H. Hurwicz and J. D. Brown, "Critical Aero-thermodynamic Parameters in Thermal Protection Design of High-Performance Re-entry Bodies," presented at the American Rocket Society Space Flight Report to the Nation/New York Coliseum, October 9-15, 1961.

95. J. Kondo and J. Sato, "Deformation of the Nose Cone by Sublimating Ablation," Japan Society for Aeronautical and Space Sciences, Transactions 5, No. 8, 69-74 (1962).

96. S. Lafazan and W. Welsh, "The Charring Ablator Concept; Application to Lifting Orbital and Suborbital Entry," pp 435-69 of "Dynamics of Manned Lifting Planetary Entry," John Wiley and Sons, Inc. (New York 1963).

97. F. W. Matting and D. R. Chapman, "Generalized Ablation Analysis with Application to Heat-Shield Materials and Tektite Glass," American Institute of Aeronautics and Astronautics, 2nd Annual Meeting, San Francisco, Calif. 26-29 July 1965.

98. D. J. Shapland, "Preliminary Design of a Mars-Mission Earth Re-entry Module," pp 525-76 in "NASA, Marshall Space Flight Center Proc. of the Symp. on Manned Planetary Missions, 1963/1964 Status 12 June 1964."

99. E. L. Strauss, "Heat Transfer and Thermal Exposure Studies of Resin Impregnated Zirconia Foam" presented at the Eighth Symposium on Ballistic Missile and Space Technology, 17 Oct. 1963, at San Diego., Calif.

100. F. T. Swann, C. M. Pittman and J. C. Smith, "One-Dimensional Numberical Analysis of the Transient Response of Thermal Protection Systems," NAS-TN-D-2976 (Sept. 1965).

(Continued)

## REFERENCES (Concluded)


101. Reproduced from data obtained on a concurrent research program at the Engineering Experiment Station of the Georgia Institute of Technology under Contract DA-01-021-AMC-14464(Z).

102. H. A. Perry, Adhesive Bonding of Reinforced Plastics, McGraw-Hill Book Co., 1959.

## BIBLIOGRAPHY

For the purpose of completeness and for the convenience of the reader, entries listed under REFERENCES in this report are incorporated in this BIBLIOGRAPHY on HEAT SHIELDS whenever they pertain.


Achard, R., "General Application of Ablators in Flight Structures," presented to the American Ceramic Society meeting at French Lick, Indiana, September 1964.

Adams, E. W., "Analysis of Quartz and Teflon Shields for a Particular Re-entry Mission," pp 222-36 of "Proceedings of the 1961 Heat Transfer and Fluid Mechanics Institute," Stanford University Press (Stanford, Calif. 1961).

Adams, J. J. and Sterry, J. P, "High Temperature Fibrous Insulations," AD 453218 (Oct. 1964).

Adams, J. J. and Sterry, J. P, "Zirconia Fibrous Insulation," AD 439841 (Dec. 1963).

Adams, M. C., "Recent Advances in Ablation," ARS Journal 29, 625-632 (Sept., 1959).

Adams, M. C., Powers, W. E., and Georgiev, S., "An Experimental and Theoretical Study of Quartz Ablation at the Stagnation Point," AVCO-Everett Research Laboratory, Research Report 57 (June 1959).

Adams, M. C. and Scala, E., "Ceramic Heat Shielding for ICBM Re-entry Vehicle," Ceramic Ind. 74, 128-33 (April 1960).

Adams, M. C. and Scala, E., "The Interaction of High Temperature Air with Materials During Re-entry," pp 54-60 of "International Symposium on High Temperature Technology, Asilomar, California, 1959 Proceedings,: McGraw-Hill (New York 1960).

Air Force Materials Laboratory, Technical Staff, "Emerging Aerospace Materials," AFML-TR-64-114 (April 1965).

Alfille, Lucien, "Laminated Material Having High Thermal Isolating Properties," British Patent No. 887,345 (Jan. 17, 1962).

Allen, W. C., "Research on Thermal Transfer Phenomena," Final Report for the Period Jan. 1 to Dec. 31, 1965, National Beryllia Corporation under Contract NASw-1197.

Anderson, R. A., "Structures Technology - 1964." Astronautics and Aeronautics 2, 14-20 (Dec. 1964).

Anderson, R. A., "Thermal Protection Systems and Structures for Re-entry Vehicles," pp 207-30 of "Virginia Polytechnic Inst., Blacksburg. Re-entry Dynamics, Part II. Proc. of the Conf. on Physics of the Solar System and Re-entry Dynamics, July 31 to Aug. 11, 1961."

Anon., "Honeycombs Bid for High Temperature Use," Chem. Eng. News -, 44 (July 23, 1962).

Anon., "Fibrous Research," Frontier 24, 6-8, 10-13 (Winter 1963).

Anon., "Early Data Indicate Success for Appollo Re-entry System," Missiles and Rockets 18, 33 (March 7, 1966).

Aves, W. L., Jr. and Hart, R. A., "Metal-Ceramic Laminated Skin Surface," U. S. Patent No. 3,031,331 (April 24, 1962).

Baltakis, F., Hurd, D., and Holmes, R., "Effects of High Temperature, High Velocity Gases on Plastic Materials," AD 243368 (June 1960).

Bashilin, P. J., Litant, I., and Walker, B. M., "Dielectric Materials for Hypersonic Re-entry Applications," Proceeding of the OSU-RTD Symposium on Electromagnetic Windows, Vol. III, 2-4 June 1964.

Batchelor, J., Vasiloff, N., McCormick, S., and Olcott, E., "Development and Evaluation of Solid Propellant Rocket Motor Case Insulating Materials Systems," AD 243969 (June 1960).

Ibid, "Part II," AD 268022 (May 1961).

Batchelor, J., Simmons, J., and West, W., "Chemical Reactions Between Plastic Composites Materials and Propellant Exhaust Products," AD 422955 (Aug. 1963).

Beecher, N. and Rosenweig, R. E., "Ablation Mechanisms in Plastics with Inorganic Reinforcement," ARS Journal 31, 532 (April, 1961).

Bendix Corporation, "Lightweight Refractories Resistant to Thermal Shock," British Patent No. 944,578 (Dec. 18, 1963).

Bethe, H. A. and Adams, M. C., "A Theory for the Ablation of Glassy Materials," Journal of the Aero/Space Sciences 26, 321-28 (June 1959).

Bilow, N. and Miller, L., "Synthesis of New Ablative Plastics for Rocket Nozzles," AD 400607 (Jan. 1963).

Ibid, "Part II" (Jan. 1964).

Bilow, N., Akawie, R., and Tuckerman, A., "Synthesis of New Plastics and Plastic Composites for Rocket Nozzles," AD 445927 (1962).

Bilow, N. and Miller, L., "Ablative Phenolic and Polyphenylene Resins," AD 463353 (March 1965).

The Boeing Company, "Evaluation of Impregnated Porous Refractory Oxide Composites," Quarterly Progress Reports One, Two, and Three prepared under Contract AF 33(657)-11222 (October 1963, January 1964, and April 1964).

Boland, Paul and Walton, J. D., Jr., "Aerospace Ceramics - Characteristics and Design Principles," AFML-TR-65-171 (June 1965).

Bond, A. C., Rashis, B., and Levin, L. R., "Experimental Ablation Cooling," NACA RM L58E15a (July 1958).

Bonin, J. H., Price, C. F., and Taylor, D. E., "Determination of Factors Governing Selection and Application of Materials for Ablation Cooling of Hypervelocity Vehicles," WADC TR 59-87 (January 1959).

Boobar, M. G., "Mariner B/Voyager Entry Capsule Preliminary Design Study. Final Report," NASA-CR-53675 (10 Oct. 1963).

Bowen, M. D., "Summary Report on Plasma Ablation Tests," Martin Company Orlando, Florida, Report OR 3240 (April 1964).

Breslich, F. N., Jr. and Stefskal, L. M., "Evaluation of Impregnated Porous Refractory Oxide Composites," ML-TDR-64-185 (May 1964).

Bridges, J. H. and Richmond, F. D., "Design Considerations for a Re-entry Vehicle Thermal Protection System," pp 761-82 of "Technology of Lunar Exploration. Progress in Astronautics and Aeronautics. Vol. 10," Cummings, C. I. and Lawrence, H. R., ed., Academic Press, Inc. (New York 1963).

Broding, W. C., Diederich, F. W., and Parker, P. S., "Structural Optimization and Design Based on a Reliability Design Criterion," Journal Spacecraft and Rockets, 1, 56-61 (Jan.-Feb. 1964).

Bromberg, R. and Lipkis, R. P., "Heat Transfer in Boundary Layers with Chemical Reactions Due to Mass Addition," ARS Jet Propulsion 28, (October 1958).

Brooks, W. A., Jr., "Evaluation of Materials in Entry Heating Simulation," NASA-TM-X-54976 (Aug. 1964).

Brooks, W. A., Jr., Swann, R. T., and Wadlin, K. L., "Thermal Protection for Spacecraft Entering at Escape Velocity," SAE Preprint 513F (April 1962).

Burgman, H. A., "Selecting Structural Adhesive Materials," Electo-Technology 75, 69-75 (June 1965).

Burgman, J. A., "Hollow Glass Fibers," pp 6B-1 to 6B-8 of "SPI Reinforced Plastics Division, Anniversary Technical Conference, 20th, Chicago, Ill., February 2-4, 1965, Proceedings."

Buhler, R., Christensen, D., and Grindle, S., "Effects of Hyperthermal Conditions on Plastic Ablation Materials," AD 274835 (Jan. 1962).

Burhard, K., Hoercher, H., Hogan, W., John, R., Megrue, J., and Recesso, J., "Characterization of Carbonized Plastic Composites in Hyperthermal Environments," ASD-TDR-62-746 (April 1963).

Burleson, W. G. and Reynolds, R. A., "Theoretical Effects of Reentry Aerodynamic Heating on the External Skin Structure of AMRAD Experiment Number One," AD 465896 (30 April 1965).

Capey, E. C., "Theoretical Evaluation and Minimum Weight Design of Thermal Protection," Royal Aircraft Establishment (England) Technical Report 65041 (Mar. 1965).

Carlson, R., Forcht, B., Medfo J., McKenney, A., McQuiston, F., and Scott, R., "Carbonized Plastic posites for Hyperthermal Environments," AD 277376 (June 1962).

Ibid, "Part II," AD 403363 (Feb. 1963).

Chamberlain, D., Van Sickle, D., and Marynowski, C., "A Study of the Mechanism of Ablation of Reinforced Plastics," AD 256558 (Feb. 1961).

Chapman, A. J., "An Experimental Evaluation of Three Types of Thermal Protection Materials at Moderate Heating Rates and High Total Heat Loads," NASA-TN-D-1814 (July 1963).

Chapman, A. J., "An Experimental Investigation of Several Ablation Materials in an Electric-Arc-Heated Air Jet," NASA-TN-D-1520 (April 1963).

Citron, S. J., "Heat Conduction in a Melting Slab," presented at the Institute of Aeronautical Sciences 27th Annual Meeting, New York (January 1959).

Clauser, H. R., Hauck, J. E., Fabian, R. J., Peckner, D., Lubars, W., and Campbell, J. B., Mater. Design. Eng. 58, 79-126 (September 1963).

Coffman, J., Kibler, G., Riethof, T., and Watts, A., "Carbonization of Plastics and Refractory Materials Research," AD 257747 (Feb. 1961).

Coffman, J., Kibler, G., Lyon, T., and Acchione, B., "Carbonization of Plastics and Refractory Materials Research, Part II," AD 297946 (Jan. 1963).

Coffman, J., and Friedman, H., "Carbonization of Plastics and Refractory Materials Research, Part III, Vol. I," AD 433021 (July 1963).

Collins, J. A., Toscano, C., Moodie, D., and Wolz, W., "Transient Behavior of Composite Thermal Protection Systems," presented at the American Rocket Society Lifting Reentry Vehicles: Structures, Materials and Design Conference, Palm Springs, California, April 4-6, 1961.

Colton, R. M. and Dobbins, E. B., "Re-entry Vehicle for Radar Selectivity Evaluations," pp 179-92 of "Army Dept. Army Sci. Conf. Proc. Vol. I" (1964).

Compton, D. L., Winovich, Warren, and Wakefield, R. M., "Ablating Heat Shields for Low-angle Re-entry," Space/Aeronautics 39, 123-25 (Jan. 1963).

Cordo Chemical Corp., "Report on Ablative Properties of Materials Molded at Autoclave Pressures. III. Molding Compounds," Cordo Research and Development Project No. CLX67 (July 15, 1963).

Cosenza, C. J., Ingram, J. C., Jr. and Guyton, R. D., "Materials and Construction Concepts for Structures Subjected to Severe Kinetic Heating," pp 847-73 of "Aeronautical Systems Div., Air Force Systems Command, Wright-Patterson AFB, Ohio, Proc. of the first USAF Symp. on Aerothermoelasticity, Dayton, Ohio, 30-31 Oct. and 1 Nov. 1961 (Feb. 1962).

Czarnecki, E. G., "Structures and Materials," Astronautics 7, 132,133, 135 (November 1962).

Dastin, S. J. and Rosenberg, Philip, "Reinforced Plastics for Project Fire Re-Entry Vehicle," in "Plastics and Adhesives in the Space Age; Regional Technical Conference, Garden City, N. Y., May 13, 14, 1964, Technical Papers."

David, D., "A State-of-the-Art on Ablative Thrust Chamber Technology," Plastics Design and Processing (August 1963).

Davidson, J. R. and Dalby, J. F., "Optimum Design of Insulated Compression Plates Subjected to Aerodynamic Heating," NASA TN D-520 (Jan. 1961).

Davis, R. M. and Milewski, C., "High Temperature Composite Structure," ASD-TDR-62-418 (June 1962).

Davis, R., Milewski, C., and Matra, J., "Ablator Attachment Techniques for Glide Re-entry Vehicles," AFFDL-TR-66-29 (April 1966).

Diaconis, N. S., Fanucci, J. B., and Sutton, G. W., "The Heat Protection Potential of Several Ablation Materials for Satellite and Ballistic Re-entry into the Earth's Atmosphere," General Electric Aerosciences Laboratory, R59SD423.

Dillon, H. P., II., "High Temperature Coatings," U. S. Patent 3,091,543 (May 28, 1963).

Donaldson, W. E. and Castonquay, T. T., "Thermal Studies of Reinforced-Plastic Materials. Part I. Diffusivity of Five Reinforced-Plastic Heat Barriers," AD 403360 (Feb. 1963).

Dooley, D. and Denison, R., "Combustion in the Laminar Boundary Layer of Chemically Active Sublimators," Aeronutronics Systems Publication U-110 (September 1957).

Dowell, John R., "Low-Modulus High-Temperature Cement," Adhesives Age 7, 26-28 (Sept. 1964).

Dukes, W. H., "Protection of Aircraft Structures Against High Temperatures," pp 781-94 in Advances in Aeronautical Sciences Vol. 4, 2nd International Congress in the Aeronautical Sciences, Proceedings, Zurich, Switzerland, Sept. 12-16, 1960," Pergamon Press, Inc. (New York 1962).

Dukes, W. H. and Anthony, F. M., "Thermal Protection of Lifting Re-entry Vehicles," Aerospace Eng. 22, 108-24 (Jan. 1963).

Economos, C., "Ablation Tests on Plastic Models in a Hypersonic Wind Tunnel," ARS Journal 32 (July 1962).

Economos, Constantino, "Results of Ablation Tests on Several Plastic Models in a Hypersonic Wind Tunnel," WADD-TN-60-273 (July 1961).

Eggers, A. J., Jr. and Wong, T. J., "Motion and Heating of Lifting Vehicles During Atmosphere Entry," ARS Journal 31 (October 1961).

Eliason, L. K., Rice, D. H., Sanford, E. L., and Poe, T. L., "Testing of Ablation Material: Preliminary Data Concerning Nondegraded Ablation Materials Nos. 1, 2, 3, and 4," NASA-CR-53658 (1964).

Erb, R. B., "Thermal Balance and Heat Protection," Chapter 11 of "Manned Spacecraft-Engineering Design and Operation," Purser, P. E., et al, ed., Fairchild Publications, Inc. (New York 1964).

Erb, R. B. and Jacobs, Stephen, "Entry Performance of the Mercury Spacecraft Heat Shield," presented at the AIAA Entry Tech. Conf., Heat Protection Session, Williamsburg, Hampton, Va. 12-14 Oct. 1964.

Evans, R. W., Crossland, F. J., and Baginski, W. A., "Development of Practical Water/Steam Transpiration Cooled Systems," presented at the AIAA 2nd Annual Meeting, San Francisco, Calif., July 26-29, 1965.

Fanucci, J. B., "Ablation Characteristics of a Glassy Material in a Decelerating Environment," Aerophysics Technical Memorandum No. 135, General Electric Company (MSVD).

Farmer, R., "Thermogravimetry of Plastics," AD 402999 (Feb. 1963).

Farmer, R., "An Arc-Imaging Furnace for Materials Research," AD 291836 (May 1962).

Farmer, R., "Ablative Behavior of Plastics in Subsonic and Supersonic Hyperthermal Flow," AD 252763 (Nov. 1960).

Farmer, R., "The Thermal Diffusivity of a Structural Plastic Laminate at Elevated Temperatures," AD 249275 (Sept. 1960).

Farmer, R., "Degradation Effects of High Intensity Thermal Radiation on Plastic Radome Materials," AD 231285 (July 1960).

Farmer, R. W., "Titania-Filled Ablative Plastics," AD 452251 (Oct. 1964).

Farmer, R. W., "Air Aging of Inorganic Fibrous Insulations," ML-TDR-64-137 (June 1964).

Farmer, R. W., "Procedural Variables in the Thermogravimetry of Plastics," AD 441169 (April 1964).

Fein, M. M., Tunkel, S. J., and Cohen, M. S., "New Developments in Ablative Cooling," Chemical Engineering Progress 60, No. 52, 99-104 (1964).

Flesher, Hal-Curtis and Hanav, W. J., "Reflective Metallic Flakes in Ablative Plastics," Society of the Plastics Industry, pp 17-F-1 to 17-F-5, (1965).

Fields, E. M., Hopko, R. L., Swain, R. L., and Trout, O. F., Jr., "Behavior of Some Materials and Shapes in Supersonic Free Jets at Stagnation Temperatures up to 4210° F, and Descriptions of the Jets," NACA RM L 57K26 (Feb. 24, 1958; Declassified Feb. 8, 1960).

Forcht, B. A., et al, "Pyrolyzed Plastic Composites," AD 454497 (Feb. 1964).

Forcht, B. A., Harder, I. E., and Carlson, R. K., "Reinforced Pyrolyzed Plastics," LTV Aerospace Corp. Report (April 1965).

Forcht, B. A., Haviland, J. K., and McKinney, A. R., "Carbonized Plastics Composites for Hyperthermal Environments, Part II, Synthesis of Improved Thermally Protective Plastics and Composites," ASD-TDR-62-352, Part II (Feb. 1963).

Freedman, S. J., "Ablation," Chapter 5 of "Developments in Heat Transfer," Rohenow, W. M., ed., The M. I. T. Press (Cambridge, Mass. 1964).

Gage, C. C., "Spacecraft and Missile Structures," Space/Aeronautics 42, 20-21 (Sept. 1964).

General Dynamics/Fort Worth, "Developments in Thermal-Structural Composites at General Dynamics/Fort Worth," AD-438471 (15 April 1964).

General Electric, "Re-entry Ablation of Reinforced Plastics," GE Report No. PIB-15.

Georgiev, S., Hidalgo, H., and Adams, M. C., "On Ablating Heat Shields for Satellite Recovery," AVCO-Everett Research Laboratory, Research Note 147 (July 1959).

Gerard, George, "Optimum Structural Design Concepts for Aerospace Vehicles: Bibliography and Assessment," AFFDL-TR-65-9 (June 1965).

Gerard, G., "Structural Interplay: Design and Materials," Aero/Space Engineering 18, 37-42, (Aug. 1959).

Glasser, Julian and Sump, C. H., "Evaluation of Manufacturing Methods for Fibrous Composite Materials," Chemical and Metallurgical Research, Inc. (July 10, 1964).

Glaser, P. E., ed., "Aerodynamically Heated Structures," Prentice Hall, Inc. (Englewood Cliffs, N. J., 1962).

Glaser, P. E., "Advances in Thermal Insulating Materials for Thermal Protection Systems," presented at the American Rocket Society Space Flight Report to the Nation/New York Coliseum, October 9-15, 1961.

Goldfein, S., "Infiltration of Porous Ceramic Materials with Plastics," Army Engineer Research and Development Laboratories, Rep.-1780-TR, AD-445878 (Jul. 1964).

Goodman, T. R., "Aerodynamic Ablation of Melting Bodies," Proceedings of the Third U. S. National Congress of Applied Mechanics, Brown University (1958).

Greco, Frank, "Contour Forming of Honeycomb," Grumman Aircraft Engineering Corporation, Note No. ADN-08-18-64.1 (15 July 1964).

Grinberg, I. M., "Determination of Analytical Techniques Available to Determine Material Suitability for Turning of Hot Gases," AD 626 430 (May 1965).

Grindle, S. L. and Todd, J. P., "Evaluation of Thermal Protection Systems Under Simulated Re-Entry Conditions," ML-TDR-64-293 (Feb. 1965).

Gross, M. E., Mehrbrodt, A. W., and McKinstry, D. G., "Low-Density Thermal Insulation Materials," a 19 page paper in "National SAMPE Symposium on Insulation-Materials and Processes for Aerospace and Hydrospace Applications, 8th, San Francisco, Calif., May 25-28, 1965."

Grosh, R. J., "Transient Temperature in a Semi-Infinite Porous Solid with Phase Change and Transpiration Effects," WADD TR 60-105 (1960).

Gruntfest, Irving and Shenker, Lawrence, "Ablation," International Science and Technology, 48-51, 54-57 (July 1963).

Gruntfest, I. J., "The Outlook for Ablating Heat Protection Systems," pp 1-6 of "Aerodynamically Heated Structures," Prentice-Hall, Inc. (Englewood Cliffs, N. J. 1962).

Guyton, R. D., "High Temperature Composite Structural Configurations: Radiative Thermal Protection Systems for 2500° to 4500° F," pp 151-69 of "Aerodynamically Heated Structures," Glaser, P. E., ed., Prentice-Hall, Inc. (Englewood Cliffs, N. J. 1962).

Hamaker, F. A., "The Ames Atmosphere Entry Simulator and Its Application to the Determination of Ablative Properties of Materials for Ballistic Missiles," NASA-TM-X-394 (Oct. 1960).

Hanna, P. A. C., "A Survey and Evaluation of Ablation Phenomena," ERR-PO-138 (Jan. 1964).

Harris, J. T., "High Temperature Metallic Fabric for Re-entry Applications," 4 page paper in "Society of Automotive Engineers, National Aerospace Engineering & Manufacturing Meeting, Los Angeles, Calif., Oct. 8-12, 1962. Paper 590A."

Harris, R. S., Jr. and Davidson, J. R., "Methods for Determining the Optimum Design of Structures Protected from Aerodynamic Heating and Applications to Typical Boost-Glide or Reentry Flight Paths," NASA TN D-990, (March 1962).

Hartman, B. T., Koubek, F. J., and Caum, D. M., "High Temperature Resistant Materials for Missile Propulsion Systems," AD 627519 (29 Nov. 1965).

BIBLIOGRAPHY (Continued)

Hartsock, J. A., "How to Select Materials for Composite Panels," Materials in Design Engineering 63, 72-3 (March 1966).

Hashin, Z. et al, "Hollow Glass Fiber Reinforced Laminates," AD 451684 (Final Report 15 June 1963-15 August 1964).

Haudenchild, C., "Determination of Properties of Sandwich Materials Subjected to Rapid Rising Temperatures," AD 2-6543 (July 1960).

Head, J. W., "Research on Phenyl Silane High Temperature Laminating Resins," AD 436 267 (31 December 1961).

Hearne, L. F., Chin, Jin H., and Lefferdo, J. M., "Reentry Heating and Thermal Protection of a Mars-Mission Earth-Reentry Module," pp 113-135 in: "American Institute of Aeronautics and Astronautics, Entry Technology Conference, Williamsburg and Hampton, Va., October 12-14, 1964, Technical Papers."

Heldenfels, R. R., "Structures for Manned Entry Vehicles," pp 197-217 of "Aerodynamically Heated Structures" Prentice-Hall, Inc. (Englewood Cliffs, N. J., 1962).

Hidalgo, Henry and Kadanoff, L. P., "Comparison Between Theory and Flight Ablation Data," AIAA Journal 1, 41-45 (Jan. 1963).

Hilhouse, R. T., "Cementitious Ceramic Materials," AD 414515 (Aug. 1963).

Hough, R., "Refractory Reinforcements for Ablative Plastics," AD 291903 (June 1962).

Ibid, "Part II, Synthesis of Zirconium Nitride and Zirconium Oxide Flakes," AD 423531 (Oct. 1963).

Ibid, "Part III, Pyrolytic Boride Reinforcing Agents," AD 449439 (Aug. 1964).

Ibid, "Part IV, Synthesis Apparatus for Continuous Filaments Reinforcements," AD 454665 (Dec. 1965).

Hough, R. L., "Ablative Plastics Containing Highly Uniform Concentrations of Particulate Refractory Material," AFML-TR-65-273 (December 1965).

Hough, R., "Continuous Pyrolytic Graphite Filaments," AD 460724 (Dec. 1964).

Hoshizaki, "Heat Transfer in Planetary Atmospheres at Super-Satellite Speeds," Presented at ARS Space Flight Report to the Nation, New York, October 1961.

Hurwicz, H. and Brown, J. D., "Critical Aero-thermodynamic Parameters in Thermal Protection Design of High-Performance Re-entry Bodies," presented at the American Rocket Society Space Flight Report to the Nation/New York Coliseum, October 9-15, 1961.

Hurwicz, H., and Brown, J., "Interaction of Ablation Material and Certain Trajectory Parameters in the Thermal Protection Design of Space Re-entry Vehicles," AVCO RAD-TR-9 (7)-59-28 (19 November 1959).

Hurwicz, H. and Fledderman, R. G., "Computer Simulation of Transient Ablation and Heat Conduction Phenomena at a Vaporizing Surface," American Rocket Society Space Flight Report to the Nation/New York Coliseum, October 9-15, 1961.

Hurwicz, H., Mascula, R. E., and Levin, L., "Glide Re-entry Vehicle Thermal Protection," pp 15-35 in "Aerospace Forum, 2nd Session, Proceedings. New York, Institute of the Aerospace Sciences, SMF Fund Paper FF-35, 1963."

Islinger, J. S., "The Structural/Material Considerations for Transpiration Cooling Systems," SAMPE Journal 2, 30-33 (Aug./Sept. 1966).

Israel, M. H. and Nardo, S. V., "An Annotated Bibliography on Ablation and Related Topics," PIBAL-686 AD-603 139 (May 1964).

John, R., Hoercher, H., Mitchel, B., Recasso, J., O'Connor, T., DeBolt, H., Hanst, P., and Rosenweig, R., "Arc Heater Characterization of Ablative Plastics," AD 452028 (Oct. 1964).

Johnson, R. H., "Advanced X-15A-2 Ablation System Design, Tests, and Analysis," North American Aviation Report NA 64-177 (1- Feb. 1964).

Johnson, R. H. and Johnston, E. W., "Development of an Ablative Protective System for the X-15A-2 Research Aircraft," pp 288-38 in "American Institute of Aeronautics and Astronautics, Entry Technology Conference, Williamsburg and Hampton, Va., October 12-14, 1964, Technical Papers."

Johnson, Read, Jr., and Yam, C. Y., "Structural and Thermal Considerations of Ablative-Covered Nonmetallic Protective Shells," presented at the AIAA Fifth Annual Structures and Materials Conference, Palm Springs, Calif., April 1-3, 1964.

Judge, J. F., "NASA, AF Funding AVCO Multidirectional Reinforced Plastics," Technology Week 19, 28-29 (Oct. 31, 1966).

Julian, A. H., "New Re-entry Shapes," Space/Aeronautics 39, 81-83 (Apr. 1963).

Kallup, Charles, Jr., Sklarew, Samuel, and Castner, S. V., "Application and Evaluation of Reinforced Refractory Ceramic Coatings," ML-TDR-64-81 (June 1964).

Kaminsky, E. L., Gluck, R., Kaplan, S., and Offenhartz, E., "Structural Requirements for Manned Spacecraft Heat Shield Materials Exposed to Environments Ranging from Deep Space Through Parabolic Earth Entry," presented at the AIAA Fifth Annual Structures and Materials Conference Palm Springs, Calif., April 1-3, 1964.

Kelble, J. M. and Bernados, J. E., "High Temperature Nonmetallic Materials," Aerospace Eng. 22, 56-75 (Jan. 1963).

Keller, L., Kimmel, B., and Schwartz, G., "New Ablative Plastics and Composites, Their Formulation and Processing, Part I," AD 464369 (April 1965).

Keller, L. B., Kimmel, B. G., and Schwartz, G., "New Ablative Plastics and Composites, Their Formulation and Processing," AD 454 497 (June 1964).

Keller, L. B. and Schwartz, S., "Formulation and Processing Techniques for New Ablative Plastics and Composites," ASD-TDR-63-568 (June 1963).

Kimmel, B. G. and Schwartz, G., "New Ablative Plastics and Composites, Their Formulation and Processing," AFML-TR-66-75 (April 1966).

King, H. A., "Materials and Techniques for Thermal Transfer and Accommodation," pp 202-34 of "Proceedings of an International Symposium on High Temperature Technology, Asilomar Conference Grounds, California, October 6-9, 1959," McGraw-Hill Book Company, Inc. (New York 1960).

Kinnard, L., "The Ablation of Phenolic Nylon," Martin Company, ER 12158 (October 1962).

Klein, Bertram, "Hollow Spheres: Versatile Design Tool," Research/Development 17, 40 (Jan. 1966).

Klein, Bertram, "Ultra-Lightweight, Highly Efficient, High-Temperature, Thermal-Insulation System," Journal of Spacecraft and Rockets 1, 352 (May-June 1964).

Knuth, E. L., "Compressible Couette Flow With Diffusion of a Reactive Gas From a Decomposing Wall," 1958 Heat Transfer and Fluid Mechanics Institute, pp 104-13 (June 1958).

Kobrin, C. L., "Cellular Materials," Iron Age 192, 147-54 (Oct. 10, 1963).

Kohn, S., "Heat-Shield Materials for Supersonic Vehicles and Space Probes," Technique et Science Aeronautiques et Spatiales (Mar.-Apr. 1963).

Kondo, J. and Sato, J., "Deformation of the Nose Cone by Sublimating Ablation," Japan Society for Aeronautical and Space Sciences, Transactions 5, No. 8, 69-74 (1962).

Kotanchick, J. N. and Erb, R. B., "The Design of Ablative Thermal Protection Systems," presented at the 7th International Aeronautical Congress on the Problems of Structures of Aviation and Engineering, Paris, France, 14-16 June 1965.

Koubek, F. J., Hartmann, B. T., and Caum, D. M., "High Temperature Resistant Materials for Missile Propulsion Systems, Summary Report, 30 June 1963 - 30 June 1964," NOLTR-64-207, AD-612504 (Feb. 1965).

Koubek, F. J. and Timins, A. R., "High Temperature Testing of Ceramics for Re-entry Body Applications," AD 227 641 (12 June 1959).

Kremith, R. D., "Thermal Erosion of Ablative Materials," AD 455774 (June 1964).

Krusos, J. N., et al, "Sheet Beryllium - Composite Structures," AD-284 842 (July 1962).

Kuno, J. K., "Tape Wrapping of Thermal Insulation, pp 15-C-1 to 15-C-12 in "Society of the Plastics Industry, Reinforced Plastics Div., Annual Technical and Management Conference, 18th, Proceedings. New York, Society of the Plastics Industry, Inc., 1963."

Lachman, W. L. and Sterry, J. P., "Ceramic Fibers Backbone for Aerospace Projects," Ceram. Ind. 84, 120-23, 134-36 (April 1965).

Lafazan, S., and Siegel, B., "Ablative Thrust Chambers for Space Application," American Institute of Chemical Engineers, 46th National Meeting, February 5, 1962.

Lafazan, S. and Welsh, W., "The Charring Ablator Concept; Application to Lifting Orbital and Suborbital Entry," pp 435-69 of "Dynamics of Manned Lifting Planetary Entry," John Wiley and Sons, Inc. (New York 1963).

Landau, H. G., "Heat Conduction in a Melting Solid," Quarterly of Applied Mathematics 8, 81-94 (April 1950).

Lapple, C., Brady, A., and Chamberlain, D., "Mechanism of Ablation of Char-Forming Ablative Plastics," AD 268946 (Sept. 1961).

Lees, L., "Similarity Parameters for Surface Melting of a Blunt Nosed Body in a High Velocity Gas Stream," American Rocket Society Journal 29, 345-54 (May 1959).

Lees, Lester, "Convective Heat Transfer with Mass Addition and Chemical Reactions," paper presented at the Third Combustion and Propulsion Colloquium, AGARD, NATO, Palermo, Sicily, May 1958.

Lees, Lester, "Laminar Heat Transfer over Blunt-nosed Bodies at Hypersonic Flight Speeds," ARS Jet Propulsion 26, (April 1956).

Licciardello, M. R., "Development of Frontal Section for Super-Orbital, Lifting, Re-entry Vehicle. Vol. III: ASSET Nose Cap," FDL-TDR-64-59, Vol. III (29 May 1964).

Licciardello, M. R. Ohnysty, B., and Stetson, A. R., "Development of Frontal Section for Super-Orbital, Lifting, Re-entry Vehicle. Vol. II: Materials and Composite Structure Development," FDL-TDR-64-59, Vol. II. (29 May 1964).

Lockheed Missiles & Space Co., "Study of Heat Shielding Requirements for Manned Mars Landing and Return Missions, Summary Report," NASA CR-308 (Oct. 1964).

Love, E. S. and Pritchard, E. B., "A Look at Manned Entry at Circular to Hyperbolic Velocities," pp 167-188 of "2nd Manned Space Flight Meeting. New York, AIAA, 1963."

Lundell, J. H., Wakefield, R. M., and Jones, J. W., "Experimental Investigation of a Charring Ablative Material Exposed to Combined Convective and Radiative Heating in Oxidizing and Nonoxidizing Environments," NASA-TM-X-54797 (1964).

Lurie, R. M., Georgiev, S., and Levine, P., "Thermal Problems of Ablative Materials in Various Planetary Atmospheres," pp 91-98 of "Chemical Engineering Techniques in Aerospace," Chemical Engineering Progress 60, Symposium Series No. 52, American Institute of Chemical Engineers (New York 1964).

Malott, J. S., "The Ablation Heat Shield," SPE Journal (May 1961).

Marolo, S., "Properties and Characteristics of Ablative Plastic Chars," AD 403050 (Feb. 1963).

Marolo, S., "Microstructure of Ablative Plastic Chars," AD 269131 (Feb. 1961).

Marolo, S. A., "Ablative Characterization of Boron Filament Reinforced Plastic Composites - Part I. Preliminary Screening in an Air Arc Environment," AFML-TR-65-348 (Dec. 1965).

Matonis, V. A., "Elastic Behavior of Low Density Rigid Foams in Structural Applications," SPE Journal 20, 1024-30 (Sept. 1964).

Matting, F. W. and Chapman, D. R., "Generalized Ablation Analysis with Application to Heat-Shield Materials and Tektite Glass," American Institute of Aeronautics and Astronautics, 2nd Annual Meeting, San Francisco, Calif., 26-29 July 1965.

Mayer, E., "Analysis of Convective Heat Transfer in Rocket Nozzles," ARS Journal 31 (July 1961).

McAllister, L. E., Bolger, J. C., McCaffery, E. L., Walker, A. C., Jr., and Ward, F. W., "Behavior of Pure and Reinforced Charring Polymers During Ablation Under Hypervelocity Re-Entry Conditions. Appendix A-Calculation of Elimination to Clevage Ratio for Char Production. Appendix B-X-Ray Diffraction Theory for Random Layer Lattices as Applied to the Structure of Graphite," pp 17-32 of "Applications of Plastics Materials in Aerospace," Chemical Engineering Progress 59, Symposium Series, No. 40, American Institute of Chemical Engineers (New York 1963).

McFarland, B. L. and Joerg, P., "A Theory for the Ablation of Heterogeneous Materials," presented at the AIChE National Meeting in New Orleans, March 10, 1963.

McFarland, B., Joerg, P., and Taft, M., "Criteria for Plastic Ablation Materials as Functions of Environmental Parameters," AD 277957 (May 1962).

Ibid, "Part II," AD 277951 (May 1962).

Mihalow, F. A., Koubek, F. J., and Perry, H. A., "Ablation Test Methods for Rocket and Heat Shield Materials," NAVWEPS Report 7314 (1 Oct. 1960).

Mitchel, B. J., "Ablative Plastics Characterization," AFML-TR-65-156, Part II. (June 1966).

Mitchel, B. and Recesso, J., "Ablative Plastics Characterization, Part I," AD 467689 (May 1965).

Mixer, R. and Marynowski, C., "A Study of the Mechanism of Ablation of Reinforced Plastics," AD 237242 (Feb. 1960).

Moeller, C. E., "New Thermal Insulations," Product Engineering 37, 91-95 (Feb. 14, 1966).

Monroe, S. F. and Chitwood, B. E., "Space Umbrella," pp 6-16 in "Plastics and Adhesives in the Space Age; Regional Technical Conference, Garden City, N. Y., May 13, 14, 1964. Technical Papers."

Morrell, J. F., Ebert, R. S., and Phillips, J. F., (A Study of the A-6A (A2F-1) Nose Radome), "Final Engineering Report, 16 Mar. 1964-1 Sept. 1965," AD-627089 (27 Sept. 1965).

Mountvala, A. J., Nakamura, H. H., and Rechter, H. L., "Development of Lightweight Thermal Insulation Materials for Rigid Heat Shields," NASA-CR-68709 (25 June 1965).

Munson, T. R. and Spindler, R. J., "Transient Thermal Behavior of Decomposing Materials, Part I: General Theory and Application to Convective Heating," IAS Paper No. 62-30, January 22-24, 1962.

Myers, Howard and Harmon, D. B., Jr., "Energy Transfer Processes in Decomposing Polymeric Systems," Douglas Aircraft Company, Inc., Engineering Paper No. 1020 (September 1960).

Myers, James R., "Materials Concepts Studied for Resistance to Space Vehicle Re-entry Temperatures," Mater. Protect. 2, 20-25 (Dec. 1963).

Nieberlein, V. A., "Materials for Reentry. A Selected Bibliography, 1959-1963," AD 433656 (12 Mar. 1964).

Norin, T. L., "The Measured Electrical Characteristics of Several Ablative and Some Non-ablative High Temperature Radome Materials," Proceedings of the OSU-RTD Symposium on Electromagnetic Windows," Vol. I, 2-4 June 1964.

Olson, G. L. and Streep, S. C., "Low Pressure Molding of Large Phenolic Nylon Parts," 6-page paper in: "Society of the Plastics Industry, Reinforced Plastics Div., Annual Technical and Management Conference, 18th, Proceedings. New York, Society of the Plastics Industry, Inc., 1963."

Papalegis, F. and Bourdeau, R., "Pyrolytic Reinforcing Agents for Ablative Erosion-Resistant Composites," AD 410254 (May 1963).

Papalegis, F. and Bourdeau, R., "Pyrolytic Reinforcements for Ablative Plastic Composites," AD 468356 (May 1965).

Papalegis, F. E. and Bourdeau, R. G., "Pyrolytic Reinforcements of Ablative Plastic Composites," AD 454952 (July 1964).

Pearl, H. A., Nowak, J. M., Conti, J. C., and Urode, R. J., "Refractory Inorganic Materials for Structural Applications," WADC-TR-59-432 (Feb. 1960).

Pears, C. D. and Shoffner, J. E., "The Thermal Response of Ablative Materials," a 28-page paper in "National SAMPE Symposium on Insulation-Materials and Processes for Aerospace and Hydrospace Applications, 8th, San Francisco, Calif., May 25-28, 1965."

Pendleton, E. L., "Synthesis and Characterization of Model Polymers for Use in the Investigation of Char Forming Heat Shields," NASA-CR-57811 (Jan. 1965).

Pirrung, P. F., "Erosion Resistant Pyrolyzed Ablative Plastics," AD 450747 (Sept. 1964).

Powers, D. J., "Thermal and Mechanical Properties of Foam Silicon Carbide," AD 284355 (29 June 1962).

Powers, D. J., "Thermal and Mechanical Testing of Foam Alumina and Foam Zirconia," AD 276983 (29 June 1963).

Price, D. E. and Wagner, H. J., "Preparation and Properties of Fiber-Reinforced Structural Materials," AD 422242 (Aug. 22, 1963).

Raech, Harry, Jr., "Prepreg Materials for High Performance Dielectric Applications," pp 11-A-1 to 11-A-6 in "SPI Reinforced Plastics Division, Anniversary Technical Conference, 20th, Chicago, Ill., February 2-4, 1965, Proceedings."

Rashis, Bernard and Hopko, R. N., "An Analytical Investigation of Ablation," NASA TMx-300 (1960).

Rashis, Bernard and Walton, T. E., Jr., "An Experimental Investigation of Ablating Materials at Low and High Enthalpy Potentials," NASA-TM-X-263 (Mar. 1960).

Reinhart, T. J., Jr. and Chase, V. A., "New High Temperature Laminates for Aerospace Applications," pp 11-G-1 to 11-G-8 in "SPI Reinforced Plastics Division, Anniversary Technical Conference, 20th, Chicago, Ill., February 2-4, 1965, Proceedings.

Reinikka, E. A. and Sartell, R. J., "Thermal Protection of Ballistic Entry Vehicles," Journal of Spacecraft and Rockets 2, 226-31, (Mar.-April 1965).

Reinikka, E. A. and Wells, P. B., "Charring Ablators in Lifting Reentry," AIAA Summer Meeting, Los Angeles, Calif., June 17-20, 1963.

Roberts, L., "An Analysis of Ablation-Shield Requirements for Manned Re-entry Vehicles," Technical Report, NASA R-62, (1960).

Roberts, L., "A Theoretical Study of Stagnation-Point Ablation," NACA-TN-4392 (September 1958).

Roberts, Leonard, "Radiation and Ablation Cooling from Manned Re-entry Vehicles," pp 1019-1044 of "Advances in Aeronautical Sciences; Vol. 4, 2nd International Congress in the Aeronautical Sciences, Proceedings, Zurich, Switzerland, Sept. 12-16, 1960," Pergamon Press, Inc. (New York 1962).

Robbins, D., "Thermal Erosion of Ablative Materials," ASD-TR-61-307 (April 1962).

Robbins, D. and Epstein, G., "Thermal Erosion of Ablative Materials," AD 274138 (Feb. 1960).

Robbins, D. and Kremith, R., "Thermal Erosion of Ablative Materials," ASD-TDR-63-254 (March 1964).

Ibid, "Part II," AD 454634 (July 1963).

Rosenbery, J. W., Smith, H. E., and Wurst, J. C., "Evaluation of Materials Systems for Use in Extreme Thermal Environments Utilizing an Arc-Plasma-Jet," WADD TR 60-926 (June 1961).

Rosensweig, R. E. and Beecher, N., "Theory for Ablation of Fiberglass-Reinforced Phenolic Resin," AIAA Journal I (August, 1963).

Rovin, S., Greening, T. A., and Adgate, F., "A Matrix Reinforced Thermal Protection System," Welding Journal, Research Supplement 43, 329-S-336-S (July 1964).

Rutner, Emile, "The Thermodynamics of Ablation," pp 140-51 in "Materials Symposium, 13-15 September 1961, Hotel Westward Ho, Phoenix, Arizona," ASD-TR-61-322 (July 1961).

Ryshkewitch, E. I., "Metal-Oxide-Gradient Ceramic Bodies," U. S. Patent No. 3,148,981 (Sept. 15, 1964).

Salmassy, O. K. and Collins, J. A., "Applications for Plastics in Aerospace Re-entry Vehicles," pp 9-16 of "Applications of Plastic Materials in Aerospace," Chemical Engineering Progress 59, Symposium Series No. 40, American Institute of Chemical Engineers (New York 1963).

Salzinger, Sam, "Continuous Bias Tape Wrapping of Re-entry Nose Cones," pp XI-3-1 to XI-3-3 of "Society of Plastics Engineers, Annual Technical Conference, 21st, Boston, Mass., March 1-4, 1965, Technical Papers. Volume II."

Scala, S. M., "The Ablation of Graphite in Dissociated Air: Part I, Theory," IAS Summer Meeting, Los Angeles, June 1962.

Scala, S. M., "A Study of Hypersonic Ablation," General Electric Company, T. I. S. Document No. R59SD438 (September 1959).

Scala, S. M., "The Thermal Degradation of Reinforced Plastics During Hypersonic Re-Entry," General Electric Company, T. I. S. Document No. R59SD401 (July 1959).

Scala, S. M., "The Thermal Protection of a Reentry Satellite," General Electric Rep. R59SD336 (March 1959).

Scala, S. M. and Gilbert, L. M., "Thermal Degradation of a Char-Forming Plastic During Hypersonic Flight," ARS Journal 32 (June 1962).

Scala, S. M. and Sutton, G. W., "The Two-Phase Hypersonic Laminar Boundary Layer, A Study of Surface Melting," 1958 Heat Transfer and Fluid Mechanics Institute, University of California, June 1958.

Schick, H. L., "An Analysis of Some of the Physical and Chemical Properties of Silica ($SiO_2$) of Importance in Ablation Behavior," AD 606 246 (27 October 1958).

Schmidt, D., "Interdisciplinary Research on Ablative Materials," AFML-TR-65-62 (August 1965).

Schmidt, D., "Ablative Plastics and Elastomers in Chemical Propulsion Environments," AD 468420 (April 1965).

Schmidt, D., "Ablation of Plastics," AD 276176 (Feb. 1962).

Schmidt, D., "Ablative Thermal Protection for Aerospace Vehicles," AD 272785 (March 1961).

Schmidt, D., "Ablative Plastics for Re-entry Thermal Protection," AD 268078 (Jan. 1961).

Schmidt, D., "Behavior of Plastic Materials in Hyperthermal Environments," AD 237362 (April 1960).

Schmidt, D., "Thermal Parameters of Re-entry Ablative Plastics," AD 237471 (March 1960).

Schmidt, D. L., "Ablative Polymers for Hypersonic Atmospheric Flight," AFML-TR-66-78 (May 1966).

Schmidt, D. L., "New Ablative Plastics and Composite Materials," SAMPE Journal 2, 10-18 (February/March 1966).

Schmidt, D. L., "Ablative Materials," pp 23-78 of "Air Force Materials Symposium/1965, 9, 10, 11 June - Technical Papers," AFML-TR-65-29 (May 1965).

Schmidt, D. L., "Ablative Materials," pp 775-815 of "Materials Symposium 13-15 September, 1961, Hotel Westward Ho, Phoenix, Arizona," ASD-TR-61-322, AD-264 193 (July 1961).

Schmidt, D. L., "Behavior of Plastics in Re-entry Environments," Modern Plastics (November-December 1960).

Schmidt, D. and Jones, W., "Carbon-Base Fiber Reinforced Plastics," AD 288289 (Aug. 1962).

Schmidt, D. and Peterson, G., "Reinforced Plastics at Very High Temperatures," AD 241595 (June 1960).

Schmidt, D. and Schwartz, H., "Experimental Evaluation Methods for Ablative Plastics," AD 277283 (March 1962).

Schmidt, D. L. and Tomashot, R. C., "Plastics in the Air Force, AD 601533 (April 1964).

Schmidt, D. L. and Hawkins, H. T., "Pyrolyzed Rayon Fiber Reinforced Plastics," AD 438892 (April 1964).

Schnitt, A., Brull, M. A., and Wolko, H. S., "Optimum Stresses of Structural Elements at Elevated Temperatures," Symposium on Structures for Thermal Flight, ASME, March 1956 (also ASME Transactions, Vol. 79, No. 5, pp 959-966, July 1957).

Schwartz, H., "Laboratory Techniques for Studying Thermally Ablative Plastics," AD 273665 (Jan. 1962).

Schwartz, H., "Comparative Erosion Resistance of Plastic Materials in a Supersonic Rocket Exhaust and Subsonic Air Arc Plasma," AD 247441L (Sept. 1960).

Schwartz, H., ed, "Conference on Behavior of Plastics in Advanced Flight Vehicle Environments," AD 247100L (Sept. 1960).

Schwartz, H. S., "New Materials and Physical Constructions for Ablative Use," pp 447-69 of "High Temperature Technology: International Union of Pure and Applied Chemistry, Commission on High Temperatures and Refractories, International Symposium, Pacific Grove, Calif., September 8-11, 1963, Proceedings," Butterworth and Co., Ltd. (London 1964).

Schwartz, H. and Farmer, R., "Thermal Irradiation of Plastic Materials," AD 267578 (Aug. 1961).

Schwartz, H. and Lisle, B., "Effects of High Intensity Thermal Radiation on Structural Plastic Laminates," AD 142181 (Dec. 1957).

Schwartz, H., Schmidt, D., Marolo, S., and Starks, D., "Properties of Thermally Degraded Ablative Plastics," AD 243683 (Nov. 1960).

Schwartz, M. A. and Greening, T. A., "Impregnated Foam Ceramic Insulating Materials," a 33-page paper in "National SAMPE Symposium on Insulation Materials and Processes for Aerospace and Hydrospace Applications, 8th, San Francisco, Calif., May 25-28, 1965."

Snapland, D. J., "Preliminary Design of a Mars-Mission Earth Re-entry Module," pp 525-76 in "NASA, Marshall Space Flight Center Proc. of the Symp. on Manned Planetary Missions, 1963/1964 Status 12 June 1964."

Shapland, D. J., Price, D. A., and Hearne, L. F., "A Configuration for Reentry From Mars Missions Using Aerobraking," presented at the 1st Annual Meeting AIAA, Washington, D. C., June 29-July 2, 1964.

Sharkitt, R. L., Hessinger, P. S., and Kyshkewitch, Eugene, "High-Temperature Resistant Beryllia Fiber-Reinforced Structural Composites," ASD-TDR-62-632, Part II (July 1963).

Sheridan, R. A., Diaconis, N. S., and Warren, W. R., "Performance of Several Ablation Materials in Simulated Planetary Atmospheres," GE Report No. R63SD35 (April 1963).

Sherrad, G. H. and Murray, C. A., "The Materials Used in Aerospace Applications for Plastics," presented at the Society of Automotive Engineers-American Society of Naval Engineers, National Aero-Nautical Meeting, Washington, D. C., Apr. 8-11, 1963.

Siegel, H. J. and Lewis, J. W., "Asset Materials Selection and Processing," pp 591-614 of "Materials Science and Technology for Advanced Applications; Proceedings of the Golden Gate Materials Conference, San Francisco, Calif., Feb. 13-15, 1964. Volume 2."

Simpkins, P. G., "On the Stable Shape of Subliming Bodies in a High-Enthalphy Gas Stream," Journal of Fluid Mechanics 15, 119-32 (Jan. 1963).

Sklarew, Samuel, "Reinforced Refractory Coatings," presented at the 1961 National Technical Symposium of the Aerospace Materials & Process Engineers, Nov. 14-15, 1961.

Sklarew, Samuel, "Reinforced Refractory Ceramic Coatings," pp 457-75 of "Composite Materials and Composite Structures. Proceedings of the Sixth Sagamore Ordnance Materials Research Conference Conducted at Sagamore Conference Center, Racquette Lake, New York, August 18, 19, 20, and 21, 1959."

Smith, F. C., et al, "Development of a Reinforced Carbonaceous and Ablative Composite for Entry Heat Protection of Manned Spacecraft," NASA-CR-56324 (30 Sept. 1962).

Smith, G. P. and Strong, G. E., "Corrugated or Cellular Bodied Ceramic Materials," French Patent No. 1,355,857 (March 20, 1964).

Smith, J. M., "Refractory Composites for Thermal Protection," presented at the Tenth Refractory Composites Working Group Meeting, Atlanta, Georgia 12-14 April 1965.

Sparrow, E. M., Minkowyez, W. J., and Eckert, E. R. G., "Diffusion-Thermo Effects in Stagnation-point Flow of Air with Injection of Gases on Various Molecular Weights into the Boundary Layer," AIAA Journal 2, 652-59 (Apr. 1964).

Spencer, S. B. and Jackson, W. O., "A New Fiber for Reinforced Plastic Aerospace Applications," pp 55-63 of "Plastics and Adhesives in the Space Age; Regional Technical Conference, Garden City, N. Y., May 13, 14, 1964, Technical Papers," Society of Plastics Engineers, Inc. (New York 1964).

Spindler, R. J. and Hurwicz, H., "Transient Heat Flow in Translucent Non-Gray Ablating Materials," Proceedings of the 4th Air Force Ballistic Missile Div., Space Tech. Lab. Symposium, Vol. 2, Pergamon Press, Inc., (1961).

Starks, D., "Ablative Plastic Chars Containing Carbon and Graphite Reinforcements," AD 466184 (April 1965).

Starks, D., "Ablative Plastic Chars Containing Vitreous and Asbestos Reinforcements," AD 464591 (April 1965).

Steg, L. and Lew, H., "Hypersonic Ablation," AD 275-292 (May 1962).

Steinberg, M. A. and Kerfoot, H. P., "Design of High Temperature Structural Systems," pp 363-387 of "High Temperature Technology: International Union of Pure and Applied Chemistry, Commission on High Temperatures and Refractories, International Symposium, Pacific Grove, Calif., September 8-11, 1963, Proceedings," Butterworth and Co., Ltd. (London 1964).

Steurer, W. H., "Materials for Thermal Protection," pp 94-121 of "Materials for Missiles and Spacecraft," McGraw-Hill Book Co., Inc. (New York 1963).

Steurer, W. H. and Sullivan, H. C., "Principles of Composites for Heat Absorption," pp 388-402 of "Proceedings of the Sixth Sagamore Ordnance Materials Research Conference Conducted at Sagamore Conference Center, Racquette Lake, New York, August 18-21, 1959," Contract DA-30-069-ORD-2566 (MET-661-601).

Steverding, B., "Surface Activity and Preferential Ablation;" AIAA Journal 2, 549-51 (Mar. 1964).

Stevens, D., "Establishment of the Potential of Flake Reinforced Composites as Engineering Structural Materials," AD 270 502 (Dec. 1961).

Strauss, E. L., "Studies of Advanced Refractory Composites Concepts for Structural and Heat Shield Applications," Martin Report RM-191 (March 1965).

Strauss, E. L., "Heat Transfer and Thermal Exposure Studies of Resin Impregnated Zirconia Foam," presented at the Eighth Symposium on Ballistic Missile and Space Technology, 17 Oct. 1963, at San Diego, Calif.

Strauss, E. L., "Structural and Heat Transfer Characteristics of Resin-Impregnated Porous Ceramics," Bull. Am. Ceram. Soc. 42, 444-47 (Aug. 1963).

Strauss, E. L., "The Historical Background of Reinforced Plastics in Aerospace Vehicles," Chemical Engineering Progress 59, Symposium Series No. 40, 1-8 (1963).

Strauss, E. L., "The Application of Resin-Impregnated Porous Ceramics to Re-entry Vehicle Heat Shields," pp 7-27 of "Aerodynamic Heated Structures," Prentice-Hall, Inc. (Englewood Cliffs, N. J. 1962).

Styhr, K. H., "Research on Low Density Thermal Insulation Materials for Use Above 3000° F," NASA-CR-57727 (1964).

Ibid., NASA-CR-59210 (1964).

Ibid., NASA-CR-60542 (1964).

Styhr, K. H., Jr., Hessinger, P. S., and Ryshkewitch, Eugene, "Research on Low Density Thermal Insulation Materials for Use Above 3000° F, Third Quarterly Status Report for the Period October 1 to December 31, 1962," prepared under NASA Contract NA3r-99 (1962).

Summers, J. L., "Evaluation of the Impact Performance of Realistic Space Structures," NASA-TM-X-51620 (1964).

Summers, J. L. and Nysmith, C. R., "The Resistance of a Variety of Composite Space Structures to Hypervelocity Impact," pp 386-93 of "AIAA Annual Structures and Materials Conference, Fifth, Palm Springs, Calif., April 1-3, 1964," (AIAA Publication CP-8).

Sutton, G. W., "Adiabatic Wall Temperature Due to Mass Transfer Cooling with a Combustible Gas," Jet Propulsion 29, 136-37 (February 1958).

Sutton, G. W., "The Hydrodynamics and Heat Conduction of a Melting Surface," Journal of the Aeronautical Sciences 25, 29-32, (January 1958).

Sutton, G. W., "Combustion of a Gas Injected into a Hypersonic Laminar Boundary Layer," in "Proceedings of the Seventh International Combustion Symposium," Butterworth and Co., Ltd. London (1958).

Swann, R. T., "Composite Thermal Protection Systems for Manned Re-Entry Vehicles," ARS Journal 32, pp 221-226 (Feb. 1962).

Swann, R. T., "An Engineering Analysis of the Weights of Ablating Systems for Manned Re-entry Vehicles," pp 65-86 of "Ballistic Missile and Space Technology, Vol. IV," Academic Press (New York 1960).

Swann, R. T., Dow, M. B., and Tompkins, S. S., "Analysis of the Effects of Environmental Conditions on the Performance of Charring Ablators," pp 259-69 of "American Institute of Aeronautics and Astronautics, Entry Technology Conference, Williamsburg and Hampton, Va., October 12-14, 1964."

Swann, R. T., Pittman, C. M., and Smith J. C., "One-Dimensional Numerical Analysis of the Transient Response of Thermal Protection Systems," NAS-TN-D-2976 (Sept. 1965).

Syvertson, C. A., "Effects of Mass Addition on the Stability of Slender Cones at Hypersonic Speeds," AIAA Journal 1, 939-40 (Apr. 1963).

Tauber, M. E. and Seiff, Alvin, "Optimization Analysis of Heating of Conical Bodies Making Lifting Hyperbolic Entries into the Atmospheres of Earth and Mars," pp 13-21 in: "American Institute of Aeronautics and Astronautics, Entry Technology Conference, Williamsburg and Hampton, Va., October 12-14, 1964, Technical Papers."

Van Driest, E. R., "The Problem of Aerodynamic Heating," Aero. Eng. Rev. 15, 26-41 (Oct. 1956).

Van Vliet, R. M., "Mathematical Optimization of Insulation," American Institute of Aeronautics and Astronautics, 2nd Annual Meeting, San Francisco, Calif., 26-29 July 1965.

Vassallo, F. A., "Internally Ablating Composites," ASD-TR-60-697 (April 1961).

Vassallo, F. A., "Dimensional Stability Together with Ablation," SAE Preprint 354E (April 1961).

Vassallo, F. A., Camnitz, H. G., and Kirchner, H. P., "Study of Thermal Radiation Within Solids and Study of Internally Ablating Composites," AD 251332 (May 1961).

Ibid, "Part II, Vol. I: Internally Ablating Composites," AD 259948 (Sept. 1961).

Vassallo, F. A. and Kirchner, H. P., "Study of Thermal Radiation Within Solids," WADD-TR-60-697, Part II, Vol. II. (July 1961).

Vassallo, F., Wahl, N., Sterbutzel, G., and Beal, J., "The Study of Ablation of Structural Plastic Materials," AD 234779 (Dec. 1959).

Ibid, "Part II," AD 240636 (April 1960).

Vogan, J., "Thermal Protection Surfaces for Structural Plastics," AD 244760L (July 1960).

Ibid, "Part II," AD 260209 (Oct. 1960).

Vogan, J. W. and Trumbull, J. L., "Metal-Ceramic Structural Composite Materials," ML-TDR-64-83 (June 1964).

Vogan, J., Trumbull, J., Munn, J., Hallerbach, K., and Kavadas, P., "Metal-Ceramic Structural Composite Materials," Boeing Airframe Company Document No. D2-11406 (Nov. 1961).

Wagner, R. B., "Process of Making an Impregnated Ceramic," U. S. Patent 3,250,833 (10 May 1966).

Wall, J. K., "Theoretical Penetration of Hypervelocity Projectiles into Finite Targets, (Normal Impact)," presented at the AIAA Fifth Annual Structures and Materials Conference, Palm Springs, Calif., April 1-3, 1964.

Warmbrod, J. D., "Calculated Results for the Transient Heating and Melting Process of Glass Shields with Various Material Properties at the Stagnation Point of a Re-entering ICBM," NASA-TN-D-1643 (May 1963).

Wells, P. B., "A Method for Predicting the Thermal Response of Charring Ablation Materials," AD 443 144 (1964).

Wheeler, W. H., "Ceramic Radiative Heat Shields," Ceram. Age 79, 161-64 (Oct. 1963).

Whipple, C. L., "Elastomeric Silicones for Aerospace Insulation. I - Ablative Materials," a 14-page paper in "National SAMPE Symposium on Insulation-Materials and Processes for Aerospace and Hydrospace Applications, 8th, San Francisco, Calif., May 25-28, 1965."

Whipple, C. L., Piper, D. G., and Smith, F. A., "Silicones for Ablative Applications," presented at the National SAMPE Symposium on Adhesives and Elastomers for Environmental Extremes, 7th, Los Angeles, Calif., May 20-22, 1964.

## BIBLIOGRAPHY (Concluded)


Wick, B. H., "Ablation Characteristics and Their Evaluation by Means of Arc Jets and Arc Radiation Sources," presented at the 7th International Aeronautical Congress on the Problems of Structures of Aviation and Engineering, Paris, France, 14-16 June 1965.

Williams, David T., "Terminal Shapes of Ablating Bodies," AIAA Journal 1, 494-96 (1 Feb. 1963).

Williamson, J. B., "Advanced Materials & New Fabrication Techniques for Ablative Hardware Composite Materials Engineering," an 8-page report in "8th National SAMPE Symposium, San Francisco, Calif., May 25-28, 1965."

Wilson, A. W., "Thermal and Strength Requirements for Reinforced Plastics," British Plastics (August 1960).

Wilson, C. O., Jr. and Maggio, F. X., "Polyborophane Resin Laminates," ML-TDR-64-183, Part II (July 1965).

Wilson, R. G., "Thermophysical Properties of Six Charring Ablators from 140° to 700° K and Two Chars from 800° to 3000° K," NASA-TN-D-2991 (ct. 1965).

Winters, C. W., "Heat-Transfer Rates and Ablation on a Blunted Cylinder-Flare Configuration in Free Flight up to a Mach Number of 3.93," NASA-TN-D-2383 (Aug. 1964).

Winters, C. W. and Witte, W. G., "A Flight Investigation of Ablation on a Blunted Cylinder-Flare Configuration to a Mach Number of 3.43," NASA-TN-D-2354 (July 1964).

Wood, R. M. and Tagliani, R. J., "Heat Protection by Ablation," pp 421-53 of "Composite Materials and Composite Structures. Proceeding of the Sixth Sagamore Ordnance Materials Research Conference Conducted at Sagamore Conference Center, Racquette Lake, New York, August 18, 19, 20, and 21, 1959."

Wurst, J. and Gerdeman, D., "Arc Heater Screening of Ablative Plastics," AFML-TR-65-110 (Aug. 1965).

Zimmerman, F. J., "Fiber Metals for Meteoroid Protection," presented at the AIAA Fifth Annual Structures and Materials Conference, Palm Springs, Calif., April 1-3, 1964.

Unclassified
Security Classification

| 14. KEY WORDS | LINK A | | LINK B | | LINK C | |
|---|---|---|---|---|---|---|
| | ROLE | WT | ROLE | WT | ROLE | WT |
| Felted Ceramics Fiber Structures | | | | | | |
| Composite Structures | | | | | | |
| Leading Edges | | | | | | |
| Thermal Protection Systems | | | | | | |
| Radomes | | | | | | |
| Silica (Fused) | | | | | | |
| Charring Ablators | | | | | | |
| Metal Films | | | | | | |
| Radants | | | | | | |
| Environmental Testing | | | | | | |
| Fabrication Processes | | | | | | |
| Slip-Casting | | | | | | |
| Embedded Ablators | | | | | | |
| Ceramic Foams | | | | | | |
| Refractory Fibers | | | | | | |
| Particle Size Distribution | | | | | | |

## INSTRUCTIONS

1. **ORIGINATING ACTIVITY:** Enter the name and address of the contractor, subcontractor, grantee, Department of Defense activity or other organization *(corporate author)* issuing the report.

2a. **REPORT SECURITY CLASSIFICATION:** Enter the overall security classification of the report. Indicate whether "Restricted Data" is included. Marking is to be in accordance with appropriate security regulations.

2b. **GROUP:** Automatic downgrading is specified in DoD Directive 5200.10 and Armed Forces Industrial Manual. Enter the group number. Also, when applicable, show that optional markings have been used for Group 3 and Group 4 as authorized.

3. **REPORT TITLE:** Enter the complete report title in all capital letters. Titles in all cases should be unclassified. If a meaningful title cannot be selected without classification, show title classification in all capitals in parenthesis immediately following the title.

4. **DESCRIPTIVE NOTES:** If appropriate, enter the type of report, e.g., interim, progress, summary, annual, or final. Give the inclusive dates when a specific reporting period is covered.

5. **AUTHOR(S):** Enter the name(s) of author(s) as shown on or in the report. Enter last name, first name, middle initial. If military, show rank and branch of service. The name of the principal author is an absolute minimum requirement.

6. **REPORT DATE:** Enter the date of the report as day, month, year or month, year. If more than one date appears on the report, use date of publication.

7a. **TOTAL NUMBER OF PAGES:** The total page count should follow normal pagination procedures, i.e., enter the number of pages containing information.

7b. **NUMBER OF REFERENCES:** Enter the total number of references cited in the report.

8a. **CONTRACT OR GRANT NUMBER:** If appropriate, enter the applicable number of the contract or grant under which the report was written.

8b, 8c, & 8d. **PROJECT NUMBER:** Enter the appropriate military department identification, such as project number, subproject number, system numbers, task number, etc.

9a. **ORIGINATOR'S REPORT NUMBER(S):** Enter the official report number by which the document will be identified and controlled by the originating activity. This number must be unique to this report.

9b. **OTHER REPORT NUMBER(S):** If the report has been assigned any other report numbers *(either by the originator or by the sponsor)*, also enter this number(s).

10. **AVAILABILITY/LIMITATION NOTICES:** Enter any limitations on further dissemination of the report, other than those imposed by security classification, using standard statements such as:

(1) "Qualified requesters may obtain copies of this report from DDC."

(2) "Foreign announcement and dissemination of this report by DDC is not authorized."

(3) "U. S. Government agencies may obtain copies of this report directly from DDC. Other qualified DDC users shall request through _____."

(4) "U. S. military agencies may obtain copies of this report directly from DDC. Other qualified users shall request through _____."

(5) "All distribution of this report is controlled. Qualified DDC users shall request through _____."

If the report has been furnished to the Office of Technical Services, Department of Commerce, for sale to the public, indicate this fact and enter the price, if known.

11. **SUPPLEMENTARY NOTES:** Use for additional explanatory notes.

12. **SPONSORING MILITARY ACTIVITY:** Enter the name of the departmental project office or laboratory sponsoring *(paying for)* the research and development. Include address.

13. **ABSTRACT:** Enter an abstract giving a brief and factual summary of the document indicative of the report, even though it may also appear elsewhere in the body of the technical report. If additional space is required, a continuation sheet shall be attached.

It is highly desirable that the abstract of classified reports be unclassified. Each paragraph of the abstract shall end with an indication of the military security classification of the information in the paragraph, represented as *(TS), (S), (C), or (U)*.

There is no limitation on the length of the abstract. However, the suggested length is from 150 to 225 words.

14. **KEY WORDS:** Key words are technically meaningful terms or short phrases that characterize a report and may be used as index entries for cataloging the report. Key words must be selected so that no security classification is required. Identifiers, such as equipment model designation, trade name, military project code name, geographic location, may be used as key words but will be followed by an indication of technical context. The assignment of links, roles, and weights is optional.

DD FORM 1 JAN 64 1473 (BACK)

Unclassified
Security Classification

Unclassified
Security Classification

**DOCUMENT CONTROL DATA · R&D**

*(Security classification of title, body of abstract and indexing annotation must be entered when the overall report is classified)*

1. ORIGINATING ACTIVITY *(Corporate author)*
Engineering Experiment Station
Georgia Institute of Technology
Atlanta, Georgia 30332

2a. REPORT SECURITY CLASSIFICATION
Unclassified

2b. GROUP

3. REPORT TITLE

CERAMIC SYSTEMS FOR MISSILE STRUCTURAL APPLICATIONS

4. DESCRIPTIVE NOTES *(Type of report and inclusive dates)* Final Summary Report (Quarterly Report No. 16 Inclusive), 1 November 1965 - 31 October 1966.

5. AUTHOR(S) *(Last name, first name, initial)*
Poulos, Nick E., Murphy, Charles A., Corbett, William J., Boland, Paul, and Gorton, Charles W.

| 6. REPORT DATE | 7a. TOTAL NO. OF PAGES | 7b. NO. OF REFS |
|---|---|---|
| December 1966 | 242 | 102 |

| 8a. CONTRACT OR GRANT NO. | 9a. ORIGINATOR'S REPORT NUMBER(S) |
|---|---|
| NOw-63-0143-d | Final Summary Report (Quarterly Report No. 16 Inclusive) |
| b. PROJECT NO. | Project A-651 |
| c. | 9b. OTHER REPORT NO(S) *(Any other numbers that may be assigned this report)* |
| d. | |

10. AVAILABILITY/LIMITATION NOTICES
Office of Technical Services
Department of Commerce

11. SUPPLEMENTARY NOTES

12. SPONSORING MILITARY ACTIVITY RMGA-8 Advanced Technology Branch, Missile Frame and Guidance Division, Bureau of Naval Weapons, Department of the Navy, Washington, D. C.

13. ABSTRACT

Five slip-cast fused silica radomes were fabricated and evaluated in a Mach 2.2, 4000° F, 140 psia Typhon ramjet exhaust at General Dynamics/Pomona Ordnance Aerophysics Laboratory July 6-18, 1966. Test data is to be presented in a separate report prepared and published by the Johns Hopkins University, Applied Physics Laboratory, Silver Spring, Maryland. Preliminary observations are presented here and it is estimated that 50 to 60 per cent of the test objectives were realized. Materials development and characterization studies of slip-cast alumina-fused silica composites and fused silica grinding for strength improvement are presented. Studies for applying metal films on slip-cast fused silica substrates for antenna applications were completed. Fabrication of felts from refractory fibers of fused silica, boron nitride, zirconia, magnesia, and silicon carbide coated graphite fibers and impregnation of a phenolic embedded ablator in these felts and comparison of thermal evaluation results of these embedded felts with standard ablators under a heat flux of 450 and 1500 BTU/ft²-sec are described.

* sq ft

DD FORM 1 JAN 64 1473

Unclassified
Security Classification